An Analysis of Transient Flow in Upland Watersheds: Interactions between Structure and Process

by

David Lawrence Brown

B.A. (University of Oregon) 1977
M.S. (University of Nevada at Reno) 1987

A dissertation submitted in partial satisfaction of the

requirements for the degree of

Doctor of Philosophy

in

Soil Science

in the

GRADUATE DIVISION

of the

UNIVERSITY of CALIFORNIA at BERKELEY

Committee in charge:

Professor T.N. Narasimhan, Chair
Professor John G. McColl
Professor William E. Dietrich

1995

The dissertation of David Lawrence Brown is approved:

T. N. Narasimhan — March 1, 1995

Chair — Date

T. N. NARASIMHAN

J. G. McCall — 3/1/95

Date

Mathew E. Dutton — 3/1/95

Date

University of California at Berkeley

1995

An Analysis of Transient Flow in Upland Watersheds: Interactions between Structure and Process

©1995

by

David Lawrence Brown

Abstract

An Analysis of Transient Flow in Upland Watersheds:

Interactions between Structure and Process

by

David Lawrence Brown

Doctor of Philosophy in Soil Science

University of California at Berkeley

Professor T.N. Narasimhan, Chair

The physical structure and hydrological processes of upland watersheds interact in response to forcing functions such as rainfall, leading to storm runoff generation and pore pressure evolution. Transient fluid flow through distinct flow paths such as the soil matrix, macropores, saprolite, and bedrock may be viewed as a consequence of such interactions. Field observations of pore pressure responses to rain events at two diverse experimental watersheds further reflect the importance of heterogeneous soil and geologic materials as they affect storm runoff responses. An existing physically-based numerical subsurface flow model was modified to incorporate infiltration partitioning and overland flow. Through a series of parametric simulations, this model was used to study storm runoff processes and pore pressure evolution in hypothetical hillslopes as affected by: nonlinearities in the conductive and storage properties of soils and bedrock; hillslope geometry; downstream (streamside) boundary conditions; and antecedent moisture

conditions. Rainfall rates of 1-year return interval magnitude were applied to convexo-concave slopes and subsurface storm flow was observed the predominant runoff generation process for the soil types considered. Simulation results suggest that soils containing significant macroporosity may enhance the contribution of a soil horizon or geologic material to hillslope discharge. For the soils considered in this study, there was correlation between runoff production and hydraulic diffusivity. Accordingly, the storage properties of soils may be more important than previous investigations have assumed, although further studies are required. Similar to the findings of previous investigations, the effects of antecedent moisture conditions were observed to be important in determining which of the flow paths may contribute to storm-induced runoff production and pore pressure responses. Results from the parametric studies also suggest that channel bank geometry and lateral heterogeneities in soil hydraulic properties along hillslope gradients are two critical factors in determining whether subsurface storm flow or saturation overland flow will be the dominant streamflow generation process. Field observations of rainfall-pore pressure responses were compared with simulations using the available field data for the sites, and were found to be in reasonable agreement following minor calibration involving storage parameters.

T. N. Narasimhan
T. N. NARASIMHAN
March 1, 95

This dissertation is dedicated to my wife Chris and our son Sean.
You have been my inspiration.

TABLE OF CONTENTS

1. INTRODUCTION 1

1.1 PREVIOUS WORK 5

1.2 GOALS AND OBJECTIVES 27

2. METHODS 30

2.1 MATHEMATICAL MODELING STUDIES 31

2.1.1 General Description of Mathematical Model 32

2.1.2 Adaptation of the Model to Hillslope Simulations 38

2.1.3 Material properties 45

2.1.4 Slope Geometries 51

2.1.5 Initial and Boundary Conditions 52

2.2 DESCRIPTION OF PARAMETRIC STUDIES USING GENERIC HILLSLOPES 53

2.2.1 Structural heterogeneities 55

2.2.2 Slope geometry 58

2.2.3 Antecedent soil moisture conditions 59

2.2.4 Downstream boundary conditions and runoff generation mechanisms 59

2.2.5 Simulations of *flow around channel heads* 61

2.3 DESCRIPTION OF FIELD SITES AND INSTRUMENTATION 62

2.3.1 Caspar Creek Experimental Watershed 62

2.3.2 Hubbard Brook Experimental Forest 66

3. RESULTS AND DISCUSSION 70

3.1 COMPARISON WITH PREVIOUS HILLSLOPE MODELING WORK 70

3.2 RESULTS OF PARAMETRIC STUDIES 71

3.2.1 Structural heterogeneities 73

3.2.2 Slope geometry 79

3.2.3 Antecedent soil moisture conditions 85

3.2.4 Downstream boundary conditions and runoff generation mechanisms 86

3.2.5 Simulations of *flow around channel heads* 90

3.3 FIELD OBSERVATIONS 94

3.3.1 Caspar Creek Experimental Watershed 94

3.3.2 Hubbard Brook Experimental Forest 96

3.4 INTEGRATION OF FIELD OBSERVATIONS AND SIMULATIONS 99

3.4.1 Caspar Creek Experimental Watershed 100

3.4.2 Hubbard Brook Experimental Forest 103

4. CONCLUSIONS 106

5. FUTURE RESEARCH NEEDS 109

6. REFERENCES CITED 110

LIST OF TABLES

Table 2.1 Summary of parametric simulations

Table 2.2 Piezometer construction details - M Swale, Caspar Creek Experimental Watershed

Table 2.3 Piezometer construction details - UNH Field Site, Hubbard Brook Experimental Forest

Table 3.1 Summary of reported subsurface stormflow discharge rates

Table 3.2 Summary of simulated subsurface stormflow discharge rates

Table 3.3 Summary of simulated subsurface stormflow discharge rates for hillslopes with saprolite

Table 3.4 Response time-scale (time constant Δt_m)

Table 3.5 Summary of simulated subsurface stormflow discharge rates for convergent slopes (20 degree wedge meshes)

Table 3.6 Summary of results for channel head simulations

Table 3.7 Summary of slug test results for Caspar Creek field site

Table 3.8 Time of peak piezometric response, January 1994 storm M Swale, Caspar Creek Experimental Watershed

LIST OF FIGURES

Figure 1.1 Conceptual hillslope flow paths

Figure 1.2 Summary of major runoff generation models

Figure 2.1 Schematic of geometric parameters used in defining conductance in TRUST

Figure 2.2 General mesh configuration

Figure 2.3 Detail of mesh discretization

Figure 2.4 Effects of horizontal grid-spacing on hydraulic head response in run 4 with Inceptisol soil, slope bottom

Figure 2.5 Typical saturation and hydraulic conductivity curves (Del Monte sand from Liakopoulos, 1965)

Figure 2.6 Idealized distribution of possible void types defined by Brewer (1974) with depth

Figure 2.7 Typical specific moisture capacity and hydraulic diffusivity curves (Del Monte sand from Liakopoulos, 1965)

Figure 2.8 Synthetic and measured hydraulic conductivity curves for soil horizons containing macropore

Figure 2.9 Pseudo 3-dimensional mesh used in simulations of convergent flow

Figure 2.10 General mesh configuration of variable angle slopes

Figure 2.11 Flow domain for a) cases where soil thickens with distance downslope; b) hillslope with fracture permeability extending to depth

Figure 2.12 Boundary conditions: a) downstream, bottom, and upstream; b) detail of downstream [seepage face, constant head and no-flow]

Figure 2.13 Possible subsurface saturation conditions affecting the pressure head ratio m (adapted from Wilson, 1988, Figure 54) .

Figure 2.14 Saturation and hydraulic conductivity curves for soils used in parametric studies

Figure 2.15 Saturation and hydraulic conductivity curves for saprolite from Wilson et al. (1992)

Figure 2.16 Saturation and hydraulic conductivity curves for bedrock used in parametric simulations

Figure 2.17 Simulation case with discontinuity in bedrock hydraulic conductivity (after Wilson et al., 1989)

Figure 2.18 Boundary condition configurations: a) 2-Part [seepage face and constant head]; and b) 3-Part [seepage face, constant head, and no-flow]
Figure 2.19 Mesh with low permeability zone in "riparian" soils near downstream boundary
Figure 2.20 Detail of mesh used in channel head simulations
Figure 2.21 Location of field sites
Figure 2.22 M Swale, Caspar Creek Experimental Watershed instrumentation
Figure 2.23 UNH Hillslope Field Site, Watershed 3, HBEF
Figure 3.1 From Freeze (1972a, Figure 4) baseflow generation homogeneous material
Figure 3.2 Simulation of base flow generation case from Freeze (1972a) - homogeneous material
Figure 3.3 Simulation of base flow generation case from Freeze (1972a) with heterogeneous conditions: Del Monte sand (Liakopoulos, 1965) and low-permeability bedrock
Figure 3.4 Effects of drainage from initial conditions used in run 4 (Inceptisol soil)
Figure 3.5 Effects of drainage from initial conditions used in nun 2 (colluvial soil)
Figure 3.6 Water table profile and runoff processes at end of 12-hour rainfall period, run 4 (Inceptisol soil), low-permeability bedrock and 1.2 m constant head downstream boundary condition
Figure 3.7 Runoff processes at end of 12-hour rainfall period for nrn 1 (Del Monte sand)
Figure 3.8 Comparison of runoff rates for different soil types (adjusted for drainage) - each with low-permeability bedrock
Figure 3.9 Hydraulic diffusivity for soils used in parametric simulations
Figure 3.10 Pressure head ratio ***m*** evolution during run 1 (Del Monte sand)
Figure 3.11 Effects of variable saprolite thickness on runoff rates
Figure 3.12 Hydraulic diffusivity relationships for saprolite cases (runs 6 - 9)
Figure 3.13 Runoff from individual flow paths for run 6
Figure 3.14 Runoff rates for low-permeability rock (run 10) and high-permeability rock (run 11)
Figure 3.15 Hydraulic diffusivity relationships for bedrock types
Figure 3.16 Pressure head evolution at soil/bedrock contact - case with midslope discontinuity (run 12)
Figure 3.17 Hydraulic head response of different materials at two slope positions during 12 hours of constant rainfall - run 4

Figure 3.18 Discharge by flow path for convergent flow domain - run 13
Figure 3.19 Discharge by flow path for convergent flow domain - run 14
Figure 3.20 Discharge rates for convergent flow domain cases (nuns 13 to 15)
Figure 3.21 Pore pressure evolution at toe of slope for convergent (runs 13 and 14) versus parallel (runs 4 and 8) flow domains
Figure 3.22 Effect of slope angle on runoff rate for cases (runs 16 to 18) with Inceptisol soil and low-permeability bedrock
Figure 3.23 Effect of slope angle on runoff rate for cases (runs 19 to 21) with Inceptisol soil and high-permeability bedrock
Figure 3.24 Effect of slope angle on runoff rate for cases (runs 22 and 23) with colluvial soil and low-k bedrock
Figure 3.25 Runoff rates for different rock permeabilities (runs 24 and 25) with variable thickness Inceptisol soil
Figure 3.26 Effect of bedrock type for hillslope with fracture permeability extending to depth (runs 26 and 27)
Figure 3.27 Effect of initial moisture conditions on runoff for cases (runs 28 to 31) with Inceptisol soil and low-permeability bedrock
Figure 3.28 Water table profiles and runoff processes for case (run 35) with 0.05 m downstream constant head boundary condition
Figure 3.29 Water table profiles and runoff processes for case (run 36) with 0.30 m downstream constant head boundary condition
Figure 3.30 Effects of different downstream boundary conditions on runoff rates - 0.05 m channel depth (nuns 32 and 35)
Figure 3.31 Effects of different downstream boundary conditions on runoff rates - 0.30 m channel depth (nuns 33 and 36)
Figure 3.32 Effects of different downstream boundary conditions on runoff rates - 1.20 m channel depth (runs 34 and 37)
Figure 3.33 Discharge by flow path for 0.05 m channel depth and 2-part boundary condition (run 32)
Figure 3.34 Discharge by flow path for 0.05 m channel depth and 3-part boundary condition (run 35)

Figure 3.35 Discharge by flow path for 0.30 m channel depth and 2-part boundary condition (run 33)

Figure 3.36 Discharge by flow path for 0.30 m channel depth and 3-part boundary condition (run 36)

Figure 3.37 Total discharge for cases (runs 36a and 37) with increasing channel depth and 3-part boundary condition

Figure 3.38 Runoff response for a 1-yr storm (run 4) versus a 100-yr storm with a 1.20 m channel depth

Figure 3.39 Discharge by flow path for case (run 39) with riparian low-k soil heterogeneity and 0.30 m channel depth

Figure 3.40 Effects of different soil types cm flow field around a 0.20-m channel head

Figure 3.41 Hydraulic head profile around a 2.0 m channel head for case (run 47) with lnceptisol soil

Figure 3.42 Relationship between seepage face height and channel head height for a uniform silt and Inceptisol soil

Figure 3.43 Relationship between ***m*** and a) channel head height (CH); b) seepage face height (SF) for uniform silt soil

Figure 3.44 Relationship between ***m*** and a) channel head height (CH); b) seepage face height (SF) for Inceptisol soil

Figure 3.45 Comparison of hydraulic diffusivity characteristics for soils used in channel head simulations

Figure 3.46 Cross-section A-C at Caspar Creek Experimental Watershed

Figure 3.47 Cross-section B-B* at Caspar Creek Experimental Watershed

Figure 3.48 Detail of cross-section B-B* showing typical winter water table profile

Figure 3.49 Rainfall and pressure head response, January - March 1994, A-transect, M Swale, Caspar Creek Experimental Watershed

Figure 3.50 Rainfall and pressure head response, January - March 1994, B-transect, M Swale, Caspar Creek Experimental Watershed

Figure 3.51 Rainfall and pressure head response, January - March 1994, C-transect, M Swale, Caspar Creek Experimental Watershed

Figure 3.52 Cross-section of UNH field site showing lower saturated zone

Figure 3.53 Storm pressure head response in piezometers monitored by data logger 1
Figure 3.54 Storm pressure head response in piezometers monitored by data logger 2
Figure 3.55 Storm pressure head response in piezometers monitored by data logger 3
Figure 3.56 Storm pressure head response in piezometers monitored by data logger 4
Figure 3.57 Soil hydraulic properties for Caspar Creek Experimental Watershed from Wosika (1981)
Figure 3.58 Cross-section along C transect at Caspar Creek Experimental Watershed showing node centers of simulation mesh
Figure 3.59 Observed and simulated rainfall patterns for a) Caspar Creek, January 1994 storm; b) Hubbard Brook, October 1993 storm
Figure 3.60 Comparison of simulated and observed pore pressure response for January 1994 rainfall event - Caspar Creek Watershed, M Swale Piezometer C1
Figure 3.61 Comparison of simulated and observed pore pressure response for January 1994 rainfall event - Caspar Creek Watershed, M Swale Piezometer C2
Figure 3.62 Cross-section A-A* at Hubbard Brook Experimental Forest showing node centers of simulation mesh
Figure 3.63 Comparison of observed and simulated pressure head response to October 1993 storm, Piezometer 321a, UNH field site, Hubbard Brook Experimental Forest

ACKNOWLEDGMENTS

I want to begin this work by expressing my thanks to the University of California at Berkeley for providing an opportunity to work in a learning environment that will always be an inspiration to me. Nari Narasimhan taught me many lessons, in the classroom, in research, and in life in general. He has convinced me that one can excel in teaching as well as research in academia, and his constant enthusiasm and willingness to question conventional beliefs when warranted will always remain an inspiration to me. I also very much appreciate the many insights he has given me on the realities of being a university professor. Bill Dietrich broadened my interests and education in process-oriented geomorphology, and he provided valuable insights and constructive criticism in my dissertation research. Beyond contributing to my dissertation work, John McColl helped me develop teaching and communication skills. I also want to acknowledge the contributions of Mary Firestone, Ron Amundson, Tetsu Tokunaga, and Harvey Doner for helping me grow as a soil scientist. The former Department of Soil Science provided my early financial support, and special thanks go to departmental staff members who facilitated my research over the last three years. I would like to express my appreciation for the financial support I received for my dissertation work from the U.S. Geological Survey Water Resources Grant Program. The Switzer Foundation provided a fellowship that helped fund my studies.

Working with my fellow students over the last four and a half years has been one aspect of my graduate education that I treasure most. I particularly appreciate

interactions with Jon Chorover, I-Wen Liu, Laurie Newman Osher, Angus McGrath Noam Gressel, Thais Winsome, Brian Schroth, Teri Balser, Trish Holden, and Rohit Salve. Jonathan Owens and Gina Wolff also provided valuable assistance in my research. The department of Material Science and Mineral Engineering was something of a second home for me, and there I had the good fortune to be able to work along side Matt Small, Zafer Demir, and Walt McNab. The prospect of working with many of these people as colleagues in the future is indeed exciting.

The collaborative nature of my dissertation research brought me into contact with many researchers outside of Berkeley. Dave Montgomery at the University of Washington shared ideas and personal insights that enhanced my work. Andy Fisher with the University of Indiana provided critical computational tools and training, and many valuable discussions as well. Breck Bowden and David Cedarholm with the University of New Hampshire furnished access to their research site in Hubbard Brook Experimental Forest, and generously shared field data.

I am particularly indebted to the research staff of the U.S. Forest Service Redwood Sciences Laboratory for their assistance and support in my efforts, including Bob Ziemer, Liz Keppeler, Rand Eads, Garth Hodgson, Lindsay Chapman, Jay Arnold, and other field staff. Norm Henry, Pete Cafferata, and many others with the California Division of Forestry contributed to the field efforts at Caspar Creek.

My field work at the Hubbard Brook Experimental Forest would not have been possible without the contributions of Wayne Martin and Amey Bailey with the U.S. Forest Service. I am grateful to the Science Advisory Committee for allowing me to

participate in the Hubbard Brook Ecosystem Study. My appreciation also goes to the many scientists with U.S. Geological Survey with whom I collaborated on this study, including Paul Hsieh, Tom Winter, Alan Shapiro, Don Rosenberry, Carol Johnson, Phil Harte, Rich Perkins, Chris Barton, and Claire Tjiedeman.

Finally, I want to offer thanks to my mother, Marian Brown, and my grandmother, Della Bartholomew, posthumously for their love, support, and enduring patience over my long years in school. I only wish they could be here to see this work completed.

1. INTRODUCTION

Upland watersheds dynamically respond hydrologically to rain events through several inter-related flow processes. These flow responses are inherently transient, reflecting temporal and spatial variations in rainfall intensity. Fluid flow is also governed by the physical framework of a watershed, including the soils and underlying shallow geologic materials, and the topography.

One means of conceptualizing transient fluid flow in upland (low-order stream) watersheds is to consider an assemblage of interacting flow paths as idealized on Figure 1.1. Surface or overland flow is coupled with subsurface flow by means of infiltration and exfiltration at the land surface. Subsurface flow may occur within soil horizons, saprolite (weathered bedrock), or bedrock (Chorley, 1978). The hydraulic properties of a given earth material as well as the spatial relations of adjoining materials determine the attributes of an actual flow path. For example, water may flow within soil horizons through the matrix as a porous medium, or through larger pores (on the order of 1 millimeter or larger) commonly referred to as macropores. By virtue of their geometry, macropores can be shown to conduct water more rapidly under high moisture conditions than the "micropores" of the soil matrix. Similarly, fractures in saprolite or bedrock may dominate the flow response under wet conditions, and thus would define a flow path distinct from the soil matrix or macropores.

The movement of water into and through these flow paths has two consequences of both theoretical and practical interest. First, surface runoff is generated on two widely

different time scales: 1) during individual precipitation events; and 2) on a seasonal basis. Runoff volume, timing, and duration affects both water supply and flood propagation. Second, transient subsurface flow is directly related to the evolution of pore pressures at the hillslope scale. Dynamic interactions between pore pressures, drainage geometry, and the material properties of soil and bedrock can significantly influence the stability of slopes and channel heads, and sediment releases to streams (Humphrey, 1982; Dietrich et al., 1986).

The earliest process studies in watershed hydrology were motivated by a need to understand and predict runoff generation phenomena. Consequently, several mechanisms of precipitation event-related stream flow generation were described, based largely on field observations in the eastern United States. Working primarily in agricultural areas, Horton (1933) proposed an infiltration-based model of runoff generation which is often referred to as Horton overland flow. Shortly thereafter, the importance of subsurface flow in runoff generation was first recognized and described based on field observations in upland forested watersheds (Hursh, 1936; Hursh and Brater, 1941). The generation of surface runoff by rising water tables recognized as a result of field studies conducted by Dunne (1970) and Dunne and Black (1970a, 1970b). Thus, the three major precipitation-induced runoff generation mechanisms commonly used today as interpretive models are:

1. Hortonian overland flow [from Horton (1933)]
2. Subsurface stormflow [from Hursh (1936)].
3. Saturation overland flow [direct precipitation and return flow, from Dunne (1978)]

Baseflow generation between storms produced by groundwater discharge to streams constitutes a fourth runoff-generation mechanism, but this phenomena is not specifically addressed in the present study. A graphical summary of these processes and the environmental factors which control their occurrence adapted from Dunne (1978) is presented on Figure 1.2.

It is useful at this point to define the important terms and phrases used in this study. Chorley (1978) provides a very useful historically-annotated glossary of terms that have evolved from the many hillslope studies conducted to date. The following definitions will be used hereafter.

> *Exfiltration*: Upward flow of water (under saturated conditions) out of the subsurface onto the land surface [The exfiltration surface is a seepage face]
>
> *Horton overland flow*: Overland flow that occurs when rainfall intensity exceeds the soil infiltration capacity and causes saturation at the soil surface (assuming a uniform soil surface without depressions)
>
> *Saturation overland flow*: Surface flow that occurs when saturation at the land surface is induced by a water table which rises to intercept the land surface
>
> *Subsurface srormflow*: Lateral saturated subsurface flow contributing to storm runoff
>
> *Variable source area*: The dynamically expanding and contracting area of a watershed that contributes to storm runoff generation

In order to understand the particular runoff generation mechanisms active in a given watershed, it will be argued that one must first characterize the physical properties and spatial arrangements of the flow paths that convey runoff and affect pore pressure evolution. Using an analogy from the biological sciences, a distinction may be made

between the "anatomy" or structure of a watershed and its "physiology" or function. Heterogeneities in the form of soil horizons, shallow underlying bedrock, and topography comprise the anatomy of a watershed. Runoff generation, subsurface water flow, and pore pressure evolution represent three of the many "physiological" processes that may occur in a watershed.

The physical structure and hydrological processes of upland watersheds interact in response to forcing functions such as rainfall, and flow paths may be viewed as a consequence of such interactions. Previous field observations and computational studies have shown that the relative importance of macropores in runoff production is highly dependent on the flow and storage of water (soil moisture conditions) in the surrounding soils (Ziemer and Albright, 1987; and Sidle and Tsuboyama, 1992). Thus it seems worthwhile to begin to systematically study runoff processes in the context of watershed structure as manifest in flow paths.

Given the transient nature of many flow processes in upland watersheds, it is very important to acknowledge two fundamental physical properties of flow systems: conductance and storage (or equivalently, capacitance). The hydraulic conductivity and specific storage of a given earth material reflect both physical structure and fluid properties. Interactions between these two properties can be represented by the hydraulic diffusivity which is simply a quotient of hydraulic conductivity to specific storage. The structure of the parabolic equation governing transient subsurface flow is such that the time scale of response to imposed forces is dependent on hydraulic diffusivity. In this

work, the importance of hydraulic diffusivity will be critically examined in the transient hydrologic response of watersheds to rain events.

Another aspect of the transient nature of flow in upland watersheds addressed in this study concerns the time scale on which different flow paths respond to rain events. The magnitude and importance of various runoff processes differ with seasonal changes in stored moisture. A question arises as to how watershed structure or material properties affect such temporal differences in runoff. Material properties such hydraulic diffusivity for different soils and rock are studied to address this question and to determine if there is a characteristic response time scale associated with different flow paths.

The following section reviews relevant hillslope studies, after which the goals and objectives of this study are introduced. Next, the attributes and development of the numerical model used in the computational studies are described, as are a suite of parametric simulations designed to address the objectives of this study. A brief description is then given of two field sites at which data were collected for simulation purposes. Next, modeling results are presented and discussed in the relation to previous and current field observations. Following a summary of the results, conclusions are presented and future research needs are identified.

1.1 PREVIOUS WORK

Beginning in the early part of this century, Horton (1933) laid the foundation for modern research efforts concerning the relationship between rainfall and runoff in watersheds. However, it is important to note that Horton's field observations were made

almost entirely on agricultural fields. Tillage and other agricultural practices significantly alter the structural and hydraulic properties of soils, and thus have a major impact on the generation of Hortonian overland flow (Hillel, 1980a).

The recognized importance of infiltration in relation to agricultural practices and runoff production has resulted in a considerable body of soil physics research (Hillel, 1980b). Many of the infiltration models developed to date either assume ponded conditions at the land surface (e.g. Philip 1957a, 1957b) or assume that ponding will occur (e.g. Smith and Parlange, 1978). These types of infiltration models have been applied to upland soils with varying degrees of success (Bonnell, 1993).

Field studies of Hortonian overland flow since the 1930's have been summarized by Dunne (1978). One significant modification of the Hortonian flow model emerged in the 1960's with the recognition that soil infiltration capacity and runoff production will vary within a watershed (Berson, 1964). Emmett (1970) and Dunne and Dietrich (1980b) (and many others at various sites) measured the overland flow hydraulic parameters at rangeland sites in Wyoming and Kenya, respectively. Saturation overland flow data collected by Wilson (1988) at a grass-covered upland watershed in the coastal mountains of Northern California generally agreed with the earlier studies. Wilson (1988) attributed an apparent anomaly between predicted laminar overland flow and observed turbulent flow to the choice of length scales in estimating Reynolds number. The importance of micro-scale topography and soil properties in controlling the magnitude and distribution of Horton overland along individual hillslopes has been described by Dunne and Dietrich (1980a) and Dunne et al. (1991).

Efforts to model overland flow on hillslopes have followed several different approaches. One example is the unit-source area analysis of homogeneous watershed subdivisions (Amerman, 1965). Due to its limiting assumptions of homogeneity, the unit-source area method was superseded by the Stanford Watershed Model (Crawford and Linsley, 1966) which incorporates spatially variable infiltration. During this period, significant progress was made in developing deterministic, physically-based overland flow models based on principles of conservation of mass, energy and momentum (Henderson and Wooding, 1964). Woolhiser and Liggett (1967) developed both a thorough solution to the Saint-Venant shallow-water equations for sheetflow, and also a kinematic approximation of simpler form. The validity of the kinematic approach in overland flow applications was found to be correlated with the Froude number. Morris and Woolhiser (1980) found that a different form of approximation, described as a diffusive wave, gave better results for certain combinations of Froude and kinematic flow numbers.

Zhang and Cundy (1989) developed a two-dimensional overland flow model that solved the hydrodynamic equations using a finite-difference scheme. They found that microtopography had the greatest effect on overland flow characteristics. The theoretical effects of moving versus stationary storms on laminar and turbulent overland flow were analyzed by Richardson and Julien (1994). Based on numerically-simulated storms, they provide criteria for evaluating the applicability of different approximation-based overland flow equations.

Most of the modern ideas concerning subsurface runoff processes have developed over the last 35 years. Freeze (1974), Kirkby (1978), Anderson and Burt (1990), and

Bonell (1993) provide useful reviews of the research that has been conducted to date concerning runoff generation and subsurface flow paths in upland watersheds. The relevant previous research can be separated into four general categories:

- Field studies focused on hydrologic processes using intensively instrumented experimental watersheds;
- Physically-based mathematical modeling of surface and subsurface flow using both field observations and hypothetical data sets;
- Geomorphic and digital terrain modeling approaches using geometric drainage units and simplified flow equations; and
- Field studies that emphasize the use of hydrogeochemical and isotopic analyses designed to identify flow paths.

Most of the watershed research efforts conducted to date have focused primarily on hydrologic processes. Far less attention has been given to flow paths, or other "structural" idealizations. Thus, the following literature review is constrained so as to focus on those studies in the four categories described above that provide insights regarding the interactions between watershed form and process.

Field Studies

Of the major subsurface flow paths, most of the field investigations performed to date have focused on flow through soils. Within the soil zone, two different flow paths can be recognized: the soil matrix itself as a "porous medium" and the macroscopic pores (macropores) including root holes, soil cracks, and animal burrows. The flow of water

through the soil matrix has been the primary focus of studies of subsurface hydrology from the earliest work by Darcy (1856) and Buckingham (1907) to the mid-1960's.

The importance of structural and biogenic pores in subsurface flow processes was recognized in at least qualitative terms prior to this time (Hursh, 1944; and Gaiser, 1952). Development of a rigorous definition of 'macropores' has been a subject of debate as seen in the classification system proposed by Luxmoore (1981) and resulting comments by Bourna (1981), Beven (1981b), and Skopp (1981). Two of the most common criteria used as a basis for defining macropores have been size (diameter) and the related capillary potential. Beven and Germann (1982) present an extensive review of macropore characteristics, function and terminology.

A variety of field studies have qualitatively described macropores in upland watersheds. Gaiser (1952), working at a forested site in Ohio, found plant roots to comprise from 2 percent to 3 percent of the soil volume to an approximate depth of 0.9 m. The decay of these roots was also observed to result in variably-empty root channels that were interpreted to be preferential pathways for flowing water. Aubertin (1971) estimated that large diameter voids can comprise as much as 35 percent of the total soil volume in the upper 0.1 m of a forest soil, declining to 10 percent or less by 0.6 m in depth. It should be noted that these pore volumes contained both root channels and animal burrows. Chamberlin (1972) observed roots, both living and in various stages of decay to comprise up to 50 percent of the upper 0.5 m of forest soils in the coastal mountains of British Columbia Wilson and Smart (1984) described the occurrence and development of macropores (referred to as soil pipes) from mole burrowing in an upland

watershed in Wales, U.K. They found 6-cm pipes to occupy approximately 3.5 percent of the upper 0.15 m of soil. Stresky (1991) found smaller large-pore volumes ranging from 0.75 percent in the upper 0.1 m to 0.2 percent at 0.5 m. The large difference in macropore pore volumes between these sites is presumed to be related to differences in soil type and vegetation.

The importance of macropores and different types of soil structure in influencing the storage and transmission of water at the plot scale has been described by Bouma and Hole (1971) and Bouma and Wosten (1979). Consequently, there was a need to modify soil sampling methods to emphasize the preservation of soil structure for the purpose of analyzing the hydraulic properties of soils (e.g. hydraulic conductivity and moisture retention). Watershed studies in which soil structure was preserved by analyzing relatively undisturbed soil cores began to appear in the literature after the mid-1970's (Yee, 1975; Wosika, 1981; Wilson et al., 1992).

Field experiments have shown that flow through macropores can rapidly transmit a significant amount of water in response to individual rain events (Whipkey, 1965, 1967; Weyman, 1973; Arnett, 1976; Beasley, 1976; Mosley, 1979, 1982; McCaig, 1983; Wilson and Smart, 1984; German et al., 1986; Ziemer and Albright, 1987; Ursic and Esher, 1988; Wilson, 1988; Smettem et al., 1991; Sidle and Tsuboyama, 1992; Montgomery and Dietrich, 1995). In all of these studies, macropores conducted water only after shallow transient water tables had risen to saturate the horizon containing the macropores. Field observations reported by Montgomery and Dietrich (1995) suggest that drainage through macropores can constrain the rise in pressure heads in response to rain events. The

rapidity of macropore flow, it appears from the work of Ziemer and Albright (1987), is influenced by antecedent moisture conditions in the vadose zone.

It can be shown from conventional soil physics that after the soil matrix surrounding a large-diameter pore becomes saturated, fluid pressure within the matrix will exceed the macropore air entry pressure and water will flow into the large pore. However, several field studies have observed significant lateral flow through soils containing macropores under unsaturated soil conditions (Aubertin, 1971; Beasley, 1976; Bouma and Dekker, 1978; Mosley, 1979; and Smettem and Trudgill, 1983). DeVries and Chow (1978) found that vertical flow through macropores seemed to dominate the infiltration process in forest soils in British Columbia, particularly under highly transient conditions. The theoretical basis for flow into cylindrical macropores under unsaturated conditions has only recently begun to emerge with the work of Philip et al. (1989).

Beyond the conductance of storm runoff, macropores have been shown to play an important role in the stability of slopes and channel heads. Using a Hele-Shaw analog model in laboratory experiments, Pierson (1983) observed that flow through long, connected macropores can lead to fluid pressures in excess of hydrostatic and conditions that might lead to slope instability. Based on field observations at an experimental watershed in New Zealand, McDonnell (1990a) reported that a connected system of soil cracks and pipes could increase infiltration rates such that excessive pore pressures and unstable conditions could develop at the soil-bedrock interface. Flow through soil pipes/macropores has been observed to be a potentially important factor in the development of stream channel networks (Jones, 1971). Dietrich and Dunne (1993)

present an extensive analysis of processes governing the occurrence and development of channel heads. They also review numerous field studies which have observed the development of channel heads through tunnel scour of various types of macropores and other structural voids (e.g. cracks).

Concurrent with measurements of soil saturation and hydraulic conductivity relationships have been efforts to quantitatively predict these relationships using a variety of empirical relations (Mualem, 1976; Clapp and Hornberger, 1978; and van Genuchten, 1980; and others). Wilson et al. (1992) present one of the more recent efforts to develop predictive equations for soils containing macropores, and their work is of particular interest since their field sampling has been carried out in forested watersheds.

Saprolite has received relatively little attention in regard to its hydraulic properties and role in subsurface flow processes. Many studies have been conducted in the eastern United States and Canada, and have focused on saprolite mineralogic properties and function in soil development (Rice et al., 1985; Wang and Ross, 1989; and Buol and Weed, 1991). Measurement of the hydraulic properties of saprolite presents a challenge, both in sampling techniques and in available analytical methodologies (Vepraskas et al., 1991; Welby, 1992). Schoeneberger and Amoozegar (1990) reported field-measured mean saturated hydraulic conductivity values for saprolite in North Carolina which ranged from 7.5×10^{-8} m/s to 2.7×10^{-6} m/s. Based on laboratory measurements, Vepraskas et al. (1991) reported a mean (geometric) saturated hydraulic conductivity of 7.5×10^{-7} m/s for saprolite from the same region. Vepraskas et al. (1991) also considered the dual flow regimes within the saprolite: channels (structural voids and root holes) and groundmass

(matrix). They estimated that the hydraulic conductivity of the channels decreased by approximately two orders of magnitude within the first 0.3 m of tension applied during desaturation. Wilson et al. (1992) present hydraulic conductivity and water retention curves for a saprolite in Tennessee, and found saturated hydraulic conductivity values that were approximately two orders of magnitude higher (2.5×10^{-4} m/s) than the highest values reported for the North Carolina study sites.

The heterogeneous nature of bedrock in terms of fracture distributions has been well documented in the literature (Domenico and Schwartz, 1990). One of the major questions that arises in studying flow through fractured rock is whether to consider discrete fractures (e.g. Moreno et al., 1985) or to focus on a continuum of fractures as an equivalent porous medium over some appropriate volume (Shapiro, 1989). Fractured rock has also been described as a double-porosity material in which the fracture domain and the matrix domain may interact (Barenblatt et al., 1960). Othmer et al. (1991) presented experimental evidence in support of the idea that soils containing macropores may function as dual-porosity media as well. Wang (1991) provides a detailed review of recent research in subsurface flow through fractured rock. While most qualitative descriptions of subsurface flow paths in watersheds include flow through bedrock, it has been customary to treat the bedrock as impermeable in quantitative analyses.

Field data on bedrock response is scarce. A review of the research efforts to date has located only five locations at which flow through bedrock in upland watersheds has been investigated by direct field measurement. Of these sites, the transient response of bedrock to rain events has been monitored at two, including the Solstice experimental

watershed in Marin County, California (Wilson and Dietrich, 1987) and an experimental watershed near Coos Bay, Oregon (Montgomery et al., 1990). These researchers have studied bedrock for its role in pore pressure development leading to slope failure. Apparent heterogeneities in shallow bedrock at this site have been observed to contribute to discontinuous areas of saturated colluvium (Montgomery et al., 1990; Montgomery, 1991). Megahan and Clayton (1986) measured the saturated hydraulic conductivity of shallow granitic bedrock (less than 10 m deep) in the Idaho batholith. They found hydraulic conductivity to be inversely related to the degree of weathering, but uncorrelated with depth.

Stephenson and Freeze (1974) present data from the Sheep Creek Watershed in Idaho on flow through bedrock in response to daily snowmelt patterns. Based on field data these authors inferred that "the mechanism of strearnflow generation is subsurface delivery of meltwater over limited distances through shallow high-permeability low porosity formations of altered and fractured basalt" (high hydraulic diffusivity by implication). Wilson and Dietrich (1987) observed "significant large- and small-scale interactions between storm flow in the bedrock and the colluvium..." Beyond these studies, to date, there has been no attempt to develop a broader understanding of either the role of bedrock flow in upland watersheds, or the factors which govern its importance. In this context, it is worth recognizing that bedrock may be characterized by high saturated hydraulic conductivity and low storativity and hence, high hydraulic diffusivity.

Physically-Based Mathematical Modeling Studies

Simulations of transient flow through watersheds have been performed in order to generate insight into runoff generation mechanisms in lieu of cost- and labor-intensive field experiments. Physically-based mathematical models have been applied using both simplified flow equations (Smith and Hebbert, 1983) and more general governing equations (Stephenson and Freeze, 1974). In the latter category, Freeze (1972a, 1972b) and Beven (1977, 1979) performed numerical simulations of rainfall-induced runoff generation for hypothetical, simplified hillslopes using finite difference and finite element models, respectively. However, neither modeling effort included macropore or bedrock flow components, and none of their simulations considered pore pressure development accompanying highly transient rain events.

The first physically-based numerical modeling studies of transient hillslope hydrologic processes were performed by Freeze (1972a) in studying base flow generation in upland watersheds, and storm runoff processes (Freeze, 1972b). Freeze (1972a) described the development of a numerical model which was used to quantitatively demonstrate the importance of soil hydraulic properties in influencing base flow generation. Using hypothetical hillslopes, Freeze (1972b) simulated rainfall-runoff events and concluded, 1) that Horton overland flow was a rare phenomena in humid, vegetated environments; 2) subsurface stormflow was not a quantitatively significant runoff generation mechanism except under certain limited conditions; and 3) simulation results provide theoretical support for the saturation overland flow mechanism as described by Dunne and Black (1970a, b).

Beven (1977), following on the earlier work of Freeze, described a suite of parametric studies which varied soil hydraulic properties, initial conditions, and slope geometry. Beven found that antecedent moisture (initial) conditions and slope convergence had a major influence on simulated runoff hydrographs. It should be noted that all of the soils data used by Beven (1977) were based on remixed samples and empirical hydraulic property relationships.

As noted previously, the experimental results reported by Stephenson and Freeze (1974) represent transient flow through a hillslope in response to snowmelt rather than rainfall. The authors compared field observations with a finite difference model and found the results of the simulations to match the field observations only to a moderate degree. They attribute the mixed success to data limitations and uncertainties related to model calibration requirements. Stephenson and Freeze (1974) summarized the major limitations in modeling complex natural flow systems with simulation models. These include: the level of theoretical development, computer limitations, difficulties in model calibration, and the lack of adequate field data.

Dietrich et al. (1986) simulated two-dimensional steady-state flow in a hypothetical homogenous hillslope to investigate the development of pore pressures leading to slope instability and failure. They used an integral finite difference method (Narasimhan and Witherspoon, 1978) to simulate the flow of water through soils and bedrock. They found that the pore pressure distribution was strongly dependent on both boundary conditions and the slope geometry.

Numerical simulations focused on slope stability have been based on individual field sites (Reid et al., 1988; and Wilson et al., 1989) and using hypothetical hillslopes (Hodge and Freeze, 1977; Humphrey, 1982). Humphrey's work is significant in that it is one of the earliest physically-based modeling studies to use soil hydraulic properties from undisturbed cores, and for its consideration of complex, 3-dimensional geometry. Using a finite-element model, Humphrey (1982) performed a set of parametric studies simulating flow through a hypothetical colluvium-filled bedrock depression of approximately 15 m in length. Among other things, he demonstrated the importance of the soil-bedrock interface topography and 3-dimensional convergent flows in the evolution of pore pressures of rainfall events.

Wilson et al. (1989) extended this work by performing 3-dimensional simulations incorporating flow through bedrock based on an extensive parallel field investigation. Their findings include: 1) the extent and duration of saturation along the axis of a hollow is affected by flow convergence both within the bedrock and colluvium; 2) colluvium-bedrock hydraulic conductivity contrasts can influence the distribution of flow out of bedrock into the colluvium; 3) small-scale (on the order of meters) heterogeneities in bedrock hydraulic conductivity can significantly affect localized pore pressures and the water table profile; and 4) the distribution of moisture conditions resulting from flow convergence (in hollows) may contribute to conditions leading to instability in locations not predicted by slope position and angle. Wilson et al. (1989) also obtained good agreement between simulated and observed piezometric responses for a 50- to 100-year return interval rain event monitored during the field component of their investigation.

Interactions between groundwater flow vectors and hillslope stability were investigated by Iverson and Major (1986). Using an analytical model for steady-state flow, they were able to relate the angle of upward flow to the stability of homogeneous, infinite, cohesionless slopes. Criteria were presented for conditions where failure would occur due to static liquefaction versus Mohr-Coulomb failure.

Smettern et al. (1991) simulated flow through a hillslope using a finite element model originally developed for consolidation modeling. Observed macropores were incorporated into the model by defining empirical hydraulic conductivity and moisture retention curves. Only drainage conditions were simulated, and the modeled water table was in reasonable agreement with field observations during the winter period. Drainage in the summer months could not be simulated due to limitations in the model parameterization.

Most recently, Jackson and Cundy (1992) took a different approach emphasizing 2-dimensional flow in the horizontal plane. However, this approach ignores the role of flow through bedrock without any justification from field observations. The degree of agreement between simulated and observed piezometric responses seems more varied than the authors imply. Jackson and Cundy (1992) also seem to be unaware of previous modeling studies (Humphrey, 1982; Wilson, 1988; Wilson et al., 1989) in contending that their approach contributes a method for modeling complex topography lacking in previous studies.

Smith and Woolhiser (1971) describe a model that couples overland flow with variably-saturated infiltration. The overland flow component employs the kinematic

cascade concept which allows the land surface to be discretized into planes with variable slope angle. Smith and Hebbert (1983) also developed a model based on kinematic wave approximations for both surface and subsurface flow. Despite its conceptually rigorous coupling of surface and subsurface flow processes, this model is also limited in its ability to handle spatially-variable material properties, especially along a hillslope gradient.

Kinematic wave approximations have been used in a variety of applications beyond overland flow analysis. Beven (1981a, 1982) presents a simplified analytical model for subsurface stormflow based on the kinematic wave theory. He reported good agreement between model results and field observations but points out that the model has several limiting assumptions, including simplified soil hydraulic properties, uniform initial moisture conditions, and constant rainfall.

During the 1980's Germann and various co-authors published numerous studies describing the application of the kinematic wave approximation to modeling flow through macropores (e.g. Germann and Beven, 1981a, 1981b; Germann and Beven, 1985; and Germann et al., 1986). While this approach has produced reasonably good predictions of flow through soil blocks, various coefficients and parameters must be determined experimentally before the analysis can be applied.

Taking a different approach, Nieber and Warner (1991) numerically simulated saturated flow through a hypothetical hillslope with a single, discrete macropore. Under the conditions considered, they reported that a 0.02 m-diameter macropore could conduct a discharge equal to that of a block of soil matrix whose outflow face was 22 m wide by 1 m deep.

The effect of spatial heterogeneity at the hillslope scale on surface runoff processes was studied by Freeze (1980) using stochastically-generated rainfall patterns and soil hydraulic property distributions. Based on simplified flow equations and Monte Carlo simulation techniques, Freeze reported that the mean hydraulic conductivity value applied on a grid-scale of 10 m by 10 m had the greatest impact on estimates of peak runoff. Using the same analysis, Loague (1988) reported that the spatial distribution of soil hydraulic properties had a greater effect on simulated runoff than did rainfall distributions.

Geomorphic/Digital Terrain Modeling Approaches

Over the last 15 years, many have attempted to develop simplified modeling approaches that avoid the difficulties associated with using comprehensive process-based numerical models as described above. Most of these models utilize a simplified flow-contributing volume or area that is based on the topography of the watershed, and often assume steady-state Darcian flow conditions to exist (e.g. Iida, 1984). One of the earliest examples of these is TOPMODEL, first proposed by Beven and Kirkby (1979) and modified through subsequent studies (Beven, 1986; Beven et al., 1988; and Wood et al., 1990). This model has been used to predict runoff from certain higher-order watersheds with reasonable success. However, TOPMODEL assumes that the saturated hydraulic conductivity declines exponentially with depth even into the underlying bedrock, and did not perform well when groundwater flow vectors are not normal to topographic contours (Hinton et al., 1992).

A second model of this type that has been widely used is TOPOG (O'Loughlin, 1986). This model also assumes that subsurface flow follows the elevational head gradient and that convergent topography controls the distribution of saturated or near-saturated areas within a watershed. Despite this limitation and the steady-state assumption, results from TOPOG have formed the basis for acceptable predictions of storm runoff (Moore et al., 1986) and shallow landslides (Montgomery and Dietrich, 1994). Bonnell (1993) provides a recent review of both TOPMODEL and TOPOG, and their anticipated future development. A final example of this class of models is the geomorphic unit hydrograph approach (GUH) first introduced by Rodriguez-Iturbe and Valdes (1979) and Gupta et al. (1980) and later extended by Sivapalan et al. (1987, 1990). In its most recent version, the GUH approach seems to emphasize Horton and saturation overland flow mechanisms (Larsen et al., 1994), and thus may have limited applicability in upland areas where subsurface stormflow is a significant runoff generation mechanism. Goodrich and Woolhiser (1991) in the reviewing work of Sivapalan et al. (1987, 1990) pointed out that the scale-independence of the GUH method precludes its ability to consider the important effects of microtopography. Recent research efforts have sought to develop models that are independent of the watershed spatial scale (Wood et al., 1990).

Recent efforts by Larsen et al. (1994) have sought to quantify the qualitative relationships portrayed by Dunne (1978) on Figure 1.2. However, this study was conducted entirely within agricultural watersheds, and thus the applicability of the methods to upland, non-agricultural watersheds remains uncertain.

Because of their emphasis on large-scale topography, models of this type are particularly well-suited to take advantage of digital elevation data. Moore et al. (1991) provide an extensive review of digital terrain modeling studies. One relevant application is to combine digital elevation data with process-models in analyzing slope stability (Okimura and Ichikawa, 1985; Dietrich et al., 1993; and Montgomery and Dietrich, 1994). Montgomery and Dietrich (1994) used digital topographic data in conjunction with TOPOG to predict the potential for shallow landslides. They found predicted landslide patterns to match observed landslide locations, despite the use of spatially averaged soil properties and constant rainfall assumptions. This general area of modeling research appears to be making progress toward providing an improved basis for forecasting runoff and slope instability potential.

Considering the different types of models that have been applied in hillslope studies, the question arises as to how to evaluate model performance. In the most detailed study to date, Loague and Freeze (1985) compared the efficiency of three different types of models in predicting runoff summary variables (total storm runoff depth, peak runoff rate, and time to peak runoff). They found that simpler models (regression and unit hydrograph) gave as good or better results than a more complex, "quasi-physically based model". It should be noted that the models included in this study were selected for their suitability for conditions where Horton overland flow is the dominant runoff mechanism. Based on a review of model comparisons and assessments, Goodrich and Woolhiser (1991) correctly point out the need for continued research concerning model evaluation.

Hydrogeochemical and Isotopic Studies

The final major area of research in storm runoff generation involves the use of tracer tests and analysis of precipitation versus surface and subsurface waters for their chemical and isotopic content. An early study by Kunkle (1965) used specific conductance measurements to differentiate groundwater contributions to baseflow and storm runoff. Pinder and Jones (1969) performed a similar study using ion concentrations and a mass-balance approach to estimate the groundwater component of peak storm runoff. They reported that groundwater contributed up to approximately 40 percent of peak discharges.

In contrast to these earlier watershed-scale studies, Pilgrim et al. (1978) used a combination of hydrometric measurements, isotopic tracers, and specific conductance measurements on a hillslope plot to distinguish between the three major storm runoff-generation mechanisms, all of which were reportedly observed. Evidence for rapid subsurface flow through macropores was obtained from all of the analytical parameters. Pilgrim et al. (1978) interpreted the specific conductance data to conclude that the subsurface flow was comprised almost entirely of event-related (new) water.

Studies at the Hillman Creek watershed in Ontario, Canada have shown that saturated flow in the soil zone is capable of producing up to 80 percent of the total storm runoff (Sklash and Farvolden, 1979). Similar results have been obtained in isotopic studies at the Maimai catchment in New Zealand, where observations have shown that subsurface stormflow is the dominant source of runoff generated during rain storms

(Sklash, 1990). Another application of hydrogeochemical studies has been associated with stream-acidification studies (e.g. Swistock et al., 1989; and others).

One of the main purposes in conducting more recent hydrogeochemical studies has been to distinguish between "old" (pre-event) water and "new" (event-related) water in storm runoff. Working in New Zealand watersheds, Mosley (1979, 1982) determined that new water delivered by rapid subsurface flow through macropores was the major source of storm runoff based on dye tracing studies and numerous subsurface flow measurements. This interpretation was disputed by Pearce et al. (1986) and Sklash et al. (1986) who, working in the same watersheds, reported that old water was the dominant source of subsurface flow. They argued that rapid subsurface flow displaced older water in the streamside zone.

McDonnell (1990b) attempted to reconcile these earlier studies using a "cracked-pipe" model in which new, rapidly-infiltrating water mixes with older water in the matrix. This water, with an older isotopic signature then rapidly moves to the channel in macropores as the rising water table saturates the matrix. McDonnell (1990b) points out that this model is not necessarily applicable to watersheds in other environments. The difficulties encountered in the New Zealand studies described above attempting to characterize runoff sources using a two-component (old vs. new water) model are not unique (Bonnell, 1993).

Another recent application of hydrogeochemical studies has been to aid in the delineation of subsurface flow paths. Ross et al. (1994) used a combination of detailed soils and geologic mapping in conjunction with analysis of stream, soil and groundwater

chemistry to explain the significant differences in pH in two nearby headwater tributaries in Vermont. Shanley et al. (in press), working at the Sleepers River Research Watershed in Vermont, identified shallow saturated subsurface flow as being the primary flow path of snowmelt water reaching streams in nested watersheds. It is clear that these types of experiments, when used in conjunction with transient observations of flow and pore pressure, can help constrain an otherwise non-unique problem.

The importance of macropores in the preferential transport of solutes has been observed in many different field studies (Hammermeister et al., 1982; Megahan and Clayton, 1983; Pilgrim et al., 1987; Levy and Germann, 1987; Wilson et al., 1991a, 1991b; and Tsuboyama et al., 1994). Flow through connected systems of macropores has also been reported in studies concerned with the transport of bacteria through groundwater (Rahe et al., 1978; and German et al., 1987). Gee et al. (1991) in reviewing the applicability of the kinematic wave approximation to solute transport in macropores points out potential limitations of this approach due to the spatial variability of macropores and temporal variability of their function. White (1985) and Gee et al. (1991) provide relevant reviews of the role of macropores in subsurface transport.

In summary, it is worth noting that subsurface stormflow and saturation overland flow were each recognized based on field observations at a single field site. Subsurface stormflow flow was first described by researchers working at the Coweeta Hydrologic Laboratory in the southern Appalachian Mountains (Hursh, 1936; Hursh and Brater, 1941). The occurrence of saturation overland flow was demonstrated in field studies conducted at the Sleepers River Experimental Watershed in northeastern Vermont

(Dunne, 1970 and Dunne and Black, 1970a, b). Despite their localized origins, the validity of these two runoff generation concepts has been confirmed by subsequent field studies at a variety of other sites, and no new runoff process has been identified

The findings of many of the hydrometric and hydrogeochemical field studies described in the preceding sections provide an interesting contrast with the conclusions of Freeze (1972b, 1974, 1978) regarding the limited conditions under which subsurface stormflow might contribute to storm runoff. The importance of rapid subsurface flow through macropores had not been well established by the time when Freeze conducted the simulations presented in the 1972b paper. Thus, there appears to be a need to continue the physically-based, numerical modeling approach in regard to the field studies described above.

In the absence of soil and/or vegetation disturbance, Horton overland flow is quite rare in upland watersheds under humid climates. The three major storm runoff generation mechanisms sized by Dunne (1978) as shown on Figure 1.2 may be viewed as a continuum of processes that occur dependent on local environmental controlling factors (disturbance, climate, vegetation, soils, and topography). Thus, it is of interest to identify the conditions under which each mechanism may control runoff generation and pore pressure evolution. Quantitatively simplified efforts (e.g. Larsen et al., 1994) to identify specific environmental controls on runoff generation processes such as the ones proposed by Dunne (1978) require a more detailed understanding of the physical structures that define those controls (soils, topography, etc.). In order to achieve this

goal, several questions must be resolved so as to address the complexity of actual watersheds. Some of these questions include:

1. How do heterogeneities, by way of discrete flow paths, affect runoff generation?
2. How important are upslope versus streamside conditions in determining the primary runoff generation process?
3. Can a particular runoff process be correlated with soil types, slope angles, or other environmental criteria that can be readily mapped in the field?

In regard to runoff generation processes, the emphasis in this study is on the factors controlling the relative importance of saturation overland flow versus subsurface storm flow (Figure 1.2). This study is entirely concerned with upland non-agricultural watersheds. As such, the computational analysis that follows allows for Horton overland flow, but the soil conditions that can be expected to produce this type of runoff are not investigated.

1.2 GOALS AND OBJECTIVES

The net result of previous and ongoing investigations is that the major subsurface flow paths have been individually identified and have been quantified to varying degrees. In general, the availability of data on subsurface flow paths and response-times decrease with depth. Very few studies have focused attention on the dynamic interactions between pathways. Montgomery and Dietrich (1995) identify climatic and topographic conditions that influence interactions between flow through the soil matrix (throughflow) and macropores at an upland headwaters watershed in California. A desire to integrate the

insights regarding flow paths and processes identified by previous studies is another motivation for the study described herein. Combining application of watershed field studies on a comparative basis with systematic application of physically-based computational analysis should contribute to insights of a more general nature regarding the interaction of watershed form and process.

Therefore, there exists a need for an integrated understanding of runoff generation as well as pore pressure evolution during and immediately following individual storm events on a time scale of minutes to hours. In a heterogeneous system, with several interacting pathways, it is hypothesized that each flowpath has a distinct time scale of response.

Accordingly, the goals of this study are:

I. To analyze the subsurface heterogeneous structure of a watershed (as manifest in its material properties and geometric attributes) in so far as it governs hydrologic processes, specifically the relationship between rainfall events, runoff, and pore pressures in upland watersheds.

II. To investigate the relationship between the spatial distribution of subsurface flow paths and the major runoff generation mechanisms.

III. To identify critical field research needs using numerical simulations of rainfall-runoff events on hypothetical hillslopes.

Within this context, specific objectives include:

1. To investigate the effects of different flow paths on: a.) the type of runoff generation process that occurs; b.) runoff production; and c.) pore pressure responses.

2. To evaluate the role of the hydraulic diffusivity parameter for different pathways in runoff production and pore pressure evolution.

3. To examine the effects of antecedent moisture conditions in determining which of the flow paths may dominate rainfall-runoff and rainfall-pore pressure linkages.

4. To study the relationship between the depth of channel incision (as represented by the downstream boundary condition) and the type of runoff generation process that occurs.

5. To investigate the time-scale of response (minutes, hours, or days) of transient flow through the soil matrix, macropores, saprolite, and bedrock.

2. METHODS

The overall approach followed in this study was to use a numerical model to investigate interactions between watershed structure and hydrologic processes. Hence the following section begins by describing the basis for choosing the mathematical model employed, its governing equations, and other pertinent attributes. Since an existing model was adapted to simulate hillslope/watershed systems, the specific extensions and new components of the model are identified. The critical material properties, slope geometries, and initial and boundary conditions are also described

After presenting the general aspects of model development, this work next provides a detailed overview of a suite of parametric simulations that were designed to explore interactions between watershed structure and process. Structural heterogeneities in the form of different soil types, saprolite, and bedrock were systematically varied to study their effects on types of runoff generation processes, runoff rates, and pore pressure responses to a typical rainfall input. The importance of slope geometry was considered next in simulations involving convergent slopes and variable slope angles. Soil-bedrock interface topography was studied by altering the depth distribution of materials along the hillslope profile. The role of antecedent moisture conditions was examined both in terms of hydrologic processes and modeling considerations. Downstream boundary conditions at the hillslope-channel interface were studied in relation to the type of runoff generation process that may result. The final set of parametric simulations focus on flow processes

around channel heads to study how material properties and small-scale geometry affect the stability of these geomorphically important features.

Following the overview of the parametric simulations, the two field sites included in this study are described. Drawing from previous investigations, the environmental conditions and prior data-gathering efforts are summarized. Field activities were conducted during this study in order to develop data sets for simulation purposes.

2.1 Mathematical Modeling Studies

The issues of model complexity and lumped- versus distributed-parameter modeling are ongoing topics of discussion among watershed researchers (Beven, 1989; Chapman, 1994). As has been clearly pointed out by Freeze (1974) and Beven (1989), there are many practical and theoretical limitations associated with physically-based modeling studies, including parameter averaging, data uncertainty, spatial variability of important parameters, and discretization. It is important to emphasize here that the purpose in applying a physically-based numerical model in this study is to obtain insights into the interaction between heterogeneities in watershed structure and hydrologic processes, rather than to make precise predictions of runoff or pore pressures. Taking a distributed-parameter approach permits several structural attributes to be varied in a controlled fashion, including the types and distribution of material properties and slope geometry. Applying average hydraulic properties on a horizonal basis facilitates a comparison of contrasting material types (e.g. soils vs. saprolite, or saprolite vs. bedrock).

2.1.1 General Description of Mathematical Model

In designing this investigation, it was deemed desirable to use a mathematical model with a minimum number of simplifying assumptions. The model used in this study is TRUST (Narasimhan et al., 1978). It is an integral finite difference algorithm designed for simulating multidimensional, saturated-unsaturated flow in deformable porous media, and is capable of handling: 1) highly non-linear, heterogeneous material property distributions leading to different flow paths; 2) complex hillslope geometry; 3) time-varying rainfall inputs; and 4) complex boundary conditions including seepage faces.

<u>Governing Equations</u>

The model solves the integral-differential equation,

$$\int_{\Gamma} \rho_w \frac{k_r k \rho_w g}{\mu} \nabla(z+\psi) \cdot \mathbf{n}\, d\Gamma + \rho_w G = M_c \frac{\delta\psi}{\delta t}, \tag{1}$$

subject to relevant initial and boundary conditions. In this equation, ρ_w is the mass density of water (M/L^3), k is the intrinsic permeability (L^2), k_r is the relative permeability, g is the gravitational acceleration (L/T^2), μ is the coefficient of dynamic viscosity (M/LT), z is elevation above datum (L), Ψ is the gage pressure head (L), **n** is the unit outer normal, G is the intensity (M/T) of source or sink integrated over a finite subregion, and M_c is the fluid-mass capacity of a finite subregion (Narasimhan and Witherspoon, 1977). The closed surface Γ bounding a finite subregion is fixed in the solid phase of the material.

Equation 1 is solved by discretizing the flow region of interest into individual volume elements; and numerically solving a discretized equivalent of the integral-differential governing equation. For an elemental volume 1, the mass conservation of water implied by (1) can be expressed in a discretized form as follows.

$$\sum_{m} U_{1,m}(\bar{\phi}_m - \bar{\phi}_1) + \sum_{b} U_{1,b}(\bar{\phi}_b - \bar{\phi}_1) + G_1 = M_e \frac{\Delta\phi_1}{\Delta t} \tag{2}$$

The quantity U is the mass conductance (M/LT), and $\bar{\phi}$ is the time-averaged hydraulic head (L) over a time interval Δt. It is defined as:

$$\bar{\phi}_m = \phi_m^\circ + \lambda\Delta\phi_m \tag{3a}$$

$$\bar{\phi}_1 = \phi_1^\circ + \lambda\Delta\phi_1 \tag{3b}$$

$$\bar{\phi}_b = \phi_b^\circ + \lambda\Delta\phi_b \tag{3c}$$

where the superscript "°" denotes the initial condition at the beginning of Δt, $\Delta\phi$ is the change in potential over Δt, and the weighting parameter λ ranges from $0 < \lambda < 1$. The subscripts "m" and "1" refer to internal volume elements, and subscript "b" refers to a boundary element. If $\lambda = 0$, the procedure is known as forward differencing (in time). If $\lambda = 1$, the procedure is known as backward differencing. And if $\lambda = 0.5$, the procedure is referred to as central differencing.

As seen in Figure 2.1, element 1 is connected to elements m = 1, 2, and 3 which are "internal" to the flow domain. Also element 1 communicates with the simulated stream across the surface segment b at which the potential is prescribed as ϕ_b. In this context, $\sum U_{1,m}$ denotes the sum of the mass conductances across the interfacial areas

between element 1 and the adjoining internal elements; and $\Sigma u_{1,b}$ represents the mass conductance of the interfacial area between element 1 and the adjoining boundary element b.

That this governing equation considers fluid flow and storage on a mass basis allows for an extremely accurate calculation of mass balances. For subsurface flow paths, the mass conductance across the interface between two adjoining elements ($U_{1,m}$) is according to

$$U_{1,m} = \overline{\rho}_{w,1,m} \frac{\overline{k}_{1,m}\overline{\rho}_{w,1,m} g}{\mu} \frac{\Gamma_{1,m}}{(d_{1,m} + d_{m,1})}, \tag{4}$$

where $\overline{\rho}$ is the mean density of water evaluated at the interface between two adjoining elements, $\overline{k}$ is the mean permeability evaluated at the interface between two adjoining elements, and *d* is the distance from a node center to the interface. Physically, the mass conductance represents the mass flux across an interfacial area per unit difference in fluid potential between adjoining elements.

The fluid-mass capacity (M_c) of a volume element is defined as (Narasimhan and Witherspoon, 1977),

$$M_c = V\left[Sn\rho_w\rho_o\beta g + \frac{\rho_w S\gamma_w \chi' a_v}{(1+e)} + \rho n \frac{dS}{d\psi}\right] \tag{5}$$

where V is the bulk volume of the soil (L^3), S is saturation, n is porosity, ρ_o is the reference density (M/L^3) at a gage pressure of 0, β is the compressibility coefficient of water (LT^2/M), γ_w is the specific weight of water (ML/T^2), χ' is Bishop's parameter (dimensionless) relating effective stress and pore pressure (Narasimhan and Witherspoon,

1977), a_v, is the coefficient of compressibility (LT^2/M), and e is the void ratio. For a variably saturated system, Narasimhan and Witherspoon (1977) defined χ' as:

$$\chi' = -\left[\chi + \frac{d\chi}{d\psi}\right] \tag{6}$$

where χ is Bishop's parameter (Bishop, 1960).

Using the relationships given above, it can be shown (Narasimhan et al., 1978) that there is a critical time constant Δt_m for each discretized elemental volume:

$$\Delta t_m = \frac{M_{c,l}}{\sum_m U_{l,m}} \tag{7}$$

where the summation term represents the sum of conductances between a given element "l" and all of its adjoining elements "m", including both internal and boundary elements. This time constant provides a measure of the time taken by the elemental volume to equilibrate itself with changes in potential in adjoining elemental volumes. Thus, a very small (Δt_m) would imply that the volume element will react very quickly to any change in its immediate surroundings. It is significant to note that the ratio of conductance to capacitance is one means of expressing hydraulic diffusivity. Thus, equation 6 implies that the critical time constant (Δt_m) is inversely proportional to hydraulic diffusivity, and that the hydrologic response (process) that occurs within a given flow path is closely linked to the material property (structure) at the scale of individual discretized elements.

Evaluation of Solvers of a System of Linear Equations

In the class of problems considered in this study, equation (1) is highly nonlinear because the material property parameters, namely permeability and fluid-mass capacity, are functions of the dependent variable Ψ. As shown by Narasimhan et al. (1978), the discretized nonlinear equations, when linearized within a time step, lead to a set of linear algebraic equations which need to be solved by matrix algebraic methods. Because of the strong nonlinearity, these equations are in general "stiff' and the resulting matrices are difficult to solve.

Accordingly, three different solvers of linear equations were evaluated during the present study, including a mixed explicit-implicit solver (Edwards, 1968), a direct solver (Duff, 1977), and a collection of conjugate gradient solvers (Moridis et al., 1994). The direct solver was found to be slow relative to the other two methods and produced the greatest errors in mass balance. The conjugate gradient solvers yielded better mass balance results, but showed unacceptable oscillations in the dependent variable Ψ for unsaturated materials with highly non-linear $k(\Psi)$ relationships. The mixed explicit-implicit solver was chosen for this study since it produced acceptable mass balance results and did not show significant oscillations in any of the materials considered.

Mesh Discretization

The simulations conducted in this study were designed to represent two-dimensional flow in the vertical cross-section from the crest of a ridge to channel below

(Figure 2.2a). Simplified three-dimensional simulations were also carried out by rotating the mesh about an axis of symmetry at the downstream boundary, as described below. A portion of the mesh showing the vertical discretization used in this study is shown as Figure 2.3. To minimize spatial discretization errors, the geometry-imbedding concept described by Narasimhan (1985) was used in discretizing the mesh.

The vertical grid spacing was chosen to facilitate application of varying soil hydraulic properties to different soil layers. Initially, three different horizontal grid spacings of 2.0 m, 1.0 m, and 0.5 m were used in trial simulations. The overall mass balance error was approximately 0.5 percent for all three cases with 30 days of drainage from initial conditions of zero tension throughout the flow domain. However, the pressure head response was observed to be sensitive to the horizontal grid spacing in simulations which included materials with highly non-linear permeability and moisture retention properties (Figure 2.4). As the horizontal grid spacing was reduced from 2.0 m to 1.0 m, small oscillations in Ψ values (caused by the presence of a soil with highly non-linear hydraulic characteristics) had disappeared. Further reduction of the grid spacing to 0.5 m increased the time required to run the simulation by an order of magnitude, from approximately 2.5 hours (1.0 m spacing) to over 24 hours (0.5 m spacing). However, since the oscillations in pore pressure had effectively disappeared with the closer spacing, a 0.5 m horizontal grid spacing was chosen for the simulations included in this study.

2.1.2 Adaptation of the Model to Hillslope Simulations

Application of TRUST to the hillslope problems considered in this study required the following modifications of the original code:

- Calculating the thickness of the elements in irregularly-shaped meshes
- Creation of a new upper boundary condition governing the partitioning of rainfall between infiltration and overland flow
- Addition of a new algorithm to simulate overland flow on the upper surface of the model domain

Overland flow was incorporated into the model primarily to simulate either return flow (exfiltration) or saturation overland flow. It is assumed here that overland flow can be simulated by the model in the same manner as subsurface flow providing that an appropriate conductance and capacitance can be defined for the elements designed to receive rainfall at the land surface.

<u>Mesh Generation</u>

The meshes used in all of the simulations in this study were created using a mesh generation program developed for use with a variant of TRUST (the PT code) that has been applied to simulating fluid flow in oceanic crust (Andrew T. Fisher, University of Indiana, unpublished code). This mesh generation program was originally created to discretize submarine ocean-floor formations, and it employs a sine curve representation of slopes over a user-defined number of wave-lengths. It also employs the concept of

Geometry-embedded Darcy's Law as defined by Narasimhan (1985) to minimize mesh discretization error. Like the parent-model TRUST, the source code for the model and mesh generator used in this study was written in FORTRAN 77.

Computational Performance

All of the simulations included in this study were performed using an IBM® RS/6000 workstation with double-precision numbers. Run-times ranged from approximately 3 minutes to 90 minutes depending on the problem. The mixed explicit-implicit solver (Edwards, 1968) allows the size of time-steps to be either controlled by the user or optimized to meet convergence criteria (Narasimhan et al., 1978). In all of the simulations performed in this study, the maximum time-step was set at 60 seconds. In conditions where potentials change rapidly or strong contrasts occur in hydraulic properties, TRUST automatically reduces time-steps. In the present simulations, time-steps as small as 0.5 seconds were not uncommon, particularly when overland flow was generated. Overall mass balance errors were always less than 1 percent, and commonly less than 0.1 percent.

Infiltration - Overland Flow Partitioning,

When rainfall is applied to the land surface in the simulations, the water will either enter the soil elements via infiltration or move laterally as overland flow if the land surface is saturated. A series of logical statements was created which compares: 1) the rainfall rate with the conductance of the interface between an overland flow element and

its associated soil element below; and 2) the local hydraulic head gradient between the two elements. The difference in flow resistance between adjoining overland flow elements versus overland flow-subsurface elements is reflected in the conductance conditions at the lateral and vertical interfaces, respectively. Accordingly, one of three conditions will exist at land surface as rainfall is applied as a source term on the upper boundary:

1. If the rainfall rate is less than the surface-soil vertical conductance, water is applied within the uppermost soil elements, because the soil will have the ability to transmit the water downward.

2. If the rainfall rate exceeds the surface-soil vertical conductance, water is applied in the overland flow element, because the soil can transmit only a part of the rainfall and the other part has to flow over the land surface.

3. If exfiltration is occurring, water is applied in the overland flow element, because the prevalent upward hydraulic gradient precludes downward infiltration.

In either of the two cases where rainfall is applied in the overland flow elements, infiltration still occurs as governed by the gradient and material properties of the adjoining overland flow and upper soil elements. Water which has exfiltrated at one point on the slope may later infiltrate at a lower point on the slope depending on the local potential gradient and conductance conditions.

Simulation of Overland Flow

If the boundary condition criteria described above are met such that overland flow is generated, the surface runoff is simulated as flow between adjoining land surface

elements which are handled computationally the same as the subsurface elements. This approach allows surface and subsurface flow computations to be performed concurrently in the same time step in a fully integrated fashion. As a consequence, mass balance is intrinsic to the partitioning process.

In this work, the overland flow node is treated as a defined volume element with a finite capacitance for which mass conservation is implemented like any other volume element in the flow domain (2). An overland flow element communicates vertically with a soil element immediately below and with upstream and downstream adjoining overland flow elements.

The capacitance of an overland flow element ($M_{c,l}$) is set equal to its plan area times the density of water. This quantity represents the mass of water released from storage within the element if the average head changes by 1 m. As a first approximation, the equation describing the mass conductance for overland flow elements was derived from the Darcy-Weisbach equation:

$$\bar{u}^2 = \frac{2ghs}{f} \tag{8}$$

where u is the overland flow velocity (L/T), h is the mean flow depth (L), *s* is the local gradient water surface (L/L), and f is the dimensionless drag coefficient, or friction factor for laminar flow.

Dunne and Dietrich (1980) present a Moody diagram of f versus the Reynolds Number (N_R) for various land surfaces. Data from various field experiments suggest that a linear relationship exists between f and NR using a dimensionless slope roughness parameter K (Dunne and Dietrich, 1980). It should be noted that the negatively sloping f-N_R relationship was observed for laminar-like (low- N_R) flow conditions. Abrahams and Parsons (1991) observed a similar f-N_R relationship for experimental plots covered by shrub vegetation in arid environment. Conversely, Abrahams et al. (1994) reported f-N_R relationships that were positively-sloping or convex for grass-covered plots at the same site. They attributed the differences between the two covers to nature of the surface roughness (e.g. grass type, gravel cover).

Overland flow elements were defined on a layer immediately above the uppermost soil elements (Figure 2.3), and an overland flow conductance (U_{of}) was derived from equation (7). For the purpose of coupling the surface and subsurface flow calculations, the surface water depth, h, is hereafter referred to as Ψ, which is the mean pressure head of water at the interface between surface flow elements. An equivalent form of equation (7) may be written as:

$$u = 2\frac{\rho g}{\mu}\frac{\overline{\Psi}^2}{K}s \qquad (9)$$

and Darcy's law for subsurface flow may be written as:

$$u = k^* \frac{\rho g}{\mu} s \tag{10}$$

where k* represents the effective permeability. Equating equations (8) and (9) yields

$$k^* = \frac{2\overline{\Psi}^2}{K} \tag{11}$$

as the effective permeability (in lieu of $\overline{k}$) that can be used for overland flow elements in equation (4). The area of the interface (Γ) for surface elements is defined by $\overline{\Psi}$ multiplied by the unit thickness of the mesh into the third dimension, and the sum of the distances between nodal centers and the interface was uniformly set at 0.5 m based on the horizontal grid spacing used. The mass conductance for overland flow cells (U_{of}) is defined as:

$$U_{of} = \overline{\rho} \frac{2\overline{\Psi}^2}{K} \frac{\overline{\rho} g}{\mu} \frac{\overline{\Psi} \cdot 1.0\,\mathrm{m}}{0.5\,\mathrm{m}} \tag{12}$$

Note that the equivalent permeability is a strong function of the surface flow depth. Field data are meager for the ***K*** parameter, especially for upland areas in humid temperate environments. Based on field data presented by Dunne and Dietrich (1980), a value of 500 was used for ***K*** in the parametric simulations. Calculations of U_{of} using different ***K*** values ranging from 50 to 5,000 resulted in estimated surface conductances that were a minimum of four orders of magnitude greater than typical subsurface conductances between overland flow elements and the soil elements below.

One consequence of taking this approach was that it became necessary to set a finite threshold surface water depth (1×10^{-4} m [0.1 mm]) below which U_{of} was set to zero. When surface water thicknesses fall below this depth, flow thicknesses are on the same length-scale as the mineral soil grains, and it becomes difficult to distinguish between flow over the soil surface versus flow through the soil as a porous medium. Setting this threshold tends to produce small oscillations in the calculated flow rates as will be noted in the results of the parametric studies, particularly when surface flow reaches the downstream boundary.

Model Credibility

Because the numerical model is used as a tool to evaluate a variety of initial-boundary value problems, model verification is essential. However, it is not possible to directly compare hillslope simulation results with analytical solutions for transient partially-saturated flow problems since such analytical solutions do not exist at present. Results presented by Wilson et al. (1989) showed that simulated runoff responses obtained from an earlier version of TRUST reasonably matched field observations at the Solstice field site. The validity of the model used in this study can also be evaluated in terms of its ability to simulate individual processes. Narasimhan and Witherspoon (1978) demonstrated that the TRUST model performs credibly in a variety of saturated and unsaturated flow problems, in particular when compared with analytical solutions for infiltration into a moderately saturated soil column (Philip, 1969) and for an extremely

dry soil column (Rubin and Steinhardt, 1963). The new algorithm for overland flow has yet to be compared with previous modeling studies (e.g. Smith and Hebbert, 1983).

Another means of testing the modeling approach is to compare it with the finite-difference model used by Freeze (1972a). The mesh and model parameters used by Freeze (1972a) in simulating base flow generation were replicated in comparable form and dimensions. The evolution of the water table was simulated using the same initial and boundary conditions. The results are presented in a subsequent section.

2.1.3 Material properties

The incorporation of heterogeneous structure into numerical flow models such as the one used in this study is accomplished by defining the material properties that capture the structures (i.e. macropores) that affect the storage and conductance of water. Of particular importance are the soil moisture characteristic (or equivalent saturation) curve, relating the moisture content to pressure potential; and the unsaturated hydraulic conductivity curve. Typical material property curves developed by Liakopoulos (1965) for a re-mixed soil with sandy texture are shown on Figure 2.5.

Macropores

Using simple calculations, it can be shown that the geometry of voids in soil horizons can significantly affect the small scale permeability of a soil (Bouma and Anderson, 1973). For capillary-shaped voids (macropores), hypothetical permeabilities can be estimated by applying Poiseuille's law for laminar flow through a pipe of finite radii. In a similar manner, inter-ped voids may be conceptualized as a planar structure,

and an approximate permeability may be estimated using the cubic law for different void apertures. Bouma and Anderson (1973) have shown that both cylindrical macropores and inter-ped voids can have permeabilities that are several orders of magnitude greater than those of the micropore structure for individual textural classes.

Of equal importance is the distribution and connectivity of structural voids. As noted earlier, field studies (Aubertin, 1971; Stresky, 1991) have shown that there can be wide variation in the volume and connectivity of hydraulically significant large voids. One consistent finding in these and other studies is that volume of macropores and other structural voids tends to decrease with depth. This observation may be explained by the vertical distribution of structural heterogeneities that tend to evolve as a result of soil horizon development and weathering of shallow bedrock. Figure 2.6 shows a hypothetical hillslope cross-section with some of the possible structural void types described by Brewer (1974) by horizon.

Structural voids constitute one manifestation of the heterogeneity of watershed form, and their role in conducting water flow has been widely recognized in previous studies (Ziemer and Albright, 1987; McDonnell, 1990; Tsuboyama et al., 1994; and Montgomery and Dietrich, 1995). The transient nature of such flow involves the storage of water as well. In hillslope modeling studies in particular, there has been a historic emphasis on hydraulic conductivity (K in units of L/T), but little discussion of the importance of specific storage (S_s in units of L^{-1}) which plays a major role in the response time-scale (Freeze, 1972a, 1972b; Beven, 1977; Freeze, 1980; and Wilson et al, 1989). This storage parameter is the sum of three components: fluid compressibility, matrix

compressibility, and desaturation due to gravity drainage. It will be shown in the following sections that the saturation characteristics of upland soils may differ significantly, and the effects of these differences on runoff will be considered. Specific storage is also more difficult to measure than hydraulic conductivity, and this may in part account for the lack of consideration in previous field studies.

The unconfined water-bearing zones (water table aquifers) found on most hillsiopes commonly tend to be transient features, even under humid climates. The duration of saturation will be affected by the balance of conductive and storative properties of the hillslope soil and geologic materials. One convenient means of conceptualizing the interaction of transient flow and storage properties is the parameter known as hydraulic diffusivity (η in units of L^2/T). Diffusivity may be defined for saturated conditions as:

$$\eta = \frac{K}{S_s} \tag{13}$$

and is a relatively constant quantity. Assuming that under medium to high saturation conditions desaturation dominates over compressibility, η may be defined as:

$$\eta(\psi) = \frac{K(\psi)}{n\frac{dS}{d\psi}} \tag{14}$$

where $K(\Psi)$ is hydraulic conductivity which varies with gage pressure head, n is the porosity, S is the percent saturation, $dS/d\Psi$ is the specific moisture capacity. An example of specific moisture capacity and hydraulic diffusivity relationships based on the data from Liakopoulos (1965) is shown on Figure 2.7. The individual materials used in the

parametric studies, including their respective saturation, K(Ψ), and diffusivity curves are described in the following section.

Soil Horizons

Early hillslope modeling studies (Freeze, 1972a; 1972b; and Beven, 1977) relied entirely on previously published soil hydraulic property analyses. Through the 1960's and early 1970's, most of the available moisture characteristic and conductivity curves had been obtained using remixed soil samples of different textural classes. In addition to laboratory analyses, various empirical quantitative approaches have been devised to estimate the moisture release and hydraulic conductivity curves (Burdine, 1953; Taylor and Luthin, 1969; Mualem, 1976; and Wilson et al., 1992; and others).

The studies by Freeze and Beven were explicitly described as assuming homogeneous conditions to exist. This was true at the hillslope scale in that only one set of material properties was used in any given simulation. By using material properties derived from remixed soil samples, a second type of homogeneity was imposed by neglecting the effects of soil structure. Clearly certain types of soil horizons will have hydraulic properties which are primarily based on the soil texture or grain size. Soils or unconsolidated parent material with a single-grained structure (aeolian sand) or which are massive (argillic horizon) (Hillel, 1980a) are two examples. Aggregated soil horizons can be expected to have more complex hydraulic properties which reflect the greater variability of pore sizes and ped structure in addition to texture.

Early in this study, an attempt was made to devise a hypothetical material property that might capture the dual porosity behavior of a combination of macropores and micropores. As a first approximation, a soil was considered with a texture based on the Del Monte sand (Liakopoulos, 1965) and a single, continuous macropore with a 0.01 m diameter. Poiseuille's law was used to define the saturated hydraulic conductivity (K_{sat}):

$$K_{sat} = \frac{\rho g R^2}{8\mu} \tag{15}$$

where R is the macropore radius (L). Macropores can be expected to drain at tensions on the order of -0.10 m or greater based on capillary theory. This limit on water retention has also been observed in experimental studies reviewed by Wilson et al. (1992). An unsaturated hydraulic conductivity ($K(\Psi)$) curve was constructed by linking the K_{sat} obtained from Poiseuille's law with the $K(\Psi)$ curve for the Del Monte sand (Liakopoulos, 1965) as shown on Figure 2.8. This approach assumes that the resulting conductivity curve represents an effective conductivity for all elements in which this material property was applied At about the same time, Wilson et al. (1992) published saturation and $K(\Psi)$ curves for a forest soil containing macropores. The $K(\Psi)$ curve for the Bw horizon from the field study is also plotted on Figure 2.8. The similarity between the two curves is intriguing as it seems to support the concept of a "dual-conductivity" material.

Saprolite

As noted earlier, very little research has been done on the hydraulic properties of saprolite. By definition, saprolite will have some relic rock structure, including fractures which may be filled to varying degrees with weathered mineral material. The lithology and degree of weathering are important considerations. For the purposes of simulation, saprolite is assumed to behave as a dual porosity material, comprised of at least residual fracture voids and a matrix with greater porosity and conductance than the parent rock. One field study in which the saturation and K(Ψ) curves were measured is presented by Wilson et al. (1992).

Bedrock

Unsaturated moisture release and conductivity curves for bedrock have been measured for a few rock types but are difficult to produce experimentally (Stephenson and Freeze, 1974). In general, there may be a much greater differential between fracture and matrix permeability in rocks than in saprolite. Permeability data presented by Wang and Narasimhan (Figure 7, 1985) show that fractures may effectively cease to conduct water at tensions less than -0.10 m, at which point the rock matrix permeability will dominate flow processes. In the absence of field data, it is possible to resort to empirical relationships to obtain saturation and K(Ψ) curves. This has been the case in all of the hillslope modeling studies to date, beginning with the study by Stephenson and Freeze (1974) who used the Burdine (1953) model to simulate flow through altered and fractured basalt. As was noted by Stephenson and Freeze, sharp contrasts in material

properties created difficulties for the line-successive over-relaxation equation solver they used. They were forced to limit the drop in hydraulic conductivity with increasing tension to a one order-of-magnitude decrease. Similar difficulties were encountered in the present modeling study, but an alternative solution was employed in which the bedrock permeability was allowed to drop several orders of magnitude as a step function at a prescribed tension. A logical statement added to TRUST specifies one hydraulic conductivity value above a certain tension, or a lower conductivity if the tension is equal to or lower than the specified tension.

2.1.4 Slope Geometries

The majority of the simulations in this study consider transient flow through two-dimensional "slices" of slopes which are of uniform 1.0 m depth in the third dimension. These meshes may be envisioned as parallel side slopes in a drainage (Figure 2.2b). A series of simulations was also conducted using "pseudo" three-dimensional, wedge-shaped meshes to study the effects of convergent flow (Figure 2.9).

The form of the generic hillslope used in the parametric studies is a convexo-concave shape of fixed relief (20.0 m) and variable slope length (35.0 m to 150.0 m). This slope shape is distinct from those used in earlier hillslope modeling studies: 1) convex slope (Freeze, 1972b); 2) concave slope (Freeze, 1972b); 3) planar, concave, and convex slopes (Beven, 1977); and 4) planar slope with a convergent depression (Humphrey, 1982); and 5) convergent planar-concave slope (Wilson, 1988). Ritter (1978) describes the convexo-concave form as being the most common shape of slopes in humid-

temperate climates, however relatively little field data exists to confirm this observation (W.E. Dietrich, personal communication). The convexo-concave slope shape used in the parametric simulations may be viewed as representing a hillslope-valley profile with an incised stream channel in the middle of the valley floor.

The relief in all of the simulations was set at 20.0 m based on the scale of the field sites considered in this study, and the "base case" utilized a slope of 15 degrees. The effects of slope angle on runoff production and pore pressure evolution were investigated by repeating certain simulation cases with 7.5 degree and 30 degree slope meshes (Figure 2.10). Soil thickness was set uniformly at 2.0 m throughout the slope except for a pair of simulations in which the soil thickness increased with distance downslope from 0.5 m at the ridge crest to 3.5 m at the downstream boundary (Figure 2.11 a). Simulations were also conducted for each rock type in which the elevation of the lower bedrock boundary was held constant (Figure 2.1 lb).

2.1.5 Initial and Boundary Conditions

Initial conditions were imposed by specifying the hydraulic head at each node at the beginning of the problem. The initial conditions in conjunction with the material properties in a given simulation form the basis for imposing different antecedent moisture conditions as described in the following section. Boundary conditions used in this study were specified as no-flow conditions for the upstream and bottom boundaries (Figure 2.12a).

Except where varied in the parametric studies, the bedrock thickness is held constant at 4.5 m. This depth was based on the observed decrease in bedrock permeability with depth (Wilson and Dietrich, 1987), and also assumes that any deeper zones with significant fracture permeability do not affect the hydrologic response of the flow domain considered in the simulations.

At the downstream boundary, a specified head was imposed that maintained a water surface at one of several elevations that were considered in the parametric simulations (Figure 2.12b). Below the constant head elevation, a no-flow boundary was imposed. The use of a no-flow boundary at the down-stream end of the flow system can be justified by assuming that the model domain occurs in a symmetric watershed Figure 2.2b). A seepage face was simulated above the constant head elevation in order to allow outflows from the hillslope to freely fluctuate with changes in the water table surface. Thus, outflow from the hillslope to the boundary condition representing a "channel" flows upward through the soil or laterally through the seepage face. Rainfall was applied as a constant source term along the upper (soil surface) boundary during the parametric studies. The rainfall was injected into either the upper soil nodes or the overland flow nodes depending on the three partitioning criteria described previously.

2.2 Description of Parametric Studies using Generic Hillslopes

In designing the scope of this study, a decision was made to assume that the hydrologic response of the hillslope is decoupled from storm-related flow processes within the channel at the downstream boundary. In future simulations, a time-varying

stream stage boundary condition could be readily incorporated. The emphasis in this study is on the hydrologic response of hillslopes in upland watersheds to rainfall events of a 1-year return interval magnitude representing the year-to-year function of an upland watershed. This approach provides an opportunity to examine the assertion by Freeze (1974) that, "there are stringent limitations on the occurrence of subsurface storm flow as a quantitatively significant runoff-generating mechanism."

Based on rainfall duration data presented by Freeze (1972a) for New England and Wosika (1981) for the northwest coast of California, an average 1-year return interval storm of 12-hour duration was estimated for use in the parametric studies. A rainfall total of 4.32×10^{-2} m (43.2 mm) was applied at a constant rate of 1×10^{-6} m/s (3.4 in/day) for 12 hours followed by 36 hours of drainage. In one simulation, a 100-year return interval 12-hour storm (3.5×10^{-6} m/s rainfall rate) was applied for comparison purposes. A summary of the parametric studies described below is presented on Table 2.1.

Previous research described earlier and preliminary simulations in this study suggested that runoff generation processes and the transient flow response of a hillslope to a rain event will be governed by four factors. These physical factors and their role in the modeling studies include: 1) the heterogeneous structure (material properties) of the hillslope; 2) local slope topography (geometry); 3) antecedent moisture conditions (initial conditions); and 4) the geometry of the downstream boundary (boundary conditions). A suite of parametric studies was designed in which each of the four factors is treated as an independent variable that can be systematically isolated to study its effect on one of two

dependent variables: the runoff generation rate from the hillslope; and pore pressure evolution.

It should be pointed out here that the pore pressure response is reported as a dimensionless ratio (***m***) of the pressure potential (ψ) to *total soil thickness* (z*). The parameter ***m*** is derived from the infinite slope analysis for shallow translational landslides (Selby, 1982). Figure 2.13 (from Wilson, 1988, Figure 54) shows the three conditions where m is less than, equal to, or greater than 1.0. The point of measurement is considered over-pressured when m is greater than 1.0, and the slope may become unstable depending on the strength characteristics of the soil or unconsolidated material involved. It should be noted that the quantity m will exceed 1.0 whenever exfiltration is occurring.

2.2.1 Structural heterogeneities

The role of structural heterogeneities was examined by varying the hydraulic properties associated with four major flow paths considered in this study (soil matrix, macropores, saprolite and bedrock). The conceptual division of soil matrix and macropores is admittedly an arbitrary distinction since the hydrologic function of virtually any type of macropore is linked to the surrounding soil. Hence, the two flow paths are considered together during the parametric simulations.

<u>Soil/Macropore Horizons</u>

Five different soil materials were simulated (runs 1-5) in order to investigate the importance of soil structure and the hydraulic diffusivity parameter. In all five cases, the

soil material comprises the upper 2.0 m of soil uniformly throughout the slope, with 4.5 m of bedrock underneath the soil. The first soil case (run 1) incorporated the homogenous Del Monte sand (Liakopoulos, 1965) used by Freeze (1972a, 1972b). This material represents a soil matrix flow path devoid of macropores since the laboratory analysis destroyed any structure the soil might have had. The second soil (run 2) considered was a colluvial soil with gravely loam texture from the Coast Range of Oregon (summarized by Humphrey, 1982), and the material properties for this soil were determined using undisturbed soil cores. The third soil (run 3) was a sandy loam Spodosol (soils with a diagnostic horizon containing an accumulation of organic material and various metal oxides) from Hubbard Brook Experimental Forest in New Hampshire (A. Federer, U.S. Forest Service, unpublished data). The empirical equations derived by Clapp and Hornberger (1978) were used to estimate the saturation and $K(\psi)$ curves for this soil. The fourth soil (run 4) used was a loamy-skeletal Inceptisol (soils which form quickly by alteration of parent material) from Melton Branch watershed near Oak Ridge, Tennessee whose hydraulic properties were determined in the laboratory using intact soil cores (Wilson et al., 1992). The final soil (run 5) was a hypothetical material synthesized by combining the Del Monte sand unsaturated hydraulic conductivity curve and the soil moisture characteristic curve of the Inceptisol to examine the importance of storage characteristic in soil hydraulic properties. Figure 2.14 shows the saturation and $K(\psi)$ curves for the five soil types.

Saprolite

Saprolite saturation and K(ψ) curves (Figure 2.15) used in the parametric studies were obtained from field data for the weathered rock in the Melton Branch watershed near Oak Ridge, Tennessee as reported by Wilson et al. (1992). Three cases (run 6-8) were considered and the thickness of the saprolite was varied relative to the soil and bedrock thicknesses.

Bedrock

Two distinct bedrock types were considered in the parametric studies. The first (run 10) was a "low" permeability bedrock (K_{sat} = 5 x 10^{-7} m/s) based on field data for fractured granitic rock from Mirror Lake, New Hampshire (Paul Hsieh, U.S. Geological Survey, unpublished data). The hydraulic conductivity curve (Figure 2.16) was assembled by selecting K_{sat} from one of the higher measured values, and the high-tension K(ψ) was arbitrarily set at the low-end detection limit (1 x 10^{-10} m/s) of the pumping tests conducted at this site. A "high" permeability bedrock (run 11) was synthesized originally by simply increasing the magnitude of the end members for the low-permeability rock K(ψ) curve by two orders of magnitude. This resulted in permeability contrasts between the soil and the bedrock that caused convergence problems for the iterative solver as mentioned earlier. This situation was remedied by specifying a step function which preserved the high permeability values and the contrast between saturated and high-tension conditions (Figure 2.16). The effects of localized discontinuities in bedrock hydraulic conductivity were simulated (run 12) by imposing a mid-slope low-K zone

within the high permeability rock type (Figure 2.17). This type of discontinuity was observed in the field by Wilson (1988, Figure 52) and included in simulations therein.

2.2.2 Slope geometry

Simulation using a wedge-shaped mesh provides a means of comparing the importance of convergent flow through headwall portions of a watershed with "parallel" flow through side slopes. This type of convergent geometry was chosen as being approximately representative of a portion of a hollow/source area configuration as suggested by Montgomery and Dietrich (1989, Figure 1). The fast pseudo three-dimensional case (run 13) included the Inceptisol soil containing macropore characteristics and low-permeability bedrock. The second case (run 14) added saprolite to the materials used in the first case. The third case (run 15) considered the added influence of “dry” antecedent moisture conditions by using a hydrostatic initial condition which induced very high tensions (> -15.0 m tension) near the land surface at the upstream boundary.

The effects of slope angle and length were investigated by conducting simulations for slopes of 7.5 degrees, 15 degrees, and 30 degrees (Figure 2.10) for the following cases: 1) the Inceptisol soil and low-permeability bedrock (runs 16-18); and 2) the Inceptisol soil and the high-permeability bedrock (runs 19-21). Simulations involving the colluvial soil and low-permeability bedrock were performed for slopes of 15 degrees and 30 degrees (runs 22-23). Variations in soil thickness (runs 24-25) and bedrock depth

(runs 26-27) for 15 degree slopes were conducted for the inceptisol soil and both types of bedrock.

2.2.3 Antecedent soil moisture conditions

Three different antecedent moisture/initial conditions were used in the parametric studies. Based on field data from the two field sites included in this study, the initial condition base case (run 28) assumed uniform "wet" soils and bedrock (-0.5 m tension). The second initial condition (run 30) was a "drained condition" obtained by allowing 5 days of drainage from an initial zero tension condition throughout the slope. The final set of initial conditions (run 31) applied was a hydrostatic condition defined by the downstream constant head boundary creating a very "dry" soil with tensions greater than -15.0 m at the upper end of the slope. This is the initial condition used by Freeze (1972a, 1972b) and Beven (1977).

2.2.4 Downstream boundary conditions and runoff generation mechanisms

Two possible downstream boundary conditions were identified for the hypothetical hillslope used in the parametric studies (Figure 2.18a, b). In the first scenario (Figure 2.18a), a seepage-face exists above the specified head elevation, and the same constant head is maintained below (runs 32 to 34). This condition might exist for a parallel segment of a headwall exiting at a channel head, for example (Figure 2.9). The second possibility (Figure 2.18b) combines a seepage-face above the specified head elevation and a no-flow boundary condition below (runs 35 to 37). This. configuration

would be likely for sideslopes leading down to a channel, recognizing that there would be flow downslope through the third dimension (i.e. down the valley). This was the primary boundary condition used as a base case.

A related issue in designing the parametric studies concerns the depth at which the constant head boundary is imposed. Early in the modeling study the downstream constant head was set at a depth of 1.6 m below land surface. This would correspond with a deeply incised channel, and for the material properties applied it was virtually impossible to induce saturation overland flow to flow directly into the channel element due to the tall seepage face. The depth of the constant head boundary was varied from 0.05 m to 1.20 m (runs 32-37) to investigate the combined effects of a seepage face boundary condition and the depth of channel incision on the type of runoff generation mechanism that occurs.

Field studies summarized by Birkeland (1984) have described the downslope variation of soil properties (texture, organic content, elemental translocation) in a variety of environments. This raises the question of what effect lateral heterogeneities in soil hydraulic properties might have on the occurrence of subsurface storm flow versus saturation overland flow. To explore this question, the effects of lateral changes in soil properties in the riparian (downstream boundary) region of the modeled domain were simulated in a case (run 39) with a 0.30 m channel depth and a low-permeability soil wedge extending from the toe of the slope to the downstream boundary as shown on Figure 2.19. The 0.30 m channel depth was selected based on the results of the earlier simulations using laterally homogeneous soil properties, as described below. A wedge of

Low-permeability soil material was chosen to represent an accumulation of clay in the streamside zone.

2.2.5 Simulations of flow around channel heads

The final set of parametric simulations was designed to study the effects of material properties and small-scale slope geometry on the pore pressure conditions around channel heads in regard to their stability and potential migration. As shown on Figure 2.20, a simplified mesh was created to represent the planar midslope portion of a larger hillslope, and the insets on this figure show the mesh configuration for each channel head height.

This set of simulations was motivated by field observations made by Montgomery (1991) at an experimental plot in Tennessee Valley, located in Marin County, California. The material properties, mesh discretization, geometries, and boundary conditions used in this set of simulations were generally based on the Tennessee Valley conditions, but it was not intended to reproduce actual field observations. Instead, the emphasis was placed on: 1) the effects of different material properties on flow around channel heads; and 2) the relationship between channel head geometry and pore pressure evolution and distributions.

Two sets of soil profiles with a total thickness of 4.0 m were simulated: 1) silt (0.5 m thick), clayey-silt (1.5 m), and silty-clay (2.0 m) included in runs 40 to 43; and 2) the Inceptisol containing macropores (0.5 m thick), clayey-silt (1.5 m), and silty-clay (2.0 m) in runs 44 to 47. Channel head heights of 0.2 m, 0.4 m, 0.8 m, and 2.0 m were

simulated for each soil profile. Below the upper 2.0 m of soil, variable depths to an impermeable bedrock were simulated, including 0.0 m, 0.4 m, 0.$, and 2.0 m (run 51). A constant head representing saturation to the land surface was specified at the upstream boundary and a seepage face was specified at the channel head and downstream boundaries. Initial conditions were set at 0.0 m pressure head, and although the simulation period lasted 5 days the system reached a quasi steady-state on a time scale of hours.

2.3 Description of Field Sites and Instrumentation

Concurrent with model development, a limited field data-gathering effort was pursued at comparative sites to provide the basis for evaluating the ability of the model to simulate actual rainfall-runoff events. The two sites include the Hubbard Brook Experimental Forest in the White Mountains of New Hampshire and the Caspar Creek Experimental Watershed in the northern Coast Range of California (Figure 2.21). These sites were chosen based on the fact that both have been the focus of long-term watershed studies. There is also a strong contrast between the two sites in their respective climate, vegetation, geology, and soils as described below.

2.3.1 Caspar Creek Experimental Watershed

The first study site is a small (1.69 ha) headwaters drainage in the North Fork of the Caspar Creek Watershed, located on the Jackson State Demonstration State Forest, in Mendocino County, California. State and federal forestry agencies have monitored

streamflow and water quality in the North and South Forks of Caspar Creek drainages since 1962 (Tilley and Rice, 1977). The purpose of this long-term monitoring effort has been to study the effects of various logging practices and road-building on runoff, water quality, and fish habitat. The specific experimental site considered in this study is an unchanneled headwaters drainage denoted as the M Swale.

Description of Field Site

The M Swale serves as a control watershed in the larger North Fork Caspar Creek drainage. The vegetation community is a coniferous forest type with a closed canopy consisting of coastal redwood (*Sequoia sempervirens* (D. Don) Endl.) and Douglas fir (*Pseudotsuga menziesii* (Mizb.) Franco) as the dominant tree species. Although not measured during this study, the diameter-at-breast height is estimated to range from approximately 0.3 m to 1.5 m. The area was clear-cut and burned in the late 1800's (Tilley and Rice, 1977), but has been undisturbed since. Other tree species occurring at this site include grand fir (*Abies grandis* (Dougl. ex D. Don) Lindl.), western hemlock (*Tsuga heterophylla* (Raf.) Sarg.), tanoak (*Lithocarpus densiflorus* (Hook. and Arn.) Rohn) and Pacific madrone (*Arbutus menziesii* Pursh.).

The soil at this site has been classified as a clayey, mixed isomesic Typic Tropudult described as the Van Damme series (California Department of Forestry, 1985). Surface soils tend to have a loamy texture and increasing clay content with depth (Wosika, 1981), and discontinuous argillic horizons have been observed in scattered soil pits (Randy Dahlgren, unpublished data). Soil thicknesses range from 1.0 m along the ridge tops to 1.5 m in the swales (Wosika, 1981). The parent material below this depth

range is a highly weathered layer of fractured saprolite derived from the underlying graywacke sandstone of Cretaceous age known as the Franciscan Assemblage (Huff et al., 1985). Geologically recent tectonic forces (1 my b.p.) acting along the San Andreas fault system just offshore have contributed to a gradual uplift of up to 200 m (Jenny, 1980). The topography of the site is shown on Figure 2.22 and contains slopes which range from 30 percent to 70 percent. The elevation at this site ranges from approximately 250 m to 300 m above mean sea level.

Local climate is heavily influenced by the site's proximity to the coast (approximately 10 km to the west). Like most of coastal California, the large majority of the rainfall occurs during late fall and winter months. The mean annual rainfall for this area is 1.190 m (46.85 in), with a range of 0.838 m to 1.753 m (Ziemer and Albright, 1987). Relatively little rainfall occurs between the months of April and October, but coastal fog may supply moisture to the soils via fog-drip. Air temperatures range from a January mean of 10° C to a high of about 13° C in July.

Field Instrumentation

Soil “pipes” with diameters ranging from 0.01 m to 1.0 m are a common feature in many of the unchanneled swales at Caspar Creek (Ziemer and Albright, 1987). Beginning in 1986, a gaging station (Figure 2.22) was installed to measure pipeflow from the M Swale. Monitored soil pipes in this swale occur at depths ranging from 1.5 m to 2.0 m and in sizes ranging from 0.02 m to 0.45 m diameter. A nest of tensiometers was also installed at depths of 0.3 m, 0.6 m, 0.9 m, and 1.2 m (Figure 2.22). Both the

pipeflow discharge and tensiometers have been monitored on 15-minute time intervals by continuous-recording data loggers.

In accord with the objectives of the present study, an array of piezometers was installed at select locations within the M Swale as shown on Figure 2.22. Two of the transects of piezometers, denoted A and C, were installed to depths of up to approximately 6.0 m using a combination of hand augers and a rock drill on the side slopes above the piping gage station. Individual piezometers were installed at about the 270 m contour within the two sub-swales shown as finely stippled bands on the site map Figure 2.22. A nest of piezometers was installed at the confluence of the two sub-swales. The saturated zones were generally thin (less than 1.0 m) and of transient duration as observed in many piezometers. Two-piezometer nests were installed at the confluence of the subswales (piezometers B1 and B2) and just upslope of the swale at the bottom of the C transect (piezometers Cl and C2). Details of piezometer construction are summarized on Table 2.2.

Each piezometer was equipped with a pressure transducer from Instrumentation Northwest, Inc. Transducers from the individual transects (A, B, and C) were connected to data-loggers designed and constructed by personnel from the Redwood Sciences Laboratory of U.S. Forest Service. These transducer/data-logger combinations provided water level heights with a design accuracy of approximately 0.01 m, and only very rarely differed from hand measurements by more than 0.02 m. Pressure heads in the piezometers were logged at 15-minute intervals during storm periods, and 2-hour intervals between storms. Beginning in December 1993, piezometers came "on-line" as

soon as they were constructed. Although not addressed specifically in this study, monitoring of the piezometers by U.S. Forest Service Research staff continued though the remainder of 1994, and will end in June 1995.

Slug tests by injecting a constant volume of water were performed in all of the piezometers which contained adequate saturated thicknesses. The pressure head response to the perturbation was measured with a pressure transducer and data logger as described above. Water level recovery data from the slug tests were analyzed using the Bouwer and Rice Method (1976) and were interpreted with respect to the evaluation of that method by Brown et al. (1995).

2.3.2 Hubbard Brook Experimental Forest

The second site considered in this study is an instrumented hillslope above Paradise Brook in Hubbard Brook Experimental Forest (HBEF), West Thornton County, New Hampshire. Managed by the Northeastern Forest Experiment Station of the U.S. Forest Service, the HBEF was originally established to study the effects of forest land management on runoff and water quality. Through subsequent cooperative studies involving a number of universities, HBEF has arguably been the leading center for small-watershed based biogeochemical cycling research (Bormann and Likens, 1967; Likens and Bormann, 1974; Martin, 1979; Bilby and Likens, 1980; Lawrence et al., 1986; and many others). The hillslope experimental site included in the present study was established in 1988 by researchers from the University of New Hampshire to study the hillslope hydrologic processes affecting streamflow in HBEF (Breck Bowden, University

of New Hampshire, personal communication). Cedarholm (1994) monitored saturated and unsaturated flow responses to natural and simulated rain events to investigate mechanisms which control subsurface storm runoff.

Description of Field Site

Along with the nearby Watershed 3, the drainage containing the hillslope site has served as a control watershed since inception of paired watershed studies at HBEF. Just as in the case of the Caspar Creek study site, this area within HBEF was completely clear-cut in the late 1800's, but has remained undisturbed since. The vegetation community is a deciduous northern hardwood forest type. The dominant tree species are: sugar maple (Acer saccharum); american beech (Fagus grandifolia Ehrh.); and yellow birch (Betula allegheniensis Britton). Although not measured during this study, the diameter-at-breast height is estimated to range from approximately 0.15 m to 0.5 m. Other tree species include red spruce (Picea rubens Sarg.), pin cherry (Prunus pennsylvanica L.s.), and striped maple (Acer Pensylvanicum L.).

The soil at this site has been classified by the Soil Conservation Service (unpublished data) as a Typic Haplorthod with sandy loam texture (Becket series). Below the 0.1 m thick organic layer (O horizon), the E, Bh, and Bs horizons have a fairly uniform texture, and the total thickness of the mineral soil ranges from 0.6 m to 1.2 m (Cedarholm, 1994). The soils have an increasing stone fraction with depth, ranging from 10 percent in the E horizon to 25 percent in the lowest Bs horizon (C.A. Federer, U.S. Forest Service). Soils in the HBEF are derived entirely from glacial till since the end of the last glaciation. The ice sheet in this area is estimated to have been 1.6 km thick (U.S.

Forest Service, 1991), and most of the soils existing prior to the most recent glaciation appear to have been completely eroded away. Till thickness is estimated to be a minimum of 10.0 m, based on a preliminary seismic survey of the study hillslope. Beneath the glacial till lies a complex metamorphic assemblage of schist and quartzite of Silurian age known as the Rangley Formation. The overall hillslope has a fairly uniform slope of 45 percent at an elevation of approximately 490 m to 510 m above mean sea level (20.0 m to 39.0 m local datum). The topography of the hillslope is shown on Figure 2.23. However, the microtopography is more complex, with pits and mounds formed by tree-throw, and numerous boulders up to 1.0 m diameter.

The climate of the HBEF is predominantly continental with a fairly uniform monthly precipitation of approximately 0.1 m (4 in, 100 mm) as recorded by the U.S. Forest Service (1991). About one-quarter to one-third of the average 1.3 m (0.187 m standard deviation) annual precipitation near the study site occurs as snow. As a result, streamflow in this region has a significant snowmelt peak runoff usually during the months of April and May. Air temperatures range from a January mean of -9° C to a high of about 19° C in July.

Field Instrumentation

An intensive instrumentation network, including piezometers, tensiometers, and neutron access tubes was installed at this site over the period 1989 to 1992. Details of the instrumentation are given by Cedarholm (1994) and the locations of the monitoring points are depicted on Figure 2.23. The high stone fraction present in this hillslope has proven to be a significant constraint on where instruments can be installed in plan view.

Of equal importance was the hardness and compaction of the till layer (C horizon), which prevented the installation of instruments into or below this layer prior to this study.

In the present study, three piezometers (B11b, B22, and B31b) were installed in the materials underlying the hard till horizon for the first time. This was accomplished using a Cobra rock drill from Atlas-Copco, Inc. to grind through the till and numerous cobbles and boulders. The locations of the three deeper piezometers (and the one shallow piezometer B11a are noted with black-filled circles on Figure 2.23, and the construction details for these piezometers and selected ones installed by Cedarholm (1994) are presented on Table 2.3.

Given the distance and logistics involved it was only feasible to monitor a single rain event in the present study. In October 1993, the pressure transducers and data loggers described above were installed in 13 piezometers at the number locations on Figure 2.23. These piezometers were logged at 15-minute intervals throughout the monitoring period and were checked by hand measurements at selected times before, during, and after the rain event. Slug tests as described above were performed in two of the deeper piezometers (B11b and B31b) as part of this study, and were performed in other piezometers as described by Cedarholm (1994).

3. RESULTS AND DISCUSSION

This section begins by presenting a comparison of the model's performance with an earlier hillslope modeling study. Next the results of parametric studies are systematically described by groups outlined above. Field observations from the two experimental watersheds are then presented in summary form. The final section strives to integrate the modeling and field efforts by simulating selected storm events at the two field sites. Throughout this section, the results are discussed and compared with previous studies.

3.1 Comparison with Previous Hillslope Modeling Work

The simulation of base flow generation presented by Freeze (1972a) provides a reasonable basis for comparing the performance of the model used in this study with one that uses a distinctly different computational basis (integral finite difference versus finite difference, respectively). The evolution of the water table surface under the simulated rainfall and drainage conditions imposed by Freeze (Figure 6, 1972a) are reproduced on Figure 3.1.

Replicating this scenario as closely as possible, a comparable set of simulations were performed using the modified version of TRUST as described in the previous section. The rise of the water table surface over time as estimated in the “new” simulations is presented on Figure 3.2. As in the case of the earlier simulation by Freeze, the water table begins to rise after approximately 64 minutes and continues to rise until

saturation occurs (about 1627 minutes) along the upper land surface where the rain is applied. After this time, a quasi-constant water table is established until the simulation period ends at 8640 minutes. The different time scale of water table over which the two flow domains respond is due to the difference in spatial scales used. The flow domain used by Freeze (1972a) was 6.0 m wide by 3.0 m deep versus the modeled domain in the present study which was 50.0 m wide by 25.0 m deep. The results from the two models seem to be comparable.

As a prelude to the parametric studies, this set of simulations was repeated with the addition of a second material property, the low-permeability bedrock synthesized for the parametric studies. Results are shown on Figure 3.3. A comparison of Figure 3.2 and Figure 3.3 shows that with a heterogeneous hillslope, the water table surface (noted by the inverted delta symbol) evolved in a different manner (Figure 3.3) than for the previous homogeneous case (Figure 3.2). Infiltrating water perches on the unsaturated bedrock, leaving an unsaturated wedge above the initial hydrostatic water table. An inverted water table forms on the bedrock surface and gradually propagates down into the bedrock.

3.2 Results of Parametric Studies

The parametric studies were designed to investigate the effects of various structural features (material properties and geometry) on runoff production and pore pressure responses. A 1-year return interval storm of 12-hour duration was applied to

focus attention on the storm runoff processes that occur on an annual basis. A summary of the parametric studies is given on Table 2.1.

One important question that arises in simulating rainfall-runoff processes in the manner described above concerns the initial moisture conditions employed. It was decided to focus mainly on rainy-season (winter conditions), and thus a uniform initial condition was selected in which the pressure potential was set to -0.5 m tension for all elements above the elevation of the downstream boundary condition. This condition is similar to field observations reported by Cedarholm (1994) and Keppeler (U.S. Forest Service, unpublished data). Beven (1977) also used this initial conditions in similar simulations based on the assumption that this tension (-0.5 m) represented 'field capacity'. In reality, the antecedent/initial moisture conditions in a hillslope will represent a sequence of rainfall, drainage, and redistribution conditions, and are thus extremely difficult to generalize. The approach taken here is a compromise, as is any other (e.g. drained over a period, or hydrostatic) as discussed below.

A consequence of this contrived initial condition is that a uniform downward gradient of potential is imposed leading to a pervasive ambient drainage. Therefore in all of the parametric study cases that utilized this initial condition, the early runoff response includes varying percentages (up to 50 percent) of flow due to drainage from initial conditions rather than a rainfall-induced flow. An example of the range of drainage effects is presented on Figure 3.4 and Figure 3.5. In the case of run 4 with the Inceptisol (Figure 3.4), there is significant drainage from initial conditions; but in run 2 with the colluvial soil (Figure 3.5) the drainage effect is much less. Thus, left uncorrected, the

absolute peak discharge and timing may be biased by the initial condition. Given the hypothetical nature of these simulations, it is argued that the absolute magnitude of discharge is less important than the differences in patterns noticed between the cases compared. In certain cases (individually noted) the runoff results were adjusted for drainage by subtracting the 48-hour drainage runoff (without rain) from the normal 12-hour rainfall, 36-hour drainage case.

3.2.1 Structural heterogeneities

In this section, the following aspects are discussed: 1) runoff generation mechanism; 2) rates of hillslope discharge, and discharge by flow path for selected cases; 3) pore pressure responses at selected locations. After presenting results for the individual flow paths, a brief discussion of the response time scales of various material types is presented.

Soils/Macropore Horizons

In all of the cases considered, subsurface storm flow was the only runoff generation mechanism by which flow was discharged to the boundary. A typical maximum water table profile at the end of the 12-hour rainfall (1-yr return interval) period is presented for the case (run 4) with the Inceptisol soil on Figure 3.6. The Del Monte sand case (run 1) was the only one in which exfiltration, saturation overland flow, and re-infiltration was noted. In this case the entire hillslope produced surface runoff with the exception of the area immediately adjacent to the downstream boundary (Figure 3.7). The seepage face and specified head boundary condition served to prevent the

saturation overland flow from reaching the channel directly. This was one of the early simulations in this study that illustrated the potential importance of the downstream boundary condition geometry. It should be noted that the fairly high saturation state of the Del Monte sand case (run 1) at the initial time has significantly influenced the saturation overland flow response.

Total hillslope runoff generated during the simulation period for the five cases with different soils is presented on Figure 3.8. Note that the Inceptisol with macropore characteristics (run 4) had the highest discharge rate, despite the fact that the colluvial soil (run 2) had a saturated hydraulic conductivity that was two times greater than that of the Inceptisol soil (4.0×10^{-4} m/s versus 1.8×10^{-4} m/s). The results shown on Figure 3.8 were adjusted for drainage from initial conditions as described above.

These results may be understood in terms of variations in hydraulic diffusivity (η) among the five soils as shown on Figure 3.9. Note that the saturated η values for the Inceptisol (run 4) and the colluvial soil (run 2) are fairly similar, but in the low-tension range (-0.2 m to 0.0 m) the η for the Inceptisol (run 4) was two orders of magnitude larger than that of the colluvial soil. The lagged increase in runoff from the colluvial soil (run 2) seems to represent a capacitance effect. The extremely steep slope in the hydraulic conductivity curve at low tensions (Figure 2.14) requires that water accumulate in the hillslope until increasing pressure heads cause $K(\Psi)$ and resultant discharge rates to rise. Hillslope discharge rates as subsurface storm flow observed or simulated in previous studies are presented on Table 3.1. Simulated discharge rates for the five soil cases

considered in this study are given on Table 3.2. The discharge rates estimated here are consistent with the range of values observed in the field and from independent numerical simulations.

An interesting result from this set of simulations was that none of the soils produced conditions of over-pressuring with the exception of the run 1 for the Del Monte sand case (Figure 3.10). The Inceptisol soil (run 4) produced a peak ***m*** value of 0.6 by comparison, and all of the other soil types had lower ***m*** values.

Saprolite

In all of the saprolite cases, subsurface storm flow was the only runoff generation mechanism observed, and exfiltration was not observed in any of the cases. The effects of variable thicknesses of saprolite on runoff generation rates is depicted on Figure 3.11. Details of the distribution of material properties and peak discharge rates are summarized on Table 3.3, comparing two different pairs of cases. First, with the soil depth held constant at 0.5 m, as saprolite thickness and bedrock thickness decreases (runs 6 and 7), there is an increase in the peak discharge rate (Figure 3.11). Second, in the case where the soil thickness (1.0 m) is similar to that of the saprolite (1.5 m), the discharge rate is virtually the same as for a case where no saprolite is present (runs 8 and 9). This latter comparison suggests that the Inceptisol soil material properties dominate the runoff response, and the presence of the saprolite has relatively little effect.

Here again, the differences in hydraulic diffusivity between the soil and the saprolite may explain the simulation results. The hydraulic diffusivity relationships for the

three materials included in this group of parametric studies are presented on Figure 3.12. It can be seen that the soil hydraulic diffusivity is an order of magnitude greater than that of the saprolite in the critical tension range near zero. Since subsurface (saturated flow) stormflow was the only runoff process observed in these cases, the importance of the saturated hydraulic diffusivity is underscored. It is interesting to note that the difference in the saturated hydraulic diffusivity between the soil and saprolite is much less than for unsaturated conditions.

In the case with thin soils and saprolite (run 6), the boundary conditions were such that all three materials were able to discharge from the hillslope. The partitioning of outflow from the different materials is presented on Figure 3.13. Since the soil layer was also thin (0.5 m), the unsaturated flow from this material exiting the seepage face was negligible. It can be seen on Figure 3.13 that the bedrock produced only a very small amount of discharge despite having the highest saturated hydraulic diffusivity of the three materials (Figure 3.12). This result can be attributed to a combination of the small porosity (10 percent) and lower saturated hydraulic conductivity of the bedrock which prevents the conductance of significant volumetric discharge relative to the other materials.

Bedrock

In the cases focused on bedrock (runs 10 and 11), subsurface stormflow was the only runoff generation mechanism observed. Exfiltration was also absent in these cases. The effect of different rock permeabilities on the hillslope runoff response is shown on Figure 3.14. Despite a two order of magnitude difference in K_{sat}, the discharge response

pattern was very similar for both bedrock cases. The peak discharge was 0.169 m^3/hr for the low-permeability rock (run 10) and 0.173 m^3/hr for the high-permeability rock (run 11). In the mesh configuration used in this set of simulations (Figure 2.18b), the soil is the only material type in contact with the seepage face or constant head boundary. This causes the soil to act as buffer of flow through the bedrock to the boundary. Under higher rainfall rates the role of bedrock may be different, especially in convergent flow systems.

Another factor in the bedrock response is the initial condition applied. The initial uniform pressure head of -0.5 m creates a strong permeability contrast between the soil and bedrock. This contrast causes the infiltrating water to perch on the bedrock surface and generate lateral saturated flow. The role during high rainfall or high antecedent moisture conditions remains to be seen.

In the simulation case (run 12) where a lateral discontinuity in bedrock permeability was included (Figure 2.17), a transient zone of saturation developed at the soil bedrock interface located immediately upslope of the permeability interface. The pressure head response for cases with and without the permeability discontinuity are presented on Figure 3.16. Similar modeling results were obtained by Wilson (1988), based on a field investigation that also mapped the bedrock permeability distribution at the hillslope scale. Montgomery et al. (1990) reported similar field observations of discontinuous zones of saturation in a steep unchanneled swale.

Response Time Scales

One means of examining the response time scale for a given flow path is to consider the hydraulic head (ϕ) response within the appropriate soil or rock material over the simulation period. On Figure 3.17, variations in ϕ are plotted over the 12-hour rainfall period for run 4 for both the Inceptisol soil (layer 8) and the low-permeability bedrock (layer 12) at two slope positions. At the lower slope position, both the soil and bedrock ϕ observation points are beneath the water table and are thus saturated. There is a gradual rise in ϕ as the rainfall continues. By contrast, at the mid-slope position, neither observation point is saturated. In the case of the soil, there is a short period during which ϕ drops due to drainage followed by a continuous gradual increase. In the midslope bedrock, ϕ remains unchanged over the entire rainfall period. This implies that under unsaturated conditions in this simulation case, there was an order of magnitude difference in the response time scale (approximately 1 hour versus greater than 12 hours) between the Inceptisol soil and the low-permeability bedrock. Responses in the unsaturated bedrock would probably occur on a time-scale of days or longer, depending on the hydraulic properties of the rock.

An alternative means of evaluating the response time scale of a given material is to consider the time constant Δt_m, of volume elements in different materials according to equation 6. At the macroscale, the time constant will be manifest primarily in the rate at which pore pressures can change. Recall that as the time constant decreases, the particular element will react more rapidly. The values of Δt_m for run 4, the case described

above are summarized on Table 3.4. The estimated time constants are consistent with the ϕ response, showing marked difference (nearly four orders of magnitude) between the unsaturated soil and rock. Layers 11 through 14 (Figure 2.12b) were bedrock layers, and it can be seen on Table 3.4 that the time constant for layer 11 decreased b orders of magnitude as the rock became saturated. Note also that under saturated conditions at the lower slope position, the rock and the soil had the same order of magnitude time constant (0.1 s to 0.3 s).

A second case was run (run 1) in which the Inceptisol soil was replaced with the Del Monte sand (Table 3.4). Here the results were similar, except that the sand had a time constant that was up to an order of magnitude greater than that of the Inceptisol under unsaturated conditions. Under saturated conditions, the difference between the sand and the Inceptisol increased to two orders of magnitude. These results for the two soils reflect the difference in hydraulic diffusivity values, particularly at saturation (Figure 3.9).

3.2.2 Slope geometry

The base case of slope geometry considered in most of the parametric simulations is a uniform (1.0 m) thickness slope (in the third dimension) at a 15 degree angle, and soil and rock layers are of uniform thickness. These parameters, thickness in the third dimension, slope angle, and horizontal thickness are varied in the following simulations. First, the effects of 3-dimensional flow are considered in convergent slopes. Next slope angle is varied at 7.5 degrees, 15 degrees, and 30 degrees. The interface topography is

considered in the final set of simulations by varying the thickness of the soils and bedrock with distance along the slope.

Convergent slopes

Simulations by Beven (1977) and Wilson (1989) have previously demonstrated the importance of convergent flow geometry in runoff and pore pressures, respectively, for different slope geometries than the form used here. The first simulation of a convergent slope using a pseudo-3-dimensional mesh (Figure 2.9) included two material types: the Inceptisol soil with macropores (Wilson et al., 1992), and the low-permeability bedrock (run 13). As seen in Figure 3.18, saturation overland flow was generated after approximately 10 hours of rainfall, and the discharge of surface and subsurface flow is shown on Figure 3.18. Subsurface flow reaches a maximum rate at the time when overland flow begins to discharge to the channel. The subsurface flow rate remains constant until the overland flow ends, after which the discharge declines.

In the second convergent slope case (run 14), three materials were included: the Inceptisol soil with macropores and saprolite from Wilson et al. (1992), and the low-permeability bedrock. Overland flow to the channel did occur in this case also, but not until after the rainfall had ended (Figure 3.19). The subsurface flow response firm both soil and saprolite followed a pattern similar to that of the first case, albeit lagged by about 2 hours.

The third convergent slope case (run 15) was identical to the first case except that the initial conditions were hydrostatic with respect to the downstream boundary condition. With the initial hydraulic head set everywhere to 78.80 m, negative pore

pressures in excess of -20.0 m were imposed at top of the mesh/hillslope. The resulting peak total discharge from the hillslope (0.058 m^3/hr) was over an order of magnitude lower than for the first case (3.030 m^3/hr) as shown on Table 3.5.

A summary of the total hillslope discharge response for the three convergent slope cases is presented on Figure 3.20. The lower magnitude and lag of the peak discharge for the 3-material case (run 14) can be explained by the presence of the saprolite with its lower hydraulic diffusivity as described above. The difference in initial conditions between run 13 and run 15 (first and third cases) had a far greater impact on the runoff response than did differences in the distribution of material types (first and second cases). The only directly comparable modeling study to date that simulated convergent flow was that of Beven (1977) who used a planar mesh with a complex convergent shape that produced a greater angle than the one used in this study. Allowing for differences in mesh configuration and material properties, the peak discharge reported by Beven (1977) of 0.765 m^3/hr is reasonably similar to the peak discharge estimated in this study (0.058 m^3/hr) for run 13. Wilson (1988) reported surface runoff rates for simulations involving convergent slopes, but the magnitude and duration of the rain event used by Wilson preclude a meaningful comparison with the present results.

The effect of convergent flow conditions on pore pressure evolution can be seen in the plot of the ***m*** parameter on Figure 3.21. The first two convergent slope cases (run 13 and run 14) are compared with their uniform (non-convergent) counterparts (run 4 and run 8). The open and closed circles are for the 2-material case (run 13 and run 4), and it can be seen that the critical ***m*** value of 1.0 is exceeded in the convergent

slope simulation. A greater relative increase in m occurred in the 3-material convergent slope cases (open and closed triangles) for run 14 and run 8. The results demonstrate the potential effects of slope convergence in leading to excessive pore pressures and potential instability. Indeed focused flow in source areas may play a vital role in the growth and evolution of channel heads. Similar results have been obtained from field studies (Anderson and Burt, 1978; Sidle and Swanston, 1981; Wilson and Dietrich, 1987) and from modeling studies (Humphrey, 1982; Wilson, 1988). However, it should be noted that soil material properties and root distributions will also influence the stability of convergent slopes.

Variable slope angles

Runoff estimates for the suite of simulations in which the slope angle was varied from 7.5 degrees to 30 degrees were adjusted for drainage from initial conditions and for differences in hillslope area. The latter adjustment was accomplished by dividing the volumetric discharge by the surface area of the slope, and thus the discharge is in units of length per unit time (m/hr). Recall that relief was held constant and slope length was varied. As a result, the higher the slope, the shorter the path length. In the first case of variable slope angle, the Inceptisol soil with macropores and low-permeability bedrock were included. The discharge responses for the three slope angles (runs 16 to 18) are shown on Figure 3.22. As slope increases, the peak discharge increases and the time to reach peak discharge decreases.

The second case combined the Inceptisol soil with macropores and high-permeability bedrock (runs 19 to 21), and the calculated discharge responses are

presented on Figure 3.23. The results from the 7.5-degree (run 19) and 15-degree (run 20) slopes for the high-permeability rock case are similar to those for the low-permeability rock case. Small oscillations in the discharge rate and a delay in the peak discharge occurs in the 30-degree slope case (run 21). This response is caused by a combination of the steep gradient and the strongly non-linear form of the hydraulic conductivity curve of the high permeability bedrock (Figure 2.16). Recall that the threshold pressure head for the step increase in the high-permeability bedrock was specified as -0.30 m tension. Since the initial condition applied was -0.50 m tension throughout most of the slope, lateral drainage associated with the rock was delayed until the local pressure head reached -0.30 m.

The final simulation in this group involved the colluvial soil and low-permeability bedrock on slopes of 15 degrees (run 22) and 30 degrees (run 23) (Figure 3.24). Total hillslope discharge follows a similar pattern for both slope angles. An early runoff peak or maximum is followed by a larger peak runoff that lags behind the end of rainfall by approximately 24 hours. That the 30-degree slope (run 23) had a higher initial peak is consistent with the first two sets of simulations described above. The small oscillations observed in the discharge from the 30-degree slope (run 23) is interpreted to be the result of the combination of the steep gradients and the strongly non-linear hydraulic properties of the colluvial soil. The greater magnitude second peak for the 15-degree slope (run 22) is an anomaly which appears to be due to a combination of the slope-related gradients and the hydraulic diffusivity properties of the colluvial soil.

Interface Topography

These simulations were designed to consider the effects of different interface topographies on runoff, including the distribution of soil thicknesses and the depth of permeable bedrock. In the simulation cases where the soil thickness increases with distance downslope (Figure 3.25), the case (run 25) with the high-permeability bedrock showed a slightly higher peak discharge rate (0.128 m^3/hr) than the low-permeability bedrock (0.102 m^3/hr) in run 24. The combination of a greater thickness of rock in the upper portion of the system (Figure 2.11a) and a higher hydraulic diffusivity of the high-permeability rock in the low-tension range below -0.3 m accounts for the observed response.

In the cases using a mesh that extended the bedrock layers to a greater depth (Figure 2.11b) than the typical "banded" type mesh, a different result was obtained. In these cases (Figure 3.26), the discharge rate was adjusted for drainage from initial conditions as described earlier. The high-permeability rock (run 27) showed a greater peak as expected, but the peak discharge occurred after just 6 hours, or about half-way through the 12-hour rainfall period. This result requires further investigation. However, the peak discharge rate for the low-permeability rock (run 26) in the “full” mesh (approximately 8.5 x 10^{-2} m^3/hr) was over an order of magnitude higher than the peak discharge rate for the "banded" mesh (approximately 1.5 x 10^{-3} m^3/hr). This suggests that the depth distribution in conjunction with the magnitude of rock permeability can directly influence runoff rates.

3.2.3 Antecedent soil moisture conditions

In a similar set parametric simulations, Beven (1977) argued that antecedent moisture conditions had a greater effect on runoff production from hillslopes than did convergent flow geometry. To test this conclusion, the effect of antecedent soil moisture conditions was investigated with the help of the three different initial conditions. The results of these simulations (runs 28 to 31) are shown on Figure 3.27. For comparison purposes, the drainage-adjusted discharge for the wet initial condition is also shown (run 29). Assuming hydrostatic conditions to exist throughout the hillslope is the optimal initial condition for isolating the runoff response strictly due to the rainfall applied Although not explicitly stated, it was probably for this reason that Freeze (1972b) employed only hydrostatic conditions. Beven (1977) considered both hydrostatic and a uniform -0.50 m pressure head. As noted above, assuming hydrostatic conditions in hillslopes of significant relief imposes unreasonably high tensions at the top of the slope. Comparing the results of run 28 versus run 31 (Figure 3.27), there is nearly an order of magnitude difference in the runoff response if hydrostatic conditions are assumed. An intermediate initial condition results from setting the pressure head everywhere to be 0.0 m and allowing the slope to drain for a specified period of time (run 30). Wilson (1988) used an observed inter-storm interval of 14 days as a drainage period. A 5-day drainage period was used to create the initial condition for run 30 as shown on Figure 3.27. However, this initial condition was accompanied by pressure heads of greater than -1.0 m

tension in the upper soil layers. This is a higher tension than the tensions observed at the two field sites considered in this study (generally less than -0.5 m).

The antecedent moisture conditions within a hillslope at any given time will reflect the effects of a sequence of rainfall and drainage episodes that may extend back days, weeks, or months depending on the season. Applying any type of uniform initial condition in numerical simulations is an approximation that will be valid in some parts of the slope, but probably not in others. Specifying a single drainage period to create initial conditions may be superior in some regards, but this approach may result in dryer moisture profiles than exist in field conditions. In future simulations, it might be possible to identify a simplified rainfall-drainage sequence that more closely resembles observed antecedent moisture conditions.

3.2.4 Downstream boundary conditions and runoff generation mechanisms

By examining the dynamic behavior of the water table for different boundary conditions, it is possible to examine the runoff generation mechanisms that occur in relation to the variable source area concept of Hewlett and Hibbert (1967). One major constraint in the simulation of a dynamic expansion and contraction of the runoff-producing zones during storm runoff is the lack of a time-varying head boundary condition representing changes in stream stage in the channel. However, as seen in run 35 even with a constant head in the 0.05 m-deep channel, saturation overland flow results in discharge directly to the channel commencing at about 5 hours. The cross-

sectional profile of the changing water table surface and the expansion and contraction of the effective channel for run 35 is shown on Figure 3.28.

A similar plot of the 0.30 m deep channel used in run 36 (Figure 3.29) demonstrates the effect of even a relatively shallow degree of incision. Exfiltration and saturation overland flow occurs over an expanding zone that extends toward the channel during the 12-hour rainfall period. For approximately 2 hours, the entire channel bank is saturated and saturation overland flow exits the flow domain at the downstream boundary. The seepage face that results from the constant head elevation is sufficient to prevent saturation overland flow from reaching the channel during the rainfall period, and thus the timing of overland flow contributions to the variable source area response appears to be constrained by the channel bank geometry in this case. Note that the surface-saturated zone expansion is of more limited duration in the 0.30 m case (run 36) than in the 0.05 m case (run 35). The peak water table profile shown on Figure 3.6 for run 4 for the deepest depth of incision (1.20 m) is typical of all of the cases simulated except for the case (run 1) using the Del Monte Sand (Figure 3.7).

Downstream Boundary Condition Configuration

The effects of the seepage face/constant head (Figure 2.18a) and seepage face/constant head/no flow (Figure 2.18b) downstream boundary configurations (hereafter referred to as the 2-part and 3-part configurations, respectively) were considered for three depths of channel incision: 0.05 m; 0.30 m; and 1.20 m. The total discharge of each type of boundary configuration at the three depths are presented on Figures 3.30 to 3.32. From these results, it can be seen that the type of boundary

employed had little effect on the total discharge rate at the end of the rainfall period. The differences in runoff rate during the first 6 to 8 hours for the 0.05 m (run 32) and 0.30 m (run 33) depths can be attributed to the greater subsurface area available to discharge flow in the 2-part configuration. At depth of 1.20 m (run 34 and run 37), there was no significant difference in the type of boundary used (Figure 3.32).

The main effect of the type of boundary configuration in the two shallow channel cases is on the time at which overland flow begins to reach the channel boundary. The partitioning of outflow between overland and subsurface flow with the 2-part boundary for run 32 with a channel depth of 0.05 m is shown on Figure 3.33. In this case, flow from the bedrock was negligible on a volumetric basis and overland flow began to reach the channel shortly after 8 hours of rainfall. This contrasts with the results for run 35 with the 3-part boundary configuration shown on Figure 3.34 in which overland flow began after 5 hours of rainfall.

For run 33 and run 36 with the channel depth of 0.30 m, the results were essentially the same (Figures 3.35 and 3.36). In these cases, overland flow was not generated during the rainfall period, but began shortly thereafter (Figure 3.30). The importance of the seepage face geometry in controlling the discharge behavior is also demonstrated by simulations in which the 3-part boundary was extended to 0.80 m (run 36) and 1.20 m (run 37) depths (Figure 3.37). A final simulation (run 38) was run with a 1.20 m channel depth in which the rainfall rate was increased to a 100-year return interval. A rainfall total of 1.51×10^{-1} m (151 mm) was applied at a constant rate of 3.5×10^{-6} m/s (12 in/day) for 12 hours followed by 36 hours of drainage. The discharge

response is presented on Figure 3.38, and it is interesting to note that the depth of the incision and corresponding seepage face combined to prevent overland flow from reaching the channel during the period of high-magnitude rainfall.

Structural Heterogeneities Near the Downstream Boundary

After examining the results thus far, one may ask the question of how realistic the uniform distribution of soil properties throughout the slope is in regard to field conditions. Hewlett (1974) in commenting on the modeling study by Freeze (1972b) asserts, “Perennial, intermittent, and ephemeral channel banks will tend toward the highest limits that he [Freeze] sets on saturated permeability.” Unfortunately Hewlett didn't provide any references for this comment. In the reported hydraulic conductivity values from hillslope studies reviewed by Dunne (1978) and more recent studies discussed above, there are very few studies that have measured hydraulic conductivity distributions along hillslope profiles (Montgomery, 1991; Shattuck, 1991; and Cedarholm, 1994). A further complication in evaluating the available conductivity data that does exist stems from the variety of field and laboratory testing methods employed.

One conceptual model that can be used to approach the question of lateral material property variation on hillslopes is that of the “catena” concept. First described by Milne (1935), the catena represents a sequence of soils distributed down a slope in response to soil-forming factors (Jenny 1941). Studies of catenas have been performed at the regional mountain range scale (e.g. McColl and McGrath, 1992; Alexander et al., 1993), and also at the hillslope scale (e.g. Swanson, 1985; Forster, 1993). The latter two studies noted a general increase in clay content with distance downslope attributed to

both translocation and weathering processes. The effect of increasing clay content on hydraulic properties of soils in the near-stream zone may be offset by a greater density of riparian vegetation and or animal activity. There is a clear need for further field studies regarding the distribution of soil hydraulic properties along catenas in different environmental settings.

The final parametric simulation (run 39) concerned with boundary conditions is something of a thought experiment. Since the simulations of boundary effects on runoff processes all employed the Inceptisol with macropores (Wilson et al., 1992) the effects of high permeability soils similar to the ones envisioned by Hewlett (1974) in the streamside zone have been considered. The consequences of a lower permeability zone in the streamside area (Figure 2.19) on the discharge rates with 0.30 m channel depth are summarized on Figure 3.39. These results may be compared with those for run 36 with the uniform Inceptisol shown on Figure 3.36. It can be seen that the magnitude of overland flow is greater by approximately a factor of four, and surface runoff begins about two hours earlier than the previous case.

3.2.5 Simulations of flow around channel heads

Montgomery (1991) described the interactions between soil material properties and subsurface flow in controlling the development and evolution of an abrupt channel at an upland watershed. The simulations conducted of flow around a hypothetical channel provide a means of examining how pore pressures behave in the vicinity of a channel head as it increases in height.

Channel head simulation results are summarized on Table 3.6. In the first set of simulations (runs 40 to 43), channel heads of four different heights were imposed within a soil consisting of a uniform silt. The pore pressure ratio m was calculated at the base of each channel head as shown on Figure 2.20. The m ratio did not exceed 1.0 for any of the simulated channel head heights (Table 3.6). Somewhat counter-intuitively, the ***m*** ratio was inversely proportional to the channel head and seepage face heights. Excessive pressuring was observed (***m*** greater than 1.0) in the surface nodes immediately below the channel head extending up to 1.90 m downslope. However, beyond an apparent threshold channel height between 0.8 m (run 42) and 2.0 m (run 43), the pore pressure as reflected in m declines such that over-pressuring does not occur below the channel head in the 2.0 m case.

Similar results were obtained in the simulations using the Inceptisol soil with macropores (runs 44 to 47). It can be seen that the ***m*** values were only slightly greater than those for the silt soil (Table 3.6). Excessive pressuring also was noted below the channel head, at distances that are apparently unrelated to soil type. Here again, ***m*** below the channel head declined to less than 1.0 as the channel head height increased from 0.8 m (run 46) to 2.0 m (run 47). The presence of pore pressures exceeding hydrostatic pressures downslope from a channel head has been observed in the field at the Tennessee Valley field site as described by Montgomery (1991). Based on the cases considered, it appears that the ratio m is relatively insensitive to soil hydraulic properties.

In the final set of simulations, a 2.0 m channel head in the silt soil was held constant while the total thickness of the two soil materials below (clayey-silt and silty-clay) was reduced from 2.0 m to 0.0 m. Results for the three cases with thicknesses ranging from 0.4 m to 2.0 m were virtually identical with the 2.0 m case (run 51) for the silt soil, and so only the case with a 0.0 m thickness "sub-soil" is presented on Table 3.6. This case represents the channel head directly overlying a surface of bedrock with negligible permeability. The resulting vertical shortening of the flow system resulted in a higher pore pressure at the base of the channel head. Although the resulting ***m*** value (0.22) was two times greater than that for the silt soil 2.0 m case (0.11) with the full thickness of soil layers below, the ***m*** was far below 1.0. Thus, it appears that the results were relatively insensitive to the proximity of the lower no-flow boundary for the simulated conditions.

The flow fields that develop around the 0.2 m channel heads for both soil types (run 40 and run 44) are shown on Figure 3.40. The overall flow is parallel with the slope, and only a very slight deviation in the equipotentials occurs due to the presence of the channel head. In both of the 0.2 m channel head cases, the seepage face occupies approximately 30 percent or more of the channel head height, and thus saturated flow is concentrated through a relatively narrow (0,06 m to 0.07 m) seepage face. By contrast, a significantly taller seepage face (1.70 m) developed in the 2.0 m channel head case (run 47) with the Inceptisol soil (Figure 3.41). The generally linear relationship between seepage face height and channel height for the two soil types is shown on Figure 3.42.

The relationship between ***m*** and channel head geometric properties (channel head height and seepage face height) for the silt soil is shown on Figure 3.43. The observed inverse relationship between ***m*** and both properties (Figure 3.43a, 3.43b) was best described by a linear equation with an r^2 of 0.836 and 0.773, respectively. A similar analysis for the Inceptisol soil is presented on Figure 3.44, and it can be seen that the same general relationships seem to occur. The linear equations gave an r^2 of 0.707 and 0.751 for the for the ***m***-channel head height and ***m***-seepage face height relationships, respectively.

Given the quasi-steady-state nature of the channel head simulations, it is not surprising that the difference in the pore pressure response between the two cases did not reflect the contrast in hydraulic diffusivity characteristics of the two soil types considered (Figure 3.45). In future simulations, rainfall events could be simulated on top of the near-saturated conditions that occurred during these simulations. Under the transient conditions that would result, it would be hypothesized that the Inceptisol soil would show a much greater pore pressure response given its greater hydraulic diffusivity.

Further simulations are also needed to explore the controls on the magnitude and extent of excessive pressuring that occurs downslope of the channel heads. The modeling approach developed in this study provides a less restrictive quantitative tool than traditional analytical expressions, particularly in terms of incorporating variable geometric factors and structural heterogeneities. As Dunne (1990) pointed out, analytical methods

such as the commonly used Dupuit-Forcheimer equation for seepage faces is limited to low slope angles.

3.3 Field Observations

Due to the different proximity of the two field sites included in this study, different levels of data-gathering efforts were achieved. The piezometer network installed at the Caspar Creek field site was monitored throughout the entire winter of 1993-94. By contrast, the logistical constraints of collecting storm data at the Hubbard Brook site limited data collection to a single storm event in October 1993. The purpose of including field research in this study was to inject a measure of realism in extrapolating the model-based theoretical analyses described in the previous sections.

3.3.1 Caspar Creek Experimental Watershed

On the basis of the soil borings excavated during piezometer installations, two geologic cross-sections (A - C and B - B*) were prepared for this site (Figure 2.22). The A - C cross-section is based on the A and C side-slope instrument transects as shown on Figure 3.46. Soil horizons and saprolite thicknesses were fairly uniform throughout both slopes. The water table throughout the entire monitoring period was only observed along the saprolite-hard bedrock interface. A typical water table profile during late February 1994 is shown on Figure 3.46. Based on field observations of the soil pipes emerging at the piping gage station, it appears that the pipes in the swale bottom occur at depth such that the water table often fluctuates into and around the pipe zone. A similar cross-

sectional profile was prepared for the transect B-B* as shown on Figure 3.47. The soil and saprolite layers also seem to be fairly uniform. In the lower portion of the transect, a late-February 1994 water table based on data from piezometers B1 and B4 is presented on Figure 3.48.

Slug test results are given on Table 3.7 and are arranged by their position within the drainage. Estimated hydraulic conductivity values (K_{sat}) for mid-slope piezometers were approximately 10^{-7} m/s and thus were consistently an order of magnitude lower than those for the piezometers in the swale bottoms (approximately 10^{-6} m/s). The one piezometer (C1) located at the toe of the slope on the C instrument transect (Figure 3.46) had the highest estimated K_{sat}. The water level in this piezometer was very close to the top of the screened interval, and thus the estimated K_{sat} obtained using the Bouwer and Rice (1976) method of slug test analysis probably represents an over-estimate of the actual K_{sat} (Brown et al., 1995). The single piezometer (C2) completed within bedrock had the second highest estimated K_{sat} at 8.7 x 10^{-6} m/s. A simplified packer test was performed in this borehole, and it was observed that the greatest conductivity seemed to be associated with uppermost 0.75 m of the rock.

The piezometric response to storms by instrument transect or cluster during the months of January, February, and March 1994 are presented on Figure 3.49 (A transect), Figure 3.50 (cluster), and Figure 3.51 (C transect). As the winter progressed, the piezometers responded more rapidly to larger rain events. The peak response was noted for the mid-February storm beginning on about day 139 (since October 1, beginning of water year). The peak rainfall occurred over an 18-hour period ending shortly after noon

on day 140. Peak piezometric responses and their lag from the end of the rainfall peak are summarized on Table 3.8.

From the calculated piezometric lag times, of the two subswales the one containing piezometer B4 showed the most rapid response. Piezometer B1 at the confluence of the subswales peaked shortly thereafter. The reason for piezometer B2 having such a rapid response is unclear, and this is the only storm that caused positive pore pressures at this location. Further data are needed to understand the behavior of the water table at this shallow depth and location, The response of piezometer B3 is also somewhat anomalous when compared with 134. In this case, subsequent soil borings near B3 indicate that this piezometer may be completed in a small-scale (less than 1.0 m thick) zone that has a limited hydraulic connection to the rest of the subswale.

Piezometric responses on the two side slope transects were fairly similar to each other and had greater lags than the B cluster. The convergence of flow in the B subswales could explain the difference in lag times with the more parallel side slopes. It is interesting to note that the bedrock piezometer responded more quickly than the other A- and C-transect piezometers which were all completed in saprolite. Although not directly measured by field tests, this result suggests a higher diffusivity in the bedrock.

3.3.2 Hubbard Brook Experimental Forest

Combining the observations of Cedarholm (1994) and field work performed during the present investigation, a cross-section was prepared for the field site as shown on Figure 3.52. The most significant finding of the field investigations at this site is

detection of a perennial lower saturated zone beneath the hard till layer at depths generally below 2.0 m.. Based on the three piezometers completed to date, it appears that this zone is continuous up the slope and is likely to mirror the terrain up to the drainage divide. Till thickness is at least 4.0 m based on the deeper soil borings, and this provides preliminary corroboration with a reconnaissance seismic survey at this site which estimated till thickness at approximately 10.0 m at the crest of the slope (Cedarholm, 1994). From the deeper borings, the till in the lower saturated zones was observed to be comprised of heterogeneous layers of unconsolidated sediments ranging in texture from silt to silty sand with a high stone content. Due to experimental difficulties in conducting the slug tests in piezometers B11b and B31b, analysis of the data gave very ambiguous results. Therefore, the tests need to be repeated before acceptable hydraulic conductivity estimates can be obtained for the deeper saturated zone.

Piezometric response data from the October 1993 storm are presented by data logger only for those piezometers showing a positive pore pressure during the monitoring period (Figure 3.53 to Figure 3.56). Piezometer locations are shown on Figure 2.23. Comparing piezometers B12 (Figure 3.53), B21 (Figure 3.54), B31a and B32 (Figure 3.55), and B41 and B42 (Figure 3.56), it can be seen that the pressure head response becomes progressively stronger and more rapid, with distance downslope. Similar observations have been reported in the field study by Wilson and Dietrich (1987).

Of the deeper piezometers, B22 did not react to the rainfall event. Deeper piezometers B11b and B31b both showed small amplitude fluctuations, but it is not clear that these pressure head changes are in response to the rainfall event. It seems more

likely that they may be related to barometric effects on the soft silt-rich layers observed in the deeper till, but further data is required to test this interpretation.

One of the most interesting results came from the lowest set of monitored piezometers attached to data logger 4 (Figure 3.56). There is a small-scale break in the slope between the stream-side terrace where piezometer B43 is located and the locations of piezometers B41 and B42. These latter two piezometers seemed to respond in the same manner as the other upslope piezometers, showing distinct peaks associated with the rainfall distribution pattern. By contrast, the rise in pressure head in piezometer B43 was sharply limited. Hand measurements during the monitoring period confirmed the data logger results. Surface saturation and overland flow were not observed in the streamside zone during the monitoring period.

The pressure head response observed in B43 is attributed to a combination of: 1) drainage effects due to macropores in the riparian zone; and 2) an extremely high capacitance in the streamside soils resulting from a large organic material content. This interpretation is based in part on observations by Stresky (1991). Working in the Hubbard Brook watersheds, he observed a significantly greater distribution of macropores in riparian soils versus soil horizon further up the slope. Field observations of the streamside soil surface made during this investigation indicate that soils within the stream terrace appear to be largely organic material mixed in with a high percentage of stones. Permission to dig soil pits in the riparian zone at this site is difficult to obtain, but should be pursued to unravel the piezometric behavior observed in B43.

The traditional interpretation of the water balance in Hubbard Brook watersheds by U.S. Forest Service scientists has been that the only form of volumetrically significant subsurface saturated flow is in the upper soil horizons. On the time scale of individual rain events such as the one described above, the lack of a discernible pressure head response in the lower saturated zone seems to support this hypothesized water balance. The role of the lower saturated zone in supplying base flow and recharge to the underlying fractured rock requires further investigation. Ongoing monthly monitoring of the deeper piezometers during the last 6 months of 1994 suggests that the lower water table fluctuates on a seasonal time scale (Amey Bailey, U.S. Forest Service, unpublished data).

3.4 Integration of Field Observations and Simulations

Thus far, a numerical tool of analysis has been developed, and applied to hypothetical hillslope conditions. Field observations have also been collected from field sites with different environmental conditions, including climate, geology, soils, and vegetation. The final group of simulations represents an attempt to integrate field observations and computational experiments to further explore inter-relationships between watershed structure and hydrologic processes under transient flow conditions. A single storm was selected from the Caspar Creek site data set for comparison with the storm monitored at the Hubbard Brook site. Within the study design, a great emphasis was placed on using existing field data where available. As a result, varying degrees of

parameter estimation had to be employed to assemble the requisite data sets for simulation purposes.

3.4.1 Caspar Creek Experimental Watershed

The January 1994 storm selected for simulation purposes followed a long drainage period with stable pressure heads in the piezometers. Piezometers C1 and C2 were selected for simulation comparison since they are located at the toe of the slope on the C transect and form an instrument nest monitoring saprolite and bedrock, respectively. Rainfall occurred over a 4-day period followed by approximately 10 days of drainage, and the pressure head response in the two piezometers is shown on Figure 3.51.

Soil hydraulic properties were obtained from the analyses reported by Wosika (1981). The saturation and hydraulic conductivity curves for the A and B horizons used in the simulations are shown on Figure 3.57. Comparable curves for the saprolite and bedrock were not available through field measurement. Saprolite hydraulic properties were estimated using the $K(\Psi)$ relationship reported by Wilson et al. (1992) adjusted to an average K_{sat} (2.9×10^{-7} m/s) obtained from slug test results. The saprolite saturation curve (Figure 2.15) presented by Wilson et al. (1992) was used without alteration. In the absence of bedrock data, a step function relationship was used similar to the one presented for the high-permeability bedrock in the parametric simulations (Figure 2.16). For bedrock, K_{sat} was set at 8.7×10^{-6} m/s based on slug test results.

The mesh used in the simulations with element centers denoted by the '+' symbols is presented on Figure 3.58 along with the geologic cross-section, and nodes

corresponding to piezometers C1 and C2 were located as indicated. As a first approximation, a specified head boundary condition was applied at the downstream boundary. Soil horizon thickness (A and B) was assumed to remain constant at 0.60 m throughout the slope. The saprolite thickness was 1.5 m at the downstream boundary and was extrapolated to about 7.0 m at the ridge crest based on the angle of the saprolite-bedrock interface between piezometers C3 and C4. A constant bedrock thickness of approximately 7.0 m was also applied Based on the time lags noted in the piezometric response described above (table 3.9), the rainfall pattern was grouped into a pattern of average generation rates and drainage periods to simplify the input data as shown on Figure 3.59a.

Observed and simulated pressure head responses for piezometer C1 are plotted on Figure 3.60. The rising hydrograph during the first two days of simulation shows very good agreement between the observed and simulated pressure heads. The peak pressure heads are over-estimated by 0.1 to 0.2 m during the remainder of the rainfall period. However, the greatest deviation between observed and simulated results occurs during the drainage period when the simulated pressure head fails to drop as rapidly as the observed pressure head. Increasing the saprolite hydraulic diffusivity would allow a more rapid drainage, but would also cause the rising hydrograph to over-estimate the pressure head to a greater extent than is shown of Figure 3.60.

Similar results were obtained for the bedrock piezometer C2 as shown on Figure 3.61. The simulated rising hydrograph departs from the observed pressure heads after the first 2 days of rainfall. In this case the drainage pattern, although offset by an

over-estimation of 0.3 m to 0.4 m, has a form that more closely follows the observed falling limb of the hydrograph. Piezometers C0, C3, and C4 were not being logged during this period, and are not available for comparison.

These results were obtained with minimal calibration of the data set to match observed pressure heads. The compressibility of the saprolite was the only parameter varied in three trial simulations to achieve the results described above. Decreasing the compressibility effectively increased the hydraulic diffusivity, and thereby served to increase the rate at which the pore pressure changed. Another 'estimated' component that is likely to affect the simulated results is the distribution of antecedent moisture conditions throughout the slope. In the simulations, initial conditions were estimated based on tensiometric data from a site near the top of the A transect (Figure 2.22). Tensions were specified as ranging from -0.15 m in upper soil layers to -0.5 m above the water table, which was specified based on data from the piezometers in the C transect.

Several factors would seem likely to account for the deviation of the simulated pressure heads from the observed pressure heads. These include: 1) the absence of measured saprolite hydraulic properties; 2) uncertainty of the actual depth of the saprolite on the upper portion of the hillslope; and 3) bedrock hydraulic characteristics and spatial distribution. The effects of these parameters on the simulated pore pressures could be evaluated in future sensitivity analyses. These data limitations are common problems in applying parameter-intensive physically-based models to real-world conditions. That the simulated hydrograph matches the observed hydrograph as well as it does suggests that the physical rationale associated with the interpretation is broadly reasonable but that the

differences are attributable to a lack of knowledge about site-specific attributes in terms of geometry, local scale heterogeneities and initial conditions. Additional field work should be performed to gather data of the three types noted above. These data should be gradually added to the simulations to determine if there is a minimum quantity and type of data required to improve the simulation results.

3.4.2 Hubbard Brook Experimental Forest

As noted earlier, only a single storm was monitored at the Hubbard Brook site during October 1993. Fortunately, there had been no rainfall over the 10-day period preceding this storm and thus the pressure heads on the hillslope were relatively stable. Piezometer B31a was selected as a representative observation point for trial simulation purposes. The rainfall period lasted for approximately 20 hours followed by about 24 hours of drainage before monitoring was halted.

A soil saturation curve developed by Cedarholm (1994) was the only field measured material property available for use in this study. A soil hydraulic conductivity curve was assembled using the Inceptisol $K(\Psi)$ relationship reported by Wilson et al. (1992) adjusted to the mean K_{sat} (1.2×10^{-4} m/s) obtained by Cedarholin (1994) from slug test results. For a trial simulation, this was the only material property applied However, the results were sufficiently poor that a second simulation was devised in which the hydraulic conductivity relationship was increased by one order of magnitude in the upper three soil layers.

The mesh used in the field simulations is shown on Figure 3.62 relative to the actual hillslope. The total soil thickness was set at a constant 0.70 m throughout the hillslope, and no attempt was made to simulate the behavior of the lower saturated zone. The dense till was assumed to form an impervious lower boundary. As in the Caspar Creek field simulation, the rainfall pattern was used to create a series of average rainfall and drainage periods as shown on Figure 3.59b.

Observed and simulated pressure heads in at the location of piezometer B31 a are presented on Figure 3.63. Simulation 1 represents a case with virtually no calibration to match the field observations. The lack of a sharp peak reveals one consequence of averaging the rainfall rate. The sharp peak of rainfall occurring at approximately 1200 minutes of the monitoring period was greatly reduced with application of the average rate (Figure 3.59b). Despite the fact that every effort was made to represent the field conditions as closely as the data would allow, the simulated response was clearly a poor underestimate.

A second simulation case was prepared to examine the effects of small-scale heterogeneities on the pressure head response. Rock fragments are often on the same spatial scale (0.10 m to 0.50 m) as the grid spacing used here. Hence, a single hypothetical low-permeability heterogeneity node representing either a boulder or dense till was placed in the node immediately downgradient of the observation node. The resulting simulated pressure head response matches the observed pressure head response to a surprisingly close degree. Based on the second simulation, it appears that structural heterogeneities at least on a small scale can directly influence the hydrologic response on

a hillslope, at least in terms of the pressure head response. In soils with high degrees of lateral heterogeneities resulting from high stone contents or collapsed macropore structure, elevated pore pressures may result leading to slope or channel head instability.

This result demonstrates the non-unique aspect of simulating complex field conditions with sparse data sets in particular, or distributed-parameter models in general. One means of constraining the interpretation of modeling results is to perform some form of tracer testing. These field techniques provide an independent means of testing assumed distributions of material hydraulic properties.

4. CONCLUSIONS

Working with the available field observations and computational tools, Freeze (1972a, 1972b), Stephenson and Freeze (1974), and Beven (1977) laid a critical foundation for future modeling studies of hillslope hydrologic processes. The study presented here should be viewed as an extension and continuation of these earlier studies. The addition of infiltration partitioning and overland flow capabilities to TRUST serves to improve its usefulness as a tool in hillslope hydrologic studies.

With regard to the effects of different flow paths on runoff generation and pore pressure responses, parametric studies using the Inceptisol soil (run 4) suggest that soil structure as manifest in the form of macropores can enhance the contribution of a soil horizon or geologic material to hillslope discharge. For the cases considered, bedrock seems to have a greater effect on the pore pressure response than on volumetric runoff production. Conductivity contrasts between soil or saprolite and unsaturated bedrock may also serve to cause perched zones of saturation leading to lateral subsurface runoff. Based on slug test data from Caspar Creek, saprolite may have higher hydraulic conductivity than the underlying bedrock, but insufficient data from other studies exist to draw conclusions regarding its larger importance in subsurface processes.

Hydraulic diffusivity, including both conductance and capacitance, appears to be a potentially important predictor of the runoff generation ability of a given soil or geologic material, and of pore pressure responsiveness. The results of this study concerning

hydraulic diffusivity suggest that the storage properties of soil and geologic materials are more important than previous studies would indicate. Considering conductive and storative properties together in the context of hydraulic diffusivity provides a very strong conceptual basis for studying transient flow in upland watersheds. This raises a challenge to develop new methods for estimating hydraulic diffusivity in remote mountainous terrain. Most of the existing aquifer testing methods that provide estimates of specific storage are not designed to handle sloping aquifers. Research is needed to determine if techniques for testing soil mechanical (compressibility) and physical (saturation) properties can provide an acceptable basis far estimating specific storage.

Similar to the findings of previous studies, the effects of antecedent moisture conditions were observed to be important in determining which of the flow paths may dominate rainfall-runoff and rainfall-pore pressure linkages. One example is the manner in which a relatively low tension (-0.5 m) served to limit the role of bedrock in conducting flow. In the wedge-shaped slope simulation (run 15) with hydrostatic initial conditions, otherwise large discharge rates produced by convergent flows were reduced by nearly two orders of magnitude. In this case, runoff generation was entirely by subsurface stormflow, versus predominantly saturation overland flow for the case with wet initial conditions (run 14).

From the parametric studies, it appears that channel bank geometry and structural heterogeneities are two critical factors in determining whether subsurface storm flow or saturation overland flow will be the dominant streamflow generation process. For the cases considered, the overall discharge rate is not significantly different if the saturation

overland flow does not reach the stream directly. However, the muting of significant flow through the seepage face might affect bank stability and solute transport to the stream. Subsurface storm flow can provide significant runoff on an annual basis under physically-realistic conditions similar to the ones considered here.

In the context of theoretical studies of transient flow through the soil matrix, macropores, saprolite, and bedrock, it is possible to define a time-scale of response based on material properties, particularly hydraulic diffusivity. The response time scale, like hydraulic diffusivity is highly dependent on antecedent moisture conditions. This is particularly true in types of bedrock with strongly nonlinear hydraulic properties similar to the hypothetical ones considered in this study.

5. FUTURE RESEARCH NEEDS

Field Research

1. Soil and rock hydraulic properties should be mapped along hillslope gradients with particular emphasis on streamside (riparian) zones.
2. More field measurements are needed of bedrock hydraulic properties and flow phenomena in upland watersheds.
3. Spatial variability studies comparable to the ones performed in agricultural fields should be conducted in upland non-agricultural watersheds.
4. Additional data gathering at the field sites considered in this study should focus on measurements of soil and saprolite hydraulic properties for the purposes of additional simulations.

Computational Research

1. Additional simulations should be performed with a time-varying boundary condition at the downstream/channel boundary, greater rainfall intensities, and different slope shapes.
2. Simulations of channel heads of height between 0.8 m and 2.0 m should be performed to identify controls on over-pressuring in surficial channel beds.
3. Channel head simulations should be performed on variable-angle slopes.
4. Fully three-dimensional simulations of flow in convergent slopes should be conducted to study the effects of heterogeneities on runoff and pore pressure responses.

6. REFERENCES CITED

Abrahams, A.D. and A.J. Parsons, 1990. Resistance to overland flow on desert pavement and its implications for sediment transport modeling, Water Resour. Res., 27:8, pp. 1827-1836.

Abrahams, A.D., A.J. Parsons, and J. Wainwright, 1994. Resistance to overland flow on semiarid grassland and shrubland hillslopes, Walnut Gulch, southern Arizona, J. Hydrol., 156, pp. 431-446.

Alexander, E.B., J.1. Mallory, and W.L. Colwell, 1993. Soil-elevation relationships on a volcanic plateau in the Southern Cascade Range, Northern California, U.S.A., Catena, 20, pp. 113-128.

Amerman, C.R., 1965. The use of unit-source watershed data for runoff prediction, Water Resour. Res., 1, 499-507.

Anderson, M.G. and T.P. Burt, 1978. The role of topography in controlling throughflow, Ear. Surf. Proc., 3, pp. 331-344.

Anderson and Burt, 1990. Hydrological forecasting, John Wiley and Sons, Inc., New York, NY.

Arnett, R.R., 1976. Some pedological features affecting the permeability of hillside soils in Caydale, Yorkshire, Earth Surf. Proc., 1, pp. 3-16.

Auberdn, G.M., 1971. Nature and extent of macropores in forest soils and their influence on subsurface water movement, USDA Forest Service Res. Pap. NE-192, NE For. Exp. Sta., Upper Darby, PA., 33 pp.

Barenblatt, G.E., I.P Zheltov, and I.N. Kochina, 1960. Basic concepts in the theory of homogeneous liquids in fissured rocks, J. Appl. Math. Mech. Engl. Transl., 24:5. pp. 1286-1303.

Beasley, R.S., 1976. Contribution of subsurface flow from the upper slopes of forested watersheds to channel flow, Soil Sci. Soc. Am. J., 40, 955-957.

Betson, R.P., 1964. ‘What is watershed runoff?’, J. Geophys. Res., 69, 1541-1552.

Beven, K.J., 1977. Hillslope hydrographs by the finite element method, Earth Surf. Proc., 2, pp. 13-28.

Beven, K.J., 1979. Experiments with a finite element model of hillslope hydrology - The effect of topography, In: Surface and Subsurface Hydrology, H. J. Morel-Seytoux, ed., Water Resources Publications, Fort Collins, Colorado, pp. 37-51.

Beven, K.J., 1981a. Kinematic subsurface flow, Water Resour. Res., 17:5, pp. 1419-1424.

Beven, K.J., 1981b. Micro-, meso-, macroporosity and channeling flow phenomena in soils', Soil Sci. Soc. Am. J., 45, pp. 1247.

Beven, K.J., 1982. On kinematic subsurface stormflow: Predictions with simple kinematic theory for saturated and unsaturated flows, Water Resour. Res., 18:6, pp. 1627-1633.

Beven, K.J., 1986. Runoff production and flood frequency in catchments of order *n*: An alternative approach, In: Gupta, V.K., I. Rodriguez-Iturbe, and E.F. Wood, eds., Scale Problems in Hydrology, Reidel, Dordrecht, pp. 107-131.

Beven, K.J., 1989. Changing ideas in hydrology - The case of physically-based models, J. Hydrol., 105, pp. 157-172.

Beven, K.J. and M.J. Kirkby, 1979. A physically-based, variable contributing area model of basin hydrology, Hydrol. Sci. Bull., 24, pp. 43-69.

Beven, K.J. and Germann, P., 1981. Water flow in soil macropore. i and II., J. Soil Sci., 32, pp. 1-29.

Beven, K.J. and Germann, P., 1982. Macropores and water flow in soils, Water Resour. Res., 18:5, pp. 1311-1325.

Beven, K.J., E.F. Wood, and S. Murugesu, 1988. On hydrological heterogeneity - catchment morphology and catchment response, J. Hydrol., 100, pp. 353-375.

Bilby, R.E. and G.E. Likens, 1980. Importance of organic debris dams in the structure and function of stream ecosystems, Ecology, 61:5, 1107-1113.

Birkeland, P.W., 1984. Soils and geomorphology, Oxford Press, New York, NY, pp. 234-259.

Bonell, M., 1993. Progress in the understanding of runoff generation dynamics in forests, J. Hydrol., 150, pp. 217-275.

Bormann, F.H. and G.E. Likens, 1967. Nutrient cycling, Science, 155(3761), pp. 424-429.

Bouma, J., 1981. Comment on 'Micro-, meso-, and macroporosity of soil', Soil Sci. Soc. Am. J., 45, pp. 1244-1245.

Bouma, J. and L.W. Dekker, 1978. A case study on infiltration into dry clay soil, I. Morphological observations, Geoderma, 20, pp. 27-4.0.

Bouma, J. and F.D. Hole 1971. Soil structure: Conductivity of adjacent virgin and cultivated pedons at two sites: A Typic Argiudoll (silt loam) and a Typic Eutrochrept (clay), Soil Sci. Soc. Am. Proc., 35, pp. 316-319.

Bourna J. and J.H.M. Wosten, 1979. Flow patterns during extended saturated flow in two, undisturbed swelling clay soils with different macrostructures, Soil Sci. Soc. Am. J., 43, pp. 16-22.

Bouwer, H. and R.C. Rice, 1976. A slug test for determining hydraulic conductivity of unconfined aquifers with completely or partially penetrating wells. Water Resour. Res., 12(3), 423-428.

Brewer, R., 1974. Fabric and mineral analysis of soils, John Wiley and Sons, Inc., New York, NY, pp. 179-204.

Brown, D.L. T.N. Narasimhan, and Z. Demir, 1995. An evaluation of the Bouwer and Rice method of slug test analysis, Water Resour. Res., accepted for publication.

Buckingham, E., 1907. Studies on the movement of soil moisture, Bur. of Soils Bull. 38, U.S. Dept. of Agric., Washington, D.C.

Buol, S.W. and S.B. Weed, 1991. Saprolite-soil transformations in the Piedmont and Mountains of North Carolina, Geoderma, 51, pp. 15-28.

Burdine, N.T., 1953. Relative permeability calculations from pore-size distribution data, Trans. ADVIE, 198, pp. 71-77.

California Department of Forestry, 1985. Unpublished soil survey, Ft. Bragg, CA.

Cedarholm, D., 1994. Dominant soil water pathways on a northern New England forested hillslope, unpub. M.S. Thesis, Univ. New Hampshire, Durham, NH, 177 pp.

Chamberlin, T.W., 1972. Interflow in the mountainous forest soils of coastal British Columbia, In: Slaymaker, H.O. and H.J. McPherson, ed., Mountain

Geomorphology: Geomorphological Proc. in the Canadian Cordillera, Tantalus Res. Ltd., Vancouver, Canada, pp. 121-127.

Chapman, T., 1994. Comment on "How much complexity is warranted in a rainfall-runoff model?" by A.J. Jakeman and G.M. Hornberger, Water Resour. Res., 30:12, p. 3565.

Chorley, R.J.,1978. The hillslope hydrologic cycle, In: Hillslope hydrology, Kirkby, M.J., ed., John Wiley & Sons, New York, NY, pp. 1-42.

Chorley, R.J., 1978. Glossary of terms, In: Hillslope hydrology, Kirkby, M.1., ed., John Wiley & Sons, New York, NY, pp. 365-375.

Clapp, R.B. and G.M. Homberger, 1978. Empirical equations for soil hydraulic properties, Water Resour. Res., 14, pp. 601-604.

Crawford, N.H. and R.K. Linsley, 1966. Digital simulation in hydrology - Stanford watershed model IV, Tech. Rep. No. 39, Dept. Civil Engr., Stanford Univ., Palo Alto, CA.

Darcy, H., 1856. Les fotaines publiques de la Ville de Dijon, Dalmont, Paris.

DeVries, J. and T.L. Chow, 1978. Hydrologic behaviour of a forested mountain soil in Coastal British Columbia, Water Resour. Res., 14:5, pp. 935-942.

Dietrich, W.E. and T. Dunne, 1993. The channel head, In: Beven, K. and M.J. Kirkby, ed., Channel Network Hydrology, John Wiley and Sons, Chichester, England, pp. 175-219.

Dietrich, W.E., C.J. Wilson and S.L. Reneau, 1986. Hollows, colluvium, and landslides in soil-mantled landscapes, In: Hillslope Processes, A. D. Abrahams, ed., Allen & Unwin Ltd., pp. 361-388.

Dietrich, W.E., C.J. Wilson, D.R. Montgomery, and J. McKean, 1993. Analysis of erosion thresholds, channel networks, and landscape morphology suing a digital terrain model, J. Geol., 101, pp. 259-278.

Domenico, P.A. and F.W. Schwartz, 1990. Physical and chemical hydrogeology, John Wiley & Sons, New York, NY, pp. 83-88.

Duff, I.S., 1977. MA28 - A set of FORTRAN subroutines for sparse unsymmetric linear equations. AERE Harwell Report R 8730, Oxfordshire, U.K., 153 pp.

Dunne, T., 1978. Field studies of hillslope flow processes, In: Hillslope hydrology, Kirkby, M.J., ed., John Wiley & Sons, New York, NY, pp. 227-293.

Dunne, T., 1990. Hydrology, mechanics and geomorphic implications of erosion by subsurface flow, In: Ground Water Geomorphology: The role of subsurface water in Earth-surface processes and landforms, C.G. Higgins and D.R: Coates, eds., Geol. Soc. Amer. Spec. Paper 252.

Dunne T. and R.D. Black, 1970a. An experimental investigation of runoff production in permeable soils, Water Resour. Res., 6, pp. 478-490.

Dunne T. and R.D. Black, 1970b. Partial area contributions to storm runoff in a small New England watershed, Water Resour. Res., 6, pp. 1296-1311.

Dunne, T. and W.E. Dietrich, 1980a. Experimental investigation of Horton overland flow on tropical hillslopes: 1. Soil conditions, infiltration, and frequency of runoff, Z. Geornorph. N.F., Suppl.-Bd. 35, pp. 40-59.

Dunne, T. and W.E. Dietrich, 1980b. Experimental investigation of Horton overland flow on tropical hillslopes: 2. Hydraulic characteristics and hillslope hydrographs, Z. Geomorph. N.F., Suppl.-Bd. 35, pp. 60-80.

Dunne, T., W. Zhang, and B.F. Aubry, 1991. Effects of rainfall, vegetation and microtopography on infiltration and runoff, Water Resour. Res., 27, pp. 2271-2285.

Edwards, A.L., 1968. TRUMP: A computer program for transient and steady-state temperature distributions in multidimensional systems, Nat. Tech. Infor. Serv., UCRL 14754, Rev. II, Springfield, VA, 265 pp.

Emmett, W.W., 1970. The hydraulics of overland flow on hillslopes, U.S. Geol. Survey Prof. Paper 662A, 68 pp.

Federer, C.A., 1992. Soil water properties and data for the Hubbard Brook Experimental Forest, unpub. USDA Forest Service rep., 11 pp.

Forster, H., 1993. Properties, dynamics and association of soils on high elevations of the Bavarian Forest (Germany) as illustrated by a toposequence on gneiss debris, Catena, 20, pp. 563-579.

Freeze, R.A., 1972a. Role of subsurface flow in generating surface runoff 1. Base flow contributions to channel flow, Water Resour. Res., 8, pp. 609-623.

Freeze, R.A., 1972b. Role of subsurface flow in generating surface runoff 2. Upstrean source areas, Water Resour. Res., 8, pp. 1272-1283.

Freeze, R.A., 1974. Streamflow Generation, Reviews of Geophysics and Space Physics 12, pp. 627-647.

Freeze, R.A., 1978. Mathematical models of hillslope hydrology, In: Hillslope hydrology Kirkby, M.J., ed., John Wiley & Sons, New York, NY, pp. 177-225.

Freeze, R.A., 1980. A stochastic-conceptual analysis of rainfall-runoff processes on a hillslope, Water Resour. Res., 16:2, pp. 391-408.

Gaiser, R.N., 1952. Root channels and roots in forest soils, Soil Sci. Soc. Am. Proc 16:1, pp. 62-65.

Gee, G.W., C.T. Kincaid, R.J. Lehnard, and C.S. Simmons, 1991. Recent studies of flow and transport in the vadose zone, In: Shea, M.A., ed., Rev. of Geophys., Suppl.. U.S. Natl. Rep. to Int. Union of Geodesy and Geophys. 1987-1990, Am Geophys. Union, pp. 227-239.

Germann, P.F. and K. Beven, 1981a. Water flow in soil macropores: I. An experimental approach, J. Soil Sci., 32, pp. 1-13.

Germann, P.F. and K. Beven, 1981b. Water flow in soil macropores: II. A combined flow model, J. Soil Sci., 32, pp. 15-29.

Germann, P.F. and K. Beven, 1985. Kinematic wave approximation to infiltration into soils with sorbing macropores, Water Resour. Res., 21:7, pp. 990-996.

Germann, P.F., R.S. Pierce, and K. Beven, 1986. Kinematic wave approximation to the initiation of subsurface stormflow in a sloping forest soil, Adv. Water Resour., 9:2, pp. 70-76.

Germann, P.F., M.S. Smith, and G.S. Thomas, 1987. Kinematic wave approximation to the transport of *Escherichia coli* in the vadose zone, Water Resour. Res., 23, 1281-1287.

Goodrich, D.C. and D.A. Woolhiser, 1991. Catchment hydrology, In: Shea, M.A., ed., Rev. of Geophys., Suppl., U.S. Natl. Rep. to Int. Union of Geodesy and Geophys. 1987-1990, Am. Geophys. Union, pp. 202-209.

Gupta, V., E. Waymire, and C. Wang, 1980. A representation of an instantaneous unit hydrograph from geomorphology, Water Resour. Res., 16:5, pp. 855-862.

Hammermeister, D.P., G.F. Kling, and J.A. Vomocil, 1982. Perched water tables on hillsides in Western Oregon: II. Preferential downslope movement of water and anions, Soil Sci. Soc. Am. J., 46, pp. 819-826.

Henderson, F.M. and R.A. Wooding, 1964. Overland flow and groundwater flow from a steady rainfall of finite duration, J. Geophys. Res., 69,1531-1540.

Hewlett, J.D., 1961. Soil moisture as a source of baseflow from steep mountain watersheds, U.S. Forest Service. Southeast. Forest Exp. Sta., Res. Pap. SE 132, 11 pp.

Hewlett, J.D. and A.R. Hibbert, 1967. Factors affecting the response of mall watersheds to precipitation in humid areas, In: Proc. of the Int. Symp. on Forest Hydrol. (1965), Pennsylvania St. Univ., Pergammon, pp. 275-290.

Hewlett, J.D., 1974. Comments on letters relating to 'Role of subsurface flow in generating surface runoff, 2, Upstream source area' by R.A. Freeze, Water Resour. Res., 10:3, pp. 605-607.

Hillel, D., 1980a. Fundamentals of soil physics, Academic Press, New York, NY, pp. 93-119.

Hillel, D., 1980b. Applications of soil physics, Academic Press, New York, NY, p. 43.

Hinton, M.J., S.L. Schiff, and M.C. English, 1993. Physical properties governing groundwater flow in a glacial till catchment, J. Hydrol., 142, pp. 229-249.

Hodge, R.A.L. and R.A. Freeze, 1977. Groundwater flow systems and slope stability, Can. Geotech. J., 14, pp. 466-476.

Horton, R.E., 1933. The role of infiltration in the hydrologic cycle, Trans. Am. Geophys. Union, 14, pp. 446-460.

Huff, T.L., D.W. Smith, and W.R. Powell, 1985. Tables for the soil-vegetation map, Jackson State Forest, Mendocino County, Soil-Vegetation Surv., Calif. Dept. of Forestry, The Resources Agency, Sacramento, CA.

Humphrey, N.F., 1982. Pore pressures in debris failure initiation, unpub. M.S. Thesis, Univ. Washington, Seattle, WA, 168 pp.

Hursh, C.R., 1936. Storm-water and absorption, in 'Discussion on list of terms with definitions; Report of the Committee on Absorption and Transpiration', Trans. Am. Geophys. Union, 17, pp. 301-302.

Hursh, C.R. and E.F. Brater, 1941. Separating storm hydrographs from small drainage areas into surface and subsurface flow, Trans. Am. Geophys. Union, 14, pp. 446-460.

Hursh, C.R., 1944. Subsurface flow, App. B - Report of the Comm. on Subsurface Flow, Trans. Am. Geophys. Union, pp. 743-746.

Eda, T., 1984. A hydrological method of estimation of the topographic effect on the saturated throughflow, Trans. Japanese Geomorph. Union, 2, 67-72.

Iverson, R.M. and J.J. Major, 1986. Groundwater seepage vectors and the potential for hillslope failure and debris flow mobilization, Water Resour. Res., 22:11, pp. 1543-1548.

Jackson, C.R. and T.W. Cundy, 1992. A model of transient, topographically driven, saturated subsurface flow, Water Resour. Res., 28:5, pp. 1417-1427.

Jenny, H., 1941. Factors of soil formation, McGraw-Hill, New York, NY.

Jenny, H., 1980. The soil resource: Origin and behavior, Ecol. Studies 37, Springer-Verlag, New York, NY.

Jones, A.J.J., 1971. Soil piping and stream initiation, Water Resour. Res., 7, pp. 602-610.

Keppeler, E.T. and P.H. Cafferata, 1991. Hillslope hydrology research at Caspar Creek, JDSF Newsletter, California Dept. of Forestry, Fort Bragg, No. 41, April, pp. 4-8.

Kirkby, M.J., 1978. Hillslope hydrology, John Wiley & Sons, New York, NY, 389 pp.

Kunkle, G.R., 1965. Computation of ground-water discharge to streams during floods, or to individual reaches during base flow, by use of specific conductance, U.S. Geol. Surv., Prof. Pap. 525-D, D207-D210.

Larsen, J.E., M. Sivapalan, N.A. Coles, and P.E. Linnet, 1994, Similarity analysis of runoff generation processes in real-world catchments, Water Resour. Res., 30:6, pp. 1641-1652.

Lawrence, G.B., R.D. Fuller, and C.T. Driscoll, 1986. Spatial relationships of aluminum chemistry in the streams of the Hubbard Brook Experimental Forest, New Hampshire, Biogeochemistry, 2, pp. 115-135.

Levy, B.S. and P.F. Germann, 1987. Kinematic wave approximation to solute transport along preferred flow paths in soils, J. Contam. Hydrol., 3, 263-276.

Liakopoulos, A.C., 1965. Retention and distribution of moisture in soils after infiltration has ceased, Bull. Int. Ass. Sci. Hydrol., 10(2), pp. 58-69.

Likens, G.E. and F.H. Bormann, 1974. Linkages between terrestrial and aquatic ecosystems, Biosci., 24, pp. 447-456.

Loague, K.M., 1988. Impact of rainfall and soil hydraulic property information on runoff predictions at the hillslope scale, Water Resour. Res., 24:9, pp. 1501-1510.

Loague, K.M. and R.A. Freeze, 1985. A comparison of rainfall-runoff modeling techniques on small upland catchments, Water Resour. Res., 21:2, 229-248.

Luxmoore, R.J., 1981. Micro-, meso-, and macroporosity of soil, Soil Sci. Soc. Am. J., 45, pp. 671-672.

Martin, C.W., 1979. Precipitation and streamwater chemistry in an undisturbed forested watershed in New Hampshire, Ecol., 60:1, pp. 36-42.

McCaig, M., 1983. Contributions to storm quickflow in a small headwater catchment - The role of natural pipes and soil macropores, Earth Surf. Proc. and Landforms, 8, pp. 239-252.

McColl, J.G. and A.E. McGrath, 1992. Soil reactions with natural and synthetic organic compounds, Proc. 13th Ann. Forest Veg. Mgmt. Conf., Jan. 14-16, 1992, Eureka, CA, pp. 64-77.

McDonnell, J.J., 1990a. The influence of macropores on debris flow initiation, Q. J. Eng. Geol. London, 23, pp. 325-331.

McDonnell, J.J., 1990b. A rationale for old water discharge through macropores in a steep, humid catchment, Water Resour. Res., 26:11, pp. 2821-2832.

Megahan, W.F. and J.L. Clayton, 1983. Tracing subsurface flow on roadcuts on steep, forested slopes, Soil Sci. Soc. Am. J., 47:6, pp. 1063-1067.

Megahan, W.F. and J.L. Clayton, 1986. Saturated hydraulic conductivities of granitic materials of the Idaho batholith, J. Hydrol., 84, pp. 167-180.

Milne, G., 1935. Some suggested units of classification and mapping particularly for East African soils, Soil Res., 4:3, 183-198.

Montgomery, D.R., W.E. Dietrich, R. Torres, S.P. Anderson, J.T. Heffner, K.O. Sullivan, and K. Loague, 1990. Hydrologic experiments in a steep unchanneled valley: 1. Experimental design and piezometric response, EOS, Trans. Am. Geophys. Union, 71, p. 1342.

Montgomery, D.R., 1991. Channel initiation and landscape evolution, unpub. PhD. dis., Univ. of California, Berkeley, California, 421 pp.

Montgomery, D.R. and W.E. Dietrich, 1989. Source areas, drainage density, and channel initiation, Water Resour. Res., 25:8, pp. 1907-1918.

Montgomery, D.R. and W.E. Dietrich, 1994. A physically based model for the topographic control on shallow landsliding, Water Resour. Res., 30:4, pp. 1153-1171.

Montgomery, D.R. and W.E. Dietrich, 1995. Hydrologic processes in a low-gradient source area, Water Resour. Res., 31:1, pp. 1-10.

Moore, I.D., S.M. Mackay, P.J. Wallbrink, G.J. Burch, and E.M. O'Loughlin, 1986. Hydrologic characteristics and modeling of a small forested catchment in south-eastern New South Wales, pre-logging condition, J. Hydrol., 83, 307-355.

Moore, I.D., R.B. Grayson, and A.R. Ladson, 1991. Digital terrain modeling: A review of hydrological, geomorphological, and biological applications, Hydrol. Proc., 5, pp. 3-30.

Moreno, L., I. Neretnieks, and T. Eriksen, 1985. Analysis of some laboratory tracer runs in natural fissures, Water Resour. Res., 21:7, pp. 951-958.

Moridis, G., K. Pruess, and E. Antunez, 1994. T2CG1, A package of preconditioned conjugate gradient solvers for TOUGH2, unpublished report, Lawrence Berkeley Lab., Berkeley, CA, 18 pp.

Morris, E.M. and D.A. Woolhiser, 1980. Unsteady, one-dimensional flow over a plane: Partial equilibrium and recession hydrographs, Water Resour. Res., 16:2, pp. 355-360.

Mosley, M.P., 1979. Streamflow generation in forested watershed, New Zealand, Water Resour. Res., 15:4, pp. 795-806.

Mosley, M.P., 1982. Subsurface flow velocities through selected forest soils, South Island, New Zealand, J. Hydrol., 55, 65-92.

Mualem, Y., 1976. A new model for predicting the hydraulic conductivity of unsaturated porous media, Water Resour. Res., 10, pp. 514-520.

Narasimhan, T.N. and P.A. Witherspoon, 1976. An integrated finite difference method for analyzing fluid flow in porous media, Water Resour. Res., 12:1, pp. 57-64.

Narasimhan, T.N. and P.A. Witherspoon, 1977. Numerical model for saturated-unsaturated flow in deformable porous media: 1. Theory, Water Resour. Res., 13:3, pp. 657-664.

Narasimhan, T.N., P.A. Witherspoon, and A.L. Edwards, 1978. Numerical model for saturated-unsaturated flow in defornyable porous media: 2. The Algorithm, Water Resour. Res., 14:2, pp. 255-261.

Narasimhan, T.N. and P.A. Witherspoon, 1978. Numerical model for saturated-unsaturated flow in deformable porous media: 3. Applications, Water Resour. Res., 14:6, pp. 1017-1034.

Narasimhan, T.N., 1985. Geometry-imbedded Law and transient subsurface flow, Water Resour. Res., 21:8, pp. 1285-1292.

Nieber, J.L. and G.S. Warner, 1991. Soil pipe contribution to steady subsurface stormflow, Hydrol. Proc., 5, pp. 329-344.

Okimura, T. and R. Ichikawa, 1985. A prediction method for surface failures by movement of infiltrated water in a surface soil layer, Nat. Disaster Sci., 7, pp. 41-51.

O'Loughlin, E.M., 1986. Prediction of surface saturation zones in natural catchments by topographic analysis, Water Resour. Res., 22:5, 794-804.

Othmer, H., B. Diekkruger, and M. Kutilek, 1991. Bimodal porosity and unsaturated hydraulic conductivity, Soil Sci.,152:3, pp. 139-150.

Pearce, A.J., M.K. Stewart, and M.G. Skalsh, 1986. Storm runoff in humid headwater catchments, 1. Where does the water come from?, Water Resour. Res., 22, pp. 1263-1272.

Philip, J.R., 1957a. The theory of infiltration: 1. The infiltration equation and its solution, Soil Sci., 83, 345-357.

Philip, J.R., 1957b. The theory of infiltration: 4. Sorptivity and algebraic infiltration equations, Soil Sci., 84, 257-264.

Philip, J.R., 1969. Theory of infiltration, Advan. Hydroscience, 5, pp. 215-296.

Philip, J.R., J.H. Knight, R.T. Waechter, 1989. Unsaturated seepage and subterranean holes: Conspectus, and exclusion problem for circular cylindrical cavities, Water Resour. Res., 25, pp. 16-28.

Pierson, T.C., 1983. Soil pipes and slope stability, Q. J. Eng. Geol. London, 16, pp. 1-11.

Pilgrim, D.H., D.D. Huff, and T.D. Steele, 1978. A field evaluation of subsurface and surface runoff, II. Runoff process, J. Hydrol., 38, pp. 319-341.

Pinder, G.F. and J.F. Jones, 1968. Determination of the ground-water component of peak discharge from the chemistry of total runoff, Water Resour. Res., 5, pp. 438-445.

Ragan, R.M., 1968. An experimental investigation of partial area contributions, Proc. Gen. Assem., Internat. Assoc. Sci. Hydrology, Berne, Publ. 76, pp. 241-249.

Rahe, T.M., C. Hagedorn, E.L. McCoy, and G.F.Kling, 1978. Transport of antibiotic-resistant *Escherichia coli* through Western Oregon hillslope soils under conditions of saturated flow, J. Environ. Qual., 7:4, 487-494.

Reid, M.E., H.P. Nielsen, and S.J. Dreiss, 1988. Hydrologic factors triggering a shallow hillslope failure, Bull. Assoc. of Eng. Geologists, 3, 349-361.

Rice, T.J., S.W. Buol, and S.B. Weed, 1985. Soil-saprolite profiles derived from mafic rocks in the North Carolina Piedmont: I. Chemical, morphological, and mineralogic characteristics and transformations, Soil Sci. Soc. Am. J., 49, pp. 171-178.

Richardson, J.R. and P.Y. Julien, 1994. Suitability of simplified overland flow equations, Water Resour. Res., 30:3, pp. 665-671.

Ritter, D.F., 1978. Process geomorphology, W.C. Brown, Dubuque, IA, 603 pp.

Rodriguez-Iturbe, I. and J. Váldes, 1979. The geomorphologic structure of the hydrologic response, Water Resour. Res., 15:6, pp. 1409-1420.

Ross, D.S., R.J. Bartlett, and F.R. Magdoff, 1994. Flow path studies in forested watersheds of headwater tributaries of Brush Brook, Vermont, Water Resour. Res., 30:9, pp. 2611-2618.

Rubin, J. and R. Steinhardt, 1963. Soil-water relations during rain infiltration, I. Theory, Soil Sci. Soc. Am. Proc., 27, pp. 246-251.

Schoeneberger, P. and A. Amoozegar, 1990. Directional saturated hydraulic conductivity and macropore morphology of soil-saprolite sequence, Geoderma, 46, 31-4.9.

Selby, M.J., 1982. Hillslope materials and processes, Oxford Univ. Press, Oxford, pp. 131-135.

Shanley, J.B., C. Kendall, T.E. Smith, and D.M. Wolock, in press. The effect of catchment size and land cover on the contributions of meltwater to stream discharge during snowmelt in a Vermont watershed, submitted to Water Resour. Res.

Shapiro, A.M., 1989. Interpretation of oscillatory water levels in observation wells during aquifer tests in fractured rock, Water Resour. Res., 25:10, pp. 2129-2137.

Shattuck, P.C., 1991. Shallow water-table response to precipitation and evapotranspiration in an ephemeral stream valley, Woodstock, New Hampshire, unpub. M.S. thesis, Univ. New Hampshire, Durham, NH, 113 pp.

Sidle, R.C. and D.N. Swanston, 1981. Analysis of a small debris slide in coastal Alaska, Can. Geotech. J., 19, pp. 167-174.

Sidle, R.C. and Y. Tsuboyama, 1992. A comparison of piezometric response in unchanneled hillslope hollows: Coastal Alaska and Japan, J. Japan Soc. Hydroi. & Water Resour., 5(3):3-11.

Sivapalan, M., K. Beven, and E.F. Wood, 1987. On hydrologic similarity, 2. A scaled model for storm runoff production, Water Resour. Res., 23:12, pp. 2266-2278.

Sivapalan, M., E.F. Wood, and K. Beven, 1990. On hydrologic similarity, 3. A dimensionless flood frequency model using a generalized geomorphologic unit hydrograph and partial area runoff generation, Water Resour. Res., 26:1, pp. 43-58.

Sklash, M.G., 1990. Environmental isotope studies of storm and snowmelt runoff generation, In: Surface and Subsurface Processes in Hydrology, M. G. Anderson and T.P. Burt, ed., John Wiley and Sons, Ltd., Sussex, England.

Sklash, M.G. and R.N. Farvolden, 1979. The role of groundwater in storm runoff, J. Hydrol., 43, pp. 45-65.

Skalsh, M.G., M.K. Stewart, and A.J. Pearce, 1986. Storm runoff in humid headwater catchments, 2. A case study of hillslope and low-order stream response, Water Resour. Res., 22, pp. 1273-1282.

Skopp, J., 1981. Comment on 'Micro-, meso-, and macroporosity of soil', Soil Sci. Soc. Am. J., 45, pp. 1246.

Smettem, K.R.J. and S.T. Trudgill, 1983. An evaluation of fluorescent and non-fluorescent dyes in the identification of water transmission routes in soils, J. Soil Sci., 34, 45-65.

Smettem, K.R.J., D.J. Chittleborough, B.G. Richards, and F.W. Leaney, 1991. The influence of macropores on runoff generation from a hillslope soil with a contrasting textural class, J. Hydrol., 122, pp. 235-252.

Smith, R.E. and R.H.B. Hebbert, 1983. Mathematical simulation of interdependent surface and subsurface hydrologic processes, Water Resour. Res., 19, pp. 987-1001.

Smith, R.E. and J.-Y. Parlange, 1978. A parameter-efficient hydrologic infiltration model, Water Resour. Res., 14, pp. 533-538.

Smith, R.E. and D.A. Woolhiser, 1971. Overland flow on an infiltrating surface, Water Resour. Res., 7:4, 899-913.

Stephenson G.R. and R.A. Freeze, 1974. Mathematical simulation of subsurface flow contributions to snowmelt runoff, Reynolds Creek Watershed, Idaho, Water Resour. Res., 10, pp. 284-294.

Stresky, S.J., 1991. Morphology and flow characteristics of pipes in a forested New England hillslope, unpub. M.S. Thesis, Univ. New Hampshire, Durham, NH, 131 pp.

Swanson, D.K., 1985. Soil catenas on Pinedale and Bull Lake moraines, Willow Lake, Wind River Mountains, Wyoming, Catena, 12, pp. 329-342.

Swistock, B.R., D.R. DeWalle, W.E. Sharpe, 1989. Sources of acidic storm flow in an Appalachian head water stream, Water Resour. Res., 25:10, pp. 2139-2147.

Taylor, G.S. and J.N. Luthin, 1969. Computer methods for transient analysis of water table aquifers, Water Resour. Res., 5, p. 144.

Tilley F.B. and R.M. Rice, 1977. Caspar Creek Watershed study: A current status report, State Forest Notes, 66, Calif. Div. Forestry, Sacramento, CA, 15 pp.

Tsuboyama, Y., R.C. Sidle, S. Noguchi, and I. Hosoda, 1994. Flow and solute transport through the soil matrix and macropores of a hillslope segment, Water Resour. Res., 30:4, pp. 879-890.

U.S. Forest Service, 1991. The Hubbard Brook Ecosystem Study: Site description and research activities, Rep. NE-NF-96-91, NE Forest Exper. Sta., Durham, NH, 61 pp.

Ursic, S.J. and R.J. Esher, 1988. Influence of small mammals on stormflow responses of pine-covered catchments, Water Resour. Bull., 24:1, pp. 133-139.

van Genuchten, M.Th., 1980. A closed-form equation for predicting the hydraulic conductivity of unsaturated soils, Soil Sci. Soc. Am. J., 44, pp. 892-898.

Vepraskas, M.J., M.T. Hoover, and J. Bouma, 1991. Sampling strategies for assessing hydraulic conductivity and water-conducting voids in saprolite, Soil Sci. Soc. Am. J., 55, pp. 165-170.

Vepraskas, M.J., A.G. Jongmans, M.T. Hoover, and J. Bouma, 1991. Hydraulic conductivity of saprolite as determined by channels and porous groundmass, Soil Sci. Soc. Am. J., 55, pp. 932-938.

Wang, C. and G.J. Ross, 1989. Granitic saprolites: their characteristics, identification and influence on soil properties in the Appalachian region of Canada. Z. Geomorph. N.F., Suppl.-Bd. 72, pp. 149-161.

Wang, J.S.Y., 1991. Flow and transport in fractured rock, In: Shea, M.A., ed., Rev. of Geophys., Suppl., U.S. Natl. Rep. to Int. Union of Geodesy and Geophys. 19871990, Am. Geophys. Union, pp. 254-262.

Wang, J.S.Y. and T.N. Narasimhan, 1985. Hydrologic mechanisms governing fluid flow in a partially saturated, fractured porous medium, Water Resour. Res., 21, pp. 1861-1874.

Welby, C.W., 1992. Field investigation of hydraulic conductivity in saprolitic materials Comparison of methods and techniques, Bull. Assoc. of Eng. Geologists, 29:2, pp. 119-130.

Weyman, D.R., 1973. Measurement of the downslope flow of water in a soil, J. Hydrol., 20, pp. 267-288.

Whipkey, R.Z., 1965. Subsurface stormflow from forested slopes, Bull. Int. Assoc. Sci. Hydrol., 10:2, pp. 74-85.

Whipkey, R.Z., 1967. Theory and mechanics of subsurface stormflow, In: Sopper, W.E. and H.W. Lull, ed., Internat. Syrnp. on Forest Hydrol., Pergammon Press, New York, NY, pp. 255-260.

White, R.E., 1985. The influence of macropores on the transport of dissolved and suspended matter through soil, Adv. in Soil Sci., 3, Springer-Verlag Inc., New York, NY, pp. 95-120.

Wilson, C.J., 1988. Runoff and pore pressure development in hollows, unpub. PhD. dis., Univ. of California, Berkeley, California, 421 pp.

Wilson, C.J. and W.E. Dietrich, 1987. The contribution of bedrock groundwater flow to storm runoff and high pore pressure development in hollows, In: Erosion and Sedimentation in the Pacific Rim, Proc. Corvallis Symp., August, 1987, pp. 49-59.

Wilson, C.J., W.E. Dietrich, and T.N. Narasimhan, 1989. Predicting high pore pressures and saturation overland flow in unchannelled hillslope valleys, Hydrol. and Water Resour. Symp., 23-30 Nov., 1989, Christchurch, New Zealand, pp. 392-398.

Wilson, C.M. and P.L. Smart, 1984. Pipes and pipe flow process in an upland catchment, Wales, Catena, 11, pp. 145-158.

Wilson, G.V., P.M. Jardine, R.J. Luxmoore, L.W. Zelazny, D.A. Lietzke, and D.E. Todd, 1991a. Hydrogeochemical processes controlling subsurface transport from an upper subcatchment of Walker Branch Watershed during storm events. 1. Hydrologic transport processes, J. Hydrol., 123, 297-316.

Wilson, G.V., P.M. Jardine, R.J. Luxmoore, L.W. Zelazny, D.E. Todd, and D.A. Lietzke, 1991b. Hydrogeochemical processes controlling subsurface transport from an upper subcatchment of Walker Branch Watershed during storm events. 2. Solute transport processes, J. Hydrol., 123, 317-336. .

Wilson, G.V., P.M. Jardine, and G.P. Gwo, 1992. Modeling the hydraulic properties of a multiregion soil, Soil Sci. Soc. Am. J., 56, pp. 1731-1737.

Wood, E.F., M. Sivapalan and K. Beven, 1990. Similarity and scale in catchment storm response, Rev. of Geophys., 28, pp. 1-18.

Woolhiser, D.A. and J.A. Liggett, 1967. Unsteady, one-dimensional flow over a plane The rising hydrograph, Water Resour. Res., 3:3, pp. 753-771.

Wosika, E.P., 1981. Hydrologic properties of one major and two minor soil series of the Coast Ranges of Northern California, unpub. M.S. Thes., Humboldt St. Univ., Arcata, CA, 150 pp.

Yee, C.S., 1975. Soil and hydrologic factors affecting stability of natural slopes in the Oregon Coast Range, unpub. Ph.D. Diss., Oregon St. Univ., Corvallis, OR.

Zhang, W. and T.W. Cundy, 1989. Modeling of two-dimensional overland flow, Water Resour. Res., 25:9, pp. 2019-2036.

Ziemer, R.R. and J.S. Albright, 1987. Subsurface pipeflow dynamics of north-coastal California swale systems, In: Erosion and Sedimentation in the Pacific Rim, Proc. Corvallis Symp., August, 1987, pp. 71-80.

TABLE 2.1 Summary of parametric simulations

Run #	Group	Focus	Case	Slope angle	I.C. ψ (m)	B.C. ϕ depth (m)
1	Structural heterogeneities	Soil/macropore horizons (w/ low-k rock)	Del Monte sand	15°	-0.5	1.2
2			Colluvial soil	15°	-0.5	1.2
3			Spodosol	15°	-0.5	1.2
4			Inceptisol	15°	-0.5	1.2
5			Mixed K(ψ), S(ψ)	15°	-0.5	1.2
6		Saprolite (w/ Inceptisol soil and low-k rock)	Thin saprolite	15°	-0.5	1.2
7			Thick saprolite	15°	-0.5	1.2
8			Intermediate saprolite	15°	-0.5	1.2
9			No saprolite	15°	-0.5	1.2
10		Bedrock (w/ Inceptisol soil)	Low-permeability rock	15°	-0.5	1.2
11			High-permeability rock	150	-0.5	1.2
12			Permeability discontinuity	15°	-0.5	1.2
13	Slope geometries	Convergent slopes	2-Materials (Inceptisol soil & low-k rock	15°	-0.5	1.2

TABLE 2.1 Summary of parametric simulations (cont.)

Run #	Group	Focus	Case	Slope angle	I.C. ψ (m)	B.C. ϕ depth (m)
14	Slope geometries	Convergent slopes	3-Materials (Inceptisol soil, saprotite, and low-k rock)	15°	-0.5	1.2
15			3-Materials hydrostatic	15°	ϕ = B.C.	1.2
16		Variable slope angle	Inceptisol/ low-k rock	7.5°	-0.5	1.2
17				15°	-0.5	1.2
18				30°	-0.5	1.2
19			Inceptisol/ high-k rock	7.5°	-0.5	1.2
20				15°	-0.5	1.2
21				30°	-0.5	1.2
22			Colluvial soil/ low-k rock	15°	-0.5	1.2
23				30°	-0.5	1.2
24	Interface topography	Soil thickness	Inceptisol/ low-k rock	15°	-0.5	1.2
25			Inceptisol/ high-k rock	15°	-0.5	1.2
26		Rock thickness	Inceptisol/ low-k rock	15°	-0.5	1.2
27			Inceptisol/ hi h-k rock	15°	-0.5	1.2
28	Initial conditions		"Wet" I.C.	15°	-0.5	1.2
29			"Wet" I.C. (adj. for drainage)	15°	variable	1.2

TABLE 2.1 Summary of parametric simulations (cont.)

Run #	Group	Focus	Case	Slope angle	I.C. ψ (m)	B.C. ϕ depth (m)
30	Initial conditions		Drained I.C.	15°	variable	1.2
31			Hydrostatic	15°	ϕ = B.C.	1.2
32	Boundry conditions (B.C.)	Configuration and B.C. depth	2-Part (Seepage face & constant head)	15°	-0.5	0.05
33				15°	-0.5	0.30
34				15°	-0.5	1.20
35			3-Part (Seepage face, constant head, and no-flow)	15°	-0.5	0.05
36				15°	-0.5	0.30
36a				15°	-0.5	0.80
37				15°	-0.5	1.20
38			100-yr storm	15°	-0.5	1.20
39		Heterogeneities at stream B.C.	Low-k soil in riparian zone	15°	-0.5	0.30
40	Channel head (CH) depth	Silt soil	0.2 m CH	15°	0	
41			0.4 m CH	15°	0	
42			0.8 m CH	15°	0	
43			2.0 m CH	15°	0	
44		Inceptisol	0.2 m CH	15°	0	
45			0.4 m CH	15°	0	
46			0.8 m CH	15°	0	
47			2.0 m CH	15°	0	
51		Bedrock at base of CH	2.0 m CH	15°	0	

TABLE 2.2 Piezometer construction details - M Swale,
Caspar Creek Experimental Watershed

Piez.	Material at screen	Borehole depth (m)[1]	Casing length (m)	Casing riser (m)[2]	Screen length (m)	Borehole radius (m)
A1	saprolite	2.34	2.44	0.10	0.15	0.09
A2	saprolite	2.95	3.23	0.28	0.30	0.07
A3	saprolite	4.93	5.03	0.10	0.30	0.07
B1	saprolite	2.48	3.08	0.60	0.15	0.09
B2		1.12	1.52	0.40	0.30	0.07
B3	saprolite	2.27	2.93	0.66	0.15	0.07
B4	saprolite	3.49	4.12	0.64	0.15	0.07
CO	saprolite	2.10	2.33	0.23	0.15	0.09
C1	saprolite	2.18	2.55	0.38	0.15	0.09
C2	bedrock	3.11	3.68	0.58	0.15	0.07
C3	saprolite	3.70	4.12	0.43	0.30	0.07
C4	saprolite	5.64	6.05	0.45	0.30	0.07

[1] Below ground surface
[2] Above ground surface

TABLE 2.3 Piezometer construction details - UNH Field Site, Hubbard Brook Experimental Forest

Piezometer	Material screened	Borehole depth (m)[1]	Casing length (m)	Casing riser (m)[2]	Screen length (m)	Borehole radius (m)
B11a	soil	0.70	1.53	0.83	0.30	0.07
B11b	lower till	3.83	4.41	0.58	0.30	0.09
B12 (1B)*	soil	1.55	2.39	0.84	0.81	0.05
B13 (2A)*	soil	0.82	1.85	1.03	0.24	0.05
B21 (2B)*	soil	0.66	1.89	1.23	0.24	0.05
B22 (2T)*	lower till	3.44	4.63	1.20	1.42	0.05
B31a (2C)*	soil	0.96	2.08	1.12	0.71	0.05
B31b	lower till	3.08	4.12	1.04	0.30	0.07
B32 (3B)*	soil	0.70	1.90	1.20	0.24	0.05
B33 (3D)*	soil	0.97	1.80	0.83	0.51	0.05
B41 (4C)*	soil	1.33	1.90	0.57	0.61	0.05
B42 (4B)*	soil	0.64	1.66	1.02	0.30	0.05
B43 (04)*	soil	0.77	1.85	1.08	0.24	0.05

(1B)* - Cross reference to piezometer installed by Cedarholm (1994)
[1] - Below ground surface
[2] - Above ground surface

TABLE 3.1 Summary of reported subsurface stormflow discharge rates

Source	Soil texture	Peak discharge per meter width (m^3 /hr)
Beven (1977)		
planar hillslope simulations	loam	0.020-0.218
Freeze (1972b)		
convex hillslope simulations	sand	0.012-0.108
concave hillslope simulations	sand	0.013-0.055
Hewlett and Nutter (1970)*		
Forested watershed	sandy loam	0.044
Whipkey (1969)		
Forested watershed	sandy loam	0.089
Dunne (1969, 1978)		
Forested hillslope converted to pasture	sandy loam	0.110
Dunne (1969, 1978)		
Forested hillslope converted to pasture	sandy loam	0.015
Ragan (1968)		
Forested watershed	sand	0.049

TABLE 3.2 Summary of simulated subsurface stormflow discharge rates

run	Simulation case	Soil texture	Peak discharge per meter width (m^3 /hr)
1	Del Monte Sand (Liakopoulos, 1965)	sand	0.014
2	Colluvial soil (Humphrey, 1982)	gravelly loam	0.044
3	Spodosol (Federer, unpubl. data)	sandy loam	0.028
4	Inceptisol with macropores (Wilson et al., 1992)	loam	0.169
4	Inceptisol with macropores - adjusted for drainage from I.C.	loam	0.087
5	Synthetic soil (mixed $K(\psi)$ and saturation curves)		0.007

TABLE 3.3 Summary of simulated subsurface stormflow discharge rates for hillslopes with saprolite

run	Simulation case	Material type	Material thickness (m)	Peak discharge per meter width (m^3 /hr)
6	Thin Saprolite			0.023
		Inceptisol soil	0.5	
		Saprolite	1.0	
		Low-k bedrock	5.0	
7	Thick Saprolite			0.114
		Inceptisol soil	0.5	
		Saprolite	3.0	
		Low-k bedrock	3.0	
8	Intermediate Saprolite			0.172
		Inceptisol soil	1.0	
		Saprolite	1.5	
		Low-k bedrock	4.0	
9	No Saprolite			0.169
		Inceptisol soil	2.0	
		Low-k bedrock	4.5	

TABLE 3.4 Response time-scale (time constant Δt_m)

Row	Material	depth (m)	Inceptisol (run 4)				Del Monte Sand (run 1)			
			slope bottom		Lower midslope		slope bottom		Lower midslope	
			t=0 hr Δt_m	t=12 hr Δt_m	t=0 hr Δt_m	t=12 hr Δt_m	t=tt Δt_m	t=12 hr Δt_m	t=0 hr Δt_m	t=12 hr Δt_m
1	soil	0.500	81	169	75	200	144	52	133	0.8
2	soil	0.150	42	75	39	135	75	1	69	1
3	soil	0.250	42	58	39	158	75	1	69	1
4	soil	0.350	42	49	39	152	75	1	69	1
5	soil	0.450	53	42	49	123	94	2	87	1
6	soil	0.625	187	62	176	261	333	6	312	5
7	soil	0.875	157	18	146	166	278	5	260	4
8	soil	1.250	0.3	0.2	207	29	9	7	367	6
9	soil	1.625	0.1	0.1	146	0.1	5	5	259	4
10	soil	1.875	0.3	0.3	355	0.3	10	10	629	11
11	bedrock	2.250	0.1	0.1	461100	0.5	0.1	0.1	461200	442800
12	bedrock	3.000	0.2	0.2	911200	909700	0.2	0.2	911200	908400
13	bedrock	4.500	0.2	0.3	855900	854200	0.2	0.3	855900	853800
14	bedrock	5.500	0.3	0.3	0.3	0.3	0.3	0.3	0.3	0.3

NOTE: Δt_m in sec

TABLE 3.5 Summary of simulated subsurface stormflow discharge rates for convergent slopes (20 degree wedge meshes)

run	Simulation case	Material thickness (m)	Peak discharge per meter width (m^3/hr)
13	2 Materials		3.030
	Inceptisol soil	2.0	
	Low-k bedrock	4.5	
14	3 Materials		2.500
	Inceptisol soil	1.0	
	Saprolite	1.0	
	Low-k bedrock	4.5	
15	2 Materials (Hydrostatic)		0.058
	Inceptisol soil	2.0	
	Low-k bedrock	4.5	
	Beven (1977)		0.765
	Loam soil/Hydrostatic	1.0	
	Planar slope		
	(greater than 25 degree wedge)		

TABLE 3.6 Summary of results for channel head simulations

run	Case	CH depth (m)	SF height (m)	ψ @ base of CH (m	***m*** @ base of CH (m/m)	ψ below CH	***m*** below CH	downslope extent of ***m*** > 1.0
40	Silt soil	0.20	0.06	0.06	0.30	0.21	1.05	0.50
41		0.40	0.11	0.11	0.28	0.22	1.10	1.30
42		0.80	0.33	0.24	0.30	0.27	1.35	1.90
43		2.00	0.76	0.42	0.21	0.17	0.85	0.00
44	Inceptisol soil	0.20	0.07	0.07	0.35	0.22	1.10	0.50
45		0.40	0.13	0.12	0.30	0.23	1.15	1.30
46		0.80	0.40	0.28	0.35	0.28	1.40	1.90
47		2.00	1.70	0.45	0.23	0.17	0.85	0.00
51	Bedrock at base of CH	2.00	0.76	0.43	0.22			

NOTE: CH - Channel head
SF - Seepage Face
ψ - Pressure head

TABLE 3.7 Summary of slug test results for Caspar Creek field site

Location	Piez.	Pressure head (m)	Saturated thickness (m)	Screen length (m)	Borehole radius (m)	Casing radius (m)	Est. K_{sat}[1] (m/s)
Mid slope	B3	0.290	0.290	0.150	0.035	0.025	1.5E-07
	B4	0.480	0.480	0.150	0.035	0.025	3.4E-07
	C3			0.300	0.035	0.025	3.4E-07
Toe of slope	C1	0.220	0.220	0.150	0.044	0.025	3.5E-05
Swale bottom	A1	1.380	1.380	0.150	0.044	0.025	2.0E-06
	B1	1.080	1.080	0.150	0.035	0.025	1.3E-06
	CO	1.310	1.310	0.150	0.044	0.025	3.0E-06
Bedrock	C2	1.530	1.530	0.150	0.035	0.025	8.7E-06

[1] - Estimated using Bouwer and Rice (1978) method

TABLE 3.8 Time of peak piezometric response, January 1994 storm
M Swale, Caspar Creek Experimental Watershed

Piezometer	Time of peak ψ (d)	Time lag (hr)
A1	141.1979	15.00
A2	141.5521	23.50
A3	141.6979	27.00
B1	140.8854	7.50
B2	140.7813	5.00
B3	141.1354	13.50
B4	140.8229	6.00
CO	141.2813	17.00
C1	140.9792	9.75
C2	141.2396	16.00
C3	141.0729	12.00

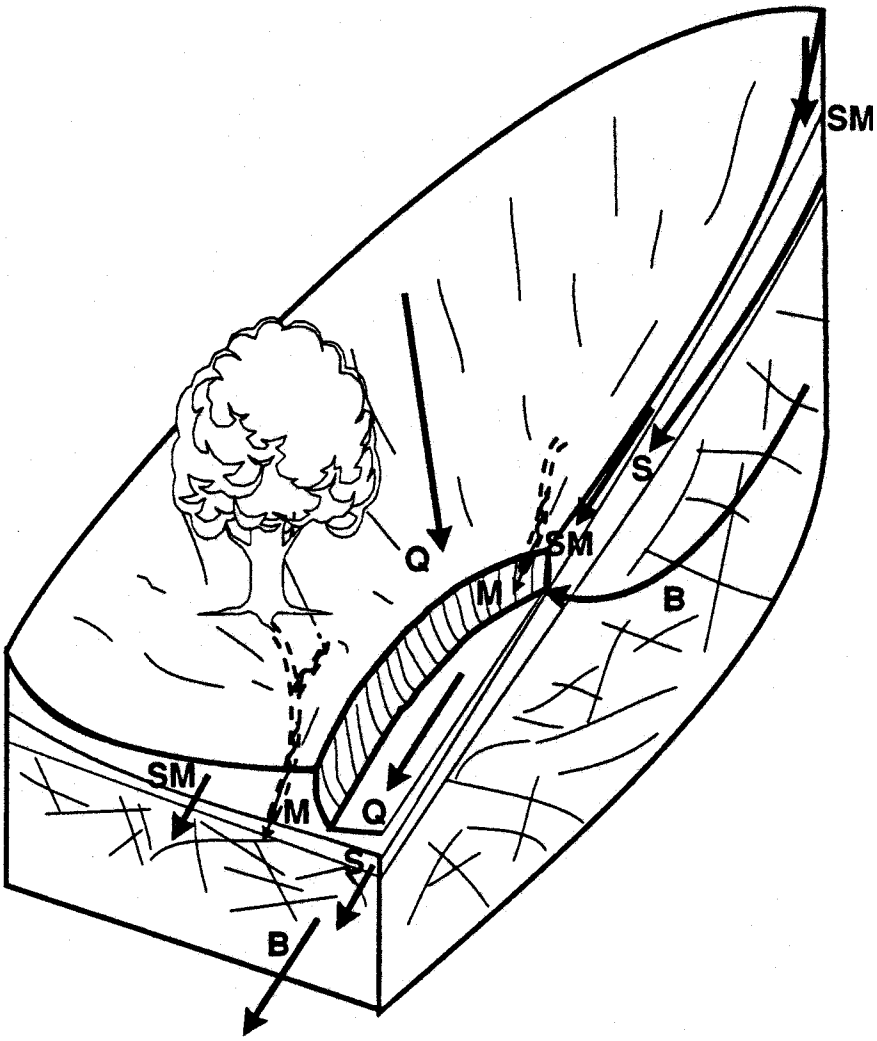

Q	Overland Flow
SM	Soil Matrix
M	Macropores
S	Saprolite
B	Bedrock

Figure 1.1 Conceptual hillslope flow paths

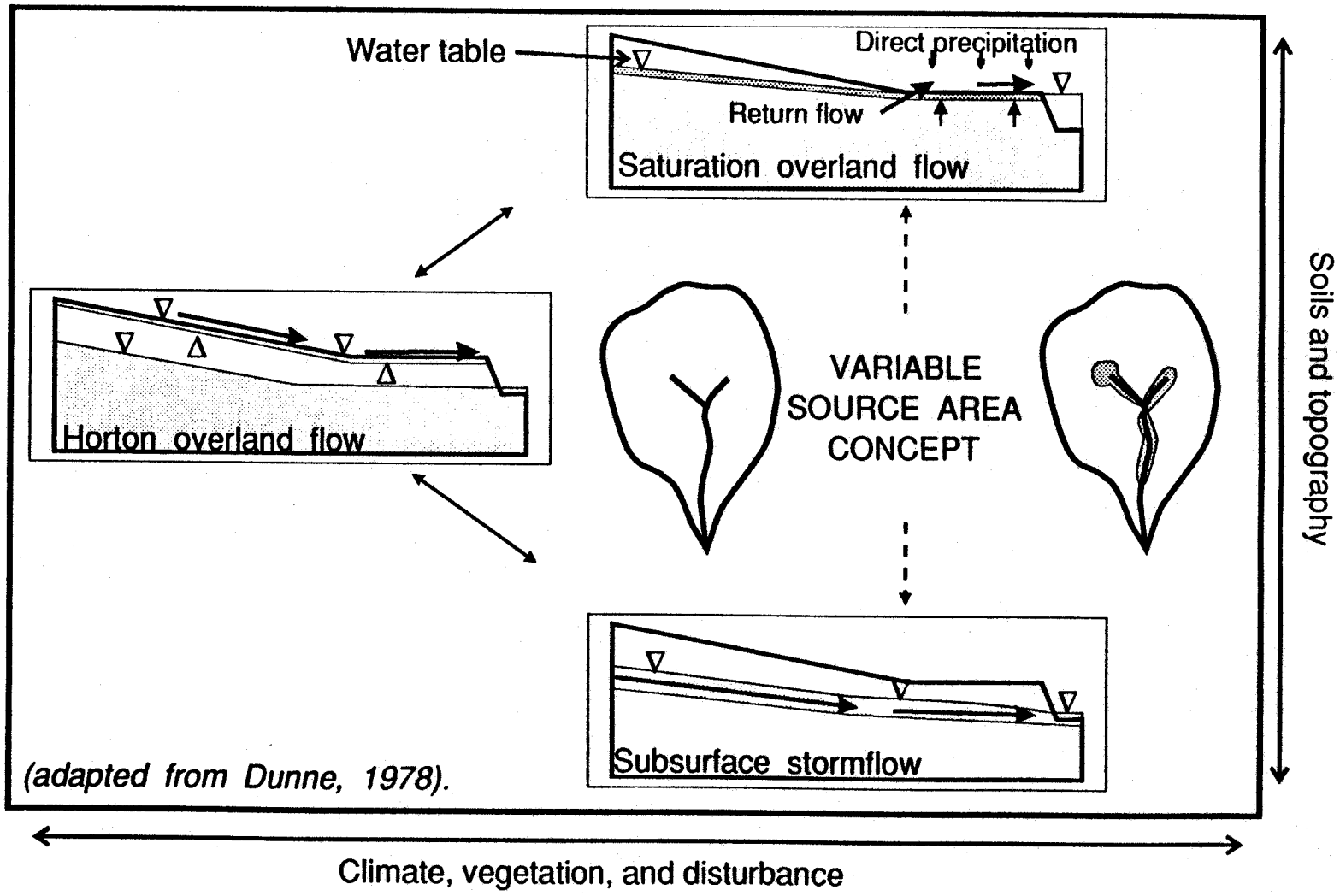

Figure 1.2 Summary of major runoff generation models

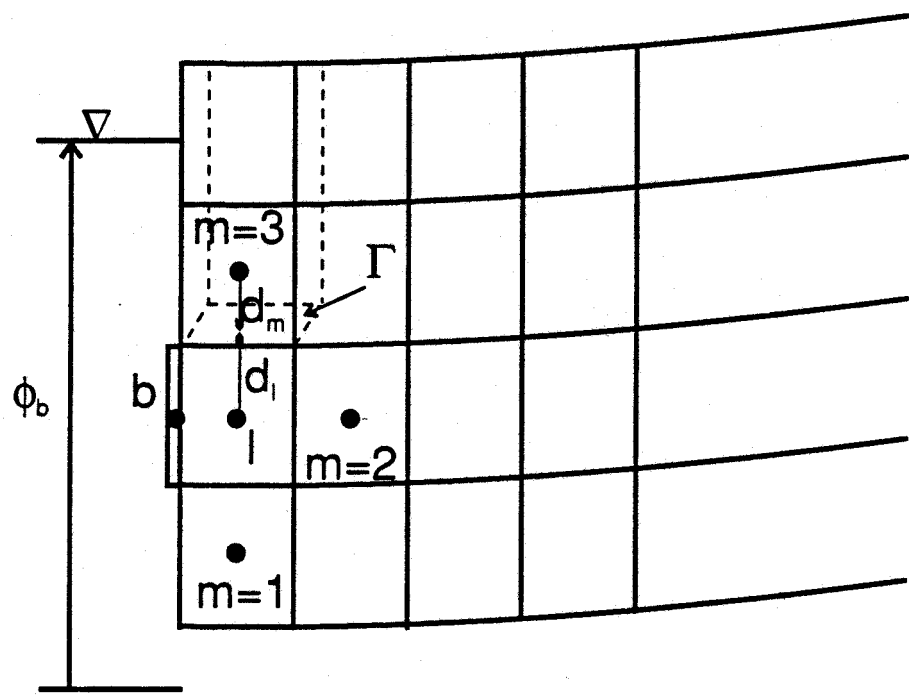

Figure 2.1 Schematic of geometric parameters used in defining conductance in TRUST

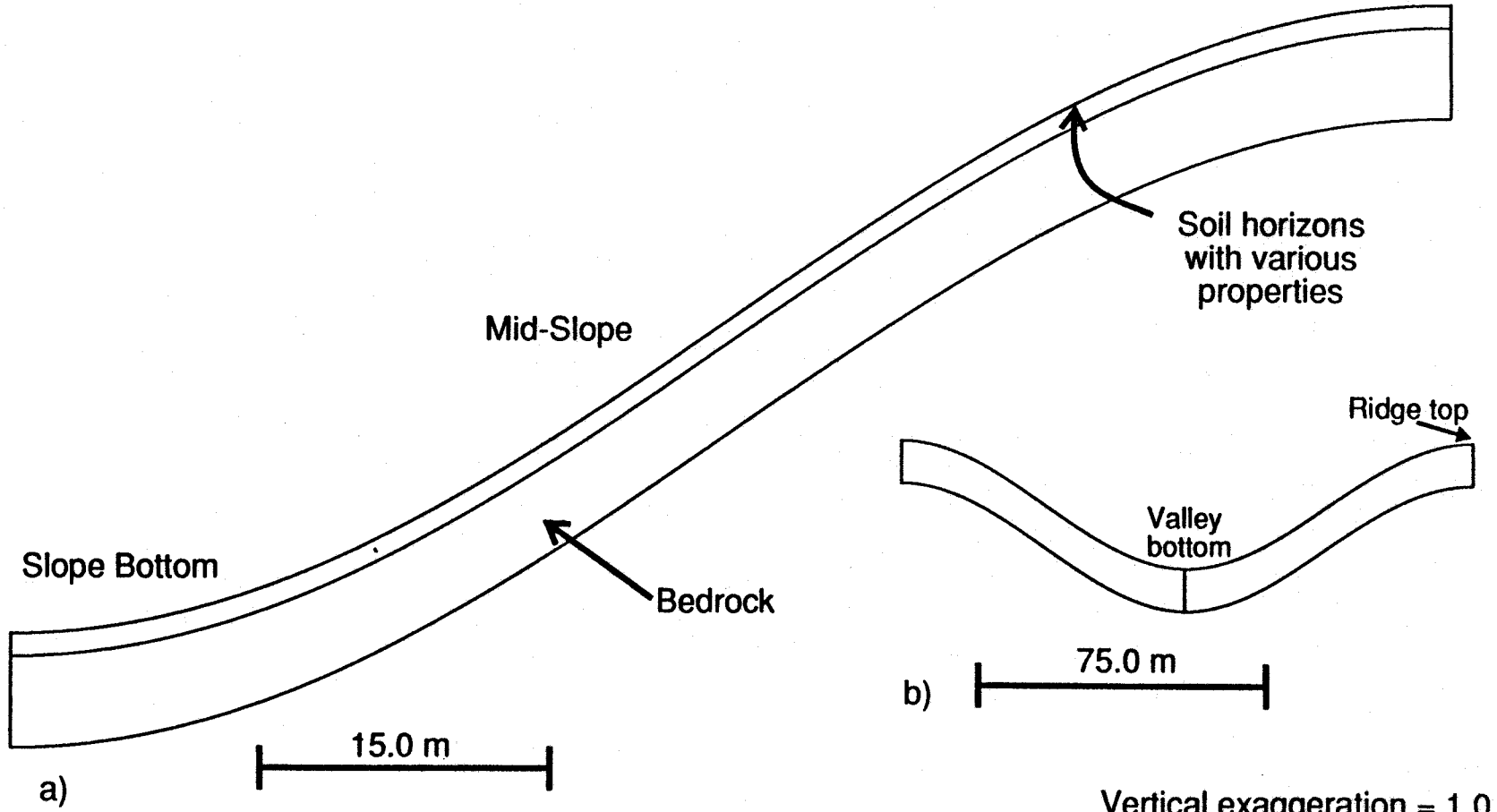

Figure 2.2 General mesh configuration

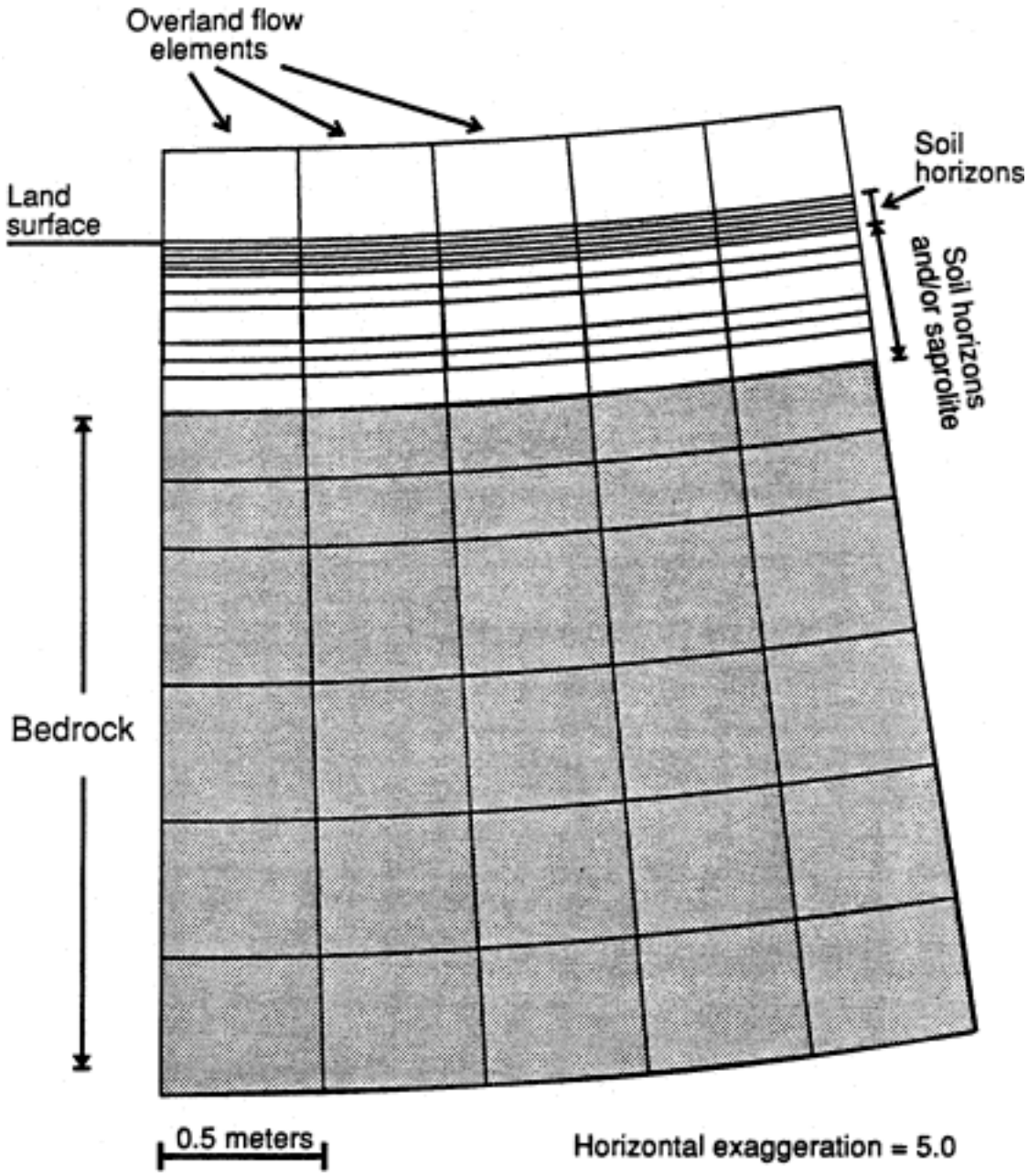

Figure 2.3 Detail of mesh discretization

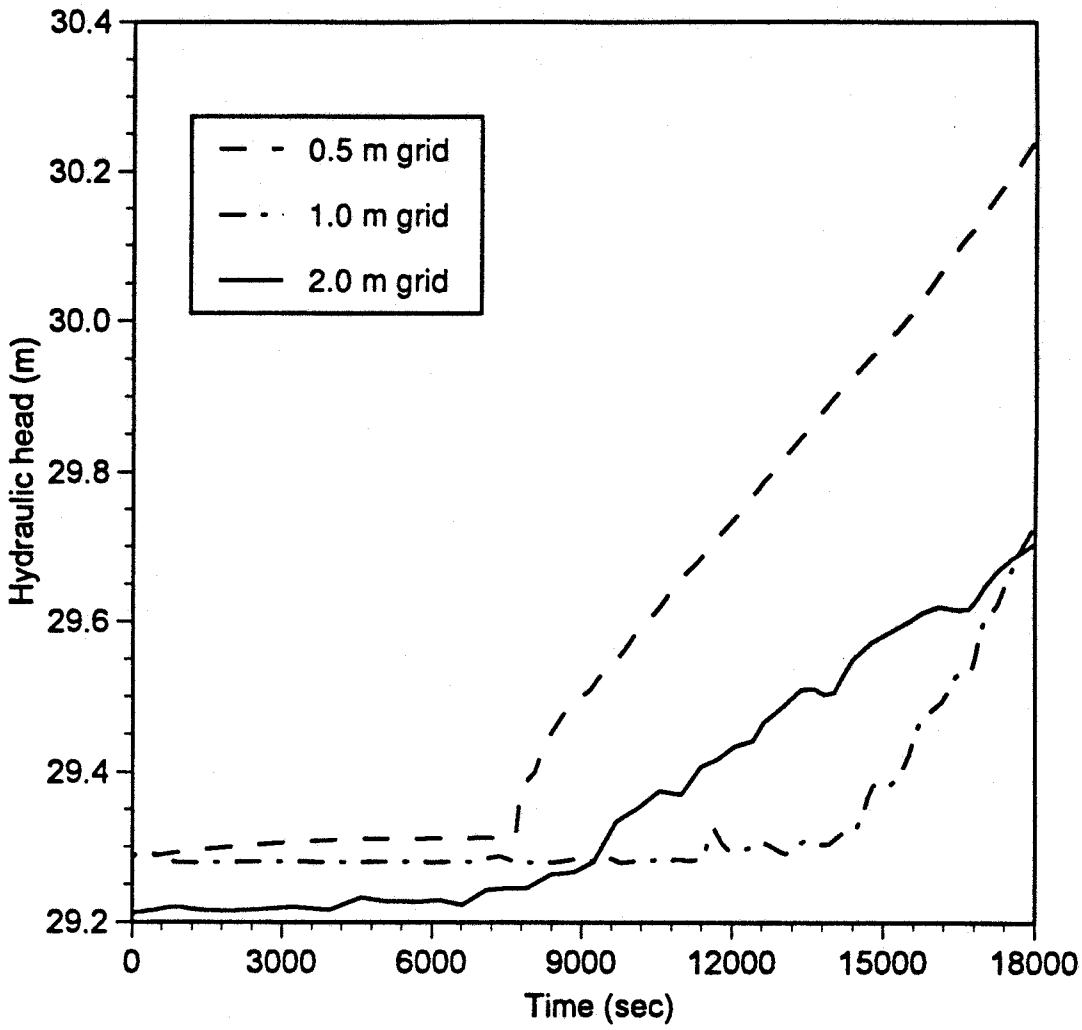

Figure 2.4 Effects of horizontal grid-spacing on hydraulic head response in run 4 with Inceptisol soil, slope bottom

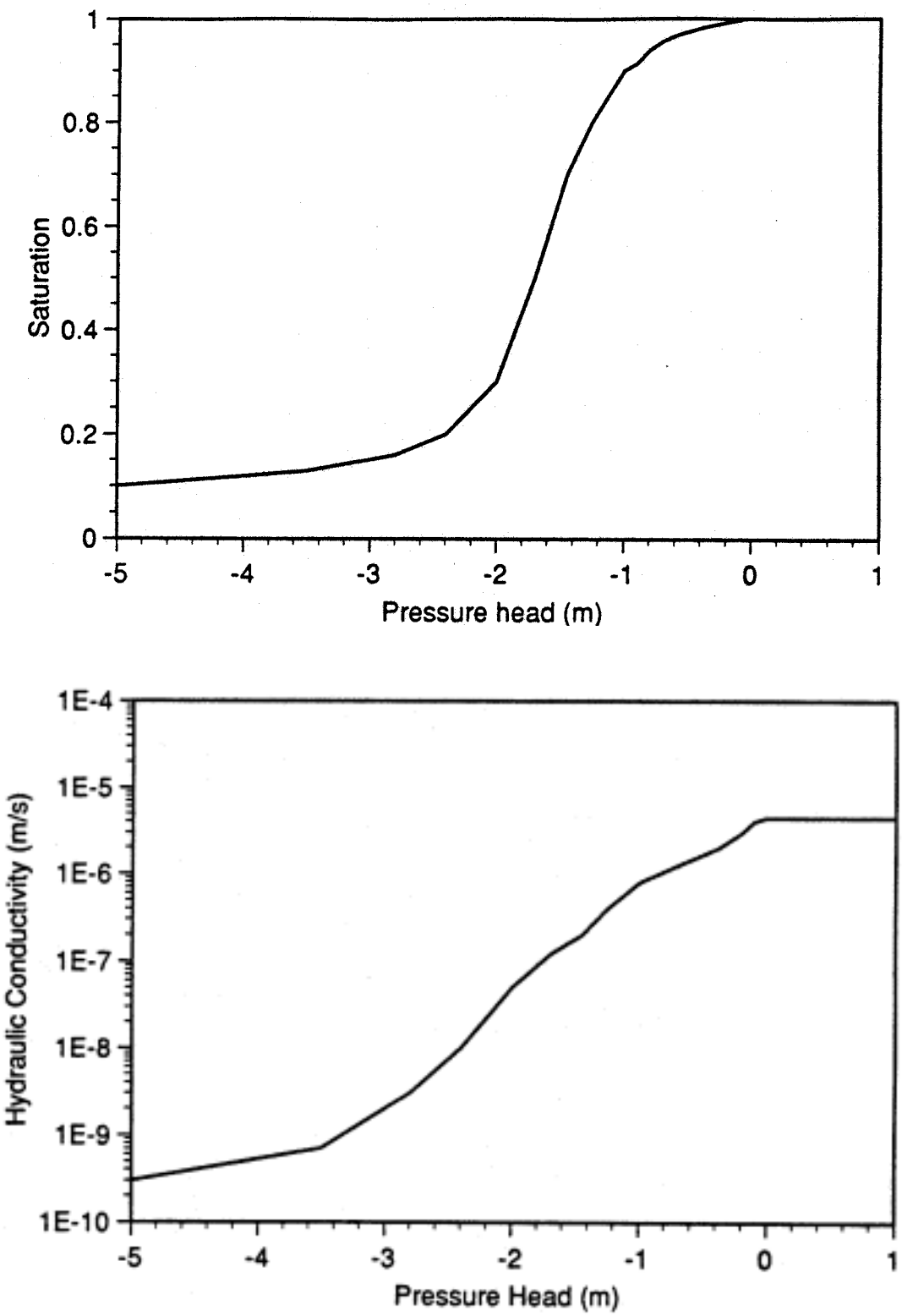

Figure 2.5 Typical Saturation and Hydraulic Conductivity Curves (Del Monte sand from Liakopoulos, 1965)

Pedogenic Horizons: biopores, pedogenic voids, structural voids, and packing pores

Parent Material: Stuctural pores, and packing pores

Saprolite: Structural voids (residual fractures), packing pores

Fractured Bedrock: Structural voids (fractures and joints)

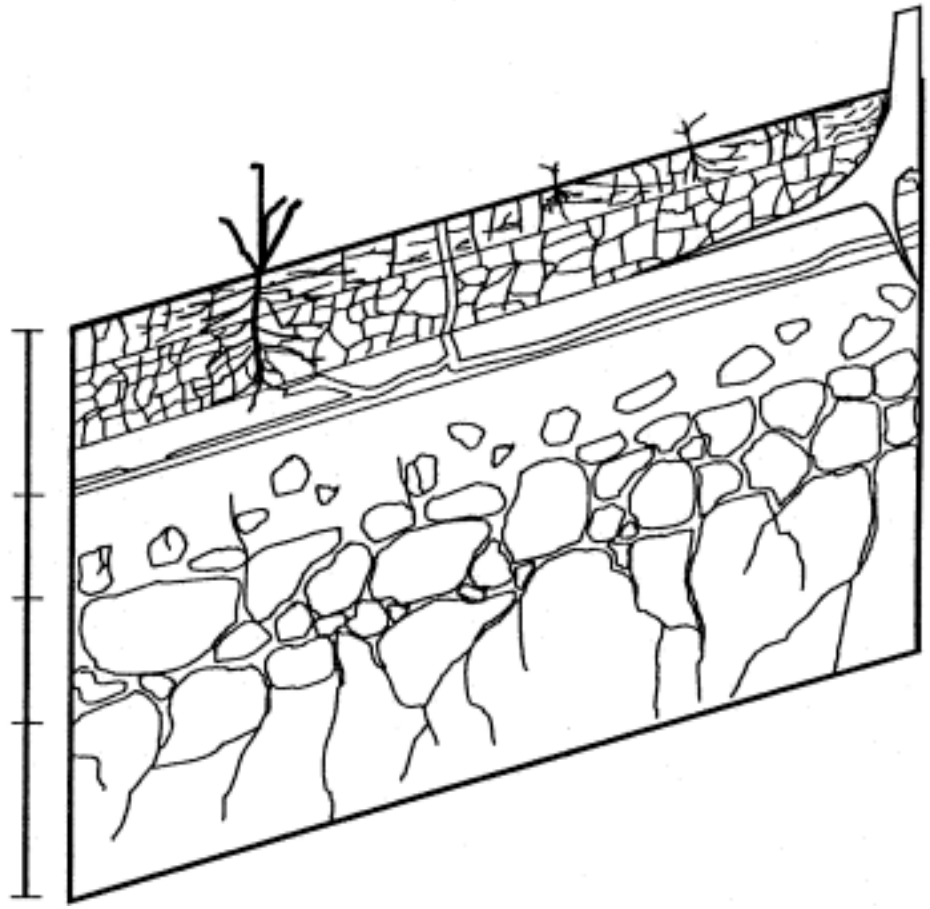

Figure 2.6 Idealized distribution of possible void types defined by Brewer (1974) with depth

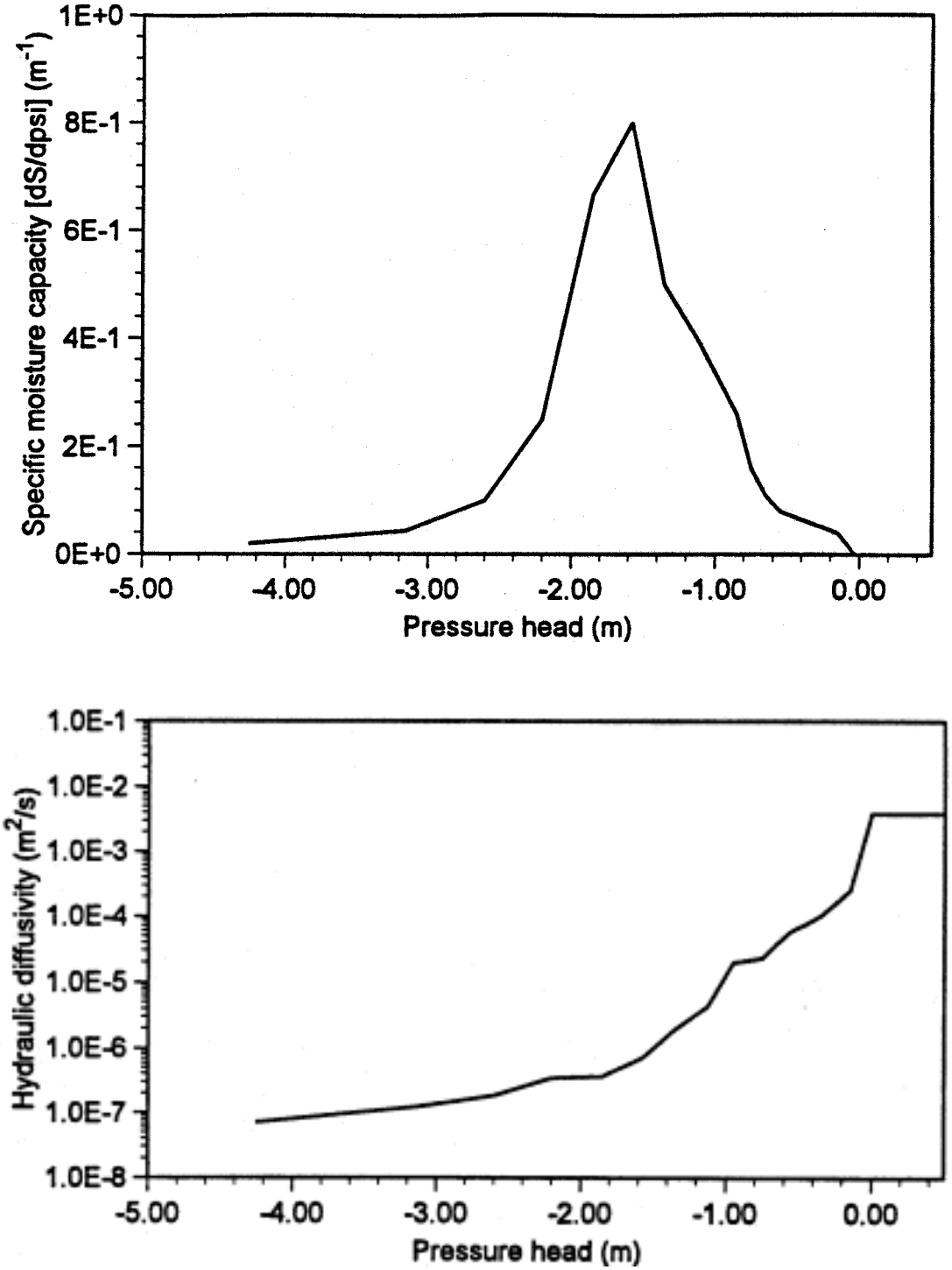

Figure 2.7 Typical specific moisture capacity and hydraulic diffusivity curves (Del Monte sand from Liakopoulos, 1965)

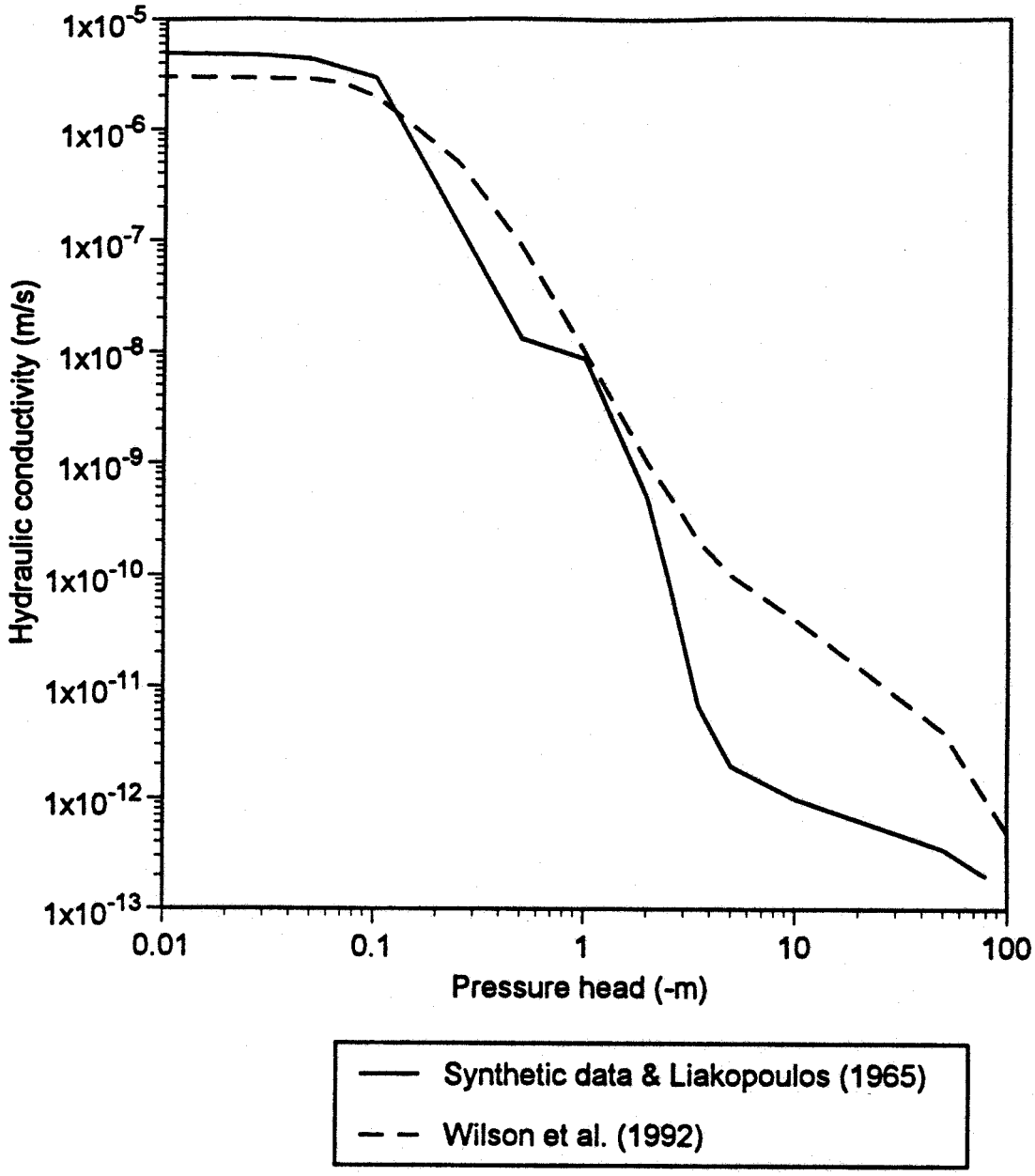

Figure 2.8 Synthetic and measured hydraulic conductivity curves for soil horizons containing macropores

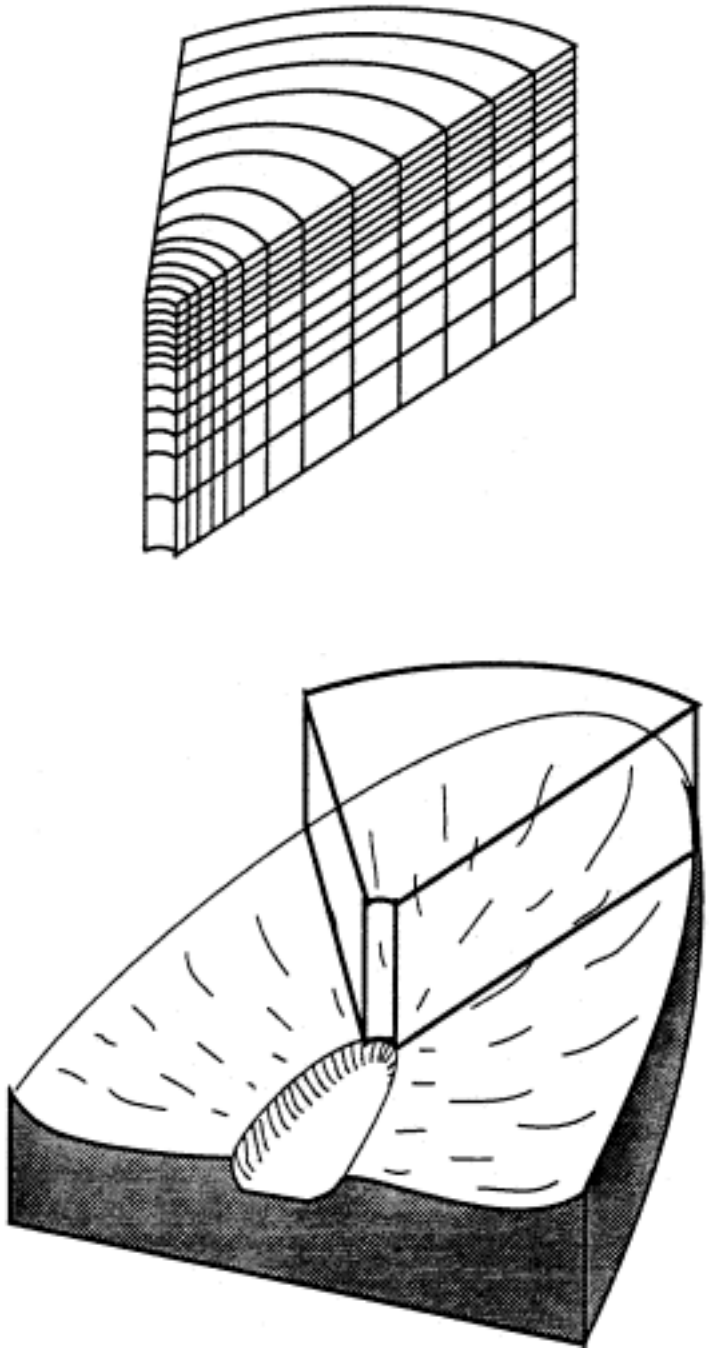

Figure 2.9 Pseudo 3-dimensional mesh used in simulations of convergent flow

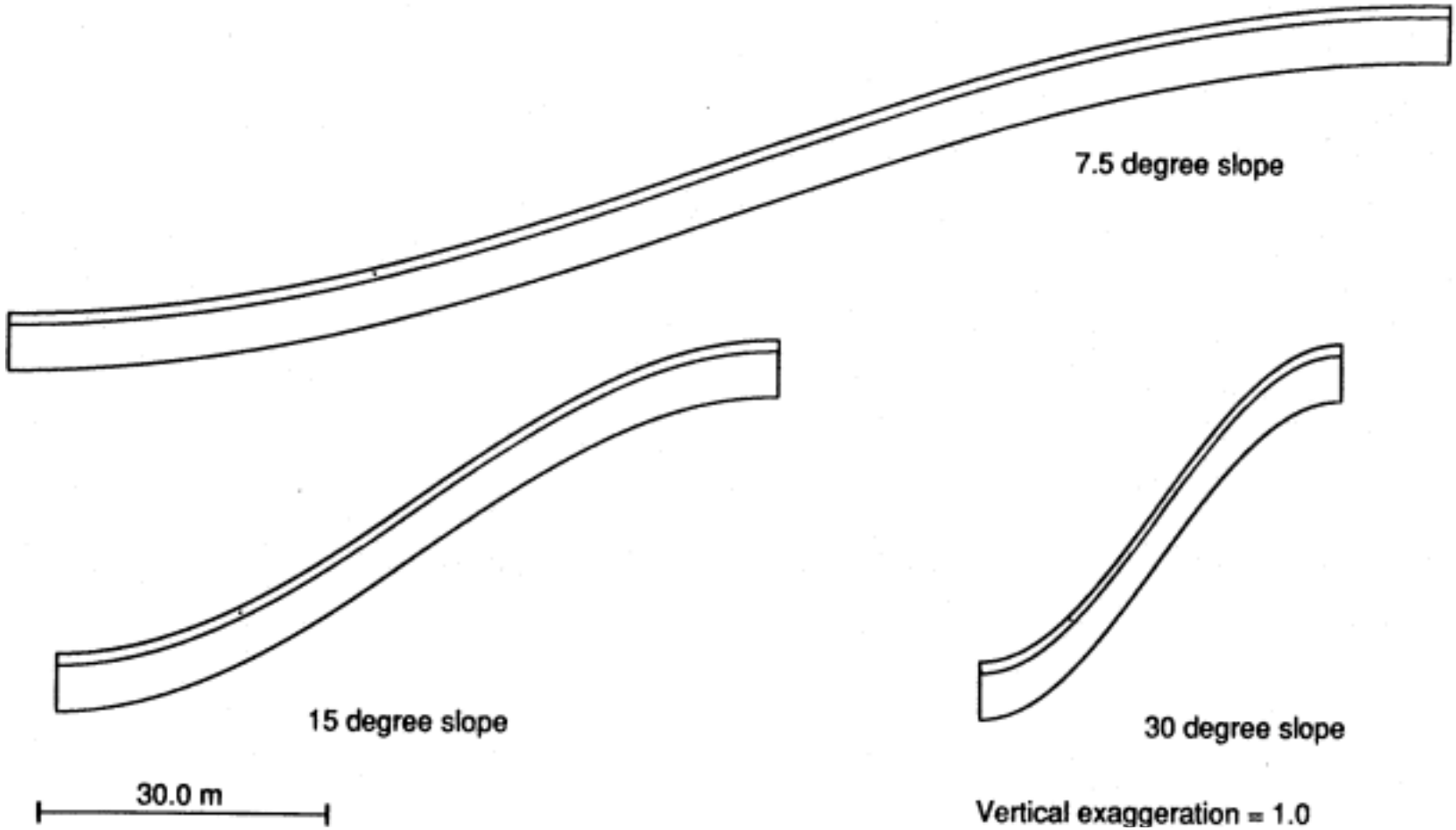

Figure 2.10 General mesh configuration of variable angle slopes

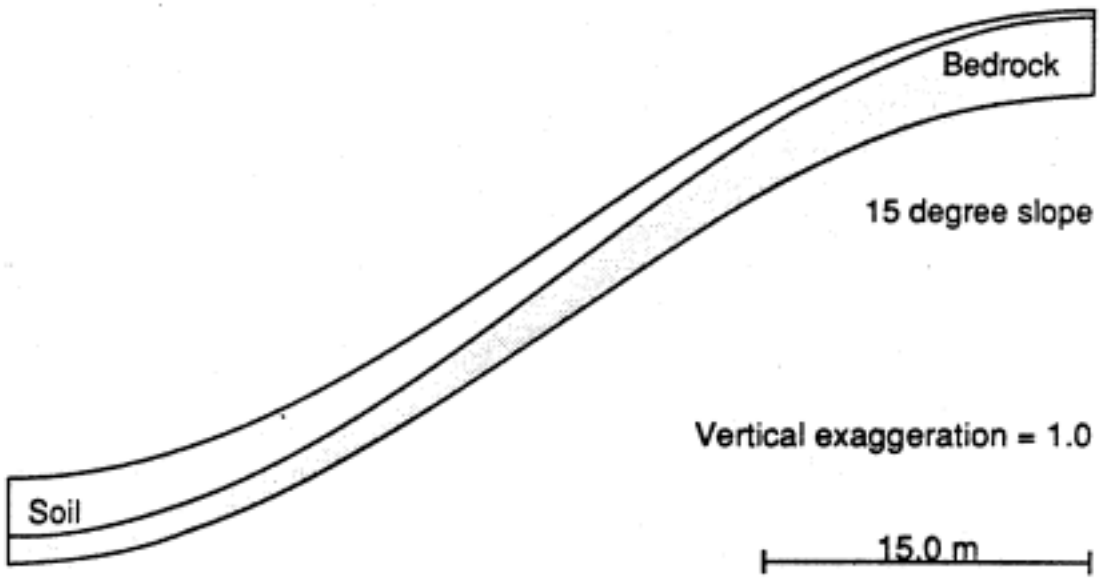

Figure 2.11 a Flow domain for cases where soil thickens with distance downslope

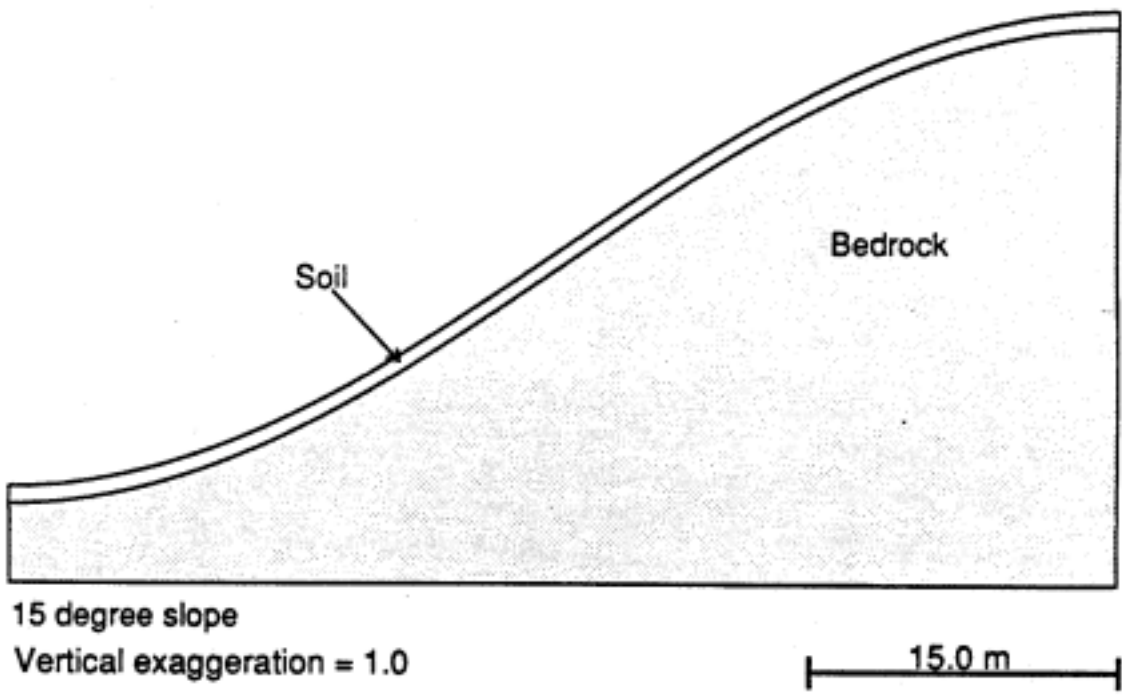

Figure 2.11 b Flow domain for hillslope with fracture permeability extending to depth

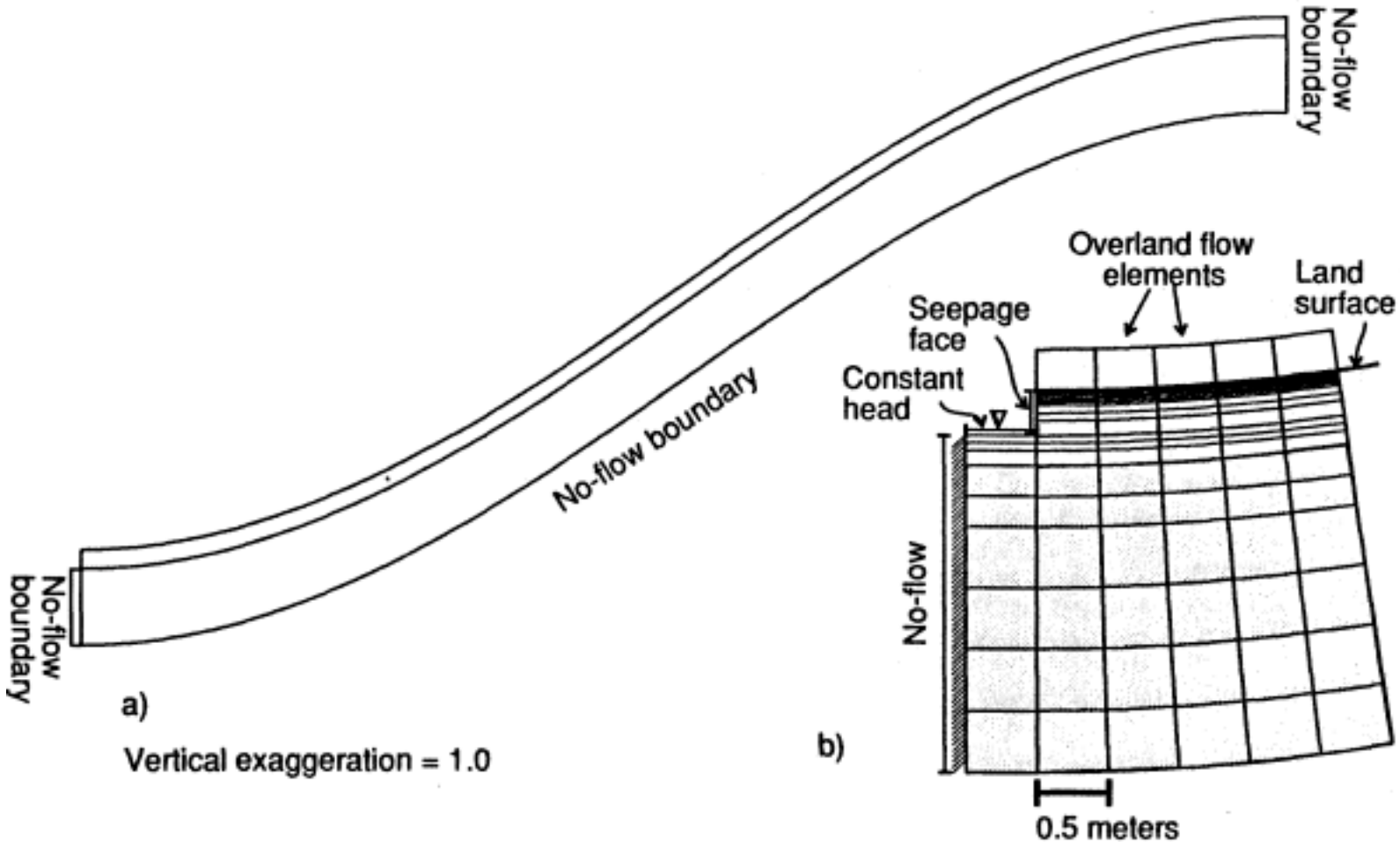

Figure 2.12 Boundary conditions: a) downstream, bottom, and upstream; and b) detail of downstream [seepage face, constant head, and no-flow]

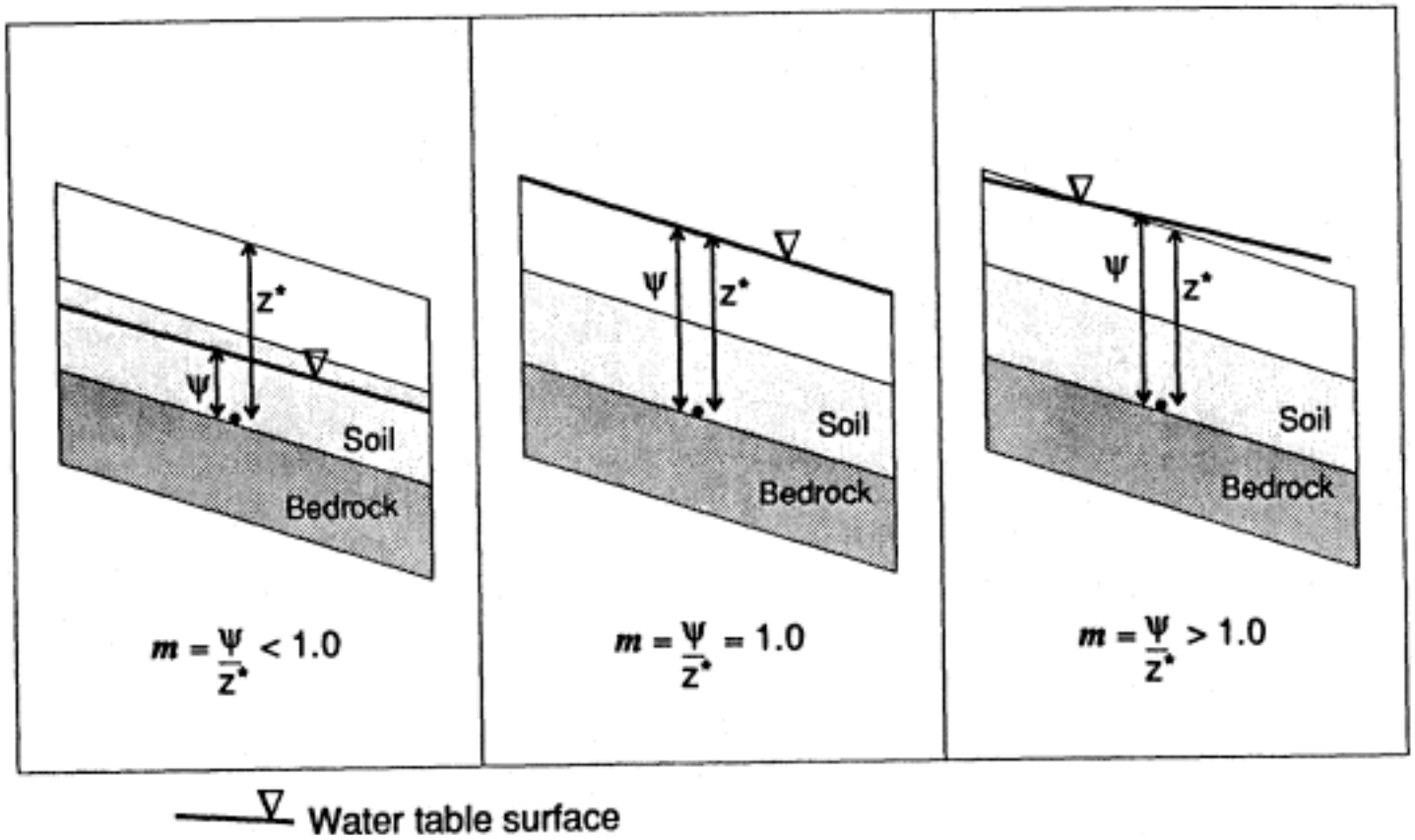

Figure 2.13 Possible subsurface saturation conditions affecting the pressure head ratio m (adapted from Wilson, 1988, Figure 54).

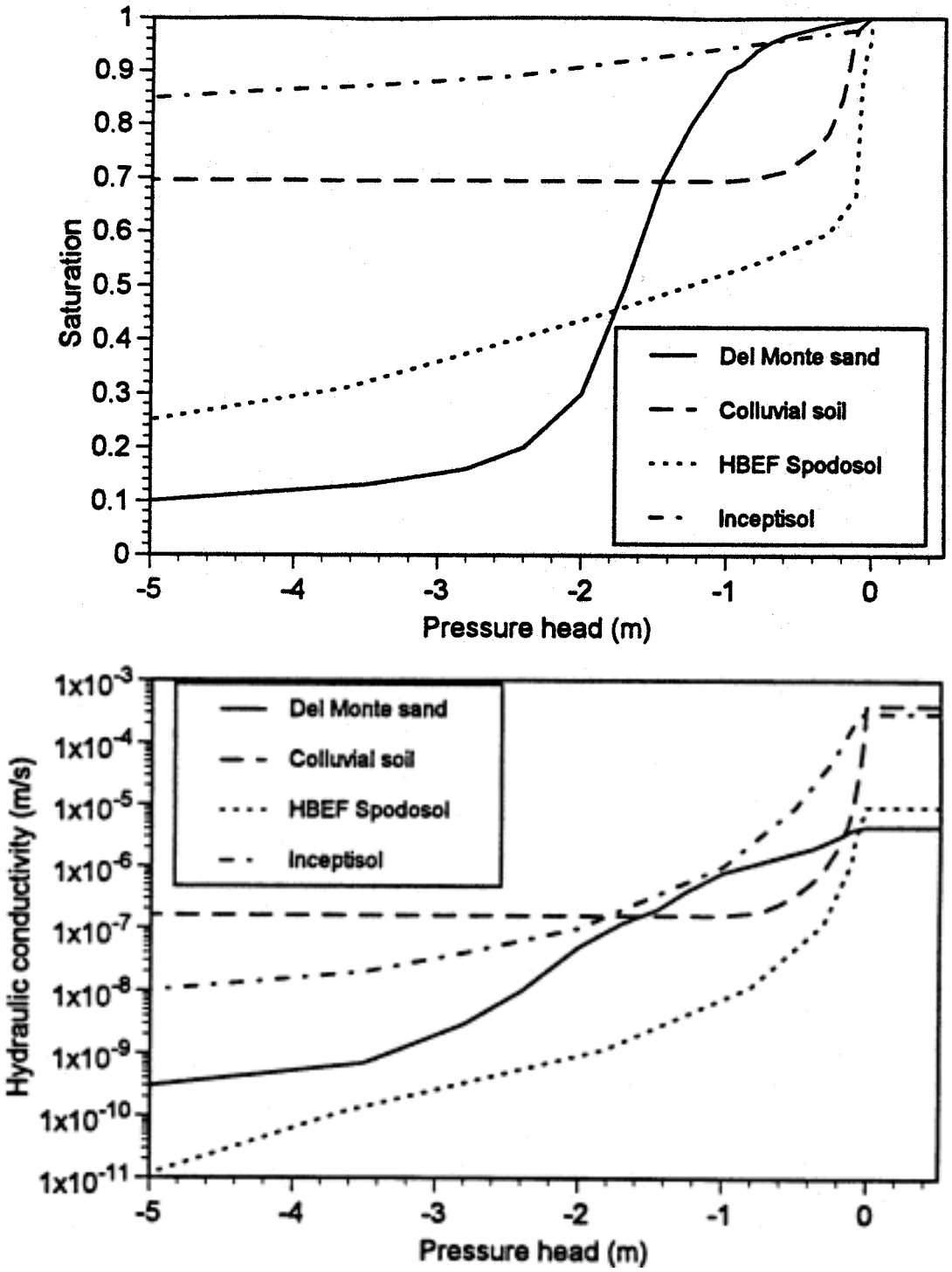

Figure 2.14 Saturation and hydraulic conductivity curves for soils used in parametric studies

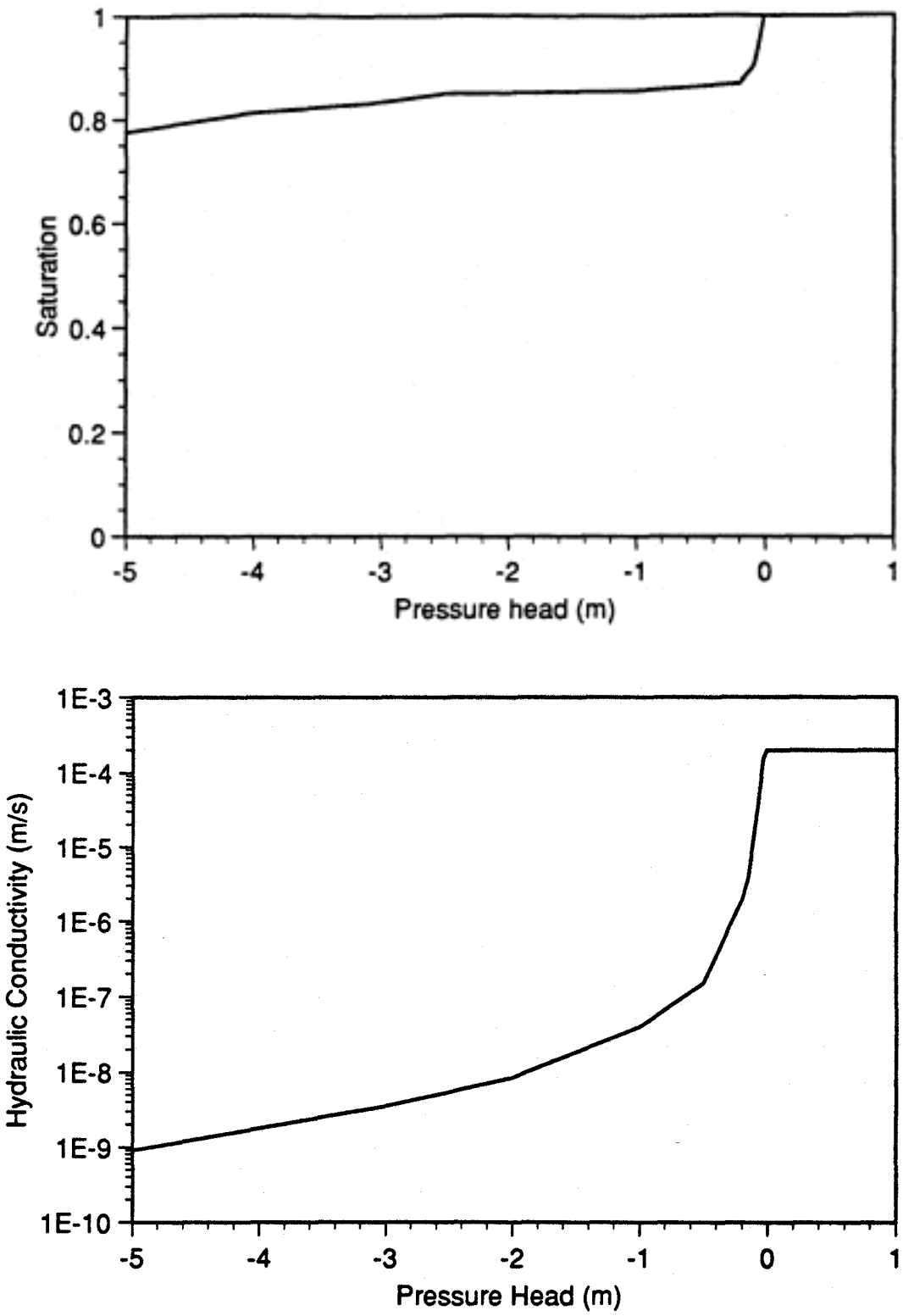

Figure 2.15 Saturation and hydraulic conductivity curves for saprolite from Wilson et al. (1992)

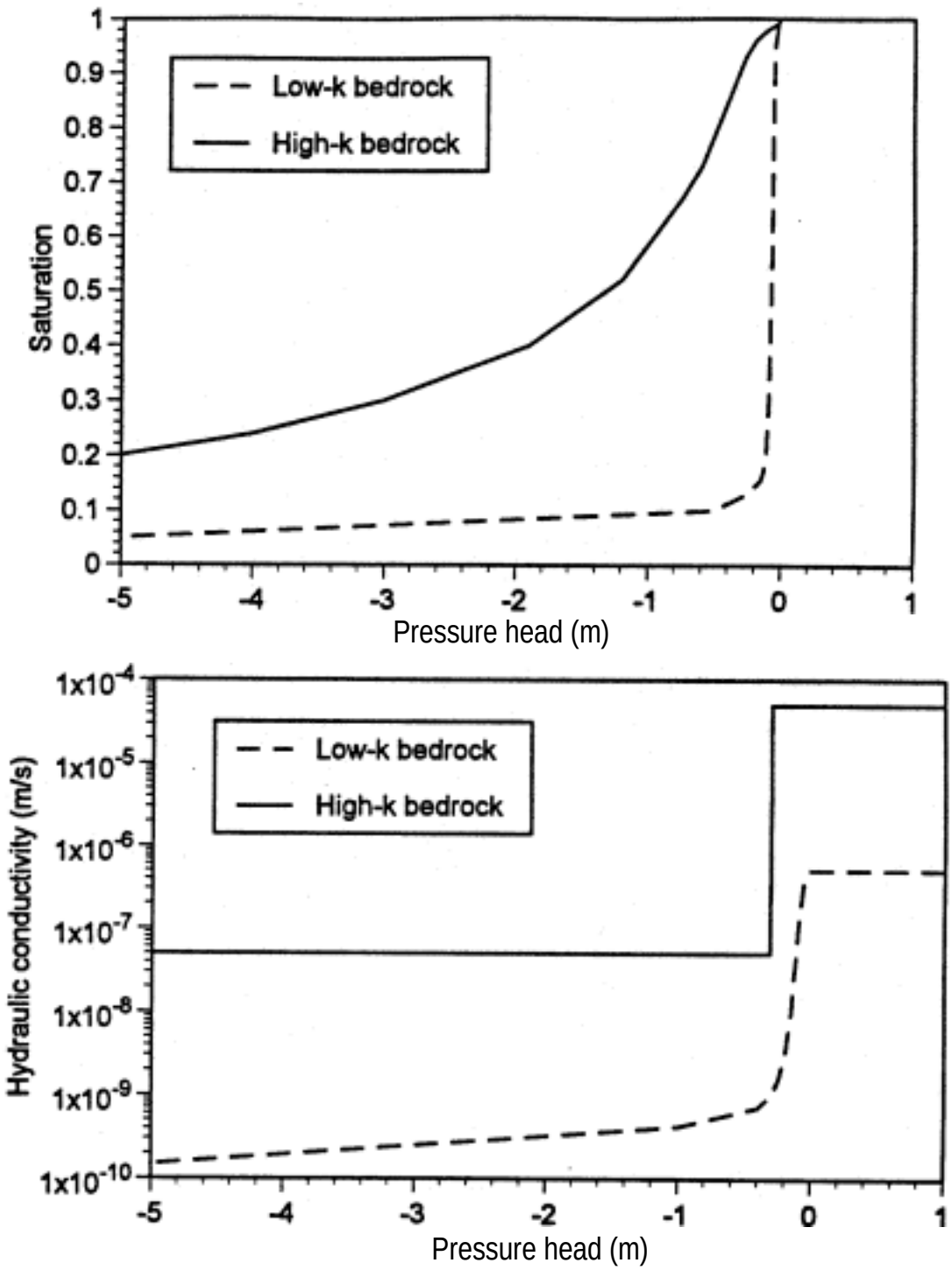

Figure 2.16 Saturation and hydraulic conductivity curves for bedrock used in parametric simulations

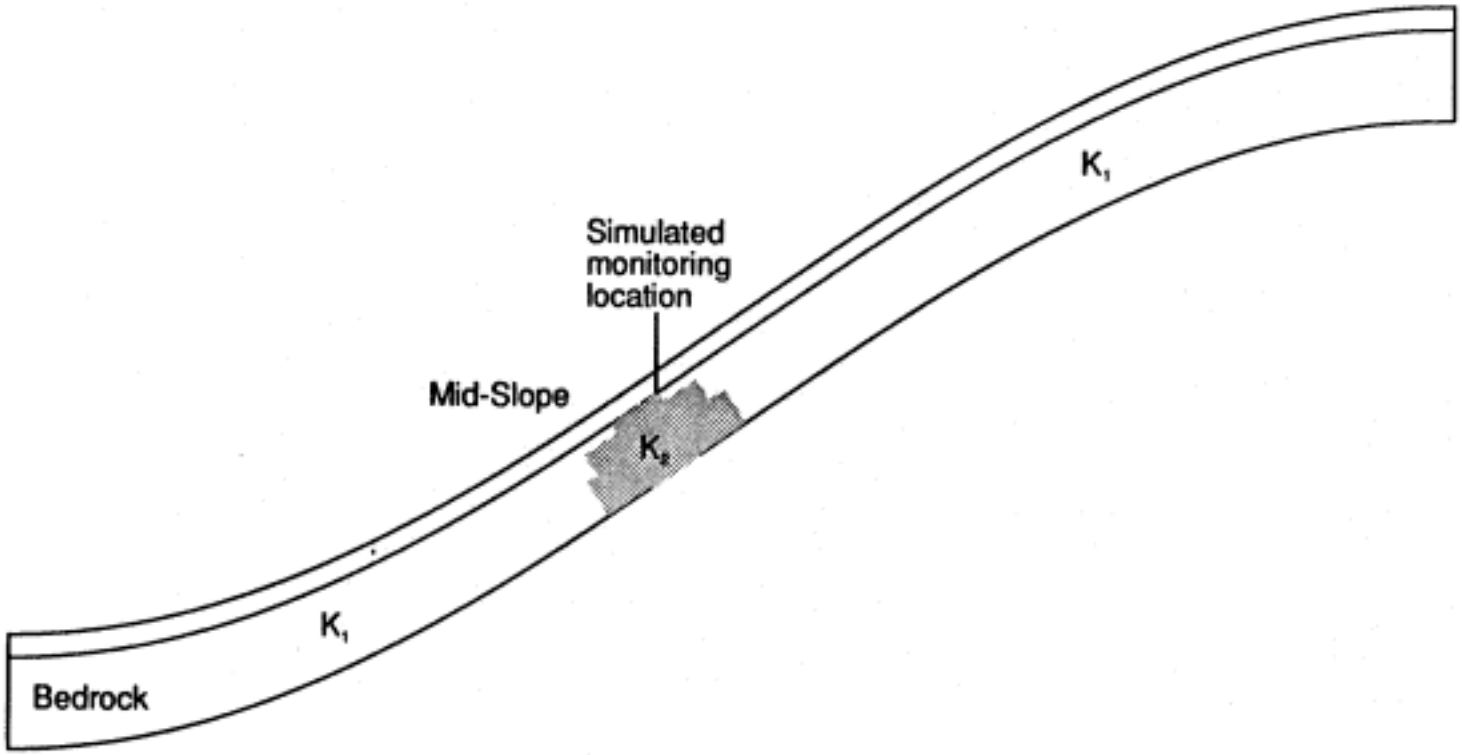

Figure 2.17 Simulation case with discontinuity in bedrock hydraulic conductivity (after Wilson et al., 1989)

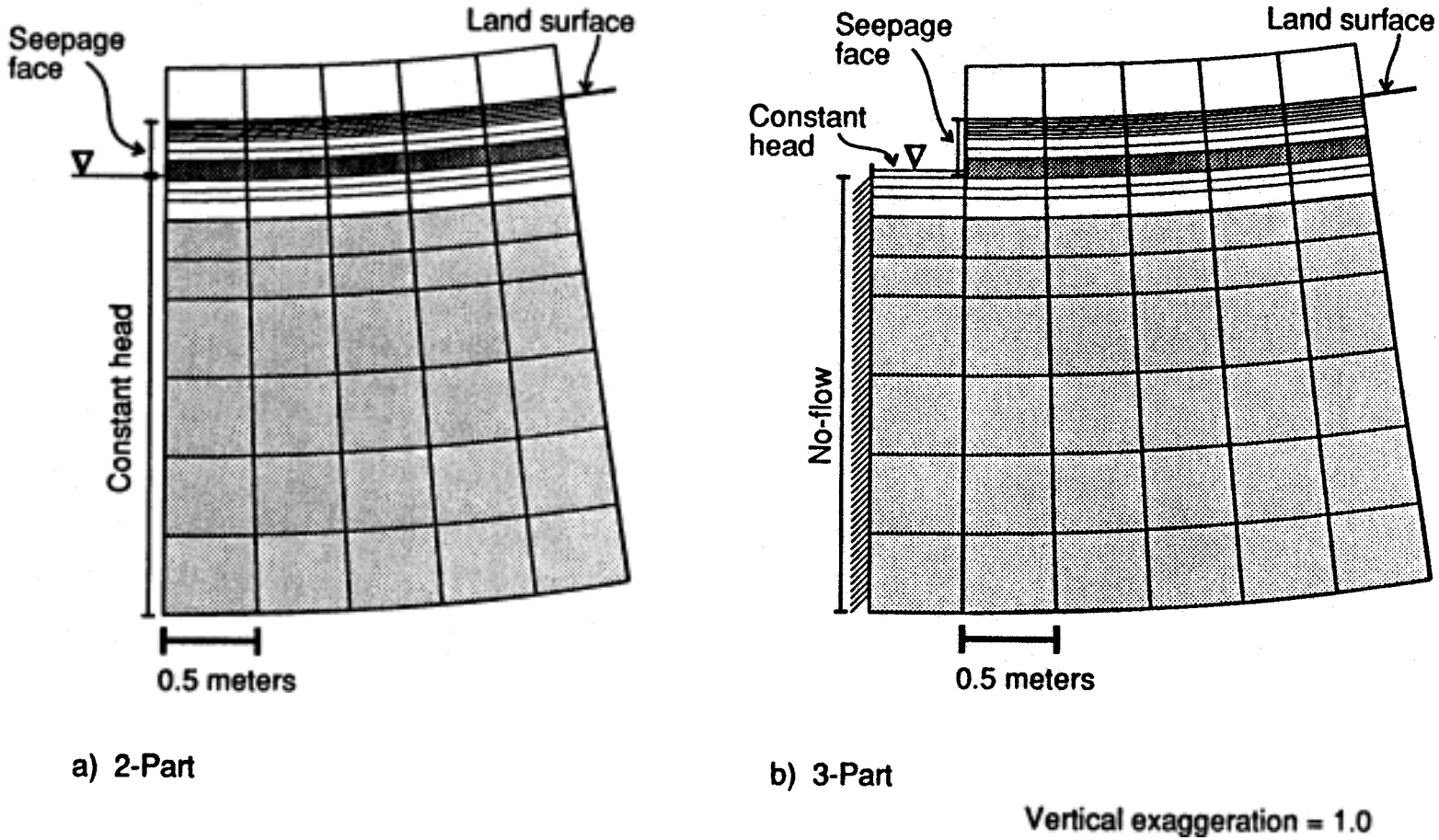

Figure 2.18 Boundary condition configurations: a) 2-Part [seepage face and constant head]; and b) 3-Part [seepage face, constant head, and no-flow]

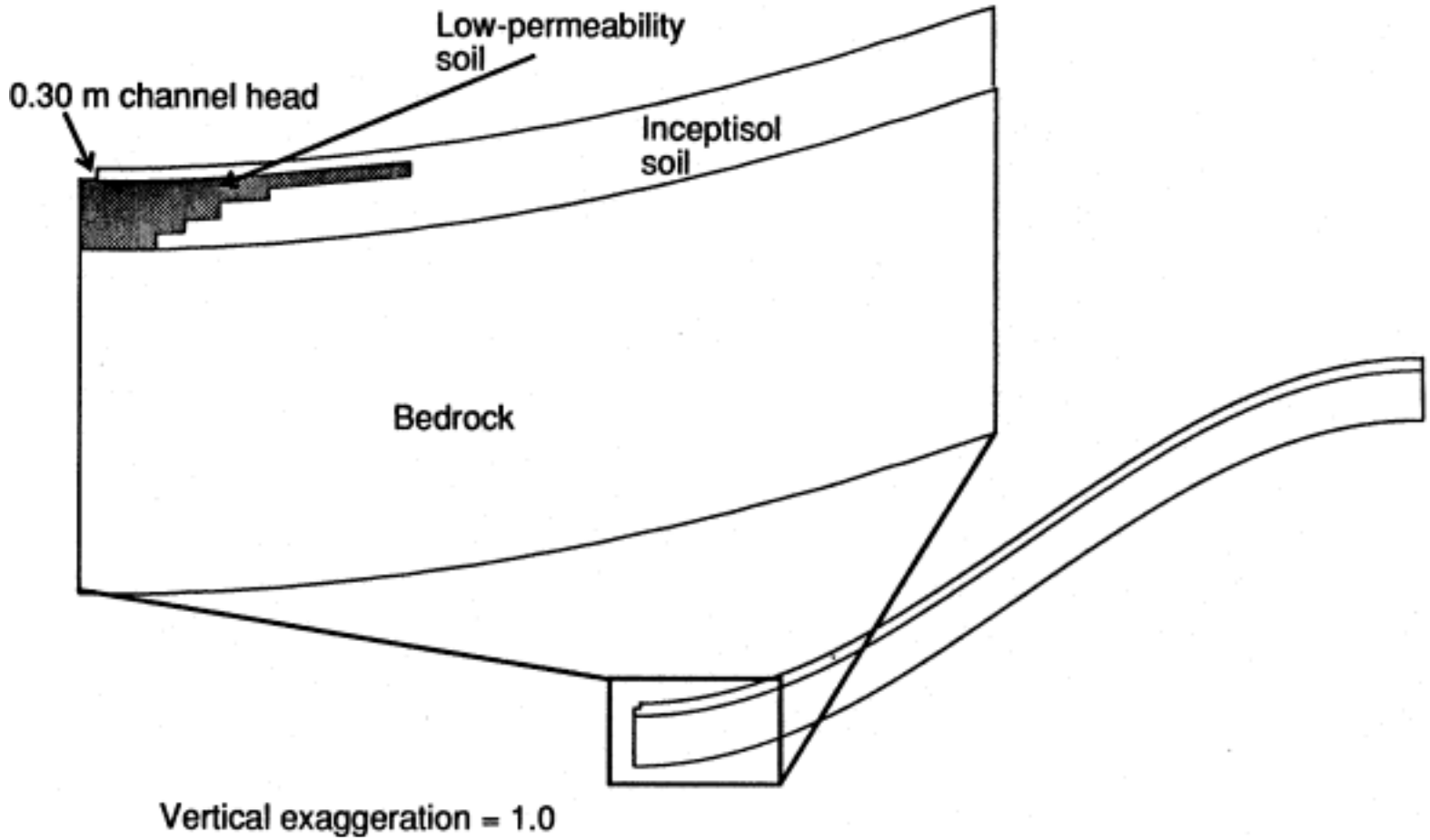

Figure 2.19 Mesh with low permeability zone in "riparian" soils near downstream boundary

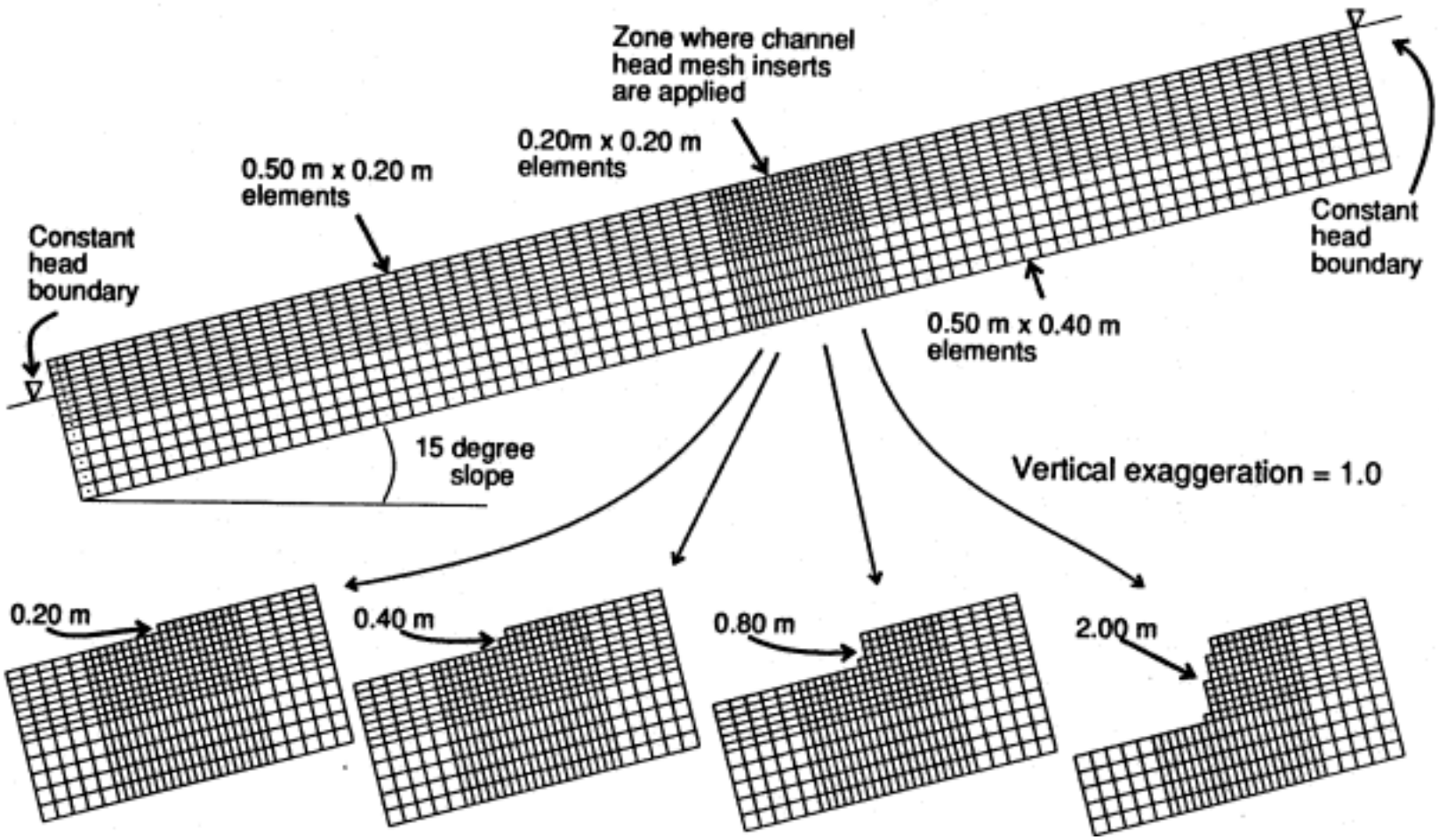

Figure 2.20 Detail of mesh used in channel head simulations

Figure 2.21 Location of field sites

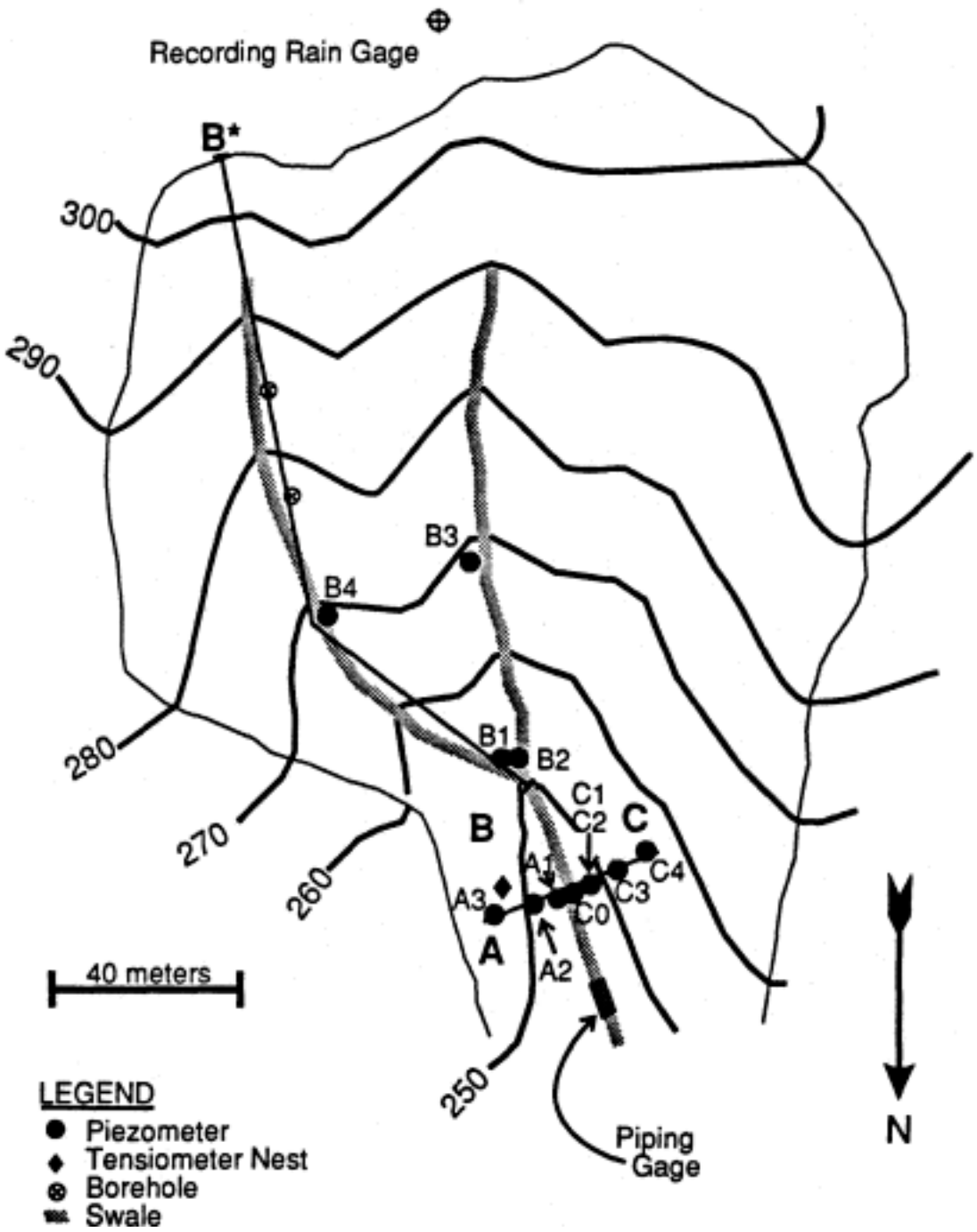

CONTOUR INTERVAL= 10 meters

SOURCE: U.S. Forest Service

figure 2.22 M Swale, Caspar Creek Experimental Watershed instrumentation

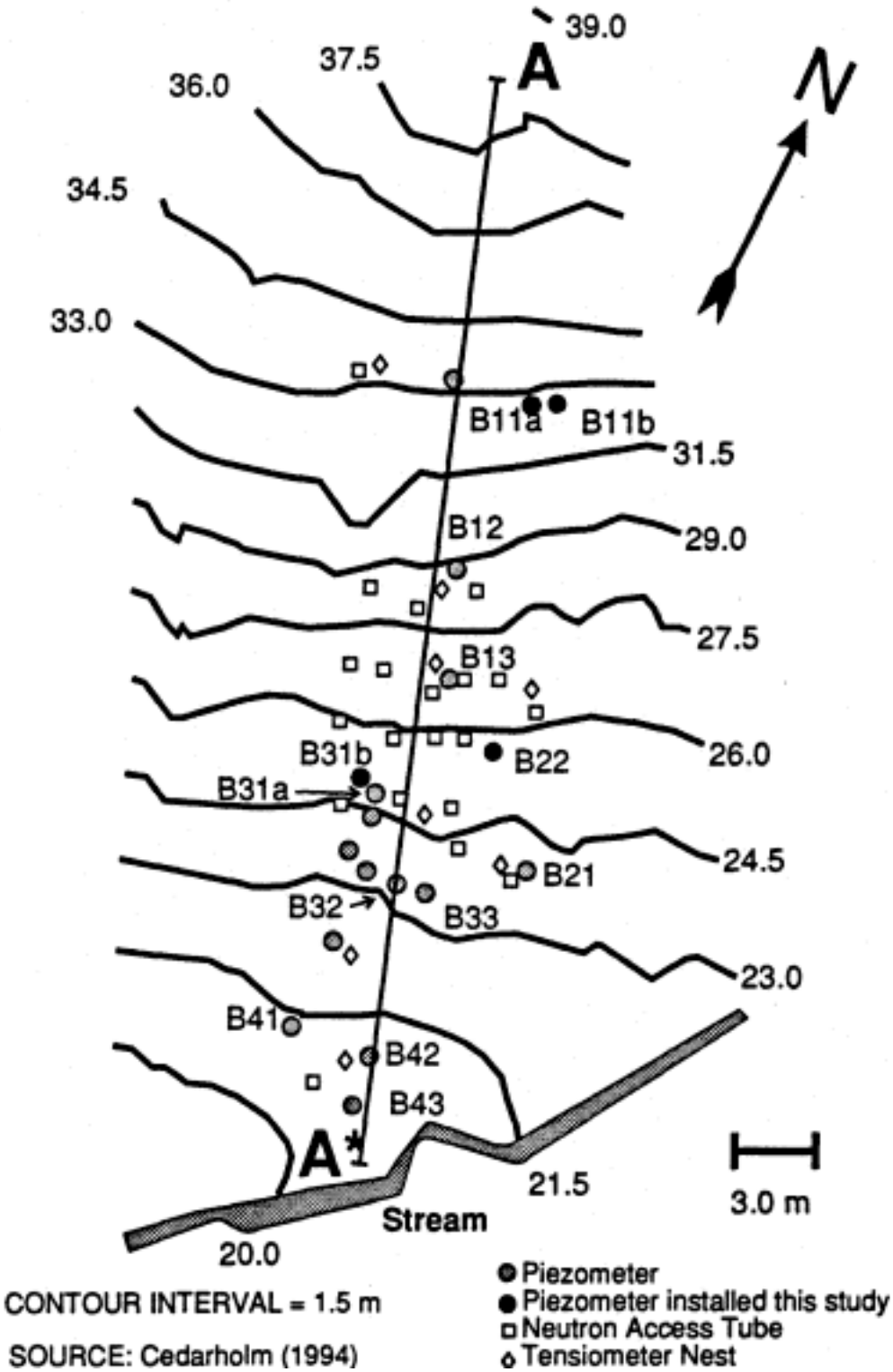

Figure 2.23 UNH Hillslope Field Site, Watershed 3, HBEF

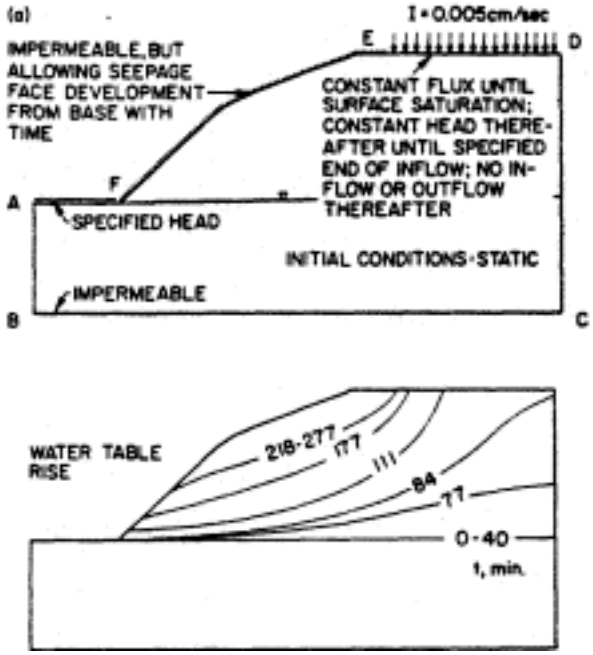

Figure 3.1 From Freeze (1972a, Figure 4) baseflow generation homogeneous material

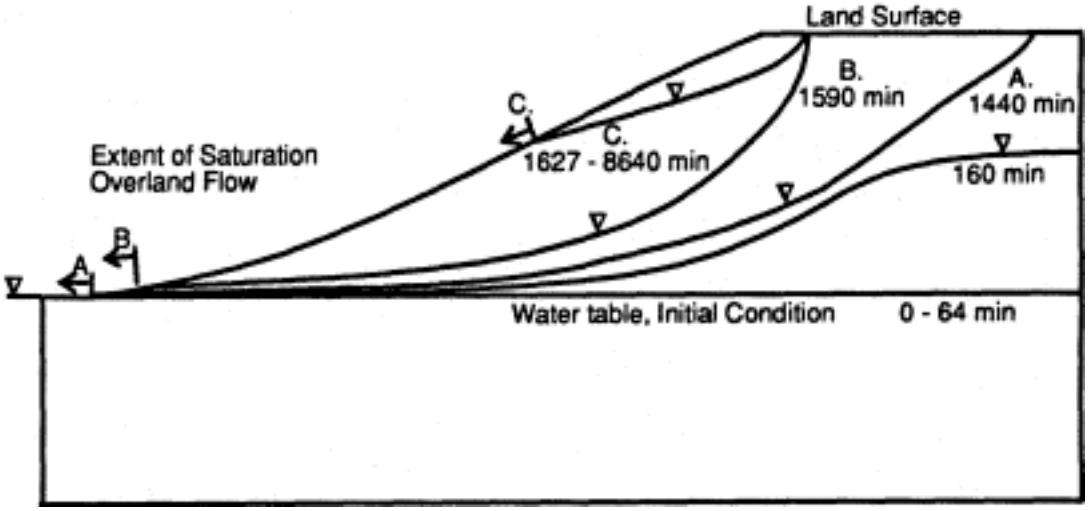

Figure 3.2 Simulation of base flow generation case from Freeze (1972a) - homogeneous material

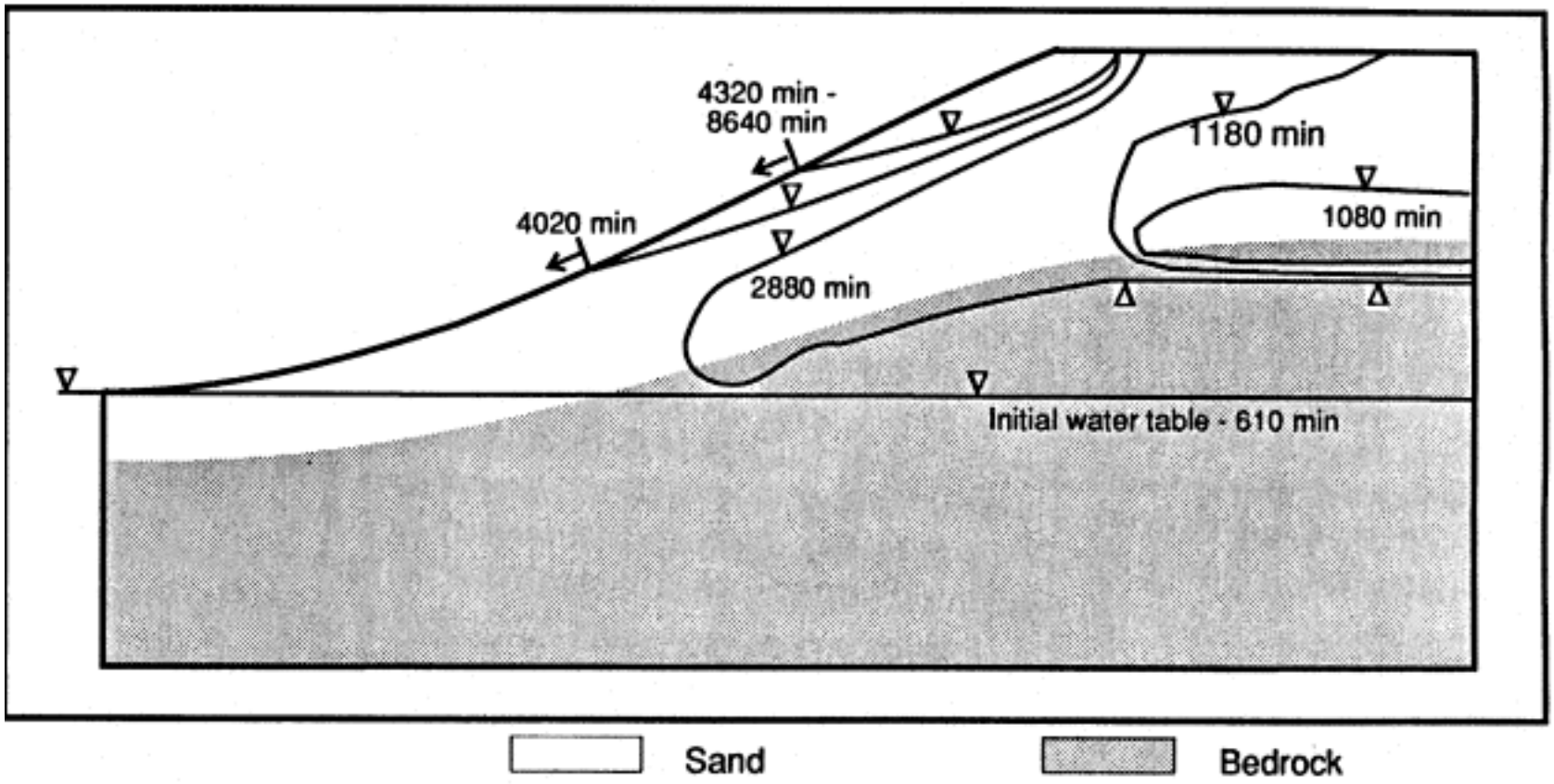

Figure 3.3 Simulation of base flow generation case from Freeze (1972a) with heterogeneous conditions: Del Monte sand (Liakopoulos, 1965) and low-permeability bedrock

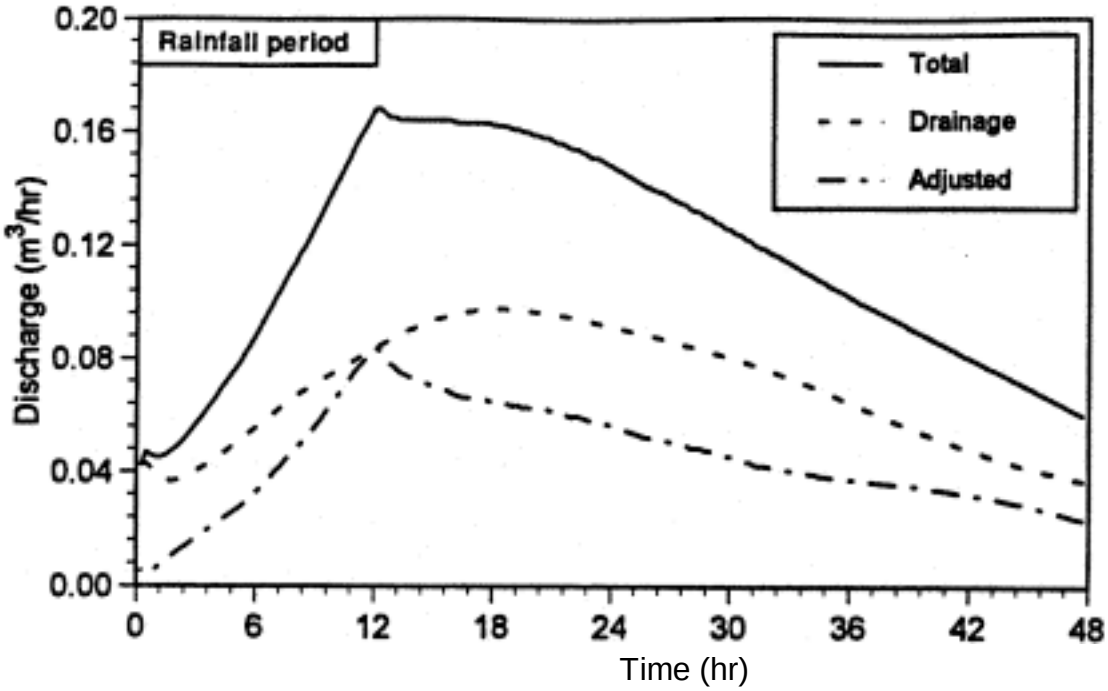

Figure 3.4 Effects of drainage from initial conditions used in run 4 (Inceptisol soil)

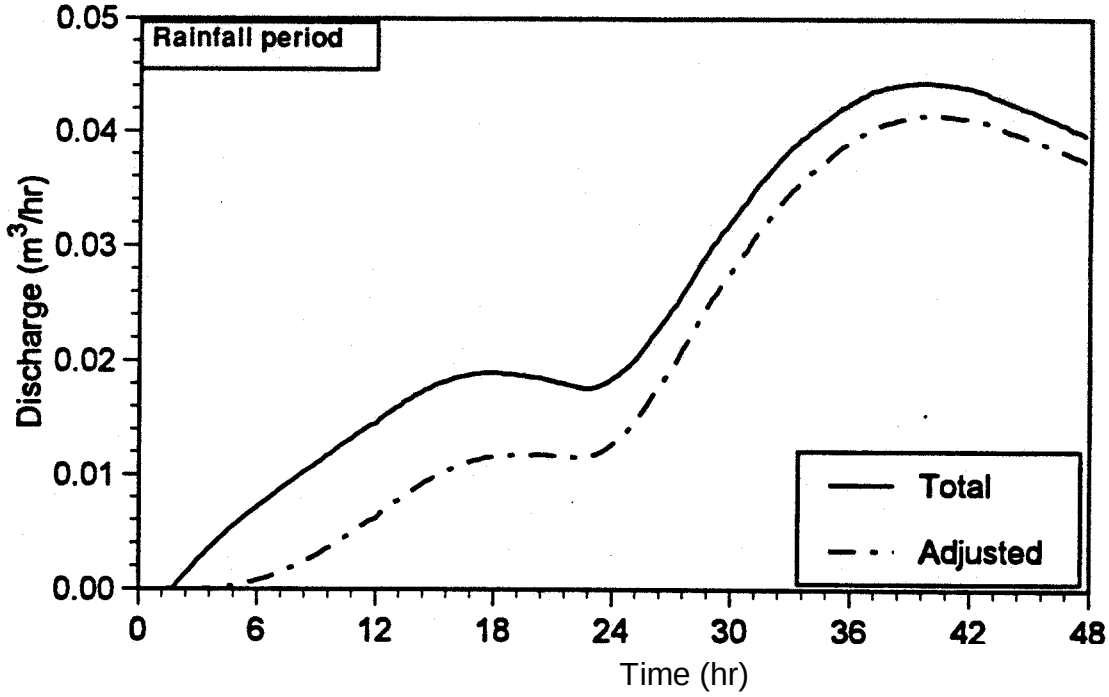

Figure 3.5 Effects of drainage from initial conditions used in run 2 (colluvial soil)

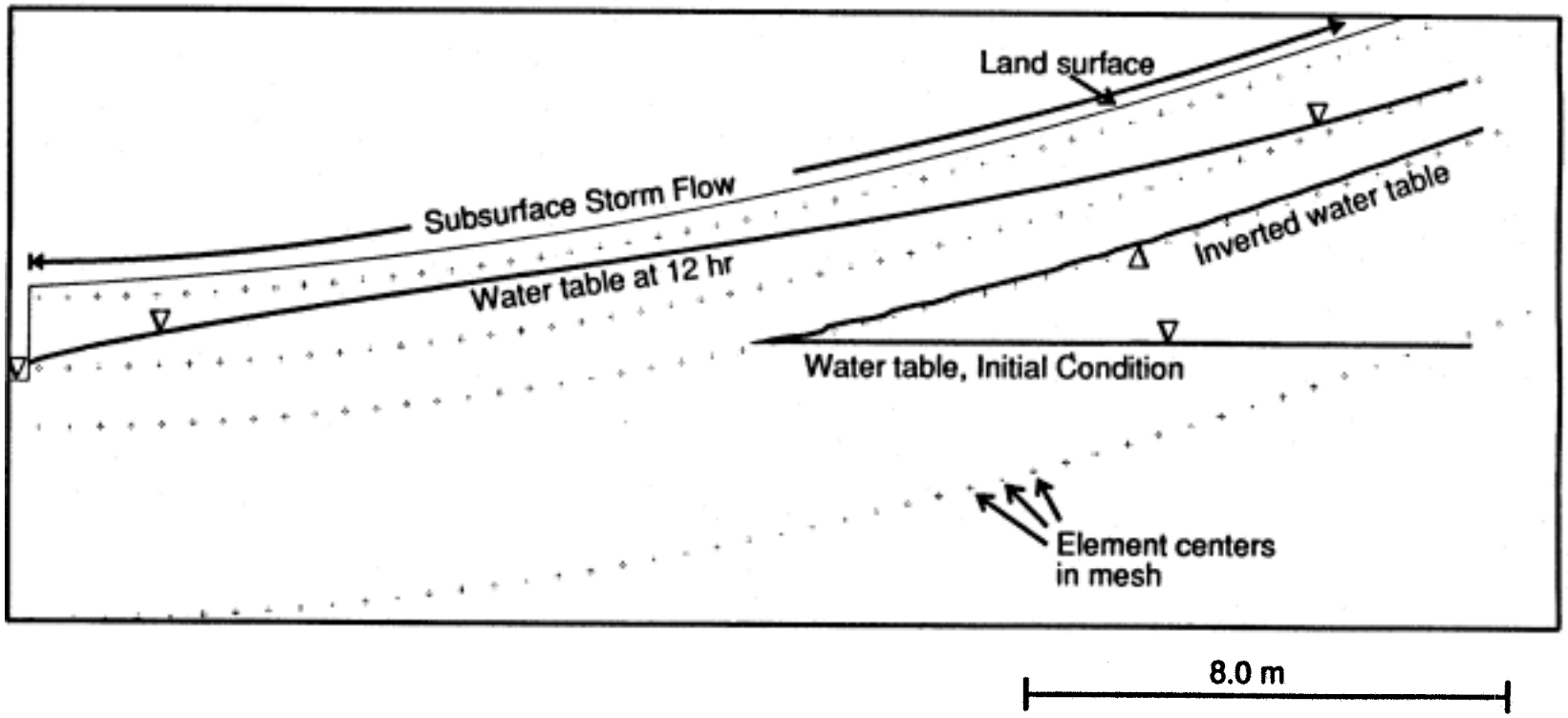

Figure 3.6 Water table profile and runoff process at end of 12-hour rainfall period, run 4 (Inceptisol soil), low-permeability bedrock, and 1.2 m constant head downstream boundary condition

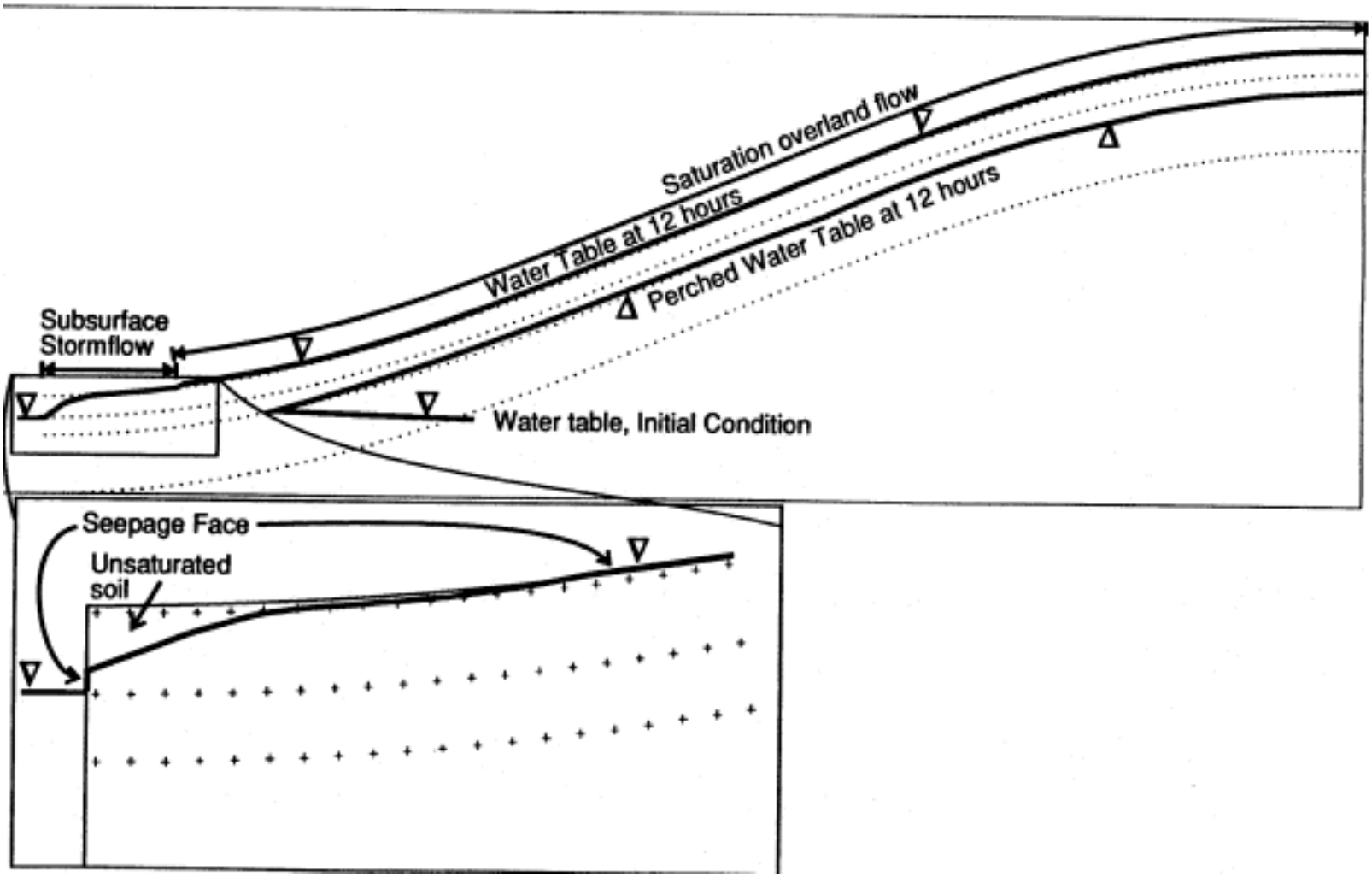

Figure 3.7 Runoff processes at end of 12-hour rainfall period for run 1 (Del Monte sand)

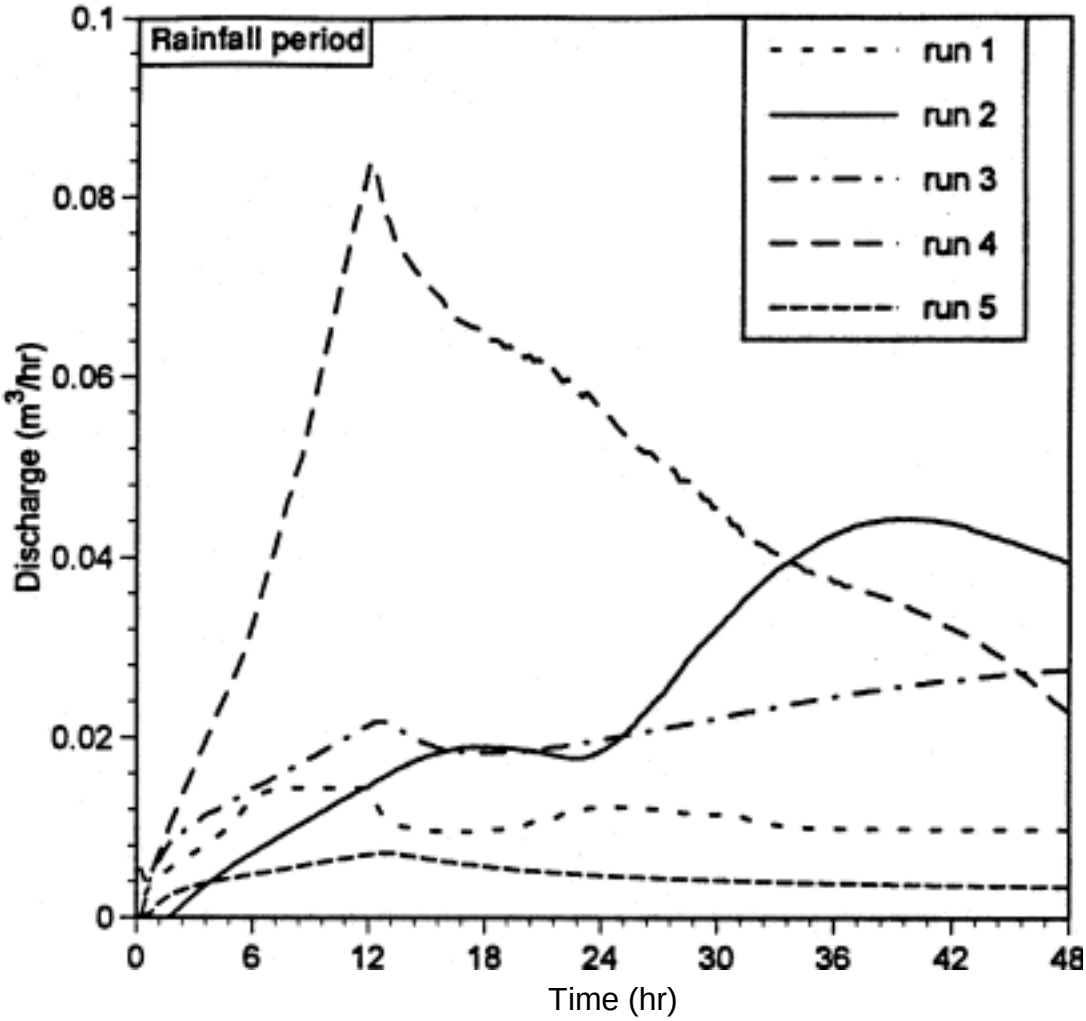

Figure 3.8 Comparison of runoff rates for different soil types (adjusted for drainage) - each with low-permeability bedrock

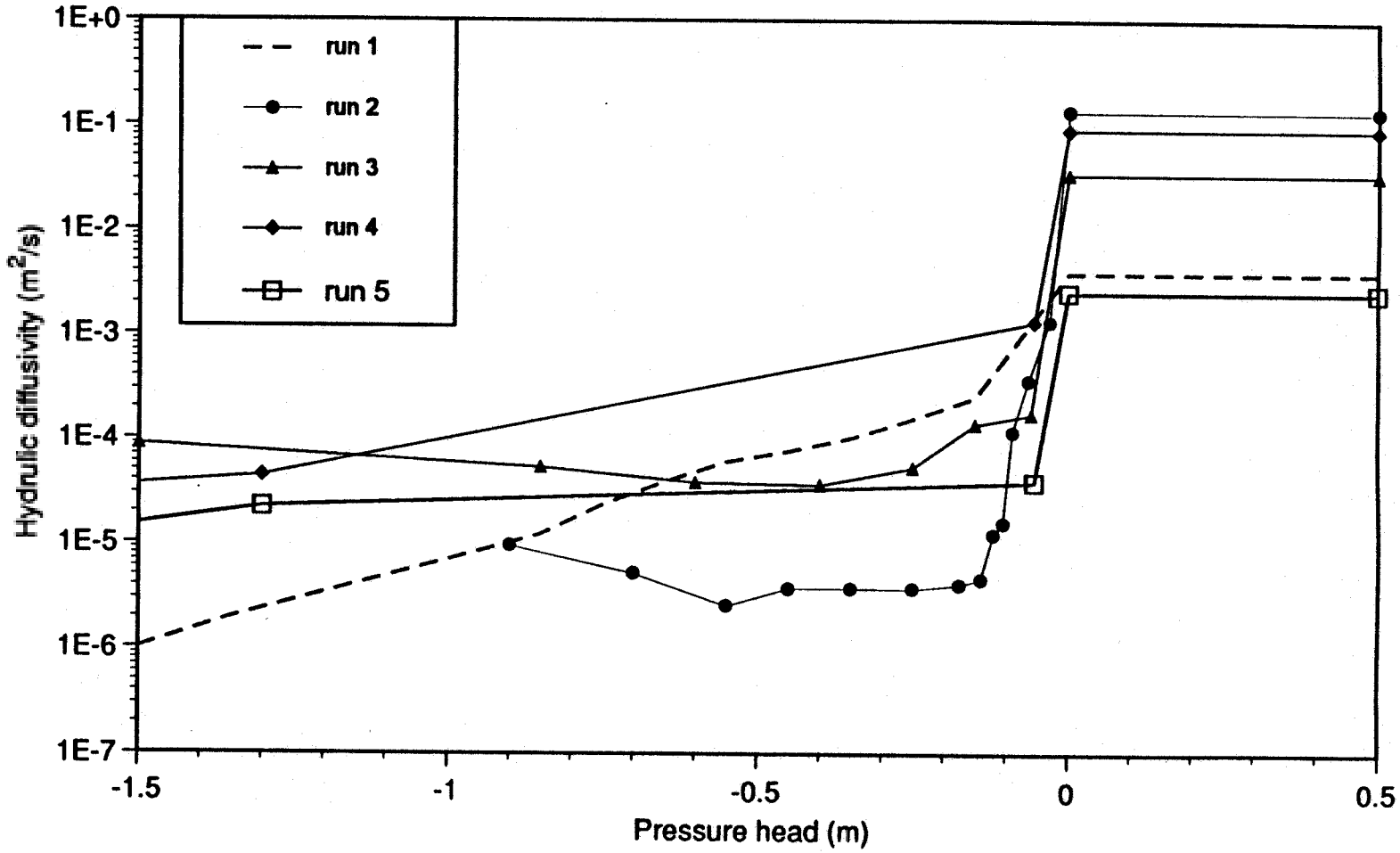

Figure 3.9 Hydraulic diiffusivity for soils used in parametric simulations

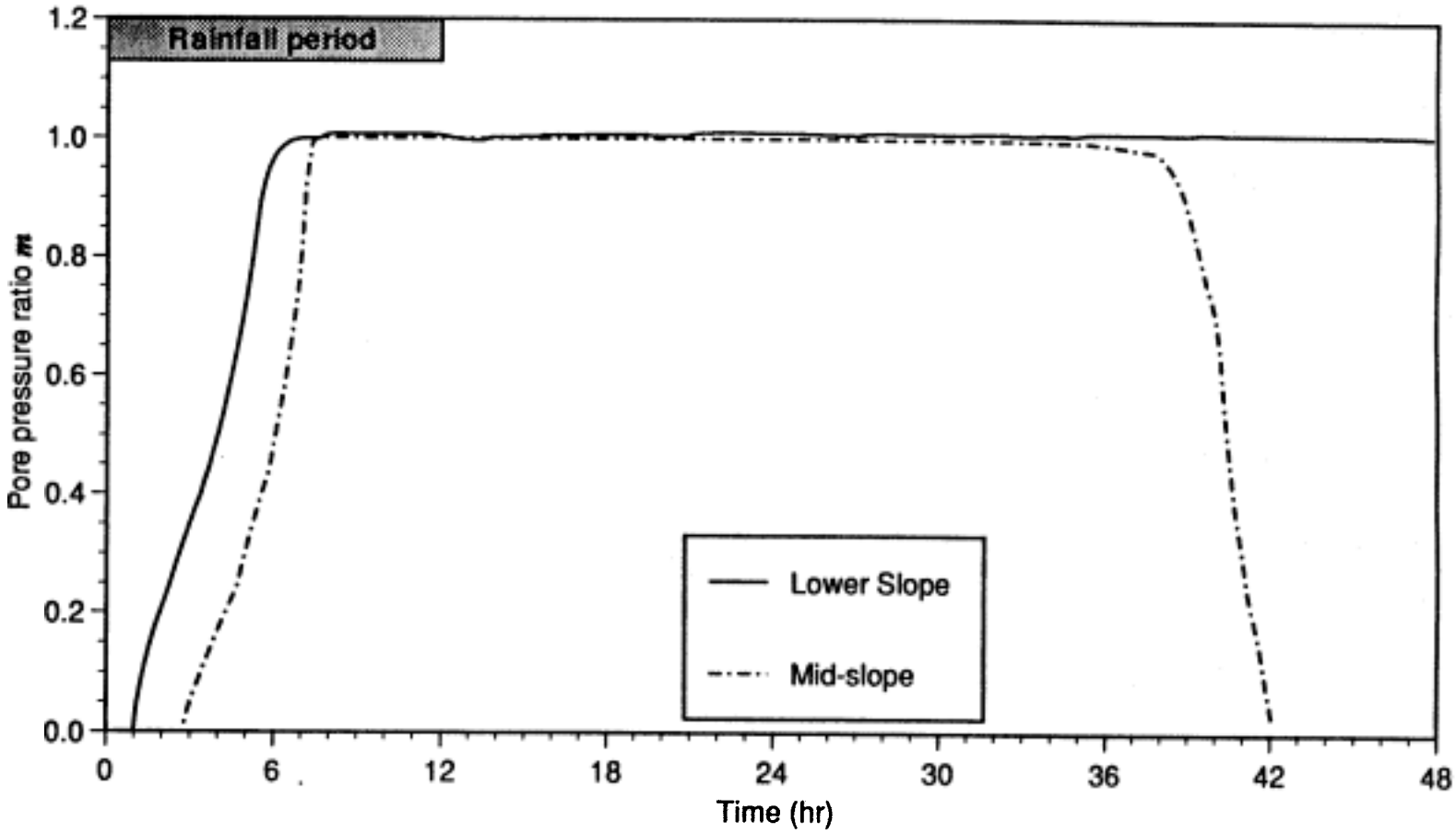

Figure 3.10 Pressure head ratio m evolution during run 1 (Del Monte sand)

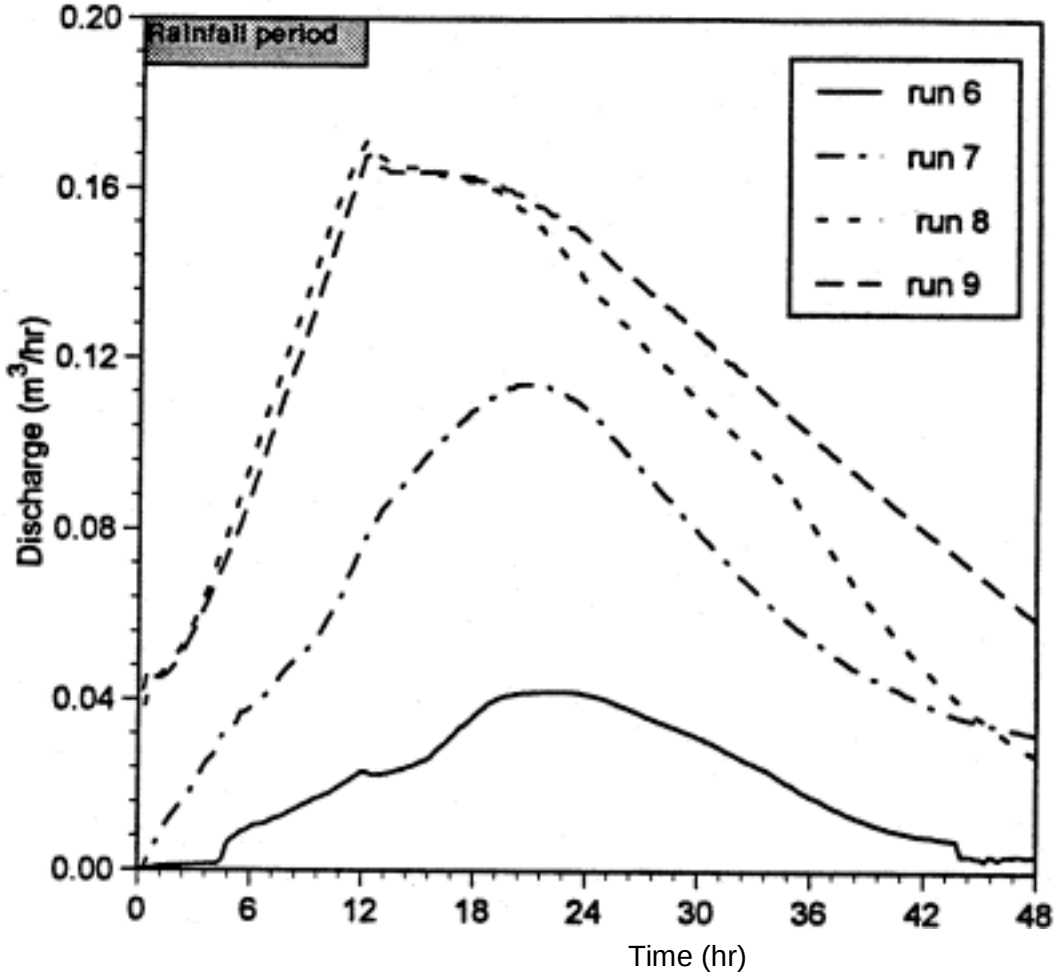

Figure 3.11 Effects of variable saprolite thickness on runoff rates

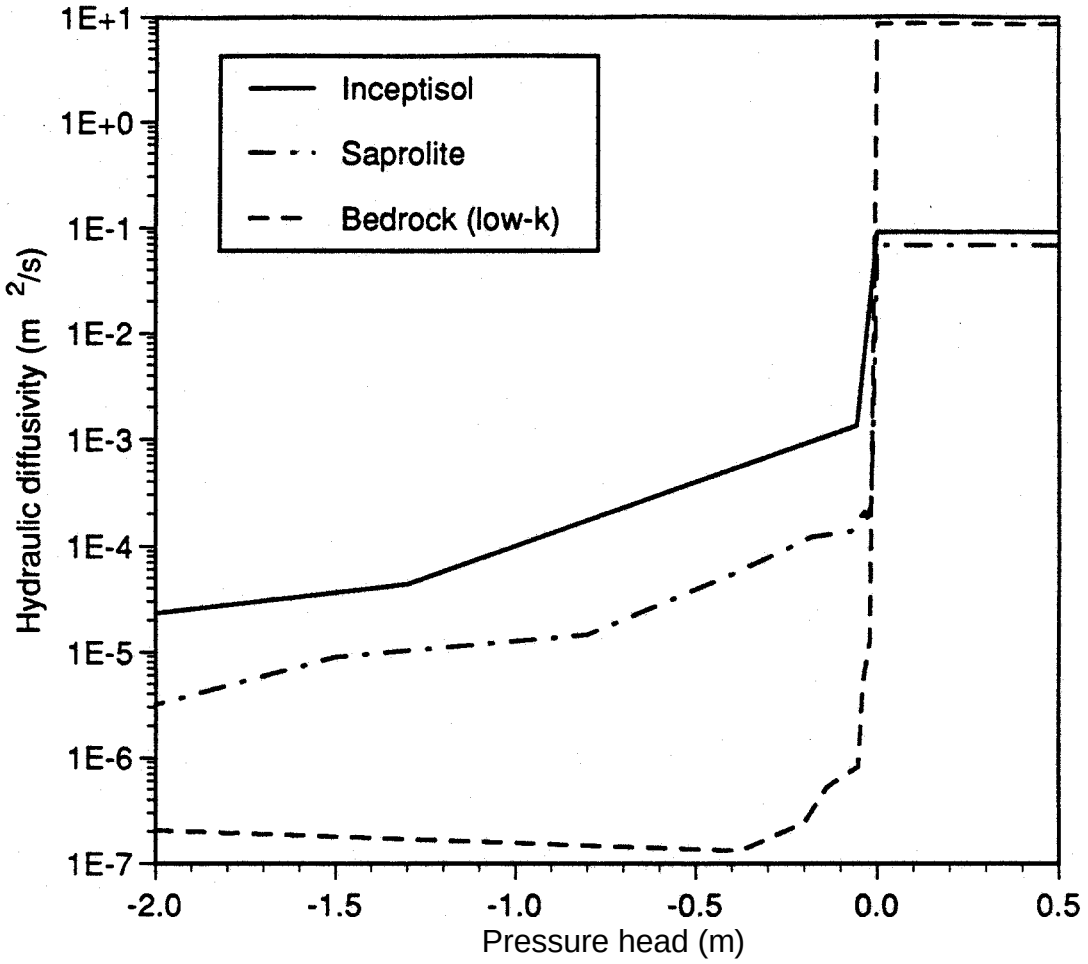

Figure 3.12 Hydraulic diffusivity relationships for saprolite cases (runs 6 - 9)

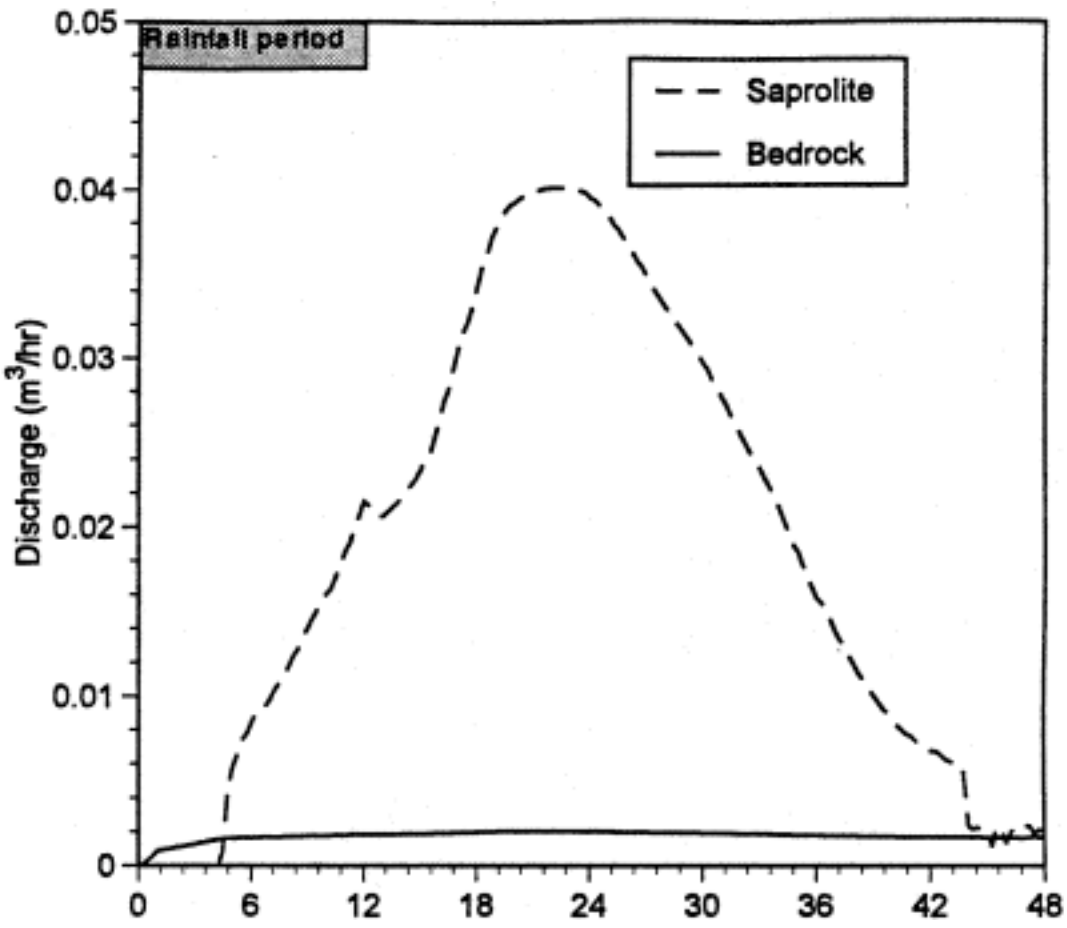

Figure 3.13 Runoff from individual flow paths for run 6

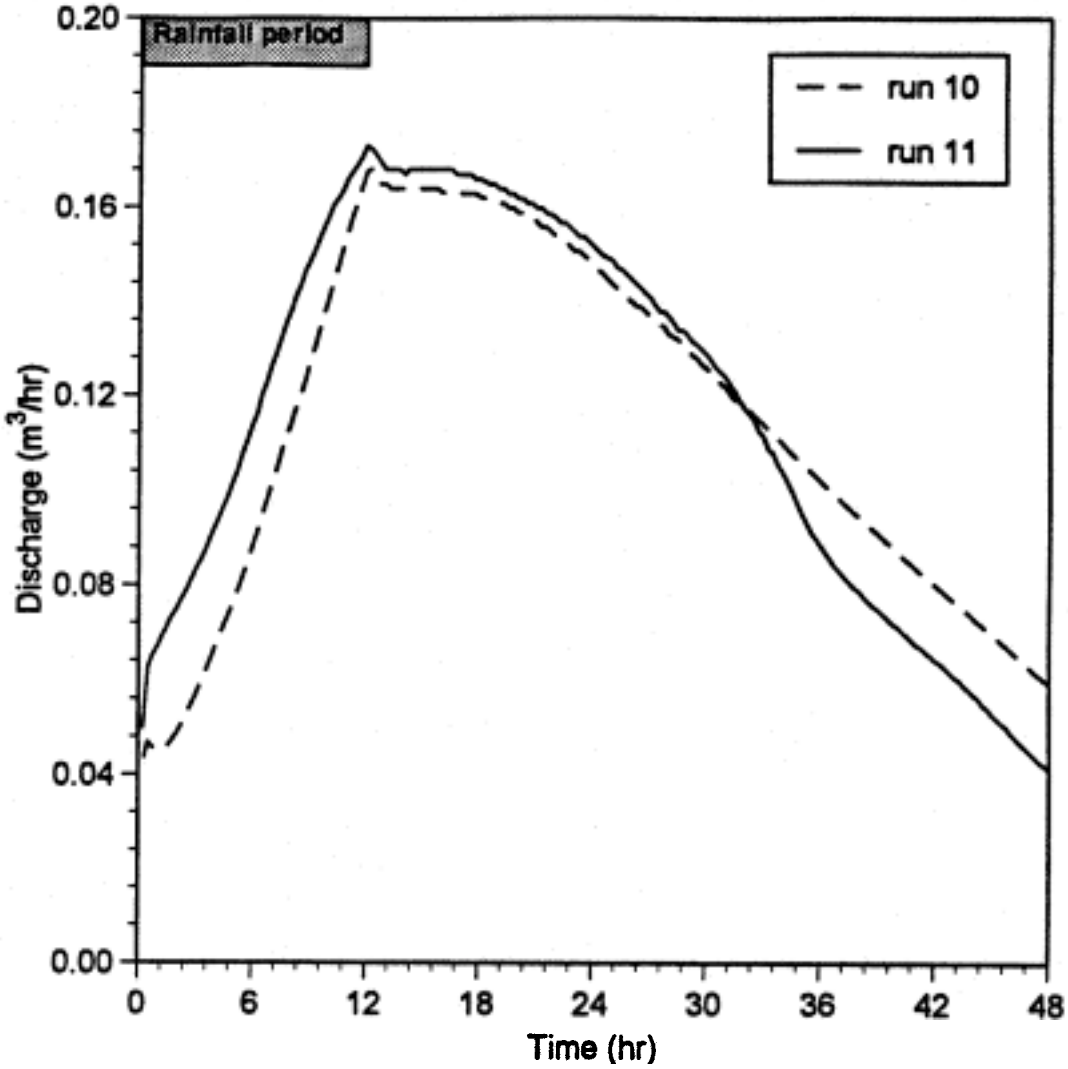

Figure 3.14 Runoff rates for low-permeability rock (run 10) and high-permeability rock (run 11)

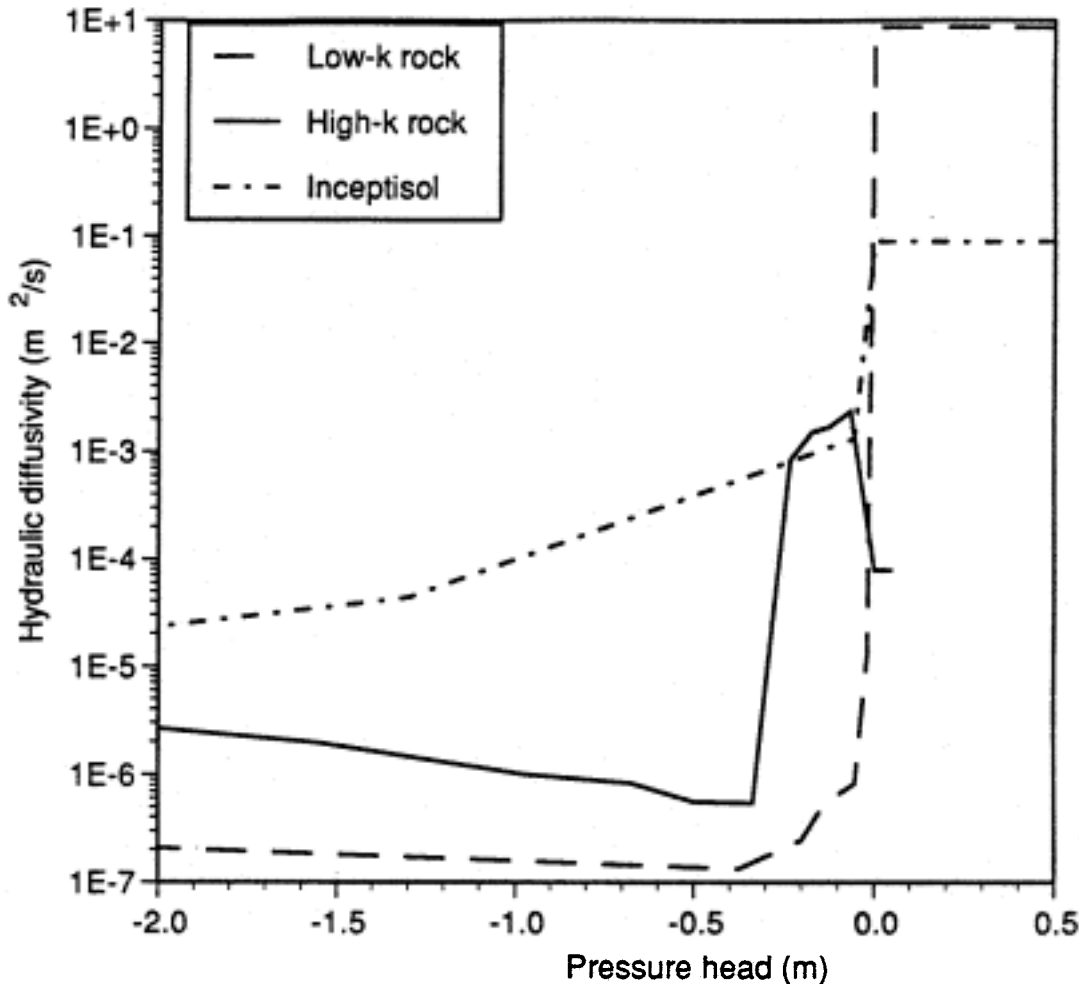

Figure 3.15 Hydraulic diffusivity relationships fior bedrock types

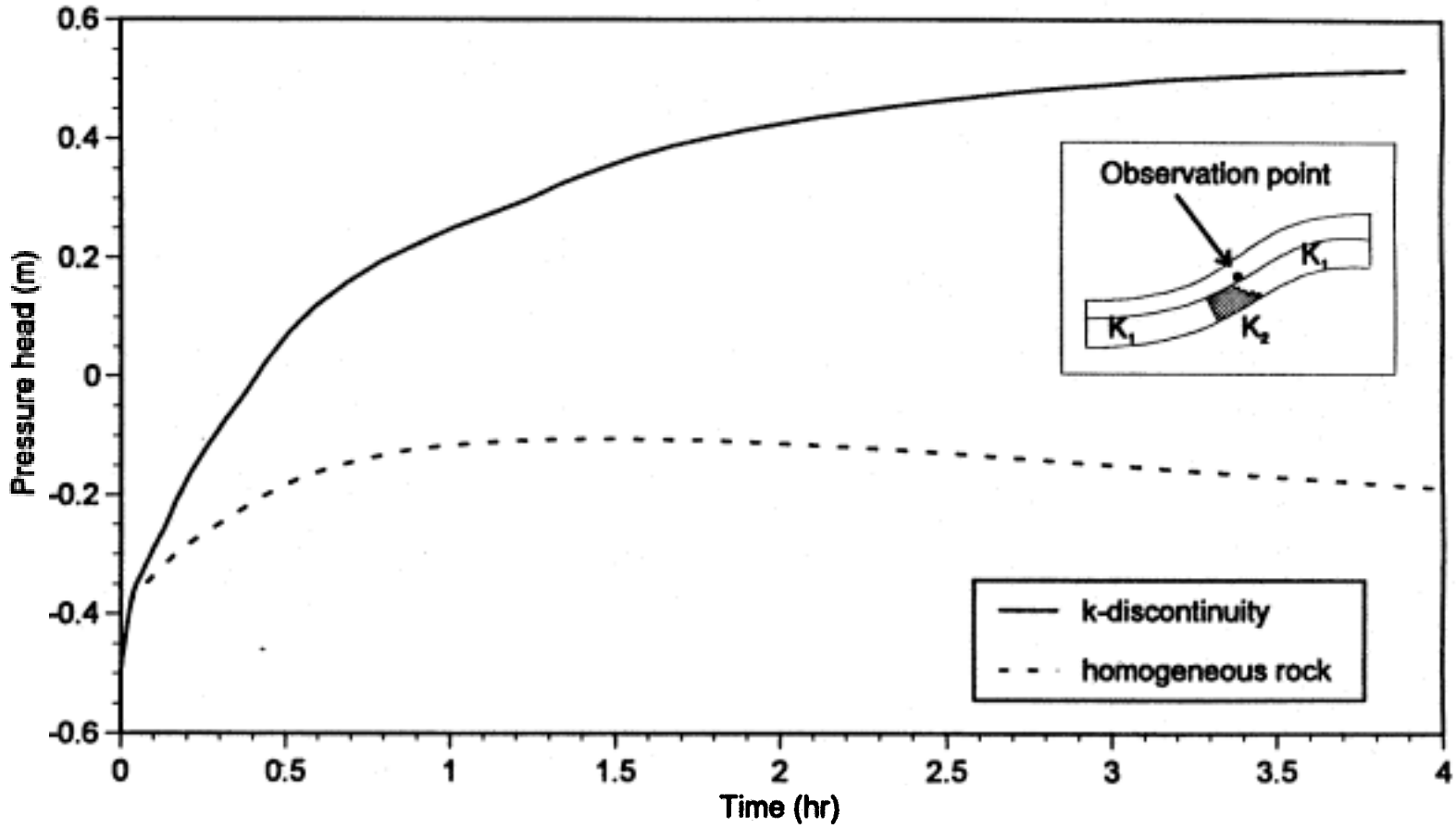

Figure 3.16 Pressure head evolution at soil/bedrock contact - case with midslope discontinuity (run 12)

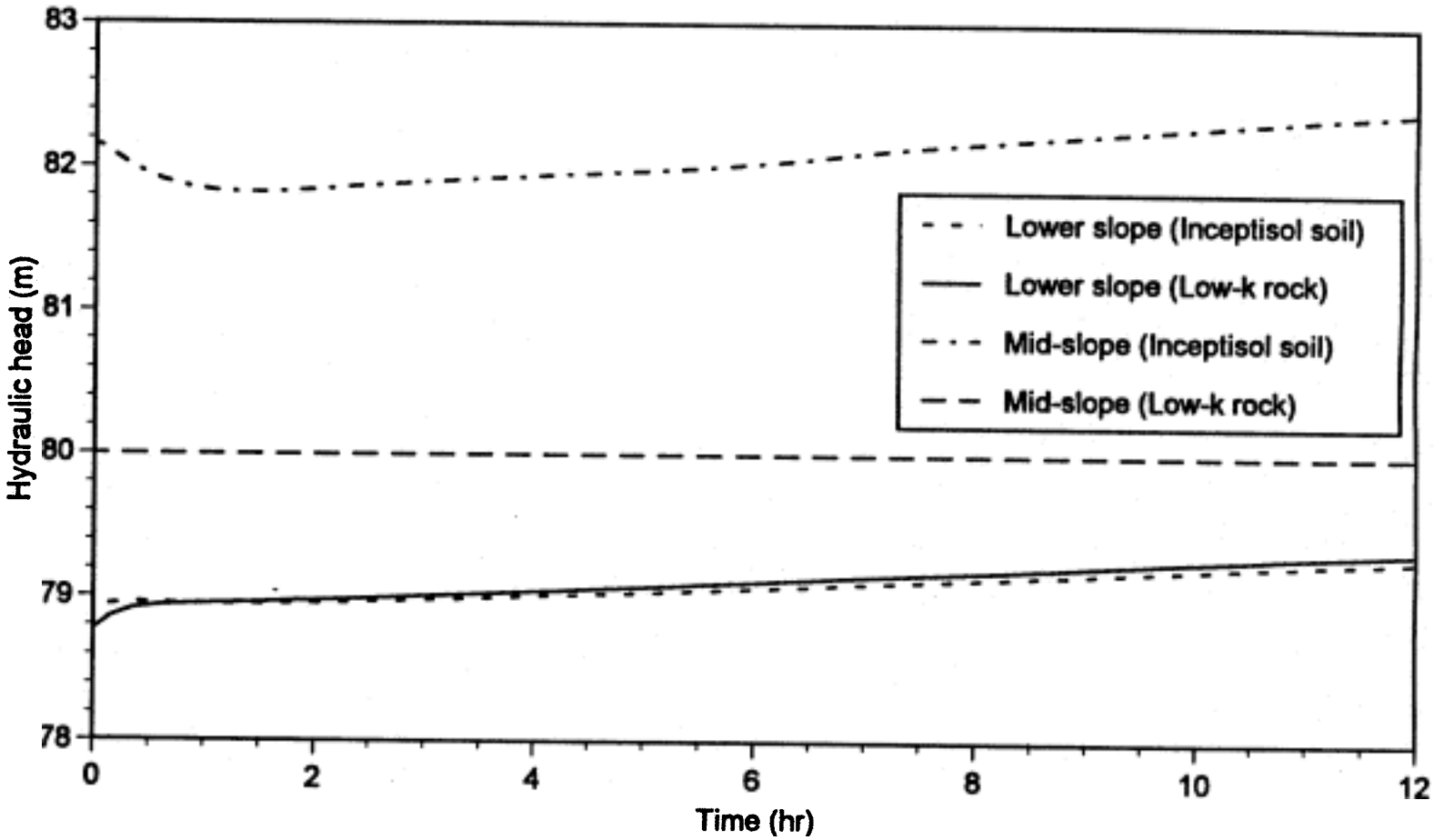

Figure 3.17 Hydraulic head response of different materials at two slope positions during 12 hours of constant rainfall - run 4

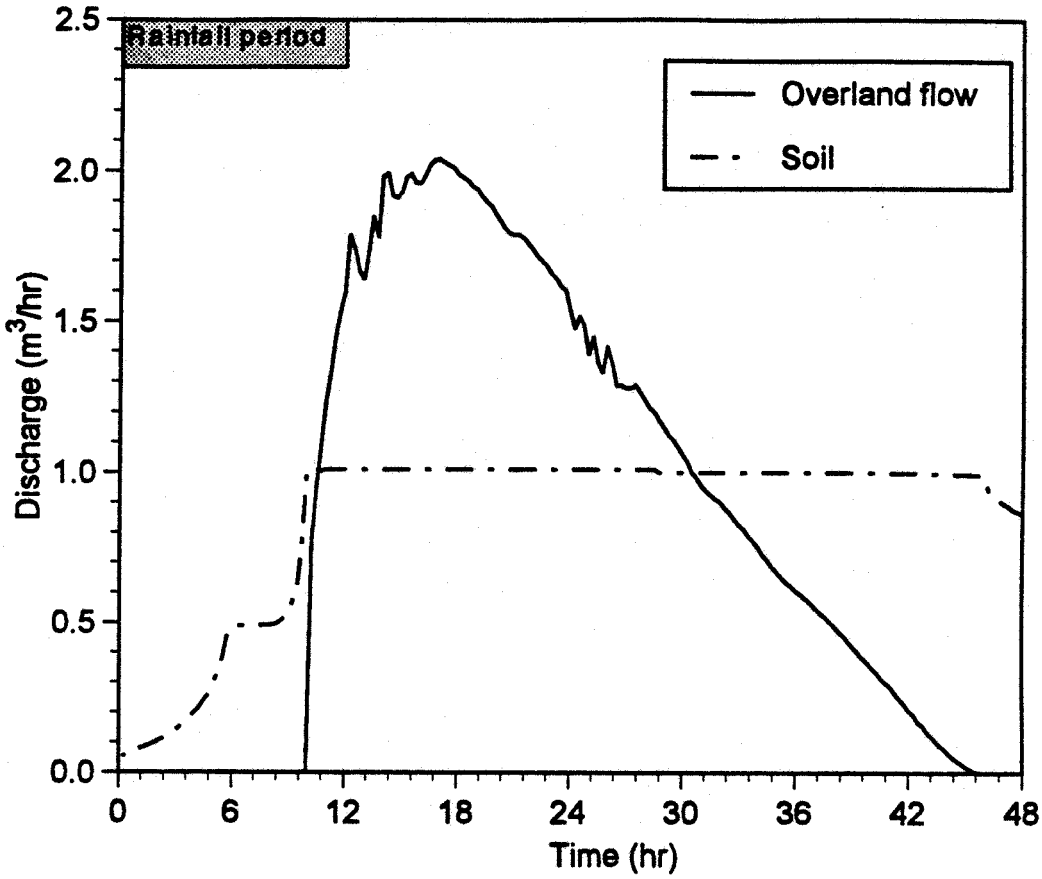

Figure 3.18 Discharge by flow path for convergent flow domain - run 13

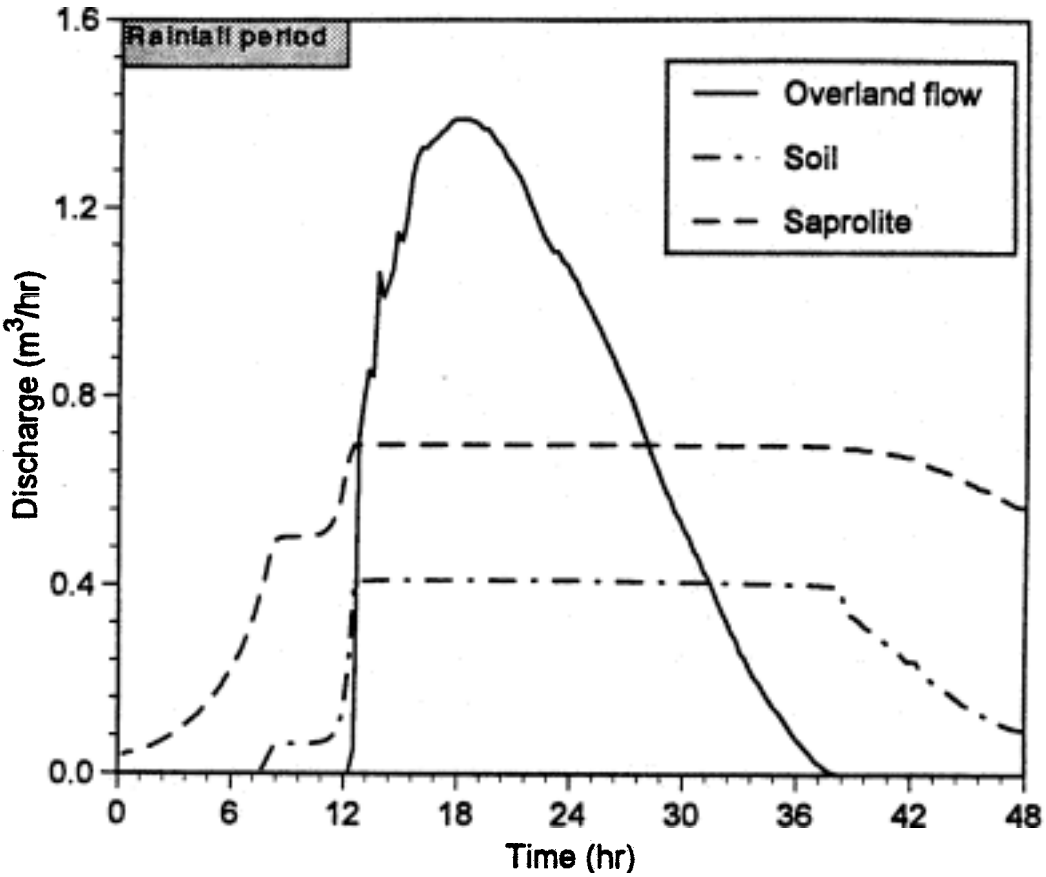

Figure 3.19 Discharge by flow path for convergent flow domain - run 14

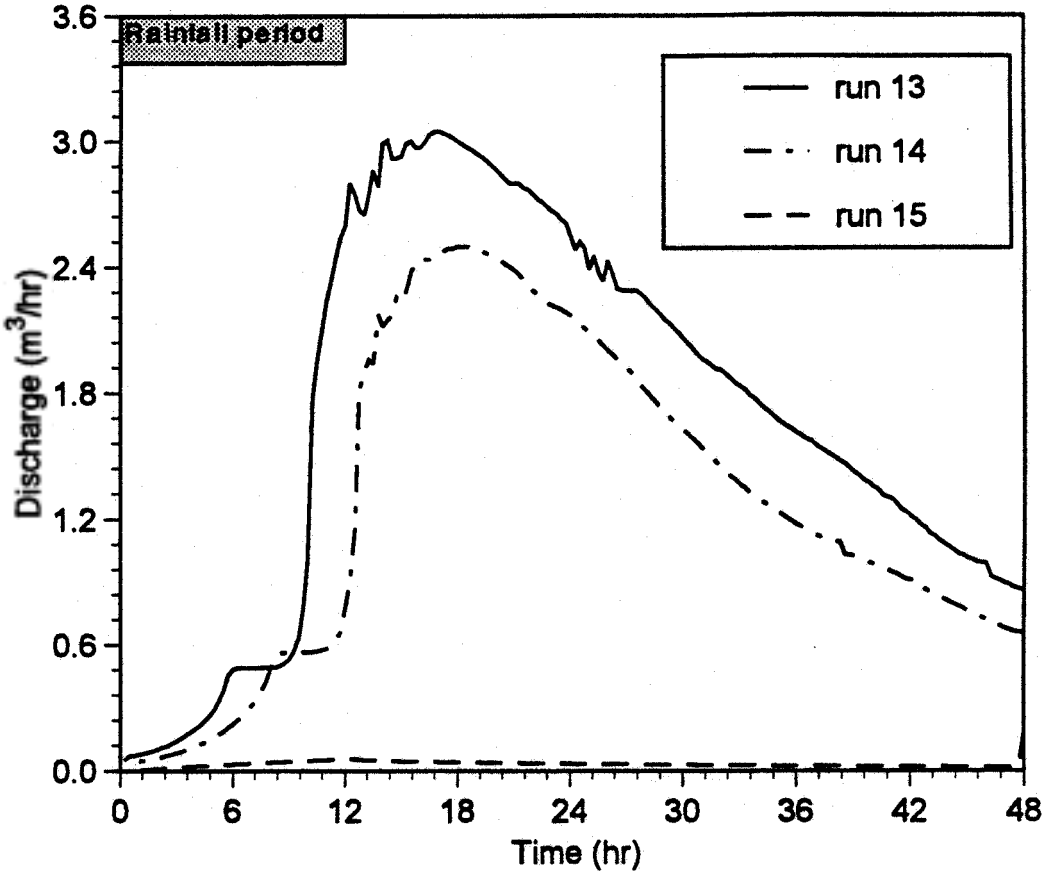

Figure 3.20 Discharge rates for convergent flow domain cases (runs 13 to 15)

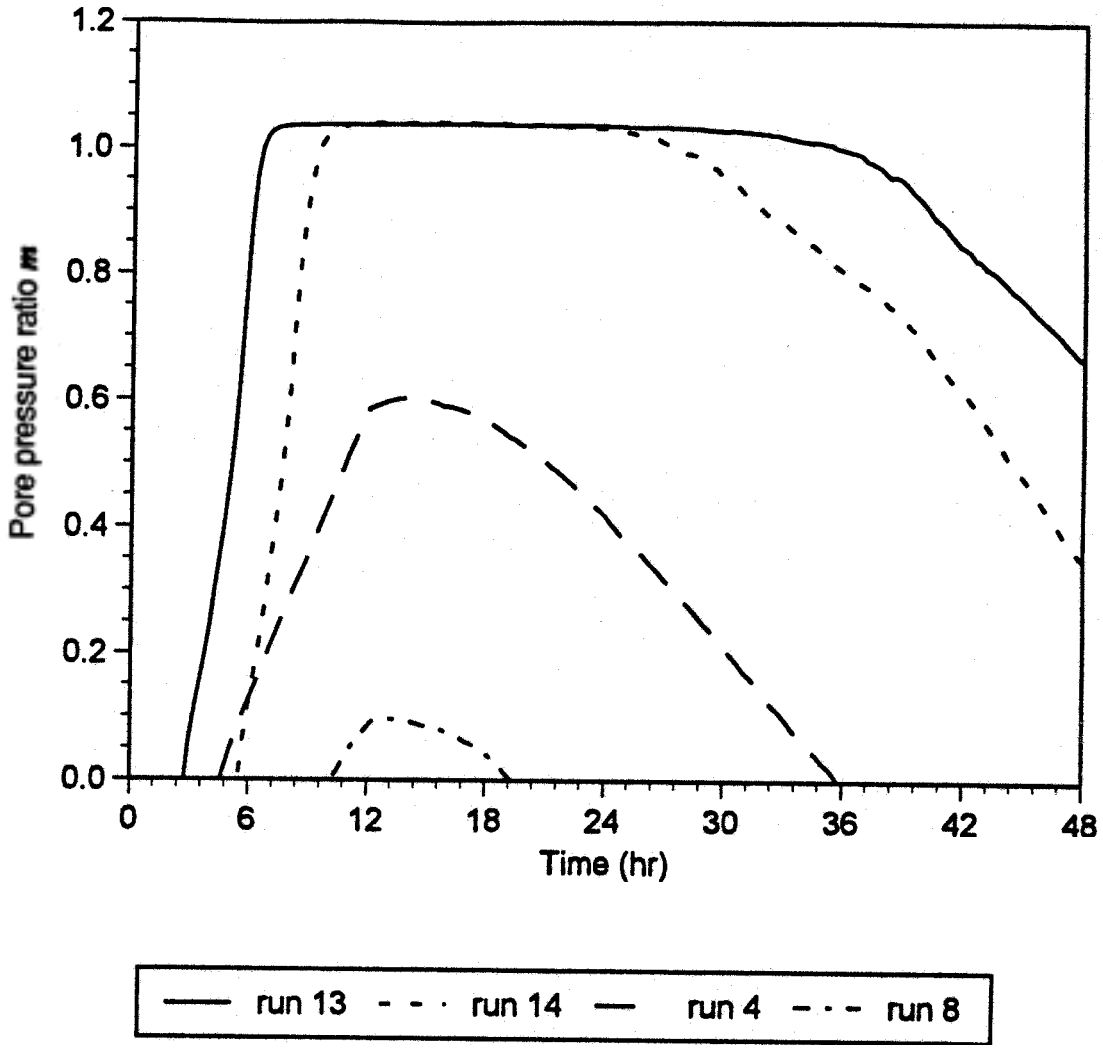

Figure 3.21 Pore pressure evolution at toe of slope for convergent (runs 13 and 14) versus parallel (runs 4 and 8) flow domains

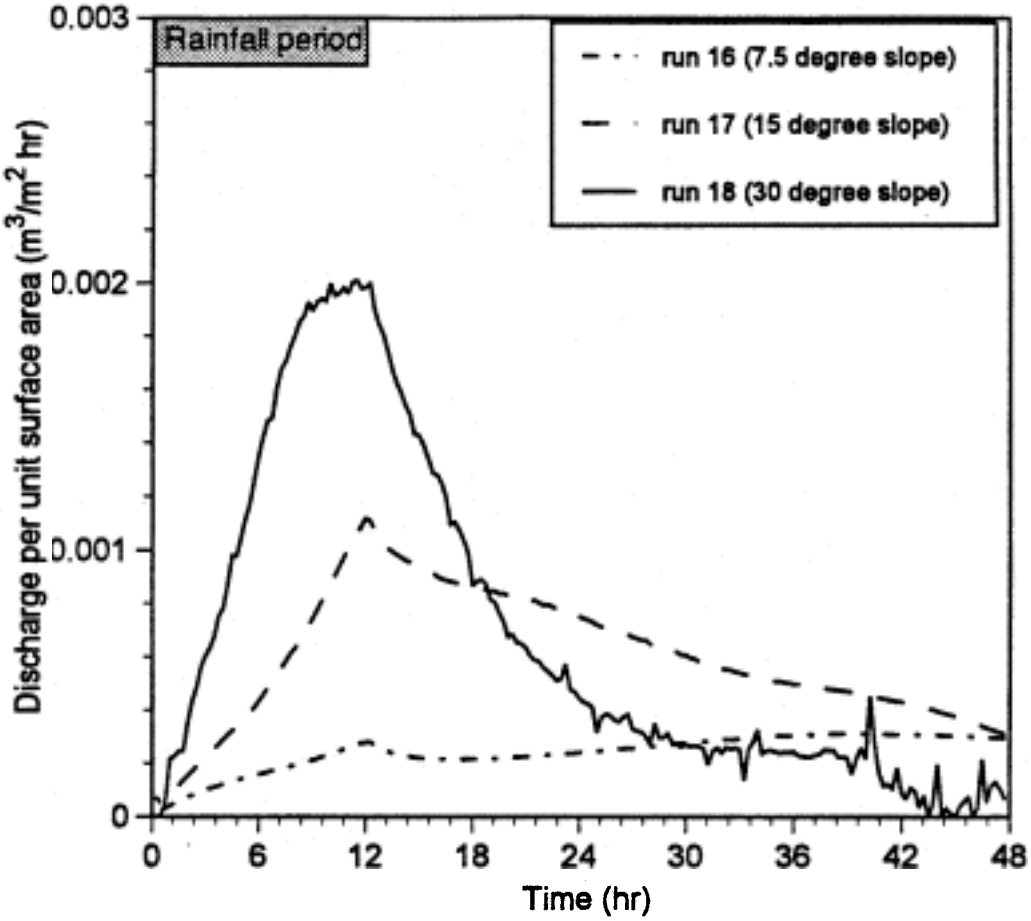

Figure 3.22 Effect of slope angle on runoff rate for cases (runs 16 to 18) with Inceptisol soil and low-permeability bedrock

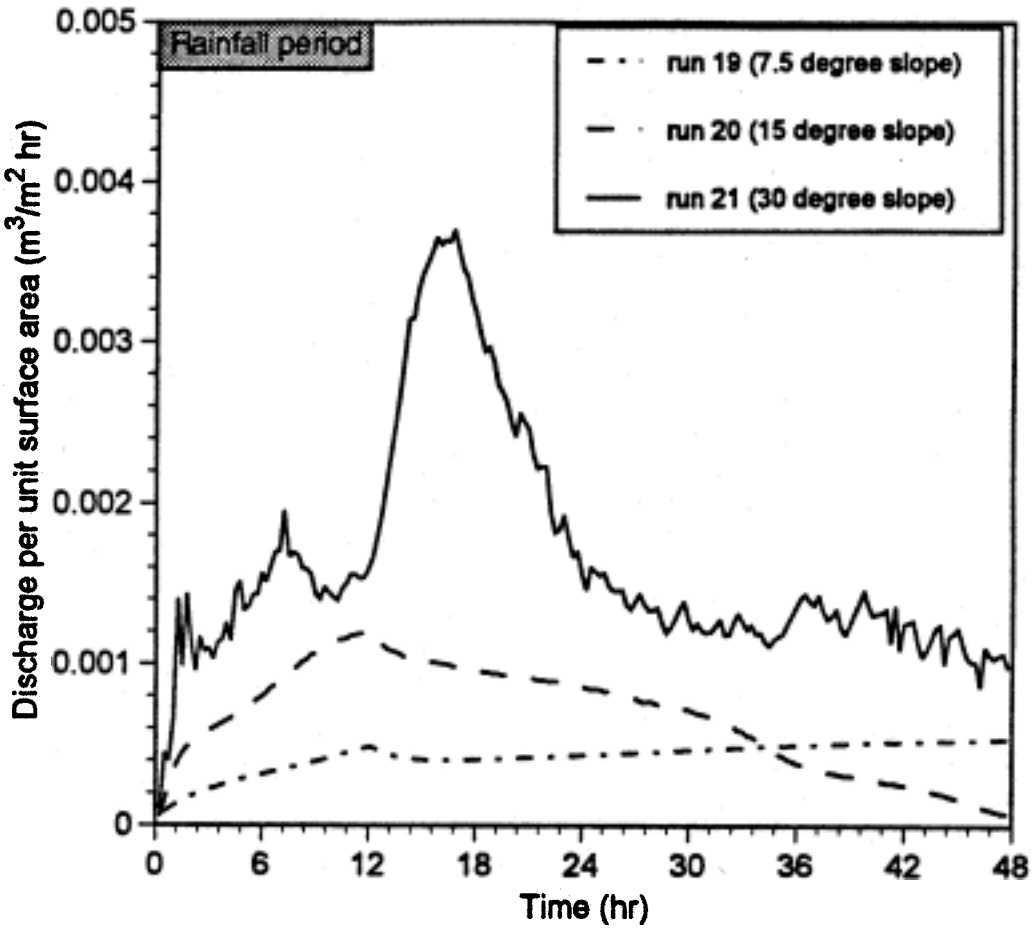

Figure 3.23 Effect of slope angle on runoff rate for cases (runs 19 to 21) with Inceptisol soil and high-permeability bedrock

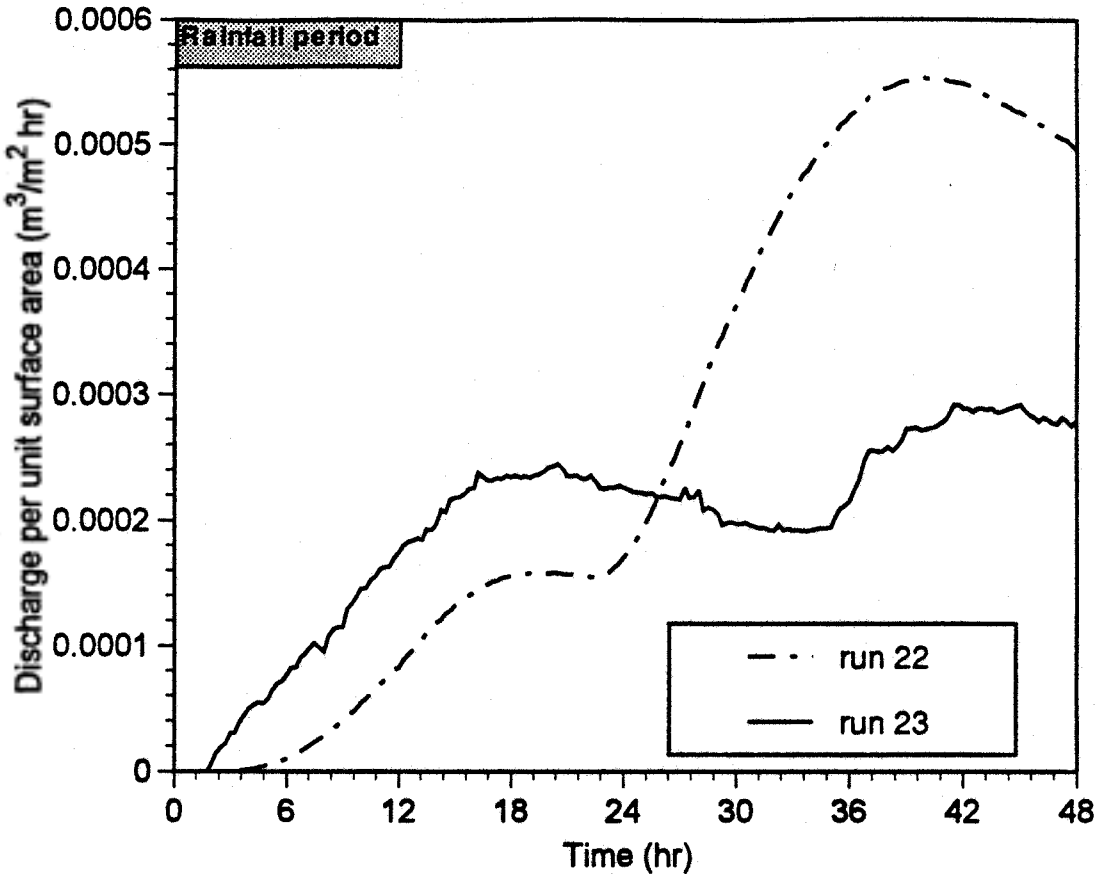

Figure 3.24 Effect of slope angle on runoff rate for cases (runs 22 and 23) with colluvial soil and low-k rock

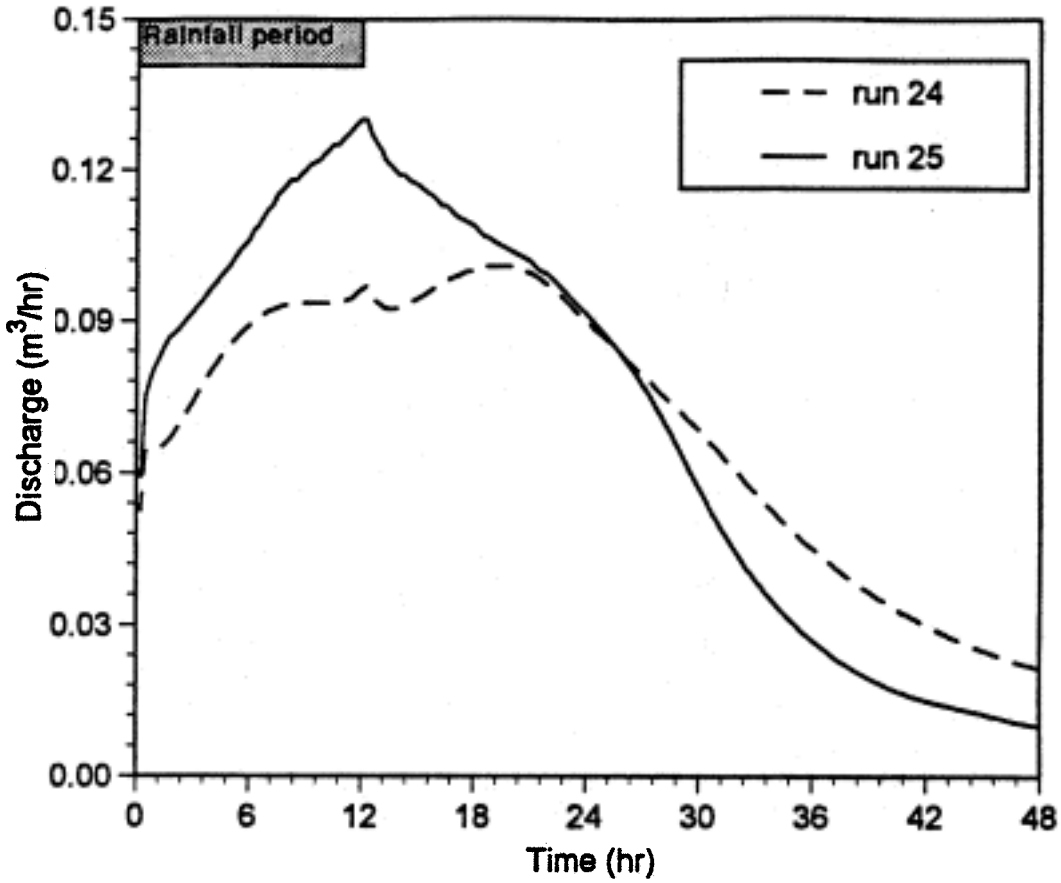

Figure 3.25 Runoff rates for different rock permeabilities (runs 24 and 25) with variable thickness Inceptisol soil

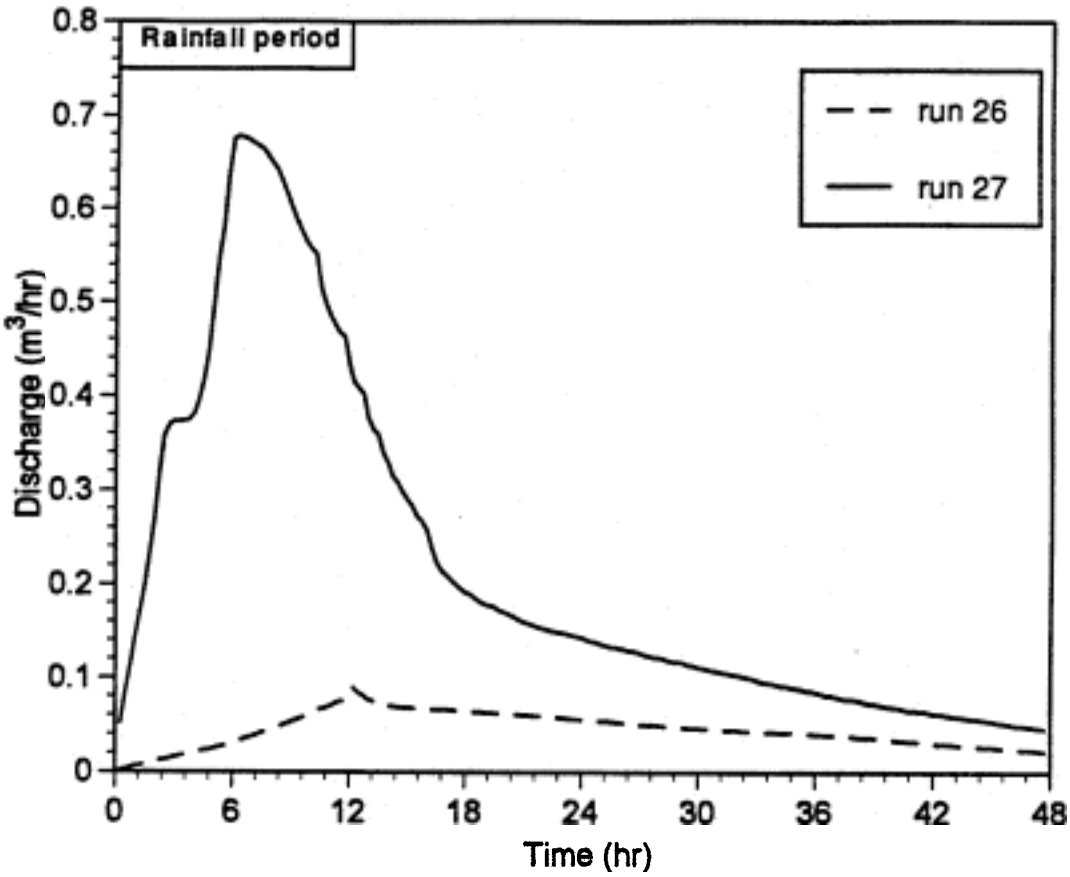

Figure 3.26 Effect of bedrock type for hillslope with fracture permeability extending to depth (runs 26 and 27)

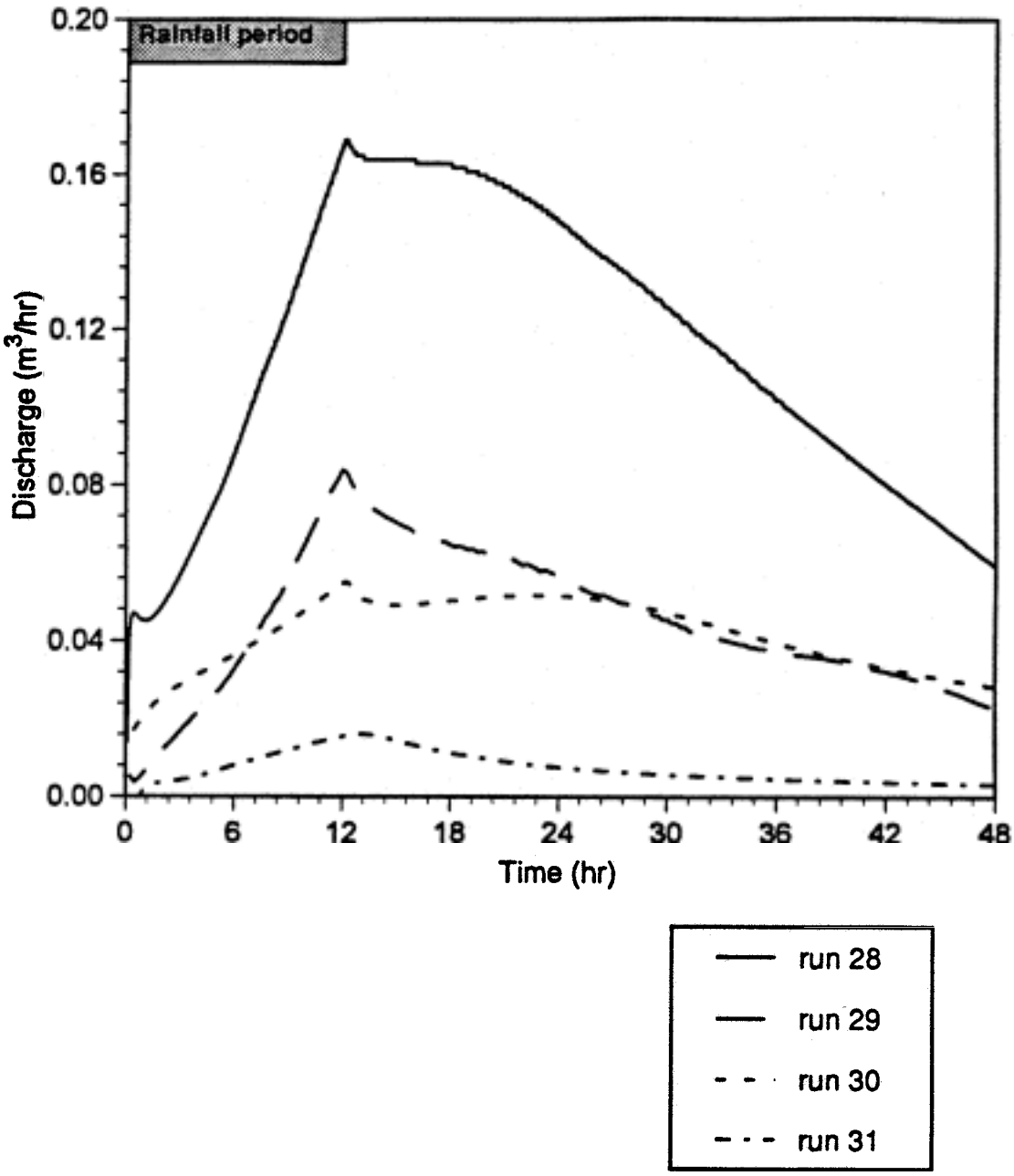

Figure 3.27 Effect of intial moisture conditions on runoff for cases (runs 28 to 31) with Inceptisol soil and low-permeability bedrock

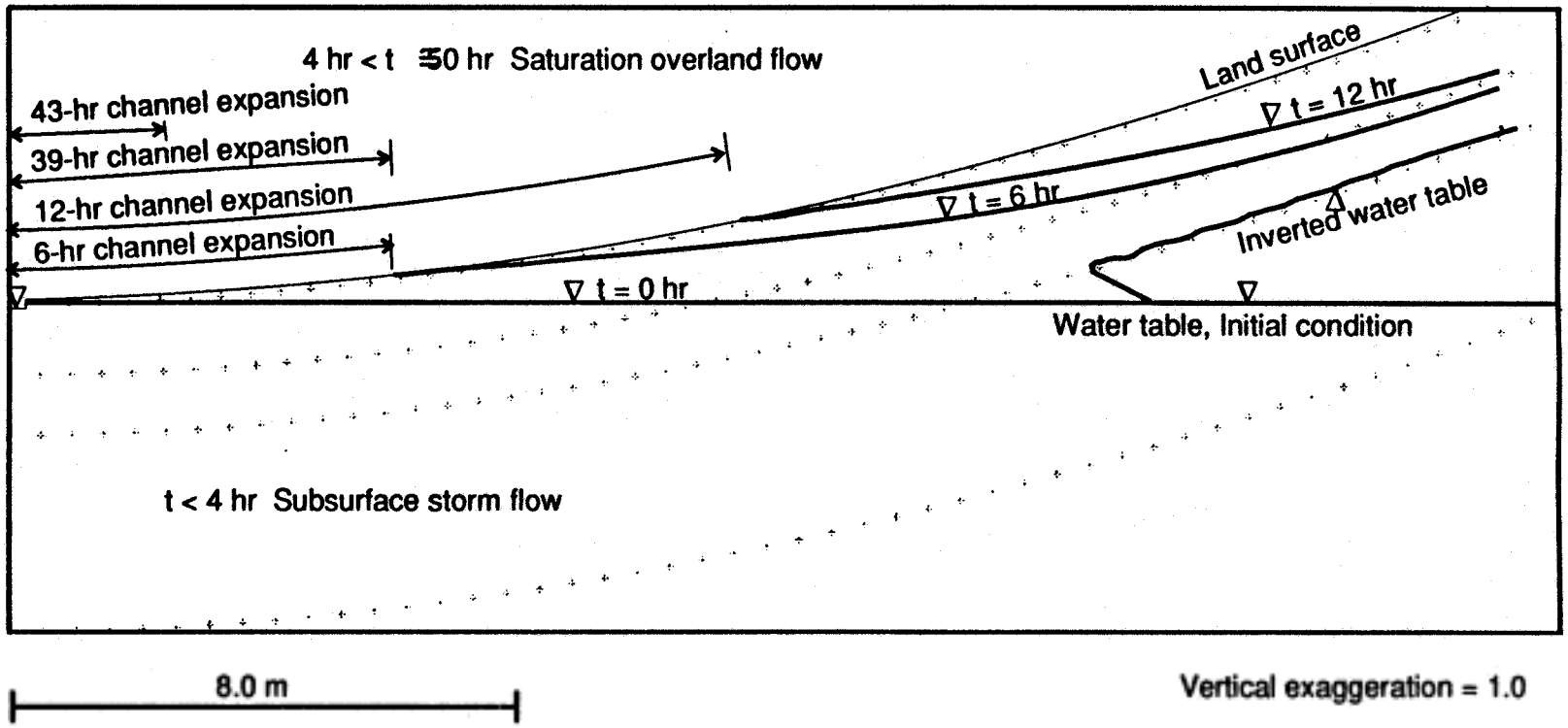

Figure 3.28 Water table profiles and runoff processes for case with 0.05 m downstream constant head boundary condition

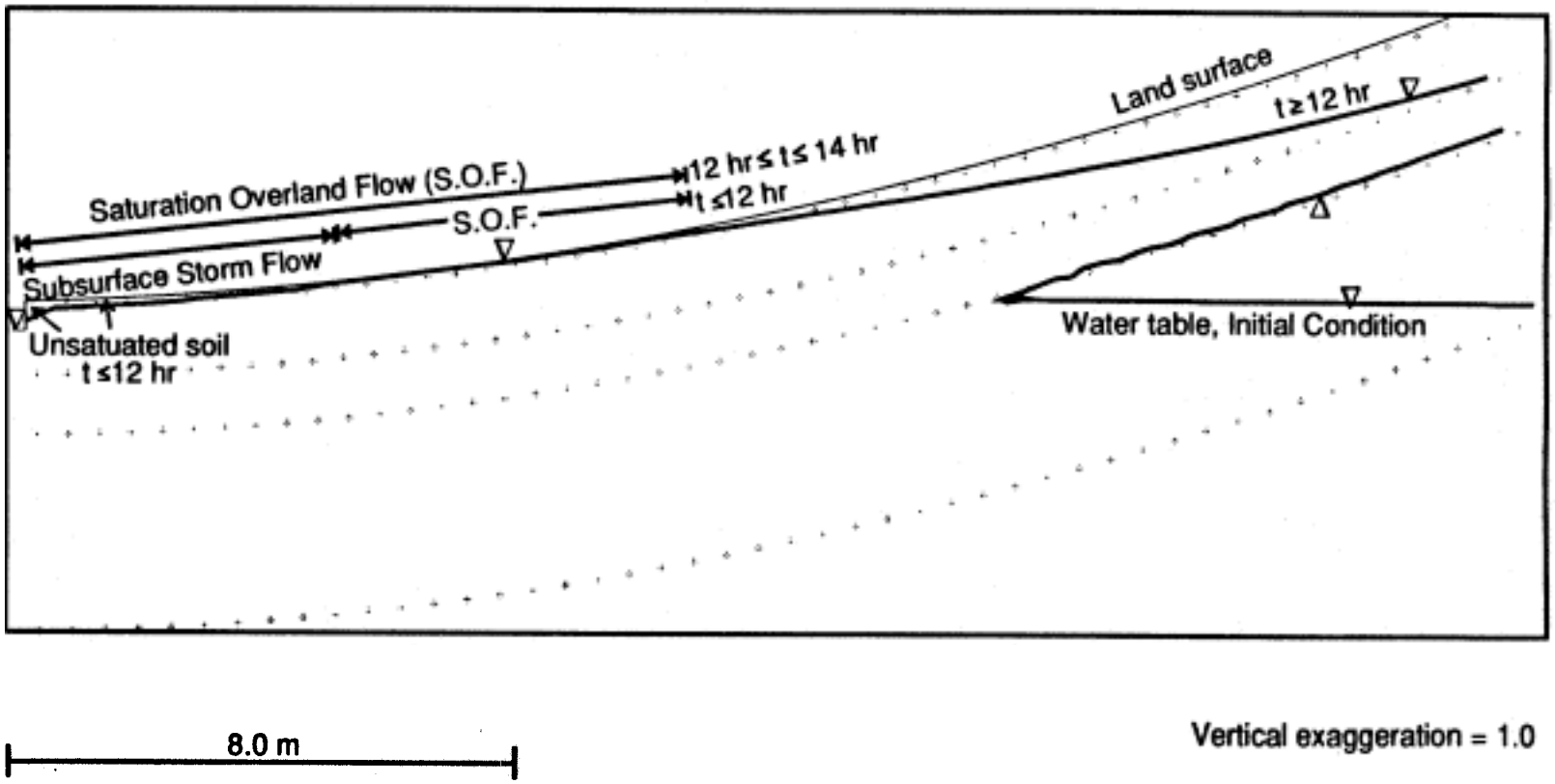

Figure 3.29 Water table profiles and runoff processes for case with 0.30 m downstream boundary condition

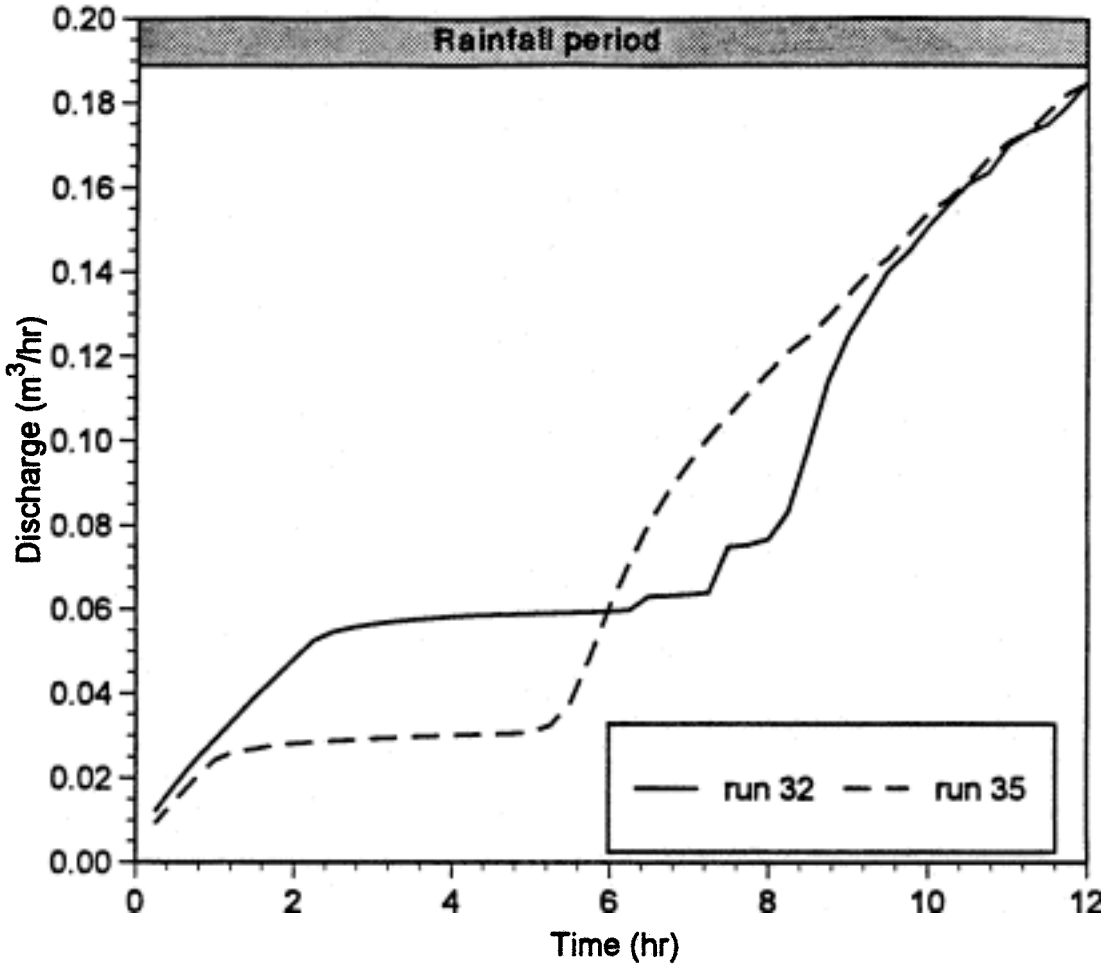

Figure 3.30 Effect of different downstream boundary conditions on runoff rates - 0.05 m channel depth (cases 32 and 35)

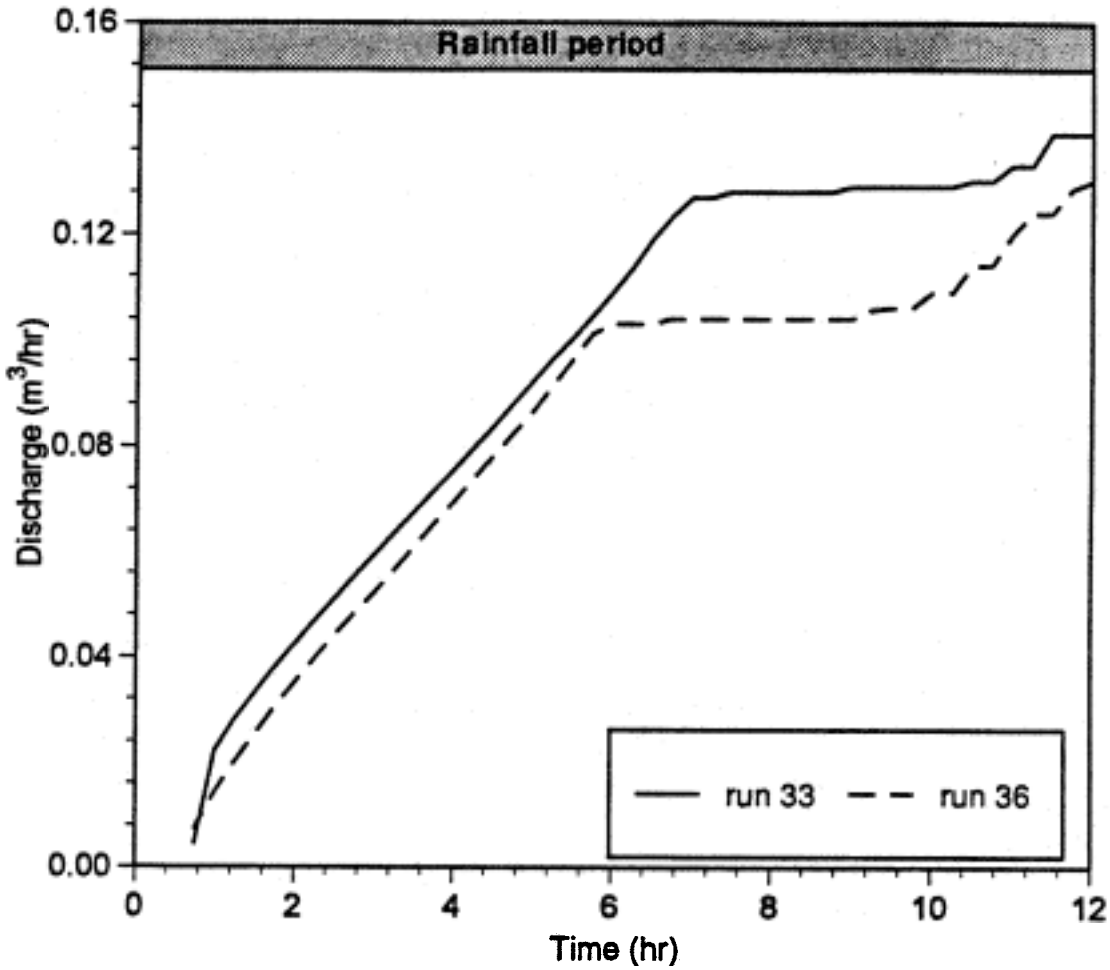

Figure 3.31 Effect of different downstream boundary conditions on runoff rates - 0.30 m channel depth (cases 33 and 36)

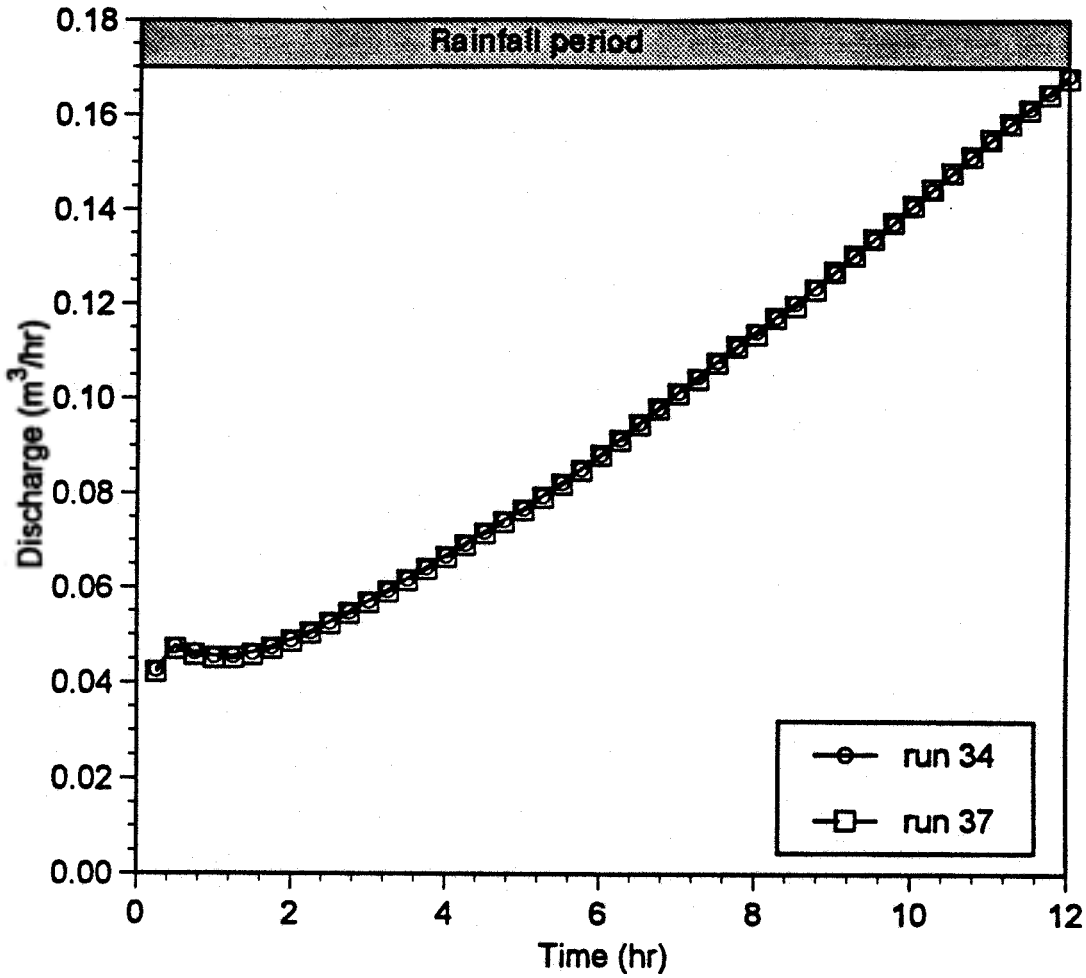

Figure 3.32 Effect of different downstream boundary conditions on runoff rates -1.20 m channel depth (cases 34 and 37)

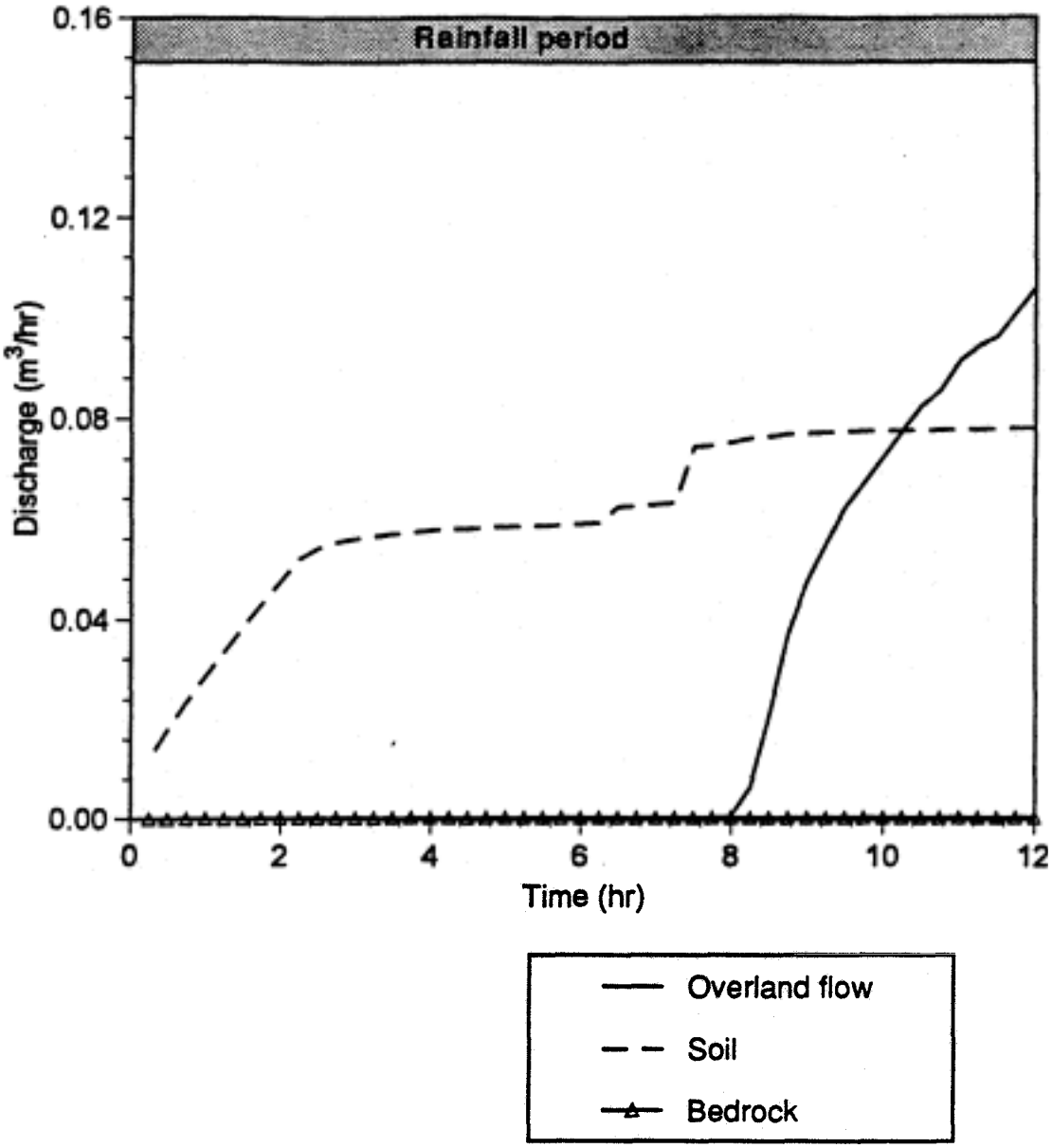

Figure 3.33 Discharge by flow path for 0.05 m channel depth and 2-part boundary condition (case 32)

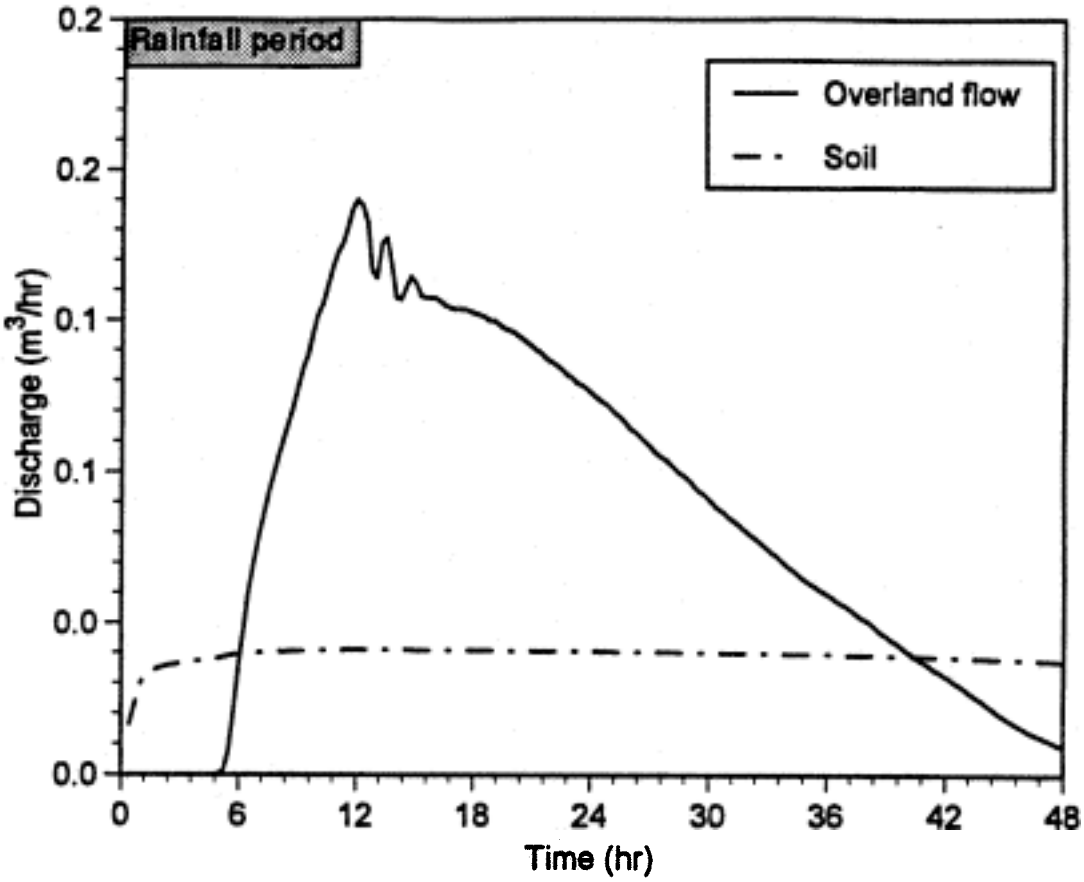

Figure 3.34 Discharge by flow path for 0.05 m channel depth and 3-part boundary condition (case 35)

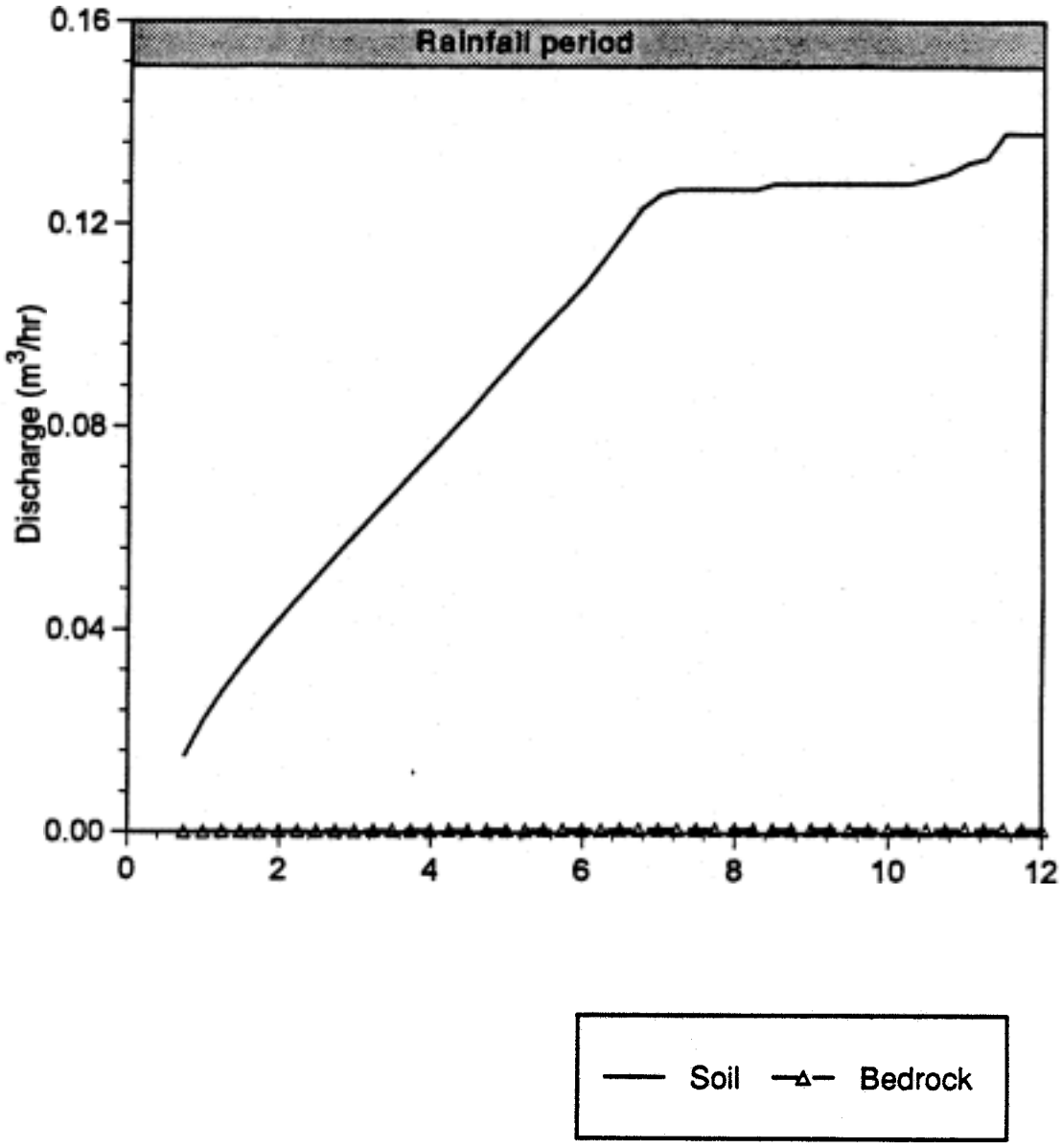

Figure 3.35 Discharge by flow path for 0.30 m channel depth and 2-part boundary condition (case 33)

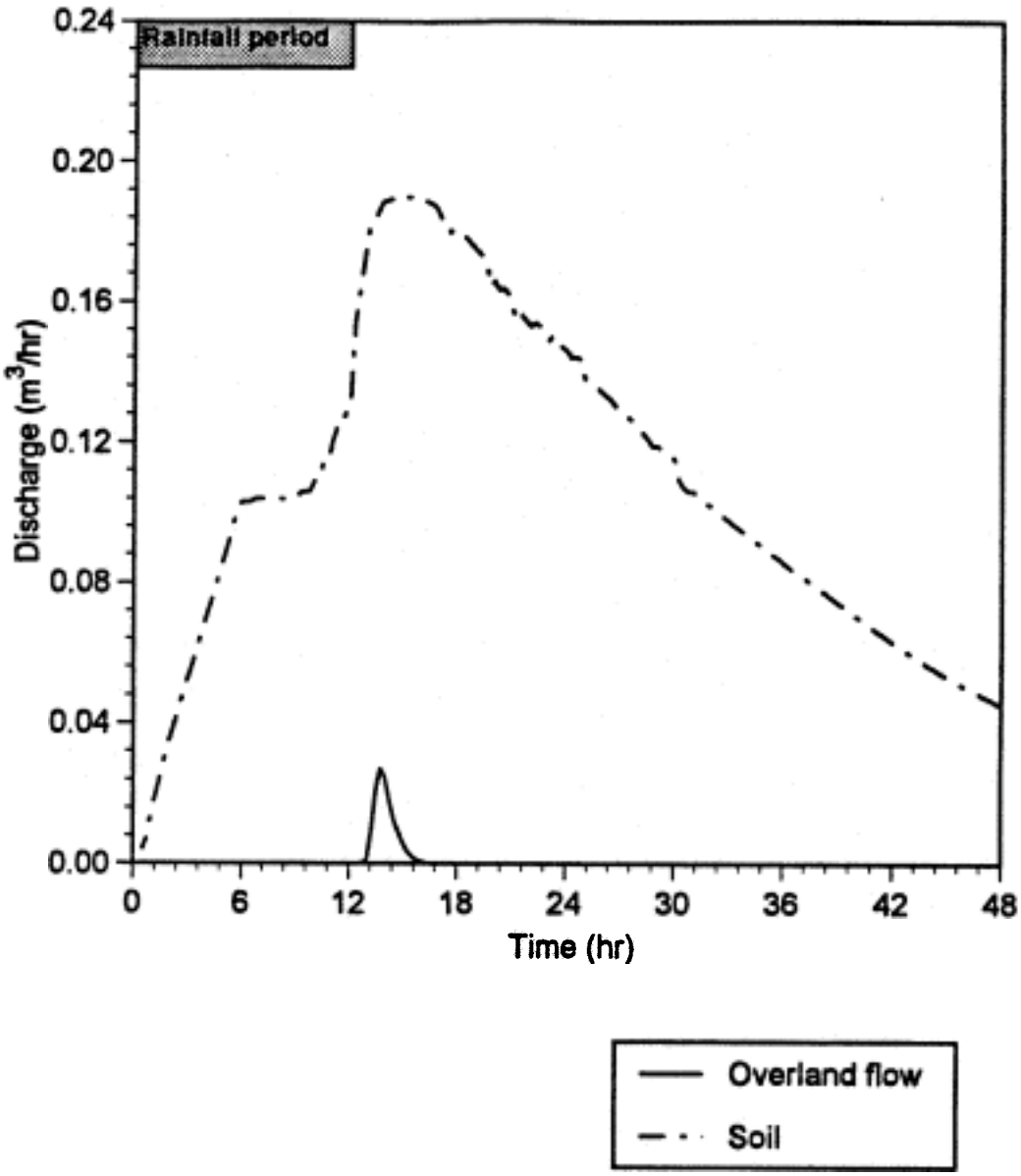

Figure 3.36 Discharge by flow path for 0.30 m channel depth and 3-part boundary condition (run 36)

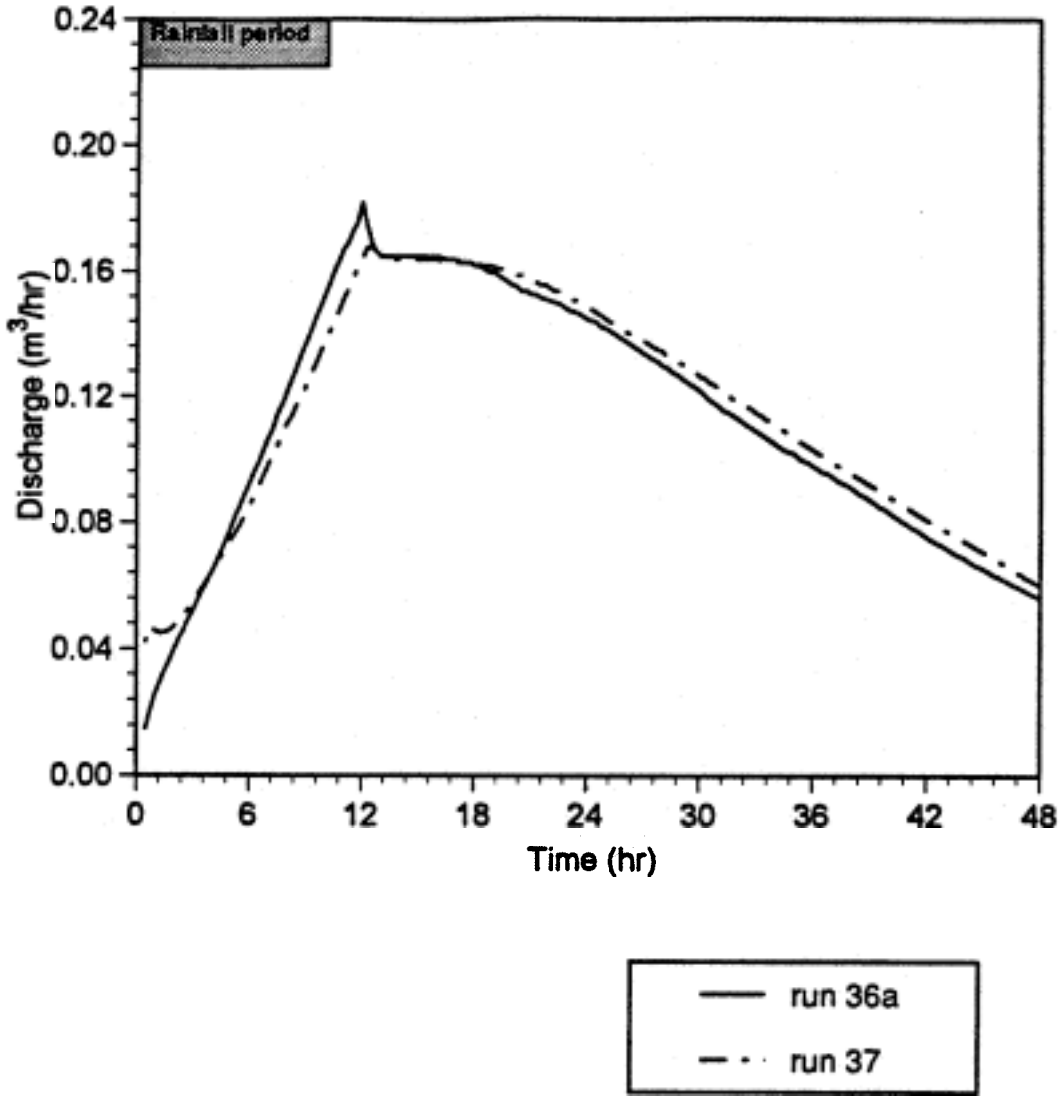

Figure 3.37 Total discharge for cases (runs 36a and 37) with increasing channel depth and 3-part boundary condition

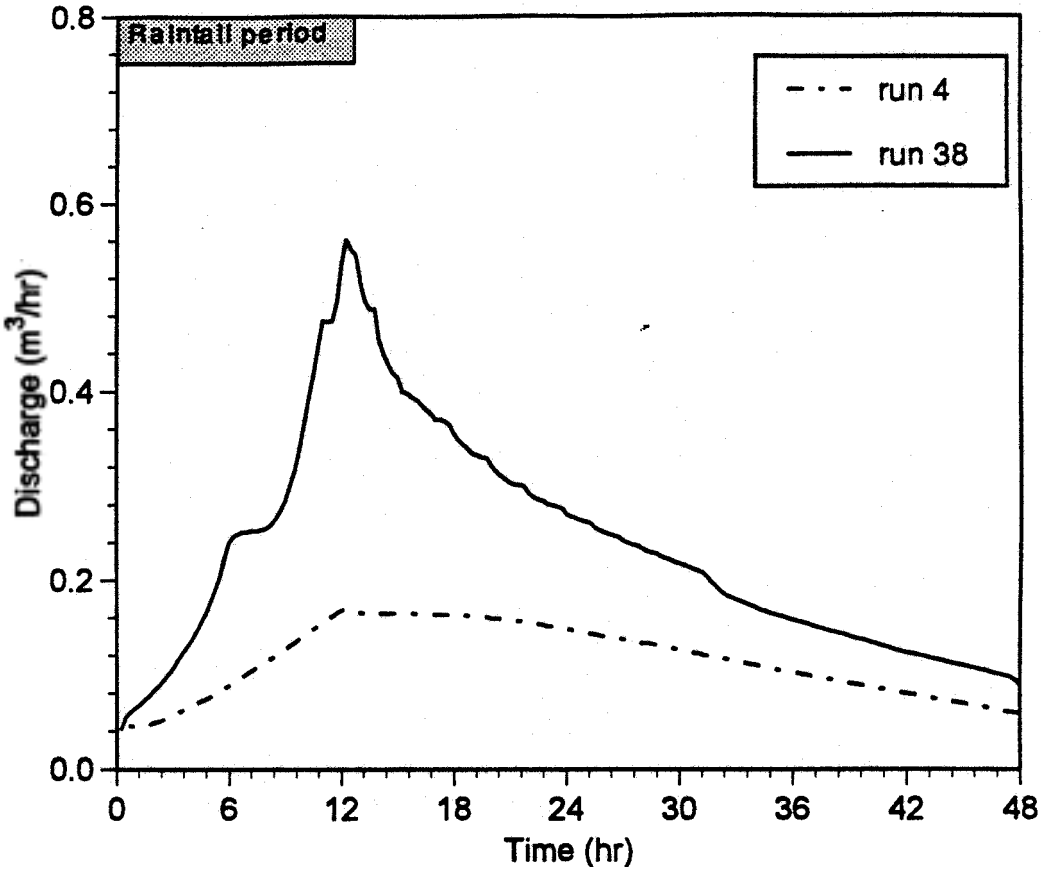

Figure 3.38 Runoff response for a 1-yr storm (case 4) versus a 100-yr storm with a 1.20 m channel depth

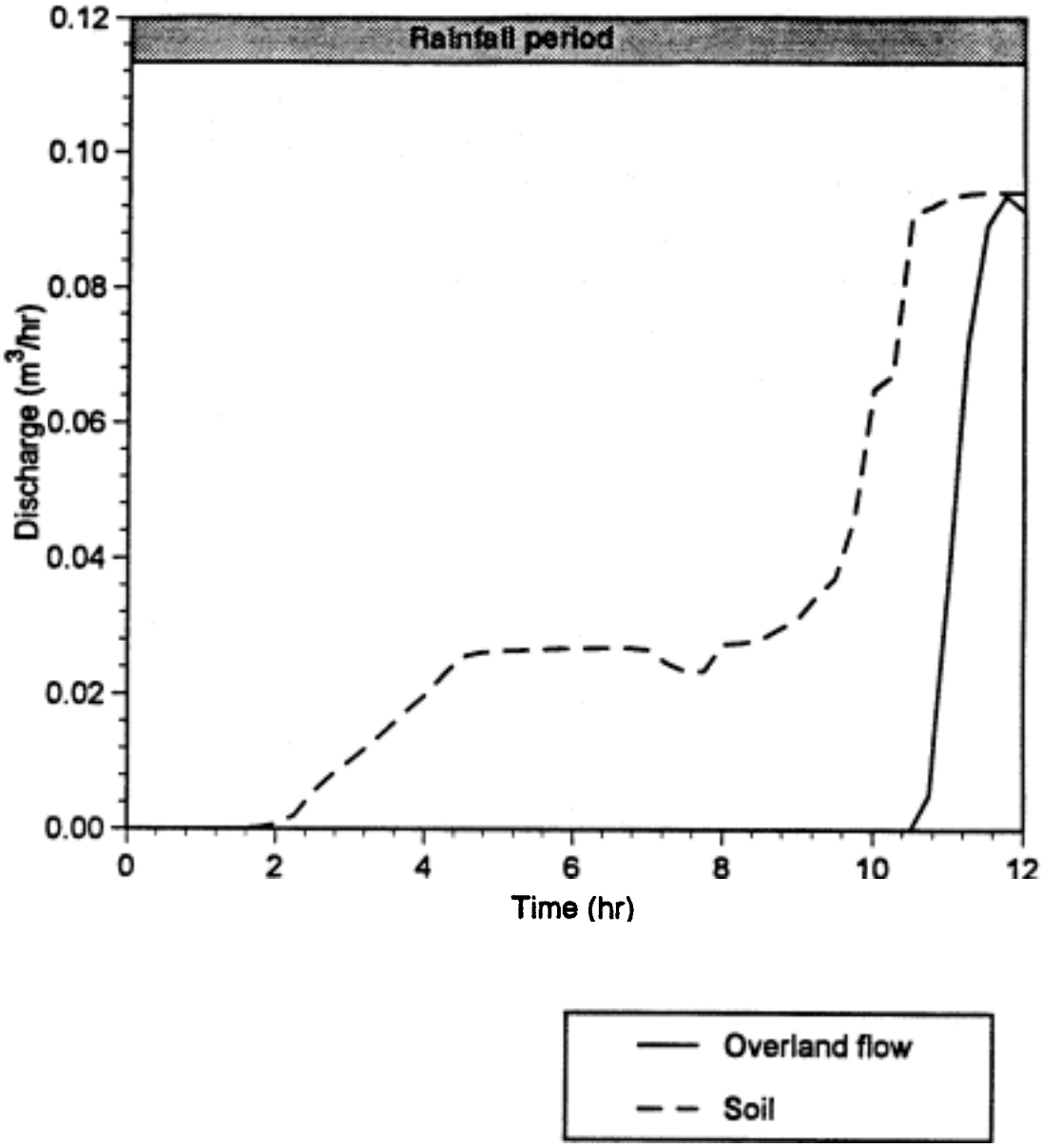

Figure 3.39 Discharge by flow path for case (run 39) with riparian low-k soil heterogeneity and 0.30 m channel depth

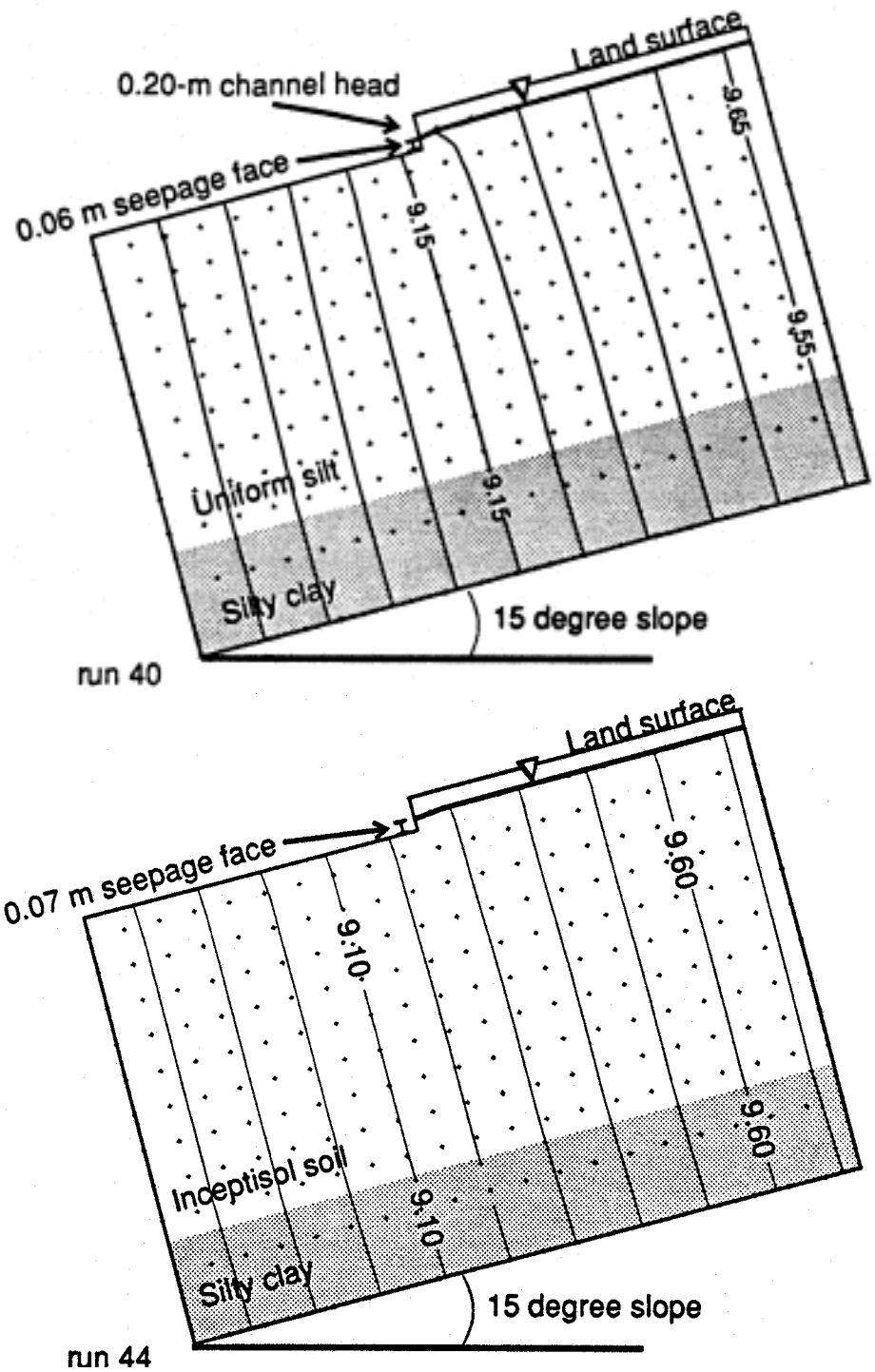

Contour interval= 0.1 m 9.00 - Hydraulic head (m)

Figure 3.40 Effects of different soil types on flow field around a 0.20-m channel head

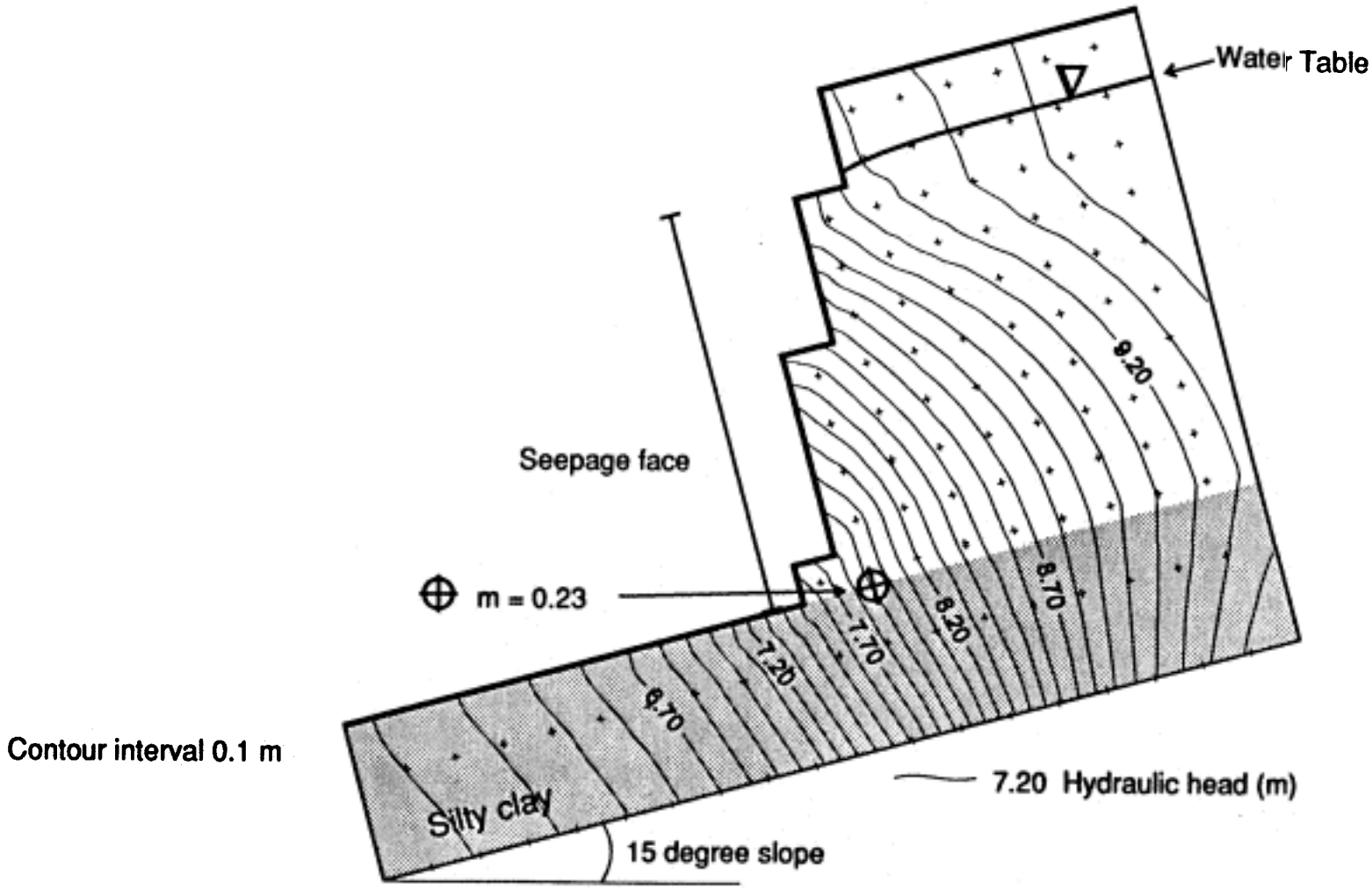

Figure 3.41 Hydraulic head profile around 2.0 m channel head for case (run 47) with Inceptisol soil

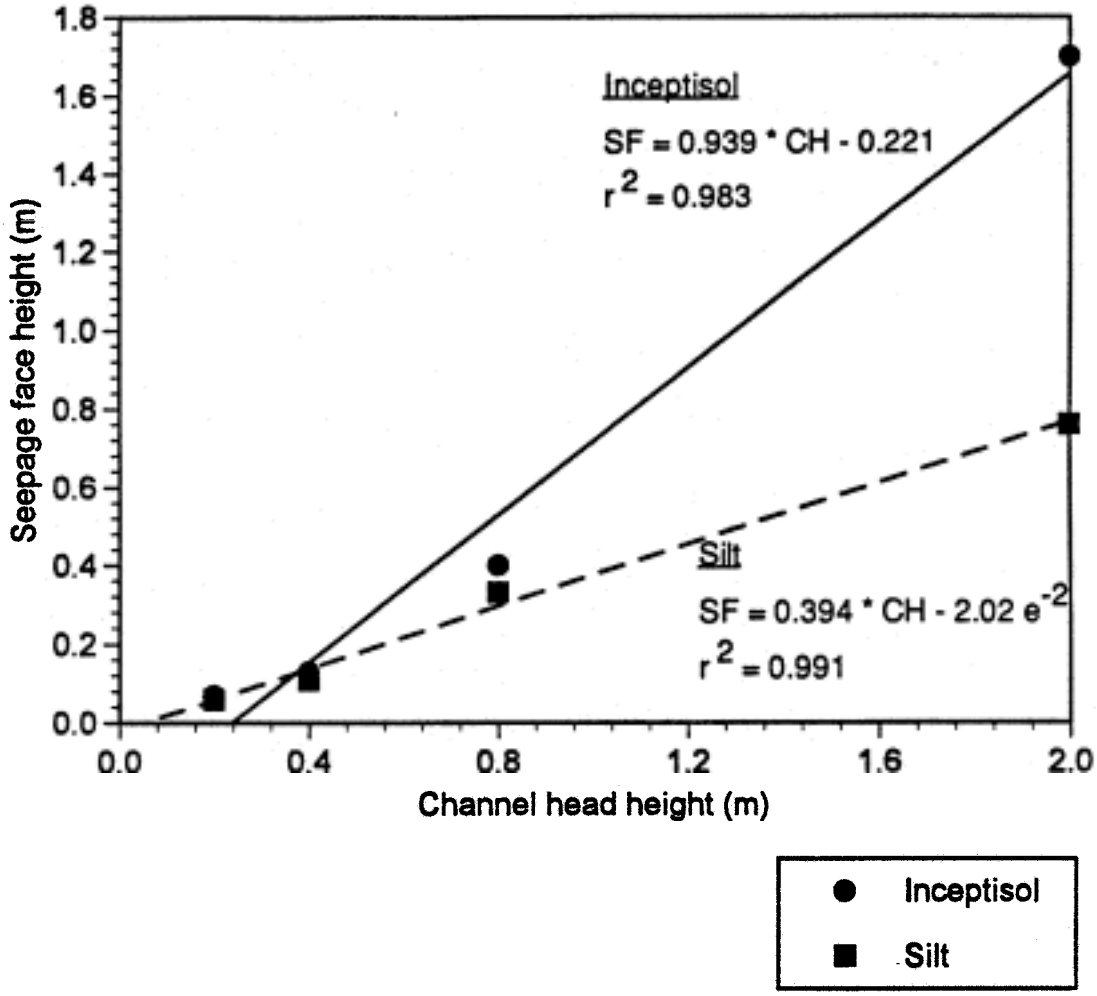

Figure 3.42 Relationship between seepage face height and channel head height for a uniform silt and Inceptisol soil

a)

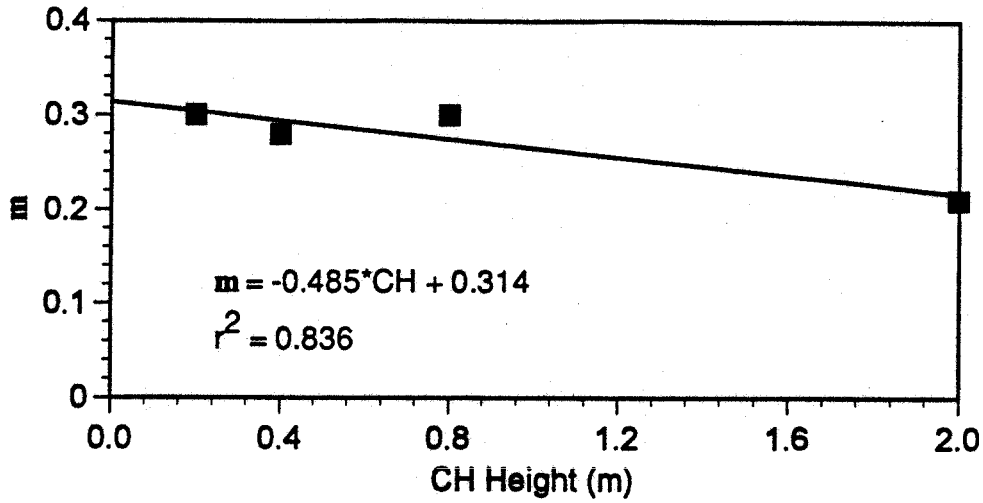

b)

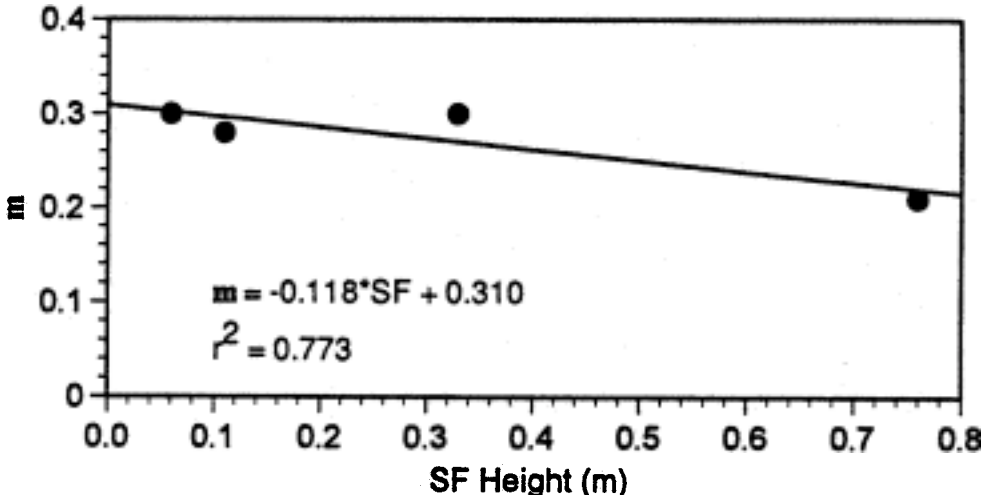

Figure 3.43 Relationship between m and a) channel head height (CH); b) seepage face height (SF) for uniform silt soil

a)

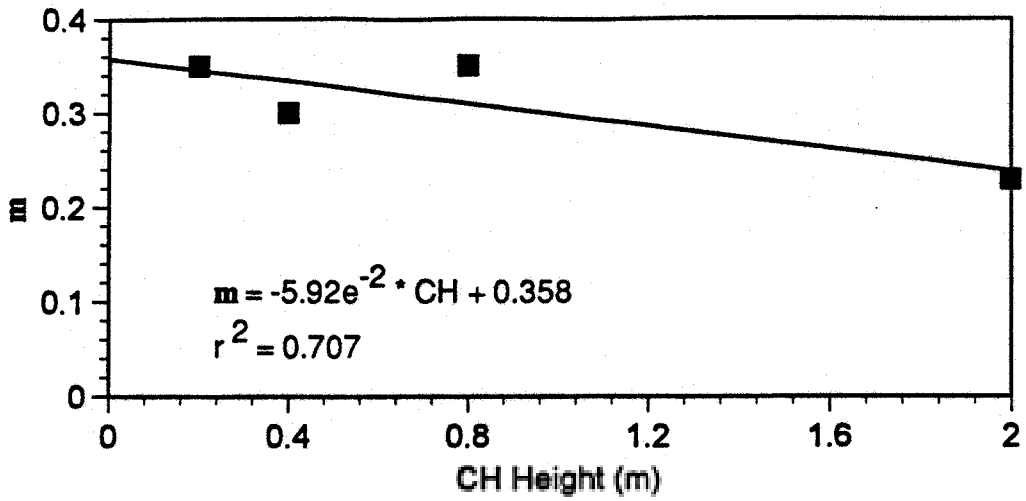

b)

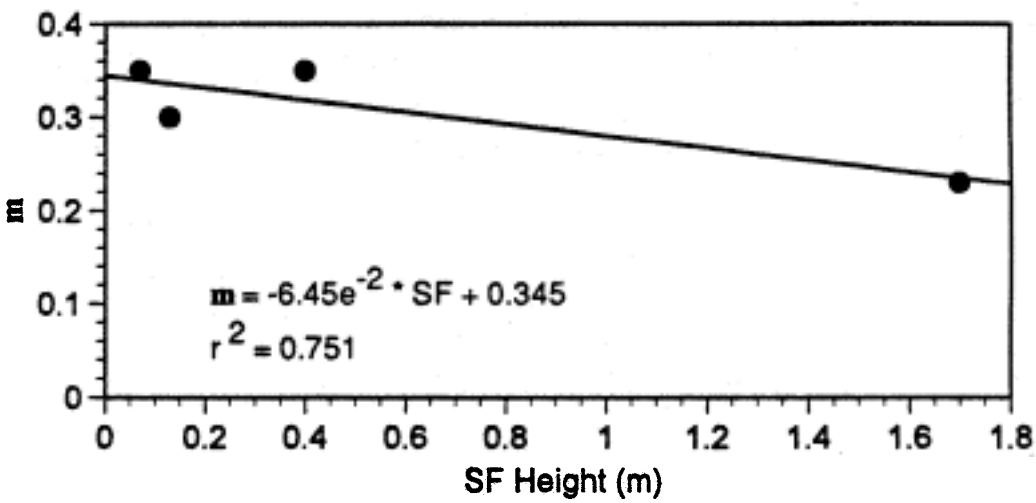

Figure 3.44 Relationship between m and a) channel head height (CH); b) seepage face height (SF) for Inceptisol soil

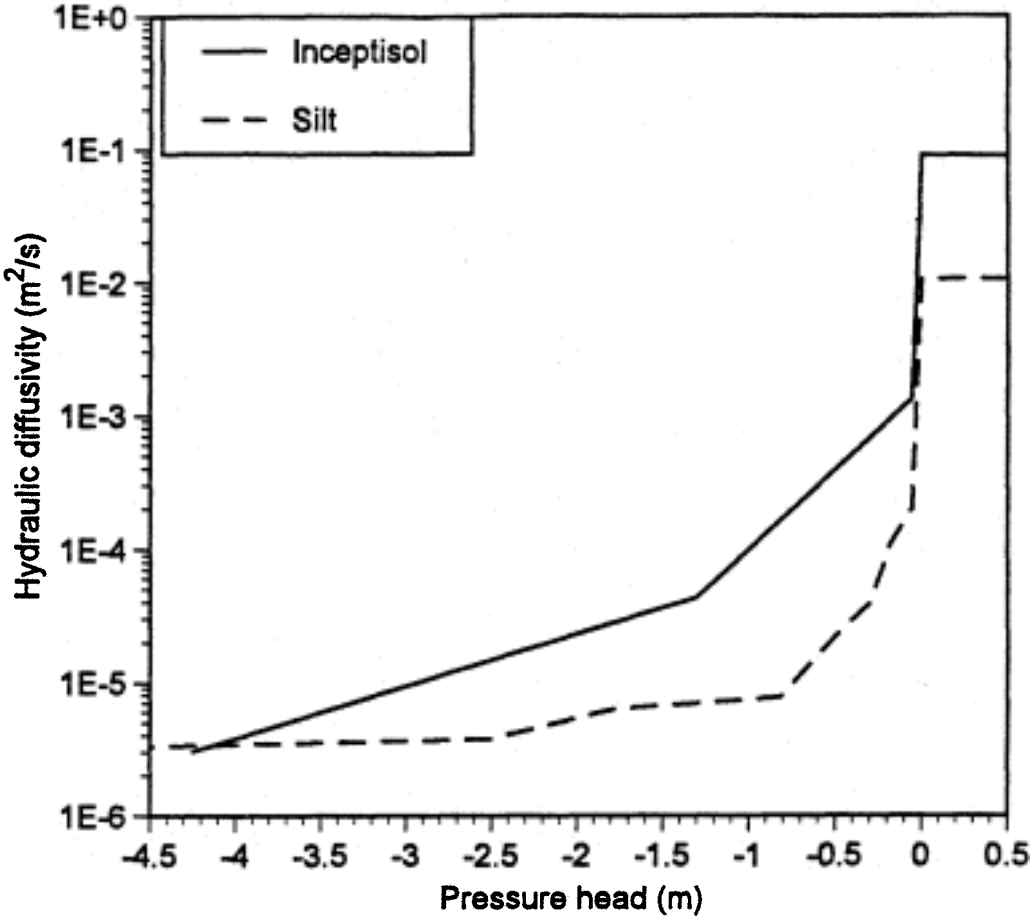

Figure 3.45 Comparison of hydraulic diffusivity characteristics for soils used in channel head simulations

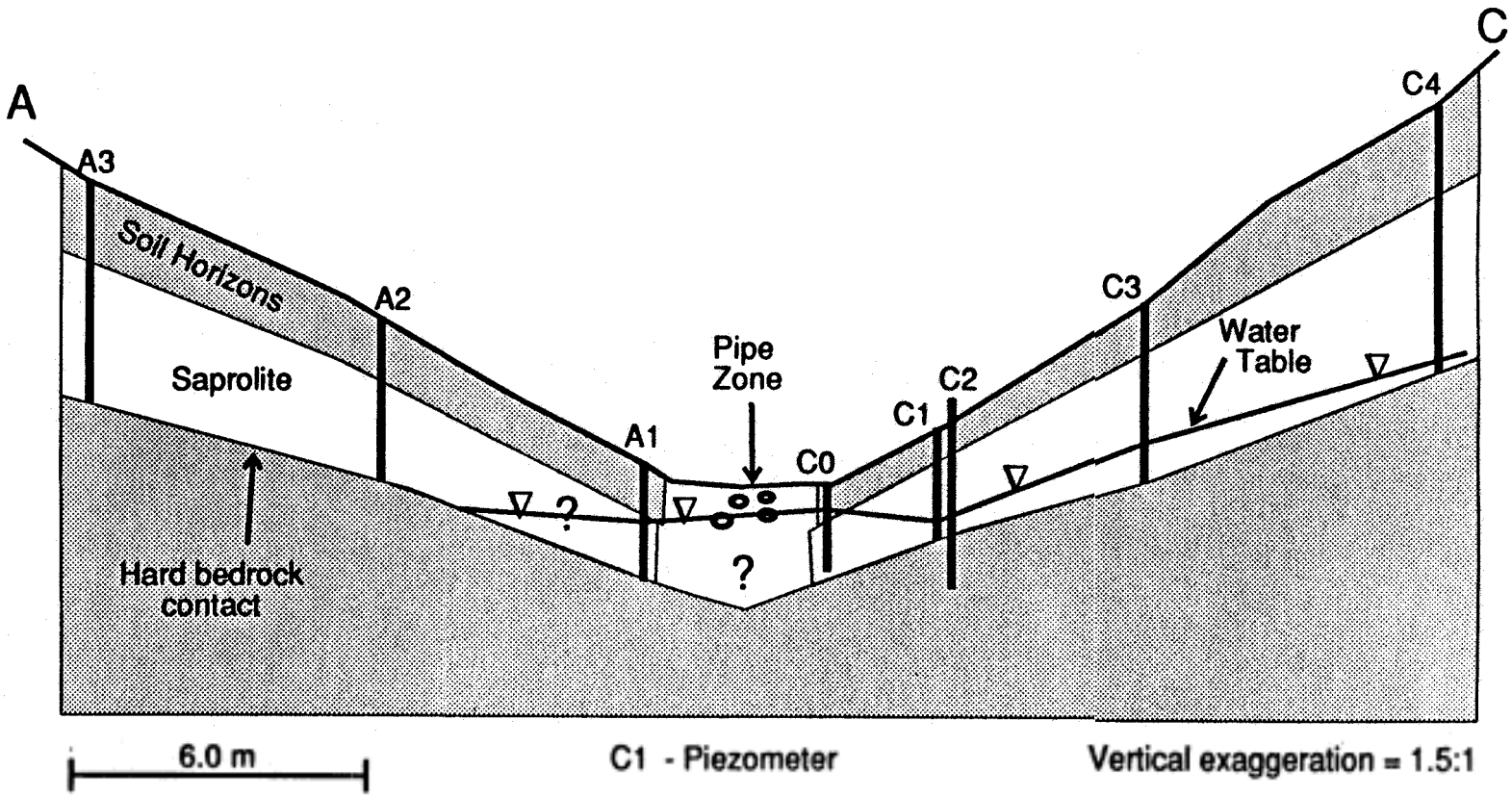

Figure 3.46 Cross-section A-C at Caspar Creek Experimental Watershed

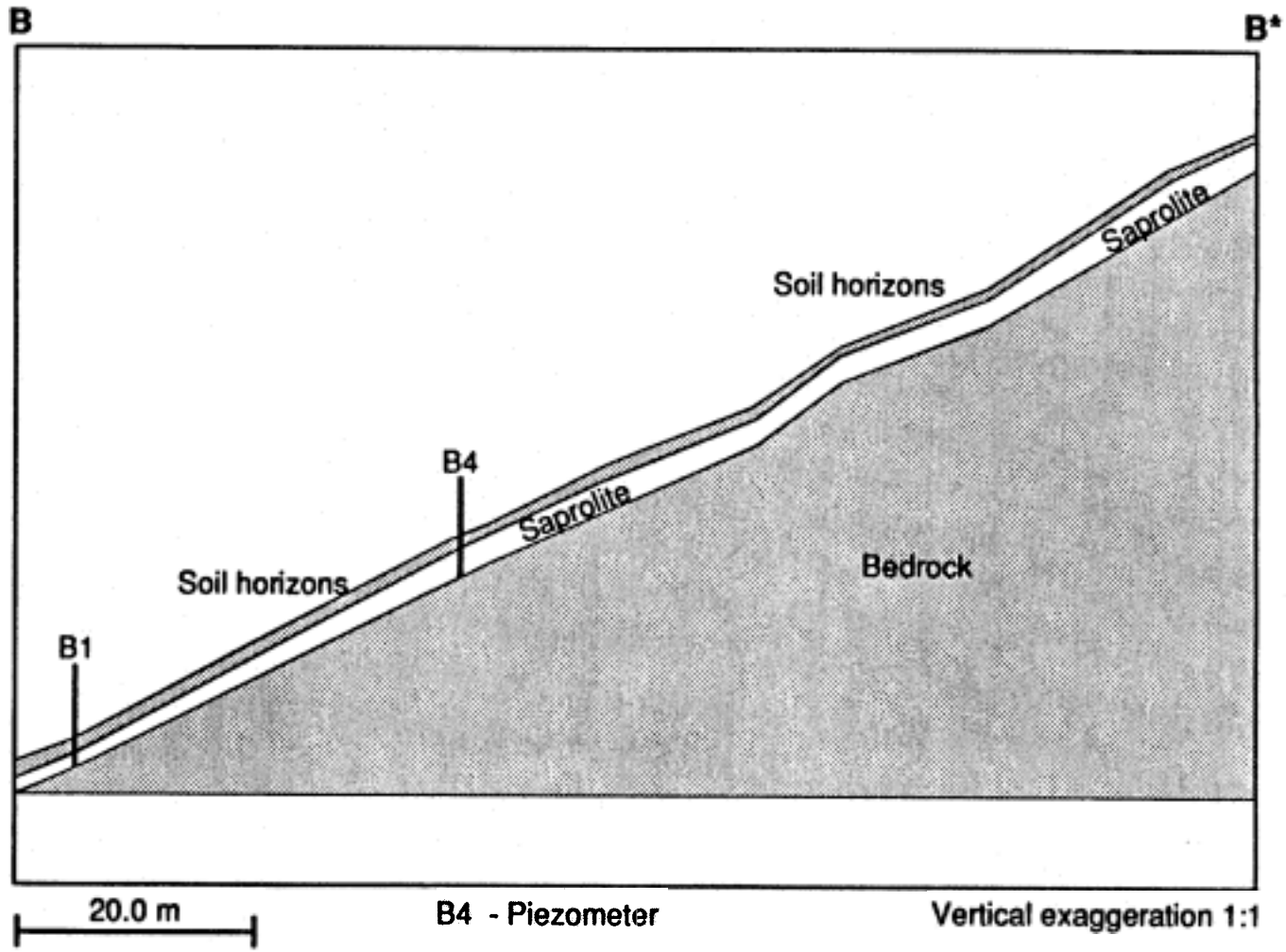

Figure 3.47 Cross-section B-B* at Caspar Creek Experimental Watershed

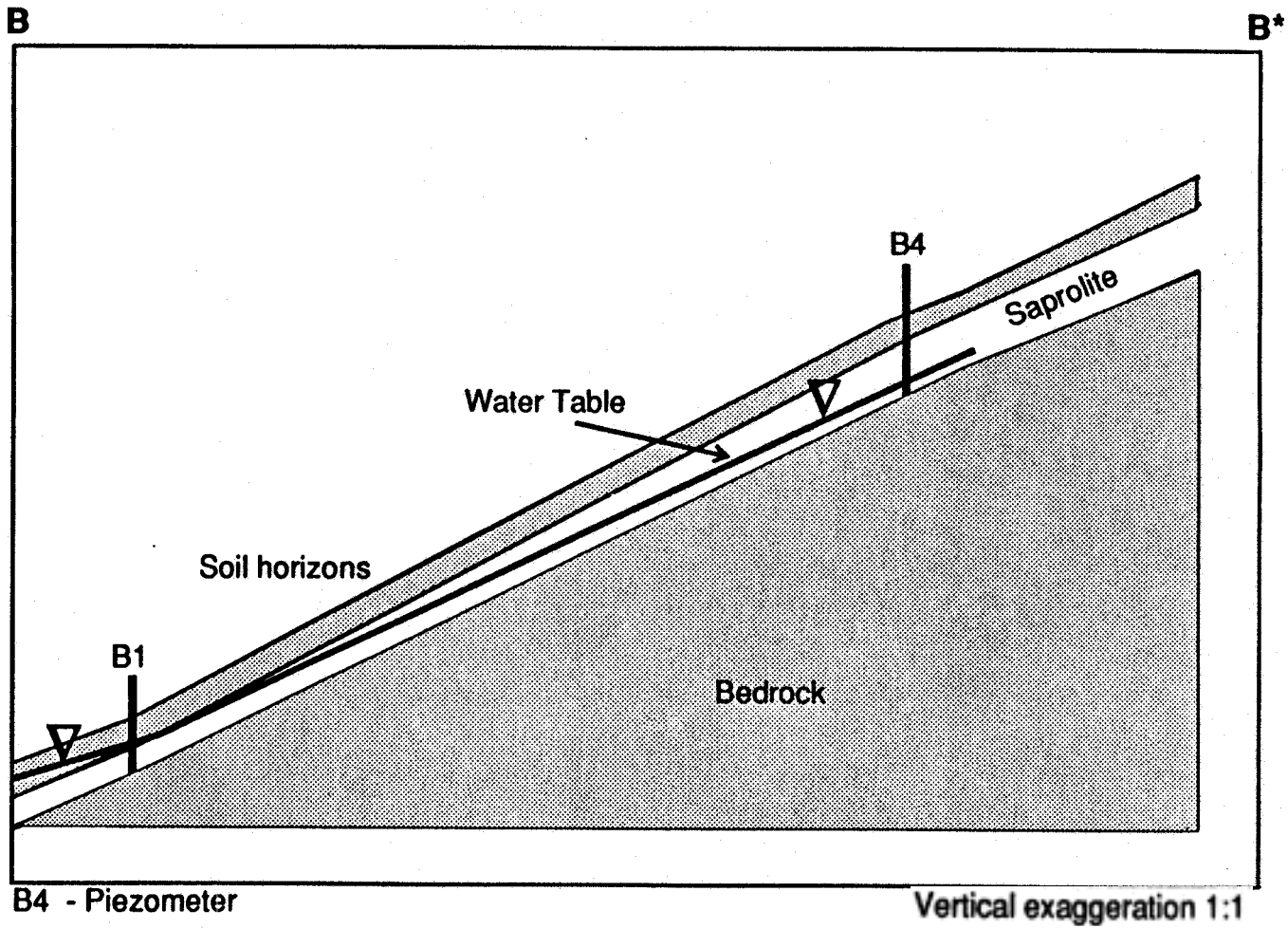

Figure 3.48 Detail of cross-section B-B* showing typical winter water table profile

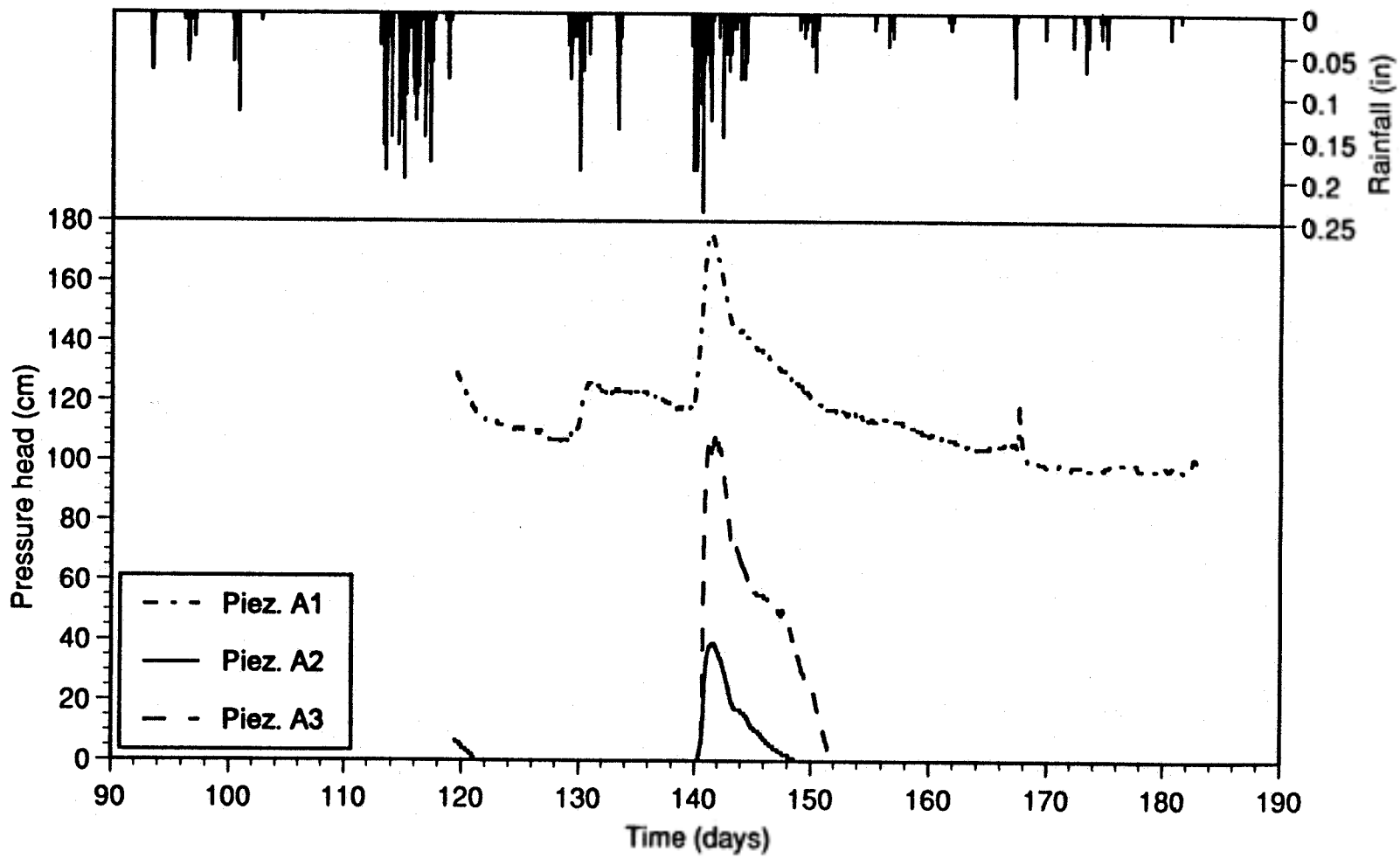

Figure 3.49 Rainfall and pressure head response, January - March 1994, A-transect, M Swale, Caspar Creek Experimental Watershed

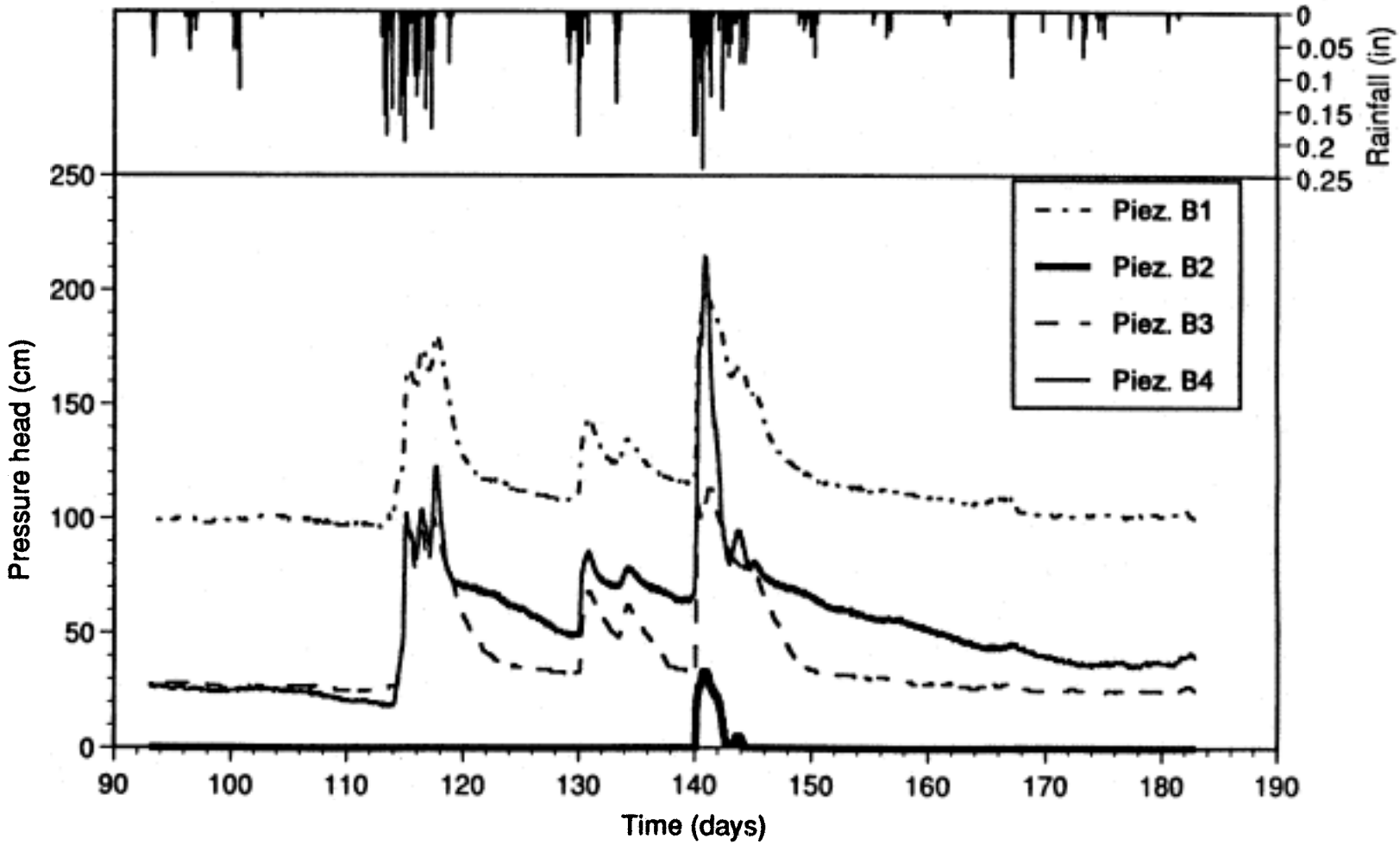

Figure 3.50 Rainfall and pressure head response, January - March 1994, B-transect, M Swale, Caspar Creek Experimental Watershed

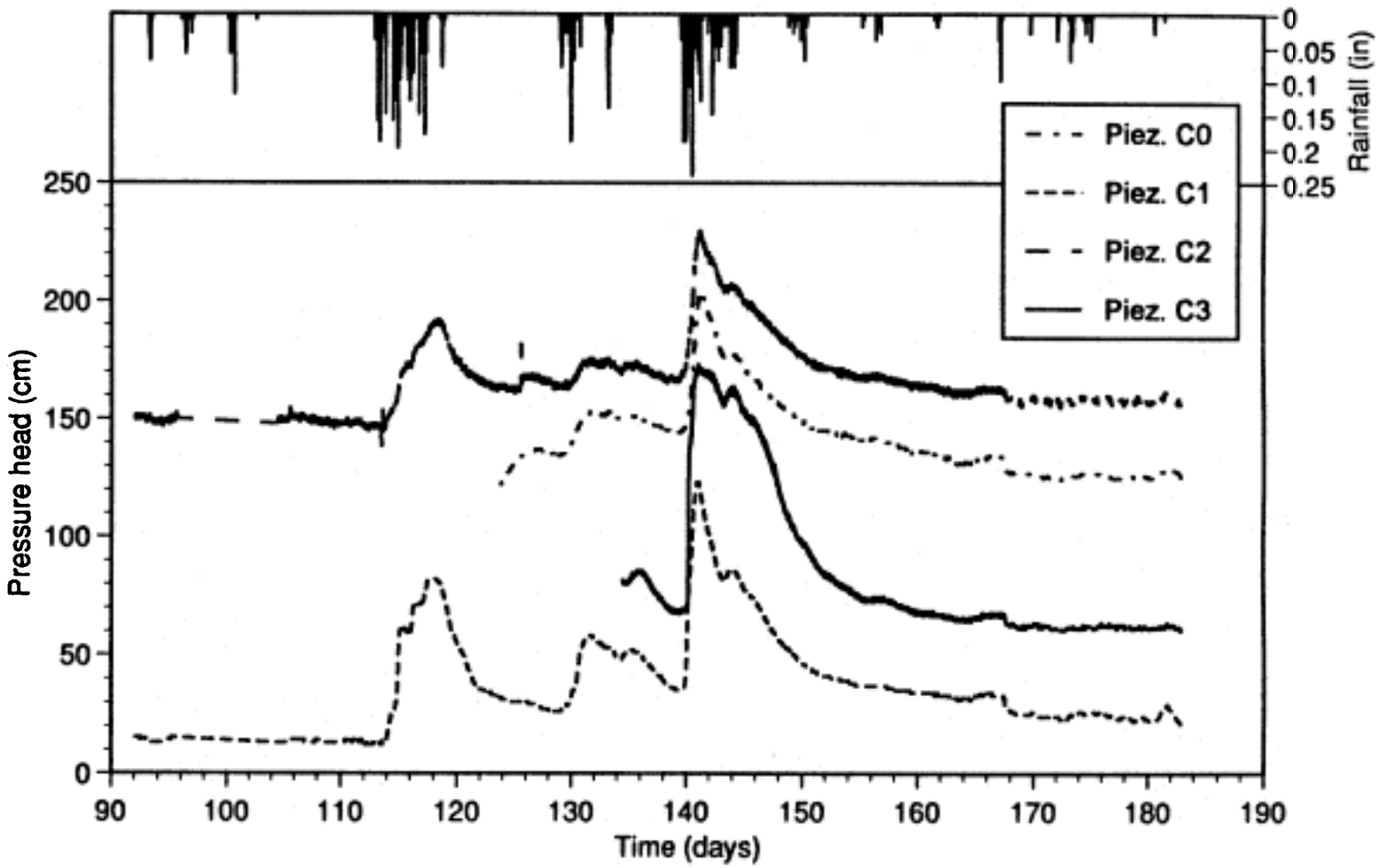

Figure 3.51 Rainfall and pressure head response, January - March 1994, B-transect, M Swale, Caspar Creek Experimental Watershed

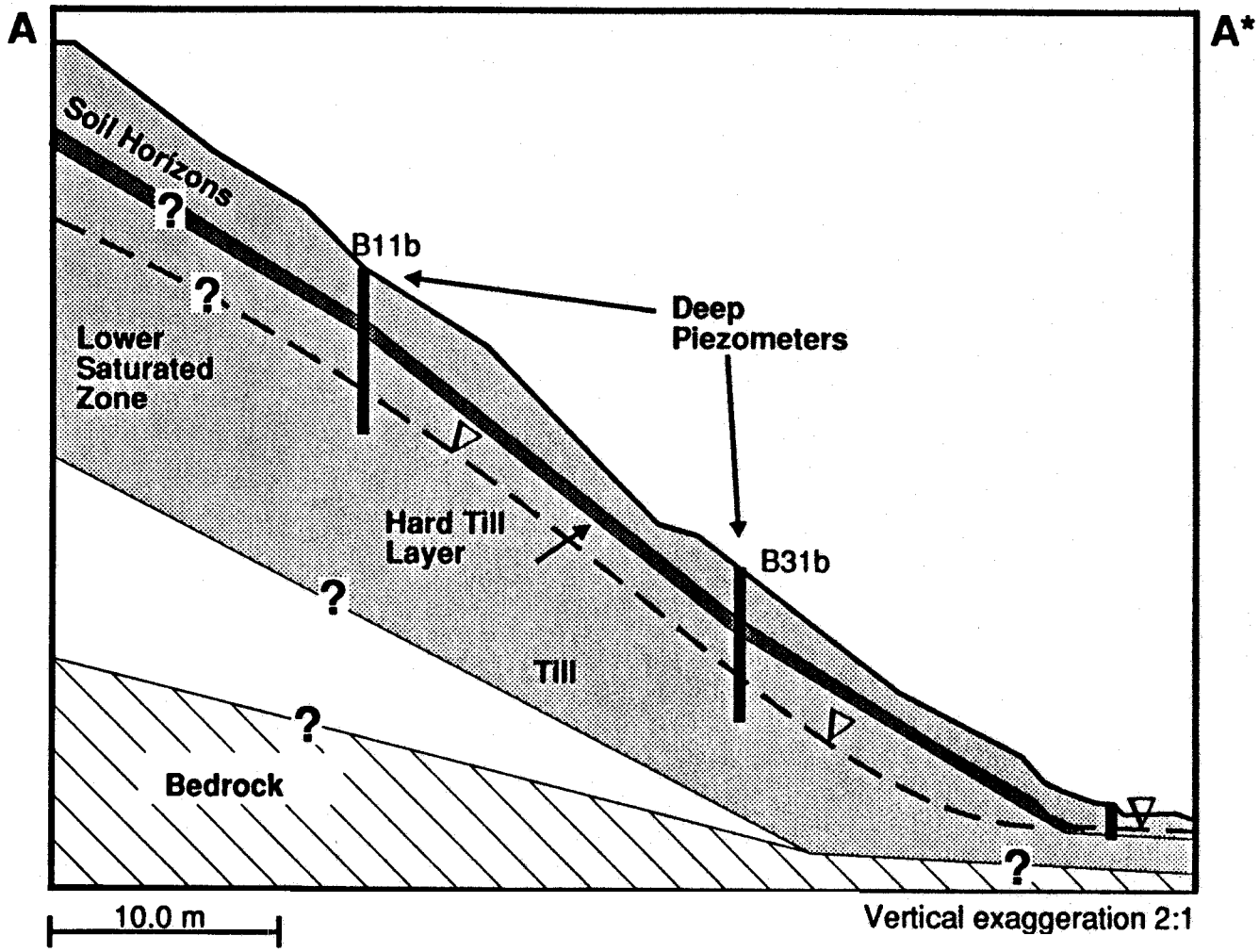

Figure 3.52 Cross-section of UNH field site showing lower saturated zone

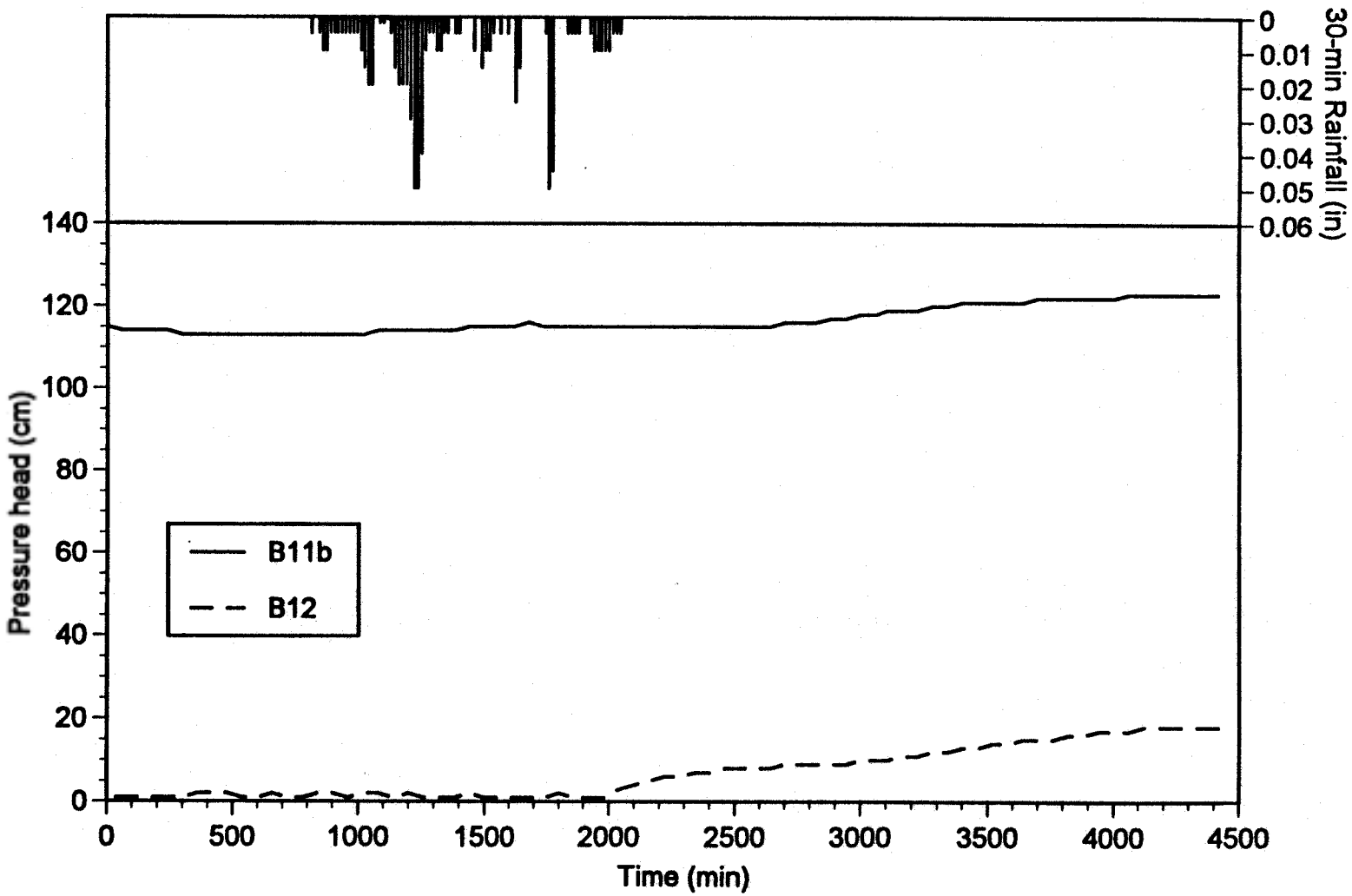

Figure 3.53 Storm pressure head response in piezometers monitored by data logger 1.

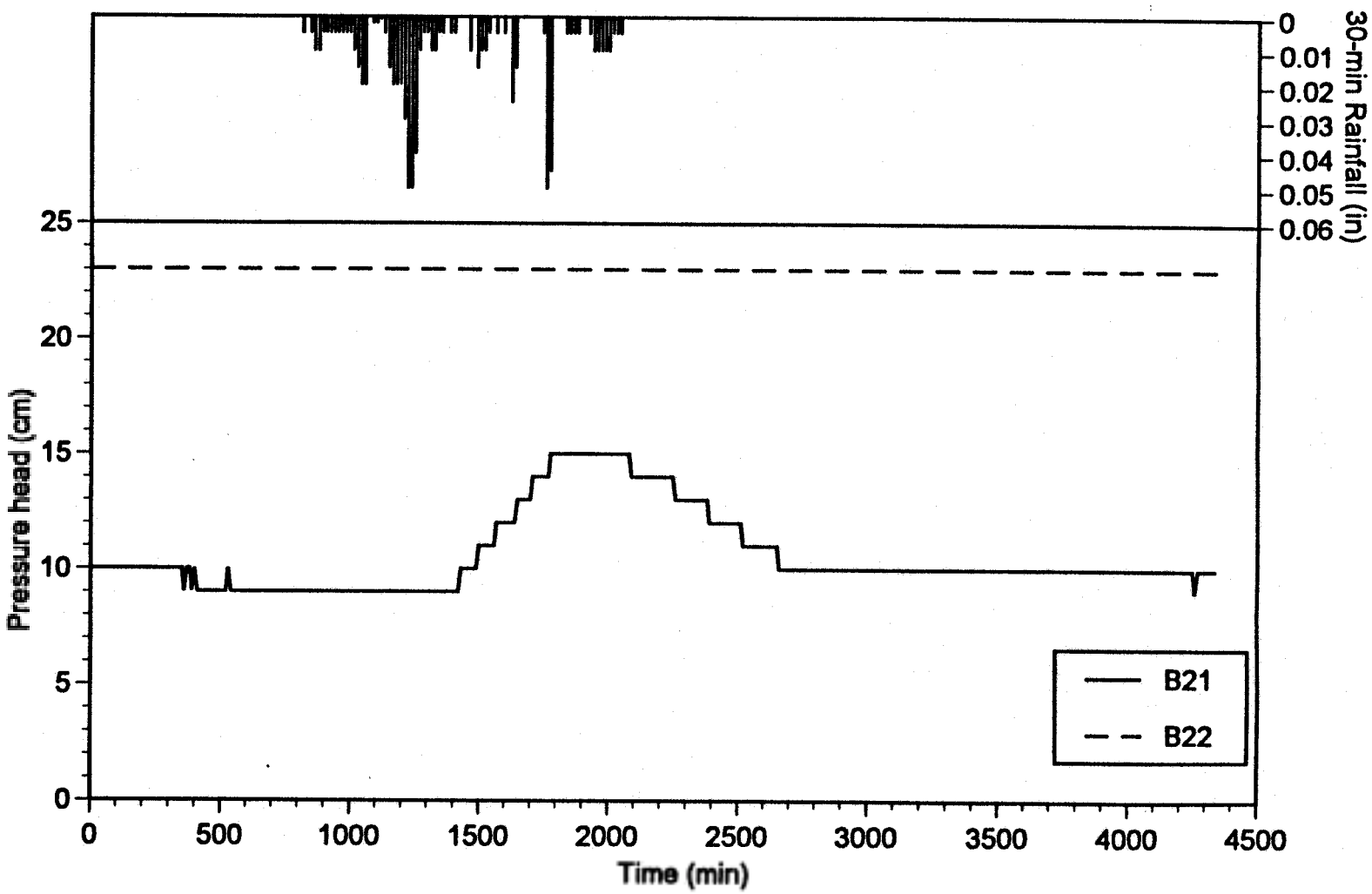

Figure 3.54 Storm pressure head response in piezometers monitored by data logger 2.

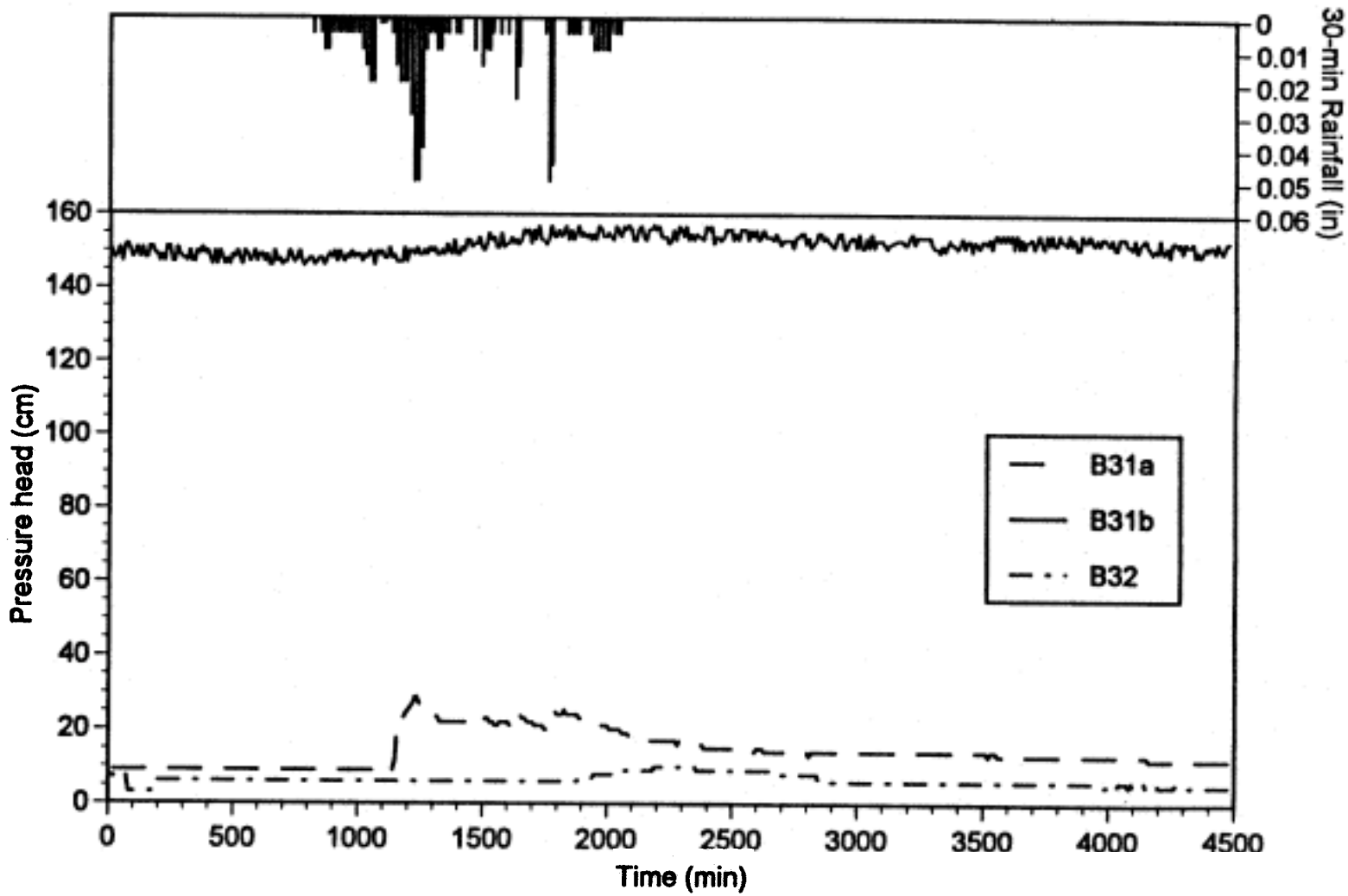

Figure 3.55 Storm pressure head response in piezometers monitored by data logger 3.

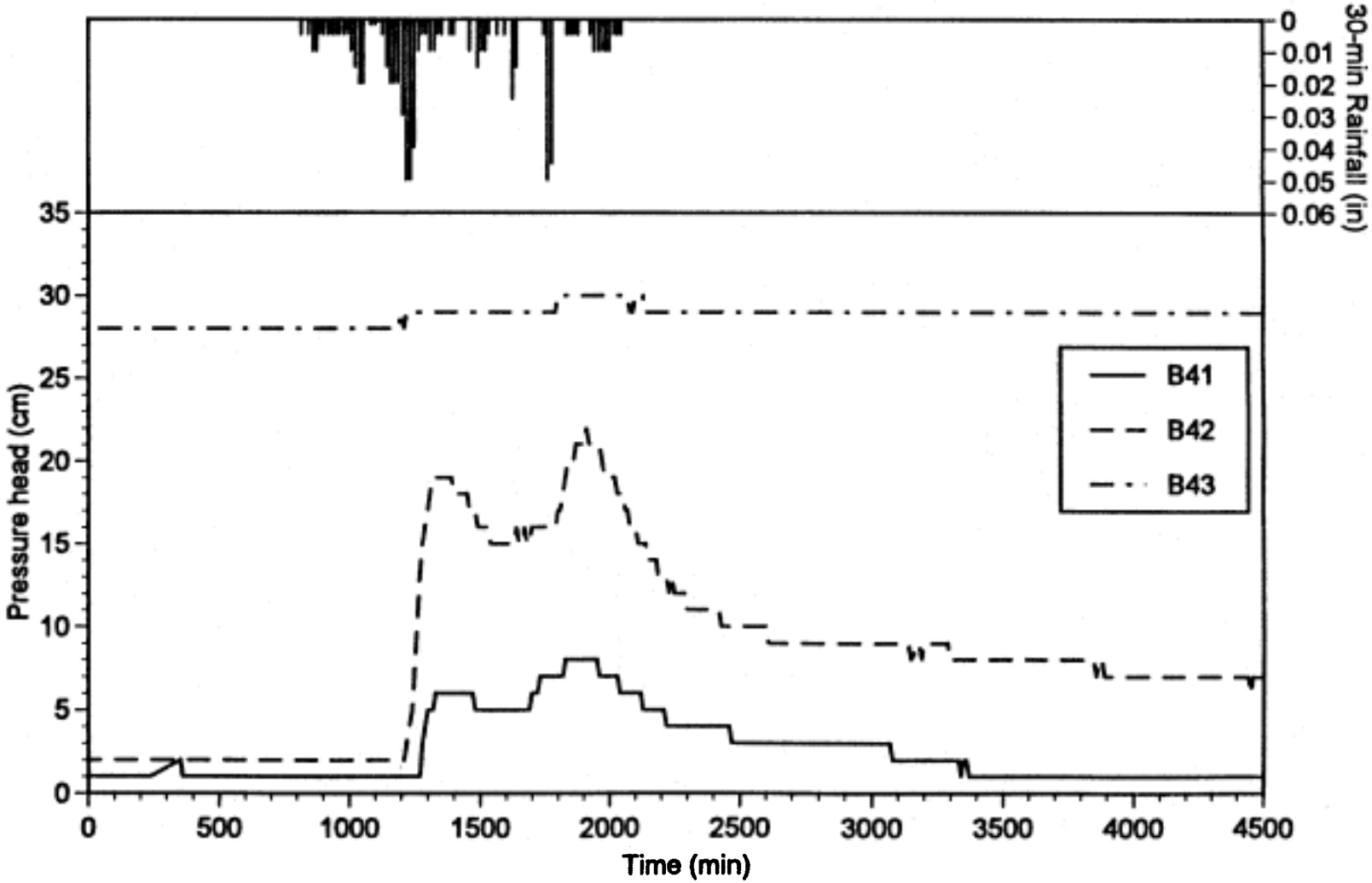

Figure 3.56 Storm pressure head response in piezometers monitored by data logger 4.

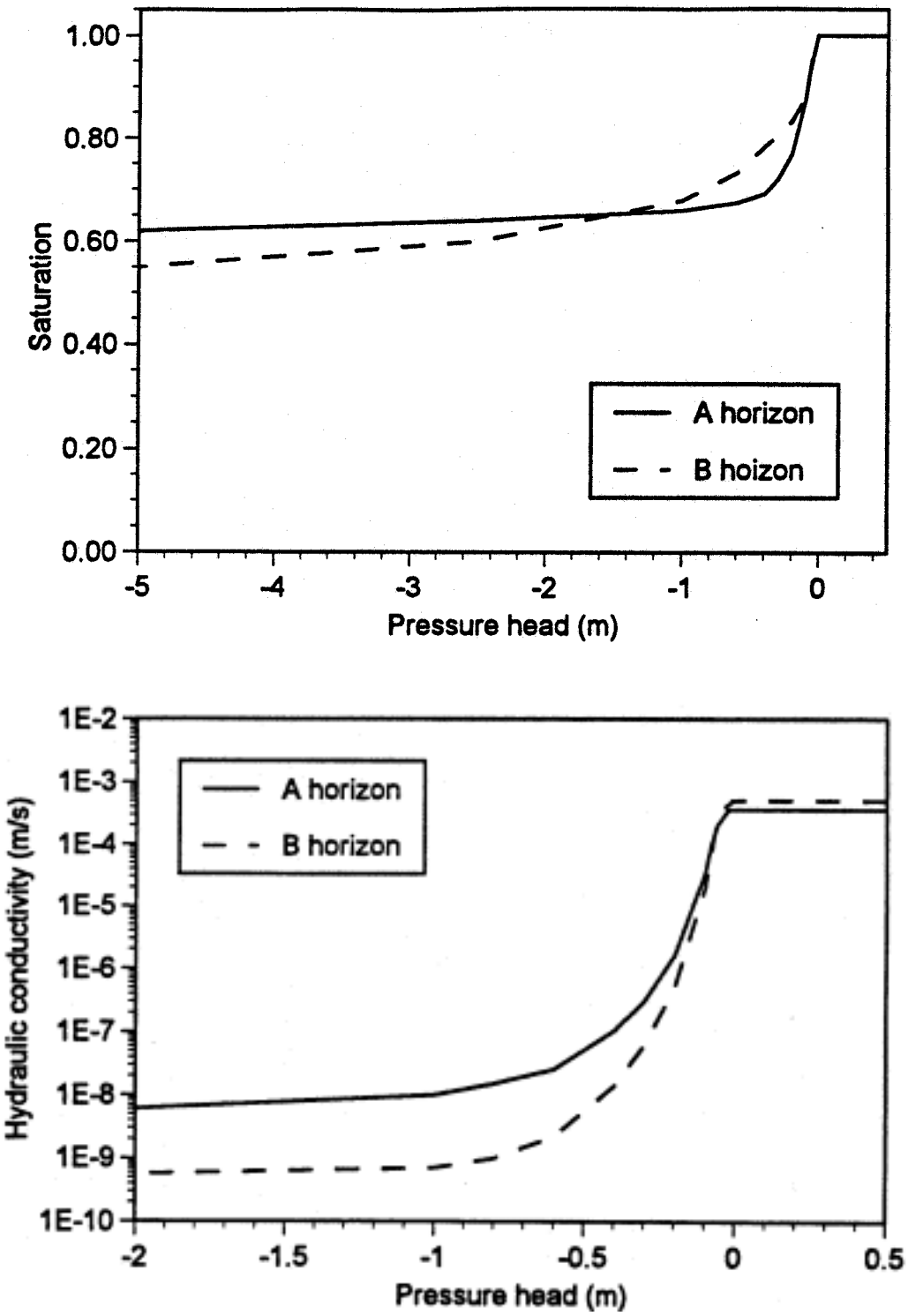

Figure 3.57 Soil hydraulic properties for Caspar Creek Experimental Watershed from Wosika (1981)

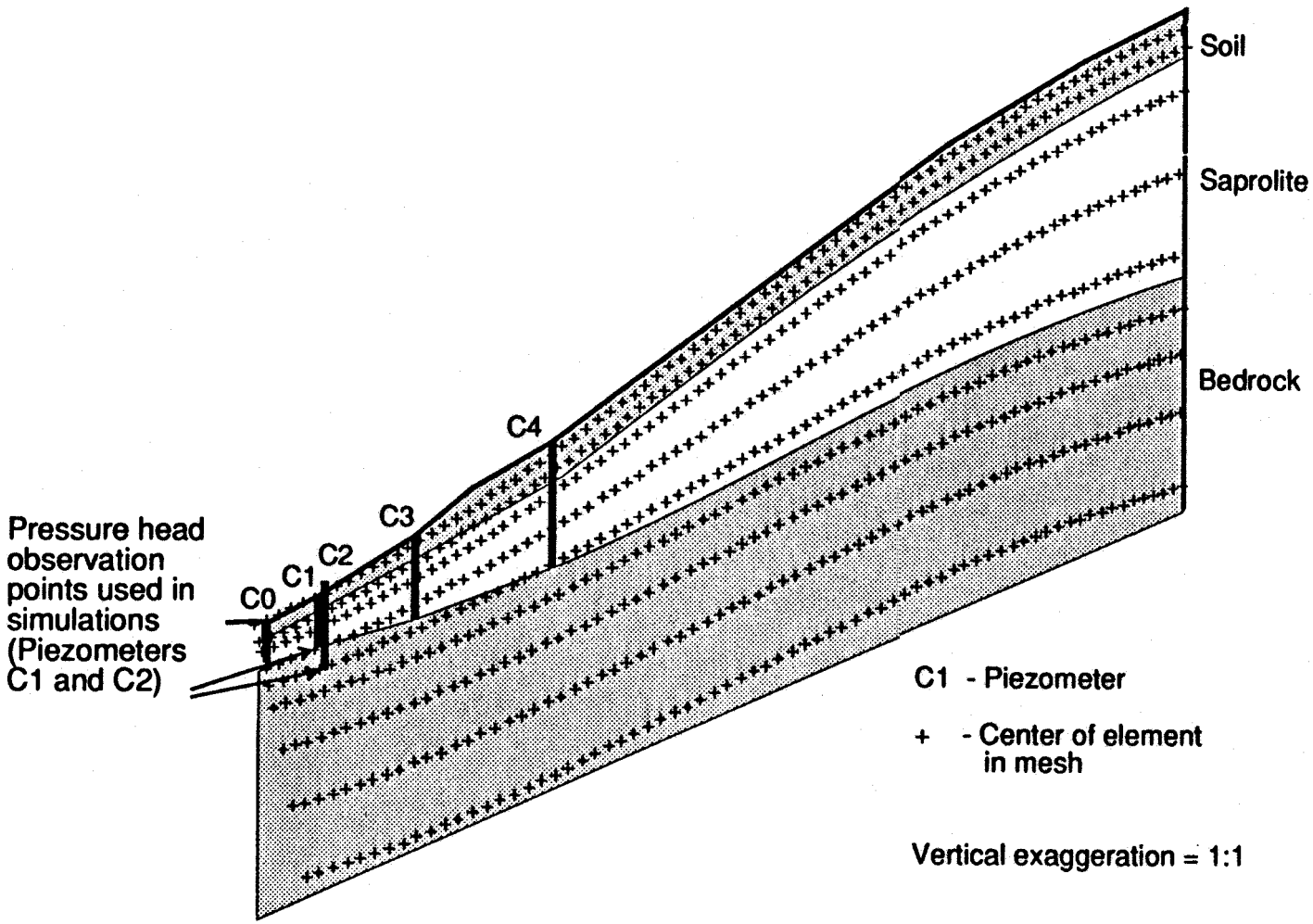

Figure 3.58 Cross-section along C transect at Caspar Creek Experimental Watershed showing element centers of simulation mesh

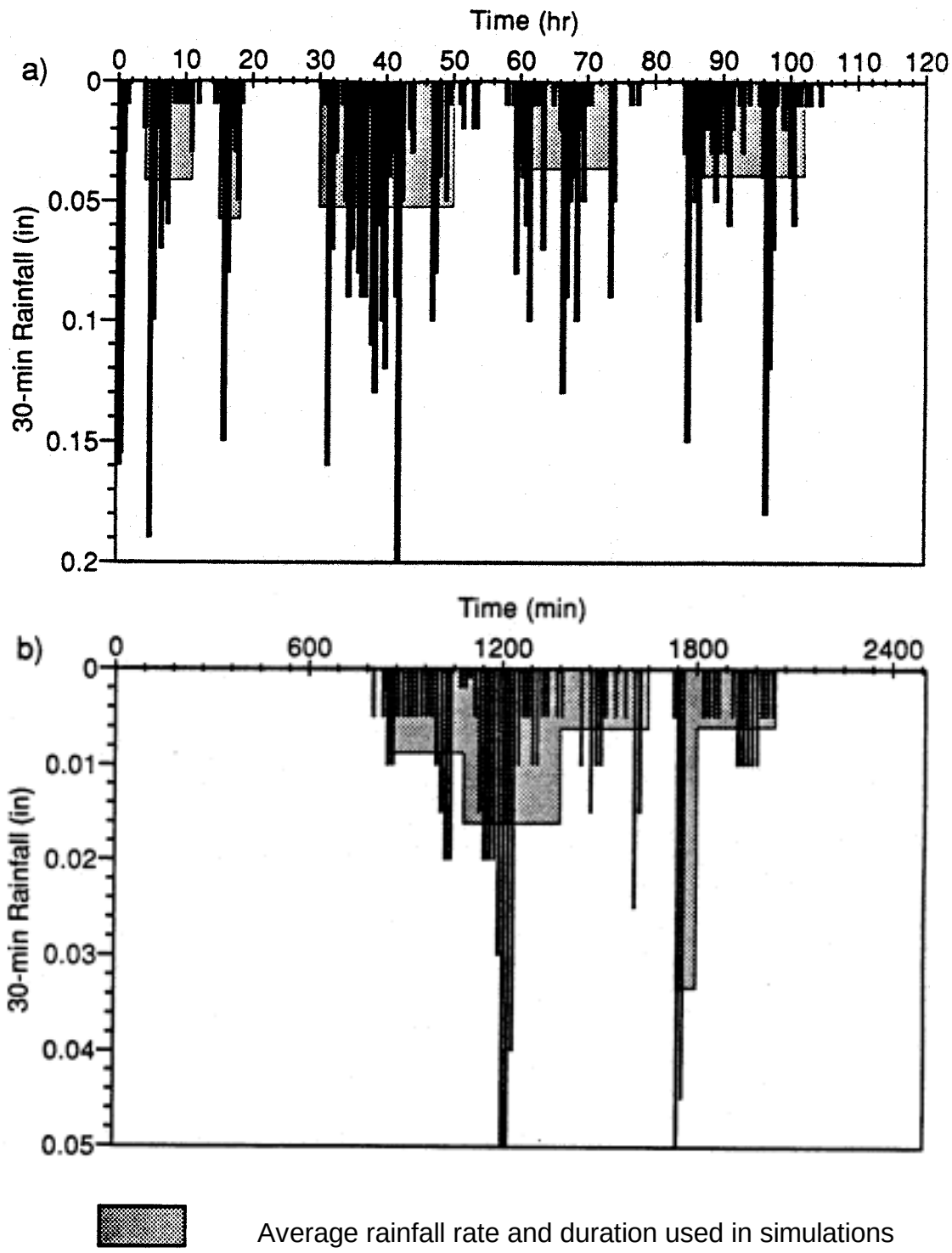

Figure 3.59 Observed and simulated rainfall patterns for a) Caspar Creek, January 1994 storm; b) Hubbard Brook, October 1993 storm

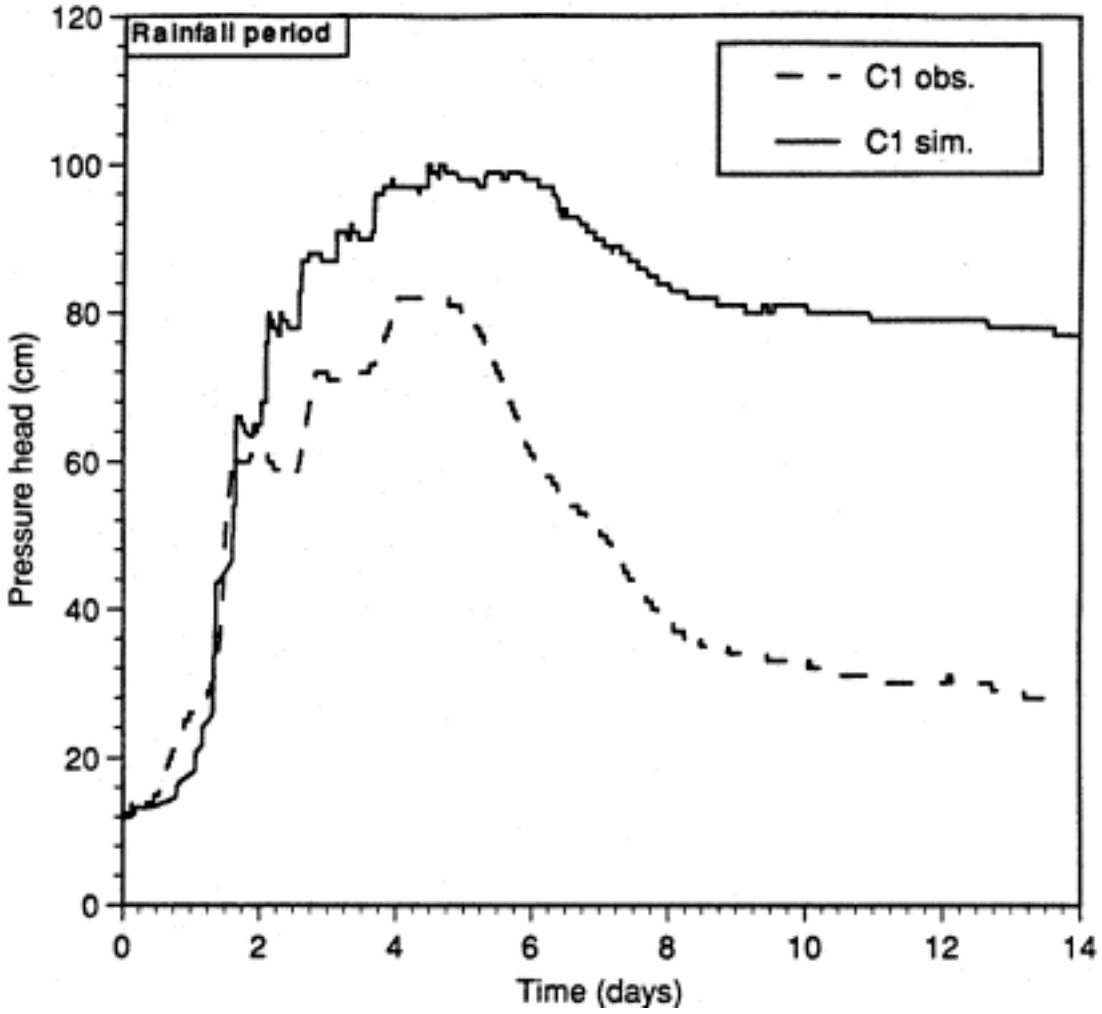

Figure 3.60 Comparison of simulated and observed pore pressure response for January 1994 rainfall event - Caspar Creek Watershed, M Swale Piezometer C1

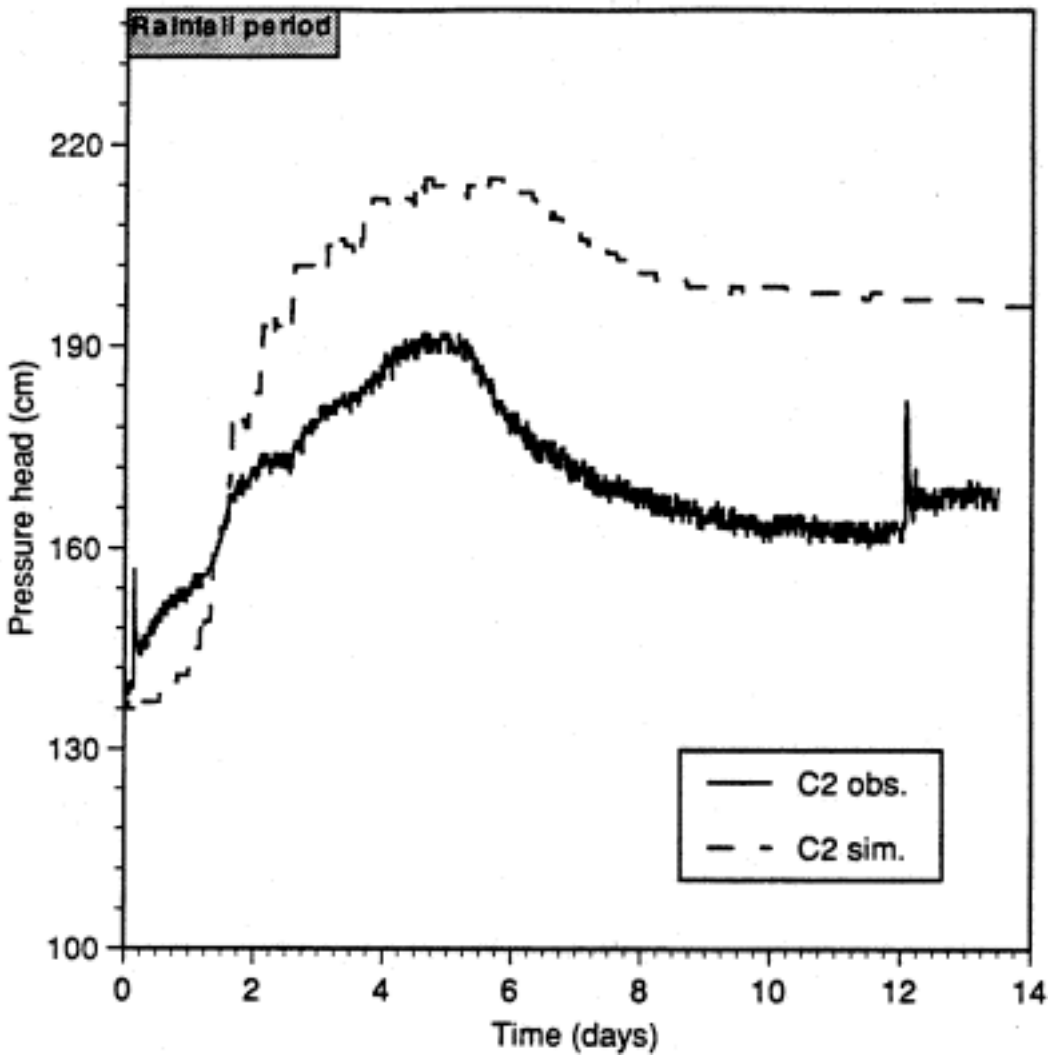

Figure 3.61 Comparison of simulated and observed pore pressure response for January 1994 rainfall event - Caspar Creek Watershed, M Swale Piezometer C2

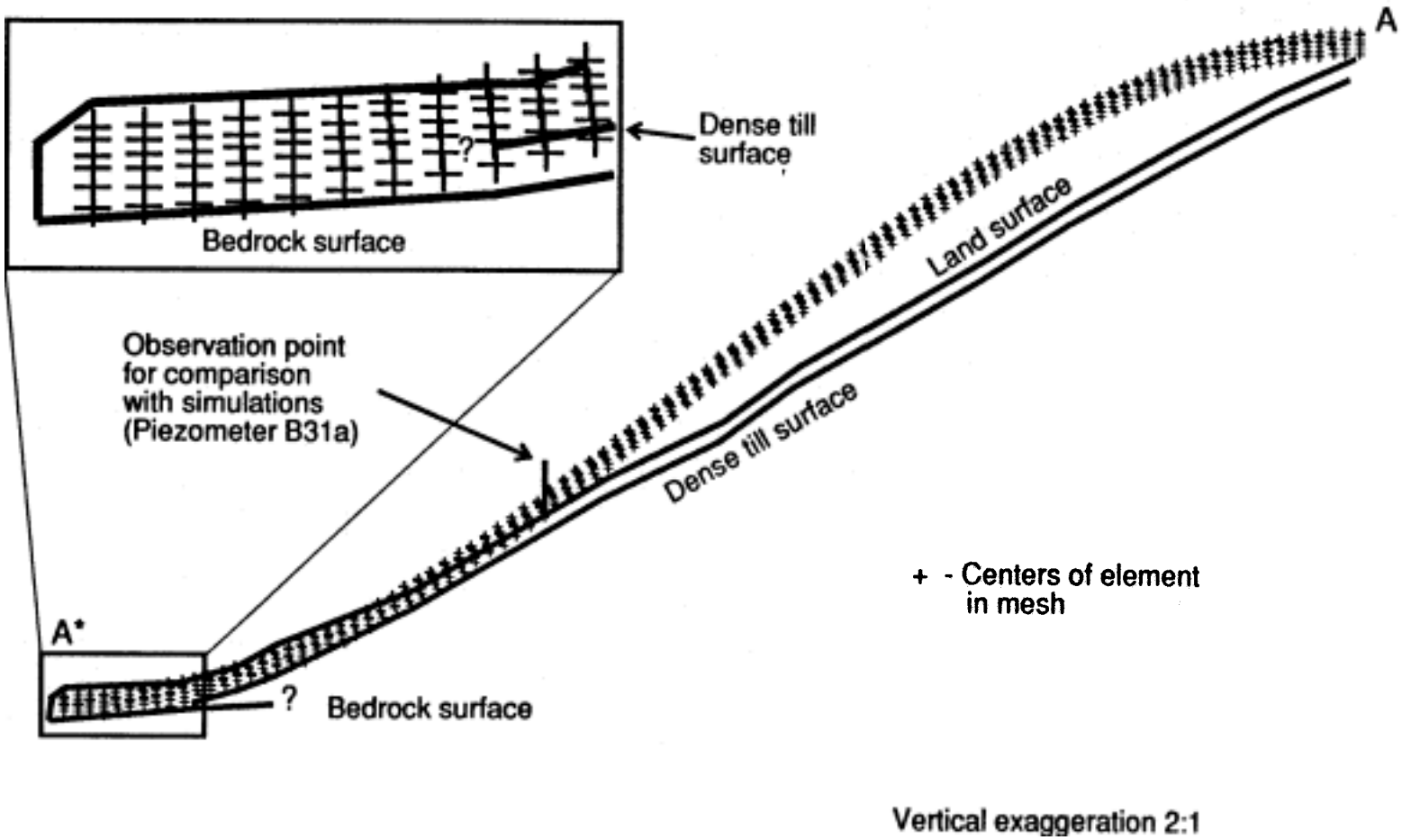

Figure 3.62 Cross-section A-A* at Hubbard Brook Experimental Forest showing element centers of simulation mesh

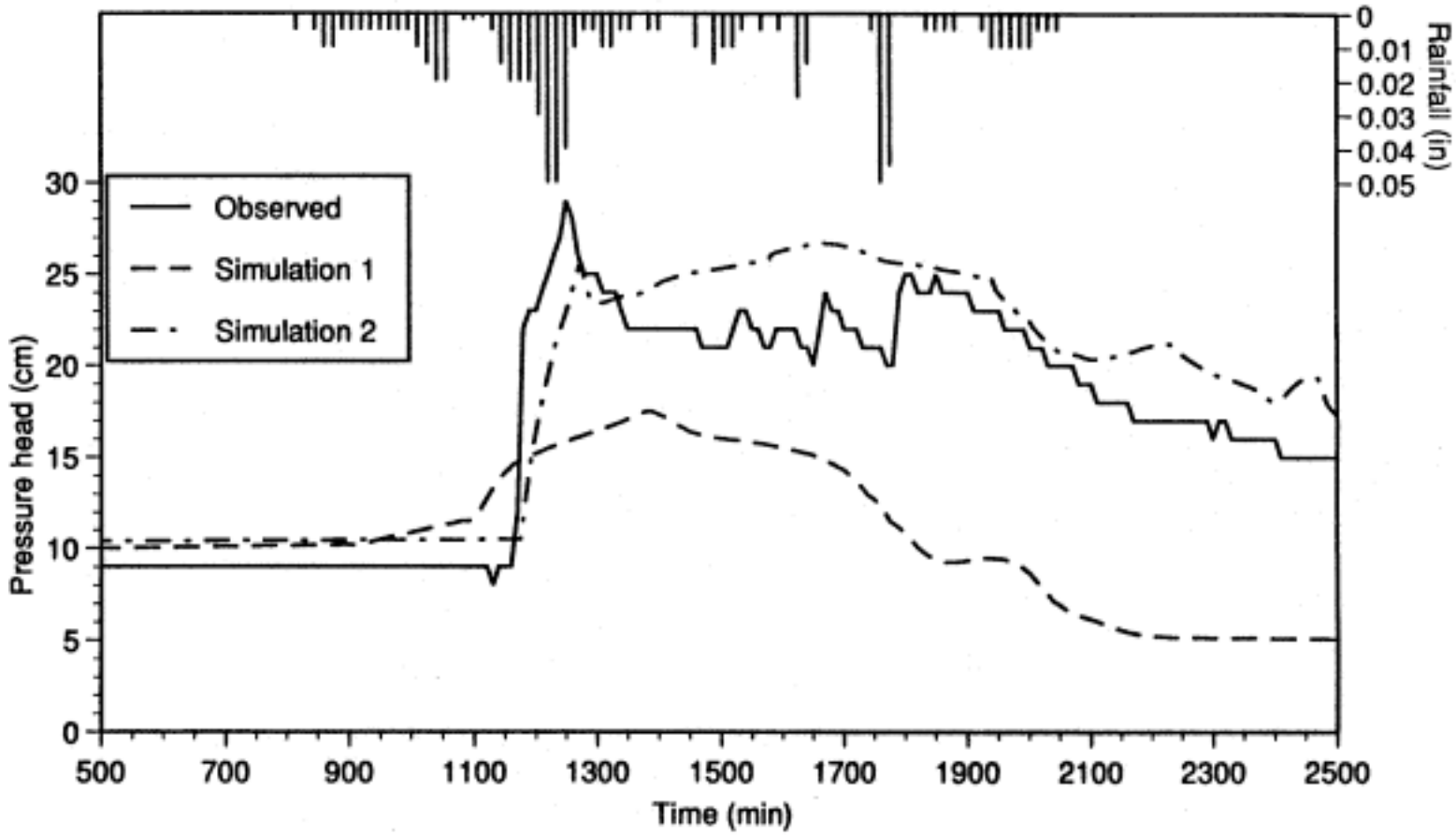

Figure 3.63 Comparison of observed and simulated pressure head response to October 1993 storm, Piezometer 31a, UNH field site, Hubbard Brook Experimental Forest